

*Return to
CRG*

34

OAK RIDGE NATIONAL LABORATORY LIBRARIES



3 4456 0548192 0

RESEARCH LIBRARY
DOCUMENT COLLECTION

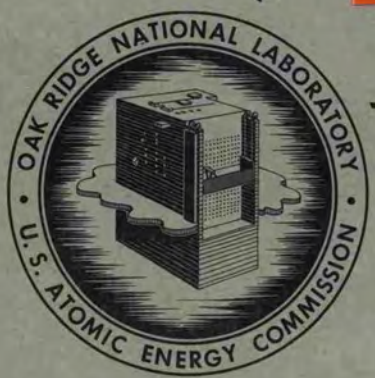
ORNL-3898
UC-33 - Propulsion Systems and
Energy Conversion
TID-4500 (46th ed.)

NASA Order No. C-220-A
(Interagency Agreement 40-14-63)

SNAP-8 CORROSION PROGRAM

SUMMARY REPORT

**CENTRAL RESEARCH LIBRARY
DOCUMENT COLLECTION
LIBRARY LOAN COPY**
DO NOT TRANSFER TO ANOTHER PERSON
 If you wish someone else to see this
 document, send in name with document
 and the library will arrange a loan.



OAK RIDGE NATIONAL LABORATORY
 operated by
UNION CARBIDE CORPORATION
 for the
U.S. ATOMIC ENERGY COMMISSION

Printed in USA. Price \$6.00. Available from the Clearinghouse for Federal
Scientific and Technical Information, National Bureau of Standards,
U.S. Department of Commerce, Springfield, Virginia

LEGAL NOTICE

This report was prepared as an account of Government sponsored work. Neither the United States, nor the Commission, nor any person acting on behalf of the Commission:

- A. Makes any warranty or representation, expressed or implied, with respect to the accuracy, completeness, or usefulness of the information contained in this report, or that the use of any information, apparatus, method, or process disclosed in this report may not infringe privately owned rights; or
- B. Assumes any liabilities with respect to the use of, or for damages resulting from the use of any information, apparatus, method, or process disclosed in this report.

As used in the above, "person acting on behalf of the Commission" includes any employee or contractor of the Commission, or employee of such contractor, to the extent that such employee or contractor of the Commission, or employee of such contractor prepares, disseminates, or provides access to, any information pursuant to his employment or contract with the Commission, or his employment with such contractor.

ORNL-3898

Contract No. W-7405-eng-26

NASA Order No. C-220-A
(Interagency Agreement 40-14-63)

SNAP-8 CORROSION PROGRAM

SUMMARY REPORT

H. W. Savage
E. L. Compere B. Fleischer
W. R. Huntley R. E. MacPherson
A. Taboada

DECEMBER 1965

OAK RIDGE NATIONAL LABORATORY
Oak Ridge, Tennessee
operated by
UNION CARBIDE CORPORATION
for the
U.S. ATOMIC ENERGY COMMISSION



3 4456 0548192 0



Contents

INTRODUCTION.....	1
SUMMARY.....	3
CONCLUSIONS.....	7
FORCED-FLOW CORROSION-LOOP EXPERIMENTS.....	9
Corrosion-Loop Program Plan.....	9
Modifications to Corrosion-Loop Program.....	12
Corrosion-Loop Design.....	12
Initial Corrosion-Loop Design.....	12
Instrumentation and Controls.....	17
Design of Hot-Spot Loops.....	20
Design of Duplex Tubing Installation.....	22
Fabrication of Corrosion Loops and Test Facilities.....	27
Purchase Specifications.....	27
Inspection Procedures for Materials.....	27
Cleaning and Assembly Techniques.....	27
Corrosion-Loop Operation.....	29
Filling and Pretest Operation.....	29
Corrosion-Loop Operating Conditions.....	29
Oxygen Control During Loop Operation.....	32
Effect of Cold Trapping on Hydrogen Concentration in the Loops.....	33
Preliminary Hydride Cold-Trapping Tests in Loop 8.....	33
Deuteride Cold Trapping in Loop 14.....	36
Argon Gas Transfer in Loops Due to Differential Temperature Solubility in NaK.....	39
Loop Shutdown and Removal Procedures.....	40
Design and Operation of Auxiliary Loop Equipment.....	40
Bypass Oxide-Removal System.....	40
Hot-Trap Design and Operation.....	41
Cold-Trap Design and Operation.....	41
Hydrogen-Injection System.....	42
Hydrogen-Detection Systems.....	44
Thermal-Conductivity Cell Hydrogen Monitoring System.....	44
Mass Spectrometer Hydrogen Monitoring System.....	46
Extraneous Hydrogen Measurements.....	47
NaK Sampling Equipment.....	49
Oxide Plugging Indicators.....	52
Other Operating Experience.....	57
Cold Finger Design and Analysis.....	57
Corrosion of Hastelloy N Underneath Lava Bushings.....	60
Analog Study of Hydrogen Concentration in the Loops.....	62
Comparison of Analog Study with Loop Performance.....	65
CORROSION-LOOP MATERIALS STUDIES.....	68
Introduction.....	68
General Pattern of Migration Observed in Corrosion Loops.....	69
Metal Migration.....	76

Effect of Hydrogen.....	76
Effect of Time.....	76
Effect of Oxygen.....	79
Effect of Temperature.....	79
Identification of Mass-Transfer Deposits and Inter- pretation of Migration Pattern	84
Effect of Hot-Spot Conditions.....	90
Carbon Migration.....	91
Character of Carbon Migration.....	91
Effect of Carbon Transfer on Material Properties.....	103
Effect of Decarburization on Microstructure of Croloy 9M.....	104
Phase Identification Studies.....	104
Mechanical Properties of Decarburized Croloy 9M.....	106
Procedure.....	106
Materials.....	106
Method of Decarburization.....	107
Tensile Tests.....	108
Strain Rate Tests.....	108
Creep-Rupture Tests.....	108
Results of Mechanical Property Tests.....	108
Tensile Tests.....	108
Strain Rate Tests.....	110
Creep-Rupture Tests.....	114
Discussion and Conclusions.....	117
CHEMISTRY STUDIES.....	119
Introduction.....	119
Materials and General Facilities.....	120
Hydrogen.....	120
Croloy 9M.....	120
Hastelloy N.....	121
Type 316 Stainless Steel.....	121
Armco Iron.....	122
NaK-78.....	122
Lithium.....	122
Inert-Atmosphere Glove Box.....	123
Experimental Comparison of Permeation Through Metals of Hydrogen from the Gas Phase and Hydrogen Dissolved in NaK.....	124
Permeation Cells and Experimental Method.....	125
Type I Cell.....	125
Type II, Iron Thimble Permeation Cell.....	129
Hydrogen Permeation Through Hastelloy N.....	131
First Cell (A).....	131
Second Cell (B).....	132
Second Cell (B), with NaK Present.....	133
Croloy 9M in the Absence of NaK (Type I Cell).....	134
Croloy 9M Iron Thimble Cell Without NaK.....	135
Permeation of Hydrogen Through Type 316 Stainless Steel in the Absence and Presence of NaK.....	136

Type I Cell.....	136
Type 316 Stainless Steel Iron Thimble Cell With and Without NaK.....	138
Deuterium Permeation of Type 316 Stainless Steel.....	140
Hydrogen Permeation After Oxidation of Stainless Steel.....	142
First Oxidation Experiment (1100°F).....	142
Second Oxidation Experiment (1100°F).....	144
Third Oxidation Experiment (1300°F).....	144
Solubility of Hydrogen in NaK-78.....	145
Experimental Results for Solubility of Hydrogen in NaK-78.....	150
Comparison of NaK Data with the Literature.....	154
Hydrogen Solubility in NaK Containing Added Lithium....	158
Calculations Relative to Hydrogen in the SNAP-8 System.....	162
Estimate of Steady-State Pressure Resulting from Hydrogen Permeation of System Walls.....	162
Removal of Hydrogen from SNAP-8 Primary NaK by Cold Traps, Windows, and Solid Getters.....	165
Direct Cold Trapping.....	165
Windows.....	166
Use of Solid Getters.....	169
Use of Soluble Getters, Including Lithium.....	170
Possibility of Lithium-Enhanced Cold Trapping.....	171
APPENDIX A, Flowsheets for Corrosion Loops.....	179
APPENDIX B, Drawing List, SNAP-8 Corrosion Loops.....	182
APPENDIX C, Chemical Analyses of Loop Materials.....	186
APPENDIX D, Loop Operating Histories.....	187
APPENDIX E, Evaluation of Chromized Hastelloy N Surface.....	198
APPENDIX F, Methods of Analyses.....	201

Introduction

This report summarizes the work completed under interagency agreement 40-14-43, NASA Order No. C-220-A, which initiated a corrosion program at the Oak Ridge National Laboratory in support of the SNAP-8 electrical-generating system. The primary objectives of the ORNL SNAP-8 program were (1) to evaluate the compatibility of the proposed structural materials with the proposed reactor coolant, NaK containing hydrogen, and (2) to provide information on the behavior, control, and disposition of the hydrogen present in the SNAP-8 primary coolant, particularly the diffusion of hydrogen from the primary circuit into the power-conversion circuit.

The SNAP-8 system utilizes a compact NaK-cooled beryllium oxide-reflected reactor fueled with uranium-zirconium hydride. The containment material for the primary-circuit coolant is type 316 stainless steel, but, in addition, the NaK is exposed to other materials in the reactor and in the primary circuit. The SNAP-8 primary circuit materials proposed at the time this program was initiated and their respective uses follow:

<u>Material</u>	<u>Use</u>
Chromized ^a Hastelloy N	Fuel cladding
Hastelloy C	Lower grid plate
Type 347 SS (later changed to 316)	BeO cladding
Type 316 SS	Reactor vessel and primary system piping
Croloy 9M and type 316 SS	Boiler material

^aApplication of chromium to the surface of a metal. Details of the process are proprietary information of the Chromizing Corporation.

Several other boiler structural materials have appeared in alternate designs, but the scope of the present corrosion program is limited to the initial choice of boiler tube material, Croloy 9M.

The reactor primary circuit operates with surface temperature in the range of 1100 to 1425°F and is designed to supply 600 kw of thermal power to the boiling-mercury Rankine-cycle power-conversion system. The design life of the system is 10,000 hr of unattended operation.

The SNAP-8 reactor differs from conventional sodium- or NaK-cooled power reactors in three important respects: (1) fuel cladding temperatures are significantly higher (by about 200°F), (2) dissimilar alloys

are employed extensively in the primary circuit (see list above), and (3) hydrogen is continuously discharged to the NaK coolant by dissociation of zirconium hydride in the fuel.

This system posed several potential problem areas that required investigation. The effects of hydrogen on corrosion were unknown. The continuous introduction of hydrogen from the fuel elements into the NaK circuit of SNAP-8 might also provide possible mechanisms for deterioration of flow in the NaK circuits as a result of hydride plugging in cold regions. In the primary pump, NaK at 1100°F is in direct (but essentially zero flow) communication with NaK at 300°F. The transfer of hydrogen by diffusion through the boiler walls to the SNAP-8 secondary mercury circuit could affect performance of the secondary circuit. Firmer estimates were therefore needed on the rate at which hydrogen diffused into this power-conversion system. The extent to which carbon migration might occur was also unknown. The adequacy of the SNAP-8 cleanup procedures for oxygen control (cold trapping during startup) needed to be established. Other imponderables included possible interactions between carbon, oxygen, and hydrogen and their effect on the mass-transfer behavior of the NaK system.

The SNAP-8 corrosion program was designed to provide some evaluation of these problems using forced-flow loop experiments that simulated as closely as possible the SNAP-8 primary NaK system. The original plan included: (1) a statistically oriented program with variable loop parameters, including oxygen and hydrogen content of the NaK and loop hot-leg temperature; (2) an investigation of the effects of time; and (3) a study of means for eliminating hydrogen egress.

Several changes were made to the loop program as work progressed. Several loops with a modified design were added to study SNAP-8 hot-spot conditions, hydrogen egress, and hydrogen control. Other loops were deferred for budgetary reasons, negating the statistical aspects of the plan.

Concurrent with the loop program, experiments were conducted to determine the relative effectiveness of gaseous hydrogen and dissolved hydride as sources of hydrogen diffusing from the primary system. The program included a study of hydrogen permeability for three SNAP-8 primary loop structural materials with and without NaK present and an investigation of the relationships between hydrogen solubility and partial pressure in NaK as a function of temperature. Mechanical-property tests of both standard and modified Croloy 9M boiler material were included to ascertain the general effects of decarburization observed in the corrosion loops.

This report describes in detail the program plan, the experiments conducted, and the test equipment used to simulate the SNAP-8 primary circuit at reduced scale. Also described are the procedures and results of the post-run examinations and the numerous supplementary experiments needed to properly complete the objectives of this program. Finally, a summary of the results is included and, in light of these results, an evaluation of the corrosion problems associated with the SNAP-8 primary circuit.

Summary

A corrosion-loop program was conducted to investigate the compatibility of the structural materials and NaK coolant in the SNAP-8 primary coolant circuit. Supplementary experiments were conducted to provide information on the behavior, control, and disposition of hydrogen, particularly with respect to its diffusion into the power-conversion system. In addition, tests were made to determine the mechanical properties of decarburized Croloy 9M, a condition observed in the corrosion loops.

The loop program entailed operation of reduced-scale forced-flow loops that closely simulate important features of the SNAP-8 primary system, including materials, temperatures, velocities, surface-to-volume ratios, and surface area ratios of the various alloys in the primary circuit. The test loops were scaled down to about 1/45 the SNAP-8 size. The loop design consisted primarily of a chromized Hastelloy N heated section and Croloy 9M heat exchanger section connected with appropriate lengths of 316 stainless steel. At appropriate locations, inserts of Hastelloy C and type 347 stainless steel were included to mock up the then current SNAP-8 design. Oxygen-control components were provided in flow bypasses.

Eleven loop experiments were completed. Eight of these loops (one a repeat loop) were operated to provide information for a study of three variables: (1) maximum temperatures of 1300 and 1400°F, (2) oxygen content of < 30 ppm and approximately 80 ppm, and (3) the effects of hydrogen addition at simulated SNAP-8 levels. The loops were operated with a minimum NaK temperature of 1100°F, and all but the repeat loop were operated for approximately 2000 hr. One loop with simulated SNAP-8 oxygen cleanup procedures was operated for 5133 hr to study the effect of time. Two loops with redesigned bypass sections were operated to simulate a SNAP-8 reactor core hot spot of 1450°F. One of the hot-spot loops contained cold traps to study hydrogen control. The eleven loops accumulated approximately 25,000 hr of operation at design conditions.

The major difficulty encountered during loop operation involved monitoring of oxygen levels in the NaK. Interpreting oxygen levels with plugging indicators was difficult initially due to multibreak plugging curves, which indicated the presence of contaminants other than oxides. Two plugging-indicator breaks other than the oxide break were observed. The first break (800 to 1100°F) is believed due to argon coming out of solution in the NaK during cooling. The precipitate causing the second break (400 to 600°F) was not identified. The third plugging curve break was consistent with the cold-trap operating temperature and represented the design oxide level.

Control of oxygen level varied with loop conditions. Cold trapping followed by hot trapping was successfully used to maintain oxygen levels

of < 30 ppm. For maintaining high oxygen levels, the system was first loaded with oxides by injecting oxygen at the surge tank, followed by cold trapping at the desired temperature. The SNAP-8 oxygen cleanup procedure of cold trapping only on startup was found to be adequate to keep an oxygen level of < 30 ppm in the long-time loop.

The investigation to provide information on the behavior and control of hydrogen in SNAP-8 led to development of a sensitive means of determining the partial pressure of hydrogen at low levels. A hydrogen-injection system was developed for introducing hydrogen into the loop NaK at rates as low as 0.6 std cc/hr to simulate hydrogen losses from the SNAP-8 reactor core fuel elements, and a hydrogen-detection system was developed in which several argon-swept annuli around the loop were monitored with thermal-conductivity cells for observing the hydrogen partial pressures within the loop. Extraneous hydrogen was observed in the effluent from the hydrogen-detection annuli prior to injection of hydrogen into the loop. The source of the extraneous hydrogen was not determined and could not be traced to the atmosphere around the loop or the moisture in the argon sweep gas. Deuterium was injected into the final loop operated in this program to distinguish between extraneous hydrogen and that injected into the loop. A mass spectrometer attached to an annular detection area around the NaK piping served successfully to observe both the extraneous hydrogen and the variations in deuterium pressure in the NaK during various modes of operation.

Cold trapping was investigated as a means of reducing the hydrogen level in NaK that could be used to minimize hydrogen diffusion from the SNAP-8 primary circuit into the secondary mercury circuit - a condition expected to cause operational problems. Cold trapping at temperatures as high as 550°F was effective in reducing the hydrogen flow from the loops. Cold-trapping tests with deuterium injection showed that at simulated SNAP-8 hydrogen partial pressures of about 2×10^{-5} atm, the flow of deuterium from the loop could be reduced by a factor of 6 for 260°F cold trapping and by a factor of 2500 for 120°F cold trapping.

Argon gas transfer by means of differential temperature solubility was noted in all loops. Argon was put in solution at the flow-through surge tank (1300 or 1400°F) and transferred to cooler regions, where it accumulated as gaseous trapped pockets. Tests were made which demonstrated that the gas transferral was by solubility and not by simple gas entrainment at the flow-through surge tank.

Analytical examinations were made on loop materials as well as specimens strategically located throughout the loops. In general, the examinations show that very little metal migration occurs in low-oxygen-content NaK at temperatures up to and including 1400°F; however, carbon migration is quite severe. This condition was found to result in carbon levels of ~0.002 wt % in the Croloy 9M and caused excessive grain growth. Corrosion of Croloy 9M in low-oxygen-content NaK is undetectable, and that of types 347 and 316 stainless steel is very low, as compared with the corrosion of chromized Hastelloy N, which ranges from three to seven times greater. The oxygen level of the NaK is an important variable governing the corrosion rates of the iron-base materials. At 1400°F, increasing the

oxygen content of the NaK to approximately 80 ppm results in a low corrosion rate for Croloy 9M and causes the corrosion rate of types 347 and 316 stainless steel to increase by a factor of 3 to 4 over that experienced at the low oxygen level; however, the effect of this level of oxygen on the corrosion rate of Hastelloy N is very small. At levels of oxygen much over 100 ppm, the corrosion rate increased dramatically for iron-base alloys and increased somewhat for the Hastelloy N. Extensive metal deposition in the cold region of the loops was observed at these very high oxygen levels.

Additions of hydrogen to the NaK have not produced any detrimental and, in fact, hardly any discernible effects on the mass-transfer rate of any of the materials. Furthermore, the extent of carbon migration does not appear to be increased by the injection of hydrogen into the loop.

Phase-identification studies performed on types 347 and 316 stainless steel specimens exposed in the loops have indicated that the loop exposures cause development of carbide phases and sigma phase. Results also indicate that in type 347 stainless steel the sigma phase gradually decomposes as carburization proceeds across the specimen.

Results of hot-spot loops showed less corrosion damage under conditions of very low NaK flow at the 1450°F hot-spot temperature than under conditions of high velocity at 1300°F. The effect of temperature on corrosion of Hastelloy N was found to be significant, but in contrast virtually no effect was noted for the iron-base alloys. Weight change data suggest that the corrosion rate for both Hastelloy N and the iron-base alloy decreases with time until an approximately linear rate results. However, intergranular corrosion of the Hastelloy N was observed and therefore must be considered when extrapolating corrosion results.

Because of the extensive decarburization of Croloy 9M in the SNAP-8 corrosion loops, a study was made to determine the effects of decarburization on selected mechanical properties. Sheet tensile specimens of standard Croloy 9M and modified Croloy 9M were decarburized to a carbon content of approximately 0.002 to 0.01% by exposure to NaK in a forced-flow type 316 stainless steel loop. Test results indicated that the tensile strength and creep strength of both materials are significantly lowered as a result of decarburization.

The fate of the hydrogen entering the NaK-78 primary coolant of the SNAP-8 reactor from the zirconium-uranium hydride fuel elements will depend on the diffusion rates of the hydrogen from the NaK through the metal walls of the system and on the solubility behavior of the hydrogen. Means of reducing the hydrogen activity may be necessary to prevent operating difficulties.

The permeation rates of hydrogen through the major structural metal, type 316 stainless steel, in the presence of NaK at temperatures of 543, 593, and 704°C were found to differ little from values obtained in the absence of NaK. Slight increases were attributed to removal of oxides

from permeation cell surfaces by the NaK. The permeabilities of Hastelloy N and of Croloy 9M were also studied.

The solubility of hydrogen in NaK-78 was determined at six temperatures from 300 to 704°C. For unsaturated solutions the solubility depended on the square root of the hydrogen pressures and varied only slightly with temperatures. At temperatures of 300 to 400°C enough hydrogen could be dissolved at pressures below 1 atm to result in precipitation of a metal hydride.

The data permitted solubility relationships to be developed for hydrogen gas in the unsaturated solution and for precipitation conditions of solid hydride as a function of pressure and temperature. Saturation pressures were consistent with the literature. However, we found the terminal solubility of hydrogen in NaK to depend less strongly on temperature than some other investigators have reported for the similar sodium-hydrogen system.

The addition to NaK-78 of 1 to 4 at. % lithium considerably diminished the hydrogen activity, both by association with it in the NaK and by precipitation. A mass action model was developed to explain the phenomenon. It was suggested that in liquid alkali metal mixtures, dissolved hydrogen exists in the form of largely undissociated metal hydride molecules, with the different metals combining with different proportions of hydrogen dependent on their proportions and their affinity for hydrogen.

Conclusions

The results of the SNAP-8 Corrosion Program led to the following conclusions concerning the SNAP-8 reactor system and the corrosion test loops:

1. The most pronounced performance-deteriorating corrosion phenomenon expected in the SNAP-8 primary circuit is carbon migration from the Croloy 9M to the rest of the system.
2. Decarburization of Croloy 9M from 0.11% C to as low as 0.002% C results in considerable loss in mechanical properties.
3. Corrosion of Hastelloy N is manifested as intergranular attack. The depth of corrosion damage is therefore greater than that expected from weight-change measurements.
4. Maximum attack in the SNAP-8 system having an oxygen level of less than 30 ppm will occur on the Hastelloy N at the outlet end of the reactor. Extrapolation of data indicates that corrosion at this point will be less than 1-1/2 mils in 10,000 hr at 1300°F.
5. Corrosion at low-flow 1450°F hot-spot areas will be less than that occurring at high-flow 1300°F areas due to influence of velocities.
6. The corrosion behavior of the system materials is not deleteriously affected by hydrogen at simulated SNAP-8 levels.
7. Oxygen was found to be the most important factor affecting corrosion of the iron-base materials. The nickel-base material, Hastelloy N, was sensitive to oxygen only at very high concentrations.
8. Initial cold trapping for removal of oxygen was found to be sufficient for oxygen control. This was demonstrated in a 5133-hr loop test in which the measured oxygen concentration remained at < 30 ppm throughout the test. Corrosion results further confirmed that low-oxygen conditions prevailed during operation.
9. The high affinity of chromium for oxygen resulted in the removal of oxygen from NaK by deposition of a chromium oxide complex, $\text{Na}_2\text{O}\cdot\text{Cr}_2\text{O}_3$, in the cold leg in high-oxygen loops. Chromium was selectively leached from all materials in the hot leg of the loops.
10. Mass-transfer deposits generally tend to build up in the electromagnetic pump cell and at flow disturbance regions in the cold leg.
11. In low-oxygen loops, deposits consisted mostly of nickel, chromium, and manganese. In the high-oxygen loops the deposits were mostly iron and chromium.

12. In the low-oxygen NaK, corrosion of the Hastelloy N was very sensitive to temperature changes while the iron-base alloys were virtually unaffected.
13. Long-time exposure of 316 stainless steel and 347 stainless steel at SNAP-8 temperatures will result in microstructure changes involving the formation of sigma phase, carbides, and other unidentified phases. Some loss in ductility can be expected from these changes.
14. Carbon diffusion from Croloy 9M is apparently a function of both the decomposition rate of Cr_7C_3 and the diffusivity of carbon in $\alpha\text{-(Fe,Cr)}$.
15. Migration of nickel to Croloy 9M causes carbon activity changes in the Croloy 9M surface which result in uphill diffusion of carbon.
16. The extent of carbon migration is not increased by injection of hydrogen into the loop.
17. Control and monitoring of oxygen level was the single most important factor in the operation of the corrosion loops.
18. Measurement of oxygen level using plugging indicators is subject to interpretation because of the multibreak results in the curve. Argon removal from NaK due to differential temperature solubilities was observed to cause a spurious break in the oxygen plugging curve.
19. Deuterium injection was a useful technique to eliminate the effects of extraneous hydrogen in studying hydrogen disposition in the loops.
20. Cold trapping is an effective means of reducing the hydrogen level in NaK and can be used in SNAP-8 to reduce diffusion of hydrogen into the mercury circuit.
21. The permeation rate of hydrogen through type 316 stainless steel is not altered by the presence of NaK.
22. The solubility of hydrogen in NaK for unsaturated solutions depended on the square root of the hydrogen pressure, and varied only slightly with temperature.
23. The activity of hydrogen in NaK can be considerably diminished by the addition of lithium. This is a potential means of controlling hydrogen egress from the SNAP-8 primary system.

Forced-Flow Corrosion-Loop Experiments

W. R. Huntley R. E. MacPherson
B. Fleischer A. Taboada

CORROSION-LOOP PROGRAM PLAN

The corrosion-loop tests were programmed to determine if there were readily detectable conditions in the SNAP-8 primary system that could contribute to serious deterioration of design performance. Ten loops (see Table 1) were to provide data for the basic corrosion investigation and two additional loops were to study methods for controlling and removing hydrogen from the primary system.

For the basic study of the effects of the design variables on the mass-transfer behavior of the SNAP-8 primary system, eight loops (1, 2, 3, 4, 7, 8, 9, 10) were planned to operate for 2000 hr each. Four of these were to operate without hydrogen addition to the NaK; the other four were to operate with hydrogen injected into the NaK at a rate simulating the maximum anticipated SNAP-8 hydrogen-infusion rate. Two loops of each set of four were to operate at a constant oxygen level (< 30 ppm), such as may be obtained by using cold or hot traps in the NaK circuit; the other two sets of two loops each were to operate at a high oxygen level (~ 80 ppm), such as might result if the NaK in the SNAP-8 system was not as thoroughly trapped during long-term operation. (The high oxygen level was initially attempted at 500 ppm, but was reduced to 80 ppm for ease of operation and oxygen level maintenance.) Of each set of two loops, one loop was to operate with a chromized Hastelloy N surface temperature which would result in a maximum NaK temperature of 1300°F , such as is expected to exist in the SNAP-8 reactor in regions where NaK velocity past the fuel elements is high, and a NaK thermal gradient of 200°F . The other loop was to operate with a maximum chromized Hastelloy N surface temperature of 1425°F , to simulate the expected SNAP-8 fuel-cladding hot-spot condition, and a thermal gradient of approximately 300°F in the NaK. All loops were operated with a minimum NaK temperature of 1100°F in the main circulating stream.

Loop 5 operated at conditions simulating the most severe hydrogen and temperature situations expected and the oxide situation resulting from procedures and methods of operation planned for the SNAP-8 primary system. In addition, loop 5 operated 5133 hr in lieu of the normal 2000-hr operating time to study the effect of time on the corrosion and mass-transfer behavior.

All the corrosion test loops included a dead-leg cold finger exposed to 1100°F NaK to simulate the narrow annulus around the shaft of the

Table 1. Operating Conditions for All Proposed and Operated Forced-Convection Loops

Loop No.	Maximum NaK Temperature (°F)	Oxygen Content of NaK (ppm)	Hydrogen Content of NaK	Variables to Be Studied	Comparison Loop	Time of Operation at Design Conditions (hr)
1	1400	< 30	0	Temperature Oxygen content Hydrogen content	1A, 10 2 4	701
1A	1400	< 30	0	Temperature Oxygen content Hydrogen content	10 2 4	2003
2	1400	~80	0	Temperature Oxygen content Hydrogen content	9 1 3	2004
3	1400	~80	SNAP-8 ^a	Temperature Oxygen content Hydrogen content	7 4, 6 2	Deferred
4	1400	< 30	SNAP-8	Temperature Oxygen content Hydrogen content	8 3, 6 1A, 1	2033
5	1400	SNAP-8 ^b	SNAP-8	Operating time	6	5133
6	1400	SNAP-8	SNAP-8	Operating time Oxygen content Hydrogen content	5 3, 4 11, 12	Deferred
7	1300	~80	SNAP-8	Temperature Oxygen content Hydrogen content	3 8 9	2021

Table 1 (continued)

Loop No.	Maximum NaK Temperature (°F)	Oxygen Content of NaK (ppm)	Hydrogen Content of NaK	Variables to Be Studied	Comparison Loop	Time of Operation at Design Conditions (hr)
8	1300	< 30	SNAP-8	Temperature Oxygen content Hydrogen content	4 7 10	2053
9	1300	~80	0	Temperature Oxygen content Hydrogen content	2 10 7	2000
10	1300	< 30	0	Temperature Oxygen content Hydrogen content	10 9 8	2000
11	1400	SNAP-8	SNAP-8	Hydrogen content	6, 12	Deferred
12	1400	SNAP-8	SNAP-8	Hydrogen content	6, 11	Deferred
13	1450	SNAP-8	SNAP-8	Hot spot	6	2000
14	1450	~30	Low	Hot spot with continuous cold trapping	13	2659
15	1450	SNAP-8	SNAP-8	No Croloy 9M in system	14, 13	Deferred

^aThe entry SNAP-8 indicates that the hydrogen content is that expected in the full-scale SNAP-8 system.

^bThe entry SNAP-8 indicates an oxygen level simulating that of the full-scale SNAP-8 system with initial oxygen removal from the NaK and no further oxygen trapping during operation.

SNAP-8 primary pump through which NaK at 1100°F in the SNAP-8 NaK primary circuit is in direct (but essentially zero flow) communication with the NaK at 300°F circulating within the SNAP-8 pump in an auxiliary closed circuit to cool windings and bearings. The cold fingers were installed to obtain a measure of the hydride and oxide accumulations in this region during prolonged operation.

Modifications to Corrosion-Loop Program

All loops proposed throughout the program are listed in Table 1. It includes the operating conditions of the loops and the major variables being studied. The loops which were deferred represent changes made as operating experience was accumulated. Loop 3 was deferred because it should give the same results as loop 2, the only difference being presence and absence of injected hydrogen. Previously operated loops had shown that hydrogen addition at SNAP-8 levels would not increase corrosion rates. Loop 6 was deferred on the basis that it should not be sensibly different from loop 4, inasmuch as it appeared that SNAP-8 oxygen levels would probably be about 30 ppm, the same as the controlled low oxide required of loop 4. (Loop 4 results, on the other hand, indicate that it operated at high, but undetected, oxide levels.) Loops 11 and 12 were originally proposed for evaluating hydrogen windows and solid chemical getters as means for reducing hydrogen concentration in the primary NaK system. These two loops were deferred when preliminary feasibility studies showed such methods unattractive for the reactor system.¹ It was concluded that excessive window area-to-thickness ratios would be required to produce significant reductions in hydrogen level. Solid getters would involve problems of compatibility with NaK, obtaining adequate surface-to-volume ratios, and avoiding undue surface oxidation and other chemical equilibrium problems. Hot-spot loops 13 and 14 were added to the initial program to study a more precise simulation of reactor hot-spot conditions. Loop 14 also featured nearly continuous cold trapping for hydrogen-removal studies. Loop 15 was proposed to simulate a reactor primary system in which no Croloy 9M was exposed to the primary NaK (simulating duplex stainless steel Croloy 9M tubing at the mercury boiler). Loop 15 was deferred at the direction of NASA.

CORROSION-LOOP DESIGN

Initial Corrosion-Loop Design

The corrosion loops used in the initial test plan were designed with configurations as nearly identical as possible. The loop design was based on matching, as nearly as practicable, the SNAP-8 NaK velocities, surface-to-volume ratios, and surface-area ratios of the various alloys in the primary circuit. The test loops were scaled down to about 1/45 the SNAP-8 size to allow the use of small components and power supplies. A summary

of the selected pipe sizes and other design data for the final loop configuration is given in Table 2. The arrangement is shown isometrically in Fig. 1 and as a simplified schematic flow diagram in Fig. 2. The main circuit of the loop was arranged approximately rectangularly in a vertical plane.

The NaK was heated at the top of the loop as it passed through 70.2 in. of 3/4-in.-OD chromized Hastelloy N tubing. Heat (~13.4 kw) was supplied externally by clamshell radiant-wire heaters. The NaK then passed through 4.0 in. of type 347 stainless steel tubing and through the bottom part of an inert-gas-pressurized, type 316 stainless steel, cylindrical surge tank containing level indicators, NaK sampling ports, and (when required) a hydrogen-injection device. Thirty inches of 3/8-in.-OD type 316 stainless steel tubing carried the flow at the maximum NaK tem-

ORNL-DWG 63-4901A

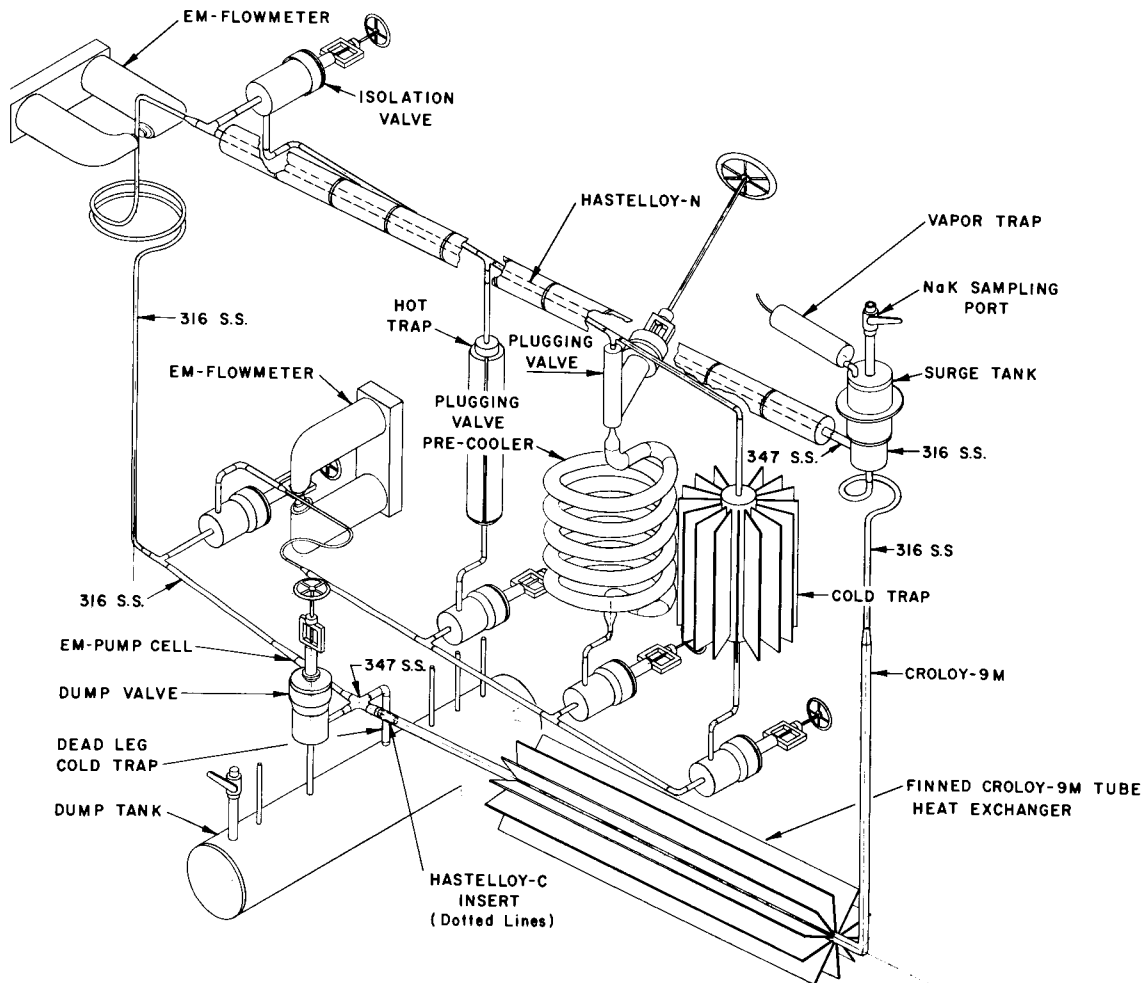


Fig. 1. Isometric Drawing of Original Loop Design.

Table 2. Summary of Original Loop Design Data

Loop Section	Material	Pipe or Specimen Size	Inside Diameter (in.)	Length (in.)	Surface Area (in. ²)	Cross-Sectional Area (ft ²)	NaK Volume (in. ³)	NaK Flow Velocity at Maximum Temperature (fpm)
Heated leg	Hastelloy N	$\frac{3}{4}$ -in.-OD, 0.072-in.-wall tubing	0.606	70.2	134	0.0020	20.3	138.5
	Hastelloy N specimen ^a				14 ^b			
	Type 347 SS	$\frac{1}{2}$ -in. sched-40 pipe	0.622	4.0	7.8	0.0021	1.2	132
Surge tank	Type 316 SS	3-in. sched-40 pipe	3.068	4.45 ^c	58.4 ^c	0.0515	41.8	5.4
		4-in. sched-40 pipe	4.026					
Surge tank baffle and level-indicator tube	Type 316 SS	$\frac{1}{8}$ -in.-thick plate and $\frac{3}{8}$ -in.-OD tubing			8.2 ^c			
Specimen in surge tank	Type 316 SS	$\frac{3}{8}$ -in.-OD, 0.020-in.-wall tubing			2.4			
Hot leg from surge tank to heat exchanger	Type 316 SS	$\frac{3}{8}$ -in.-OD, 0.049-in.-wall tubing	0.277	30	26.1	0.00042	1.8	660
Heat exchanger	Croloy 9M	1-in.-OD, 0.109-in.-wall tubing	0.782	84.1	207	0.00334	40.4	82.5
	Croloy 9M specimen ^a	0.030-in.-thick sheet			5.5 ^b			
	Type 316 SS specimens ^a	0.010-in.-thick sheet and $\frac{3}{32}$ -in. rod			6.9			

Table 2 (continued)

Loop Section	Material	Pipe or Specimen Size	Inside Diameter (in.)	Length (in.)	Surface Area (in. ²)	Cross-Sectional Area (ft ²)	NaK Volume (in. ³)	NaK Flow Velocity at Maximum Temperature (fpm)
Cold leg (1100°F)	Hastelloy C insert ^d		0.415	3.06	4.0	0.00094	0.4	285
	Type 347 SS	1/2-in. sched-40 pipe	0.622	4.0	7.8	0.0021	1.2	128
	Type 316 SS	1/2-in.-OD, 0.065-in.-wall tubing	0.370	24	28.0	0.00075	2.6	357
	Type 316 SS	3/8-in.-OD, 0.049-in.-wall tubing	0.277	96	83.7	0.00042	6.9	637
Total					593.8		116.6	

^aMetal specimens listed are those that fit loosely inside piping and therefore present added area in contact with flowing NaK.

^bArea of four specimens.

^cBased on 4.45-in. depth of NaK in surge tank.

^dLocated at exit of Croloy 9M tubing.

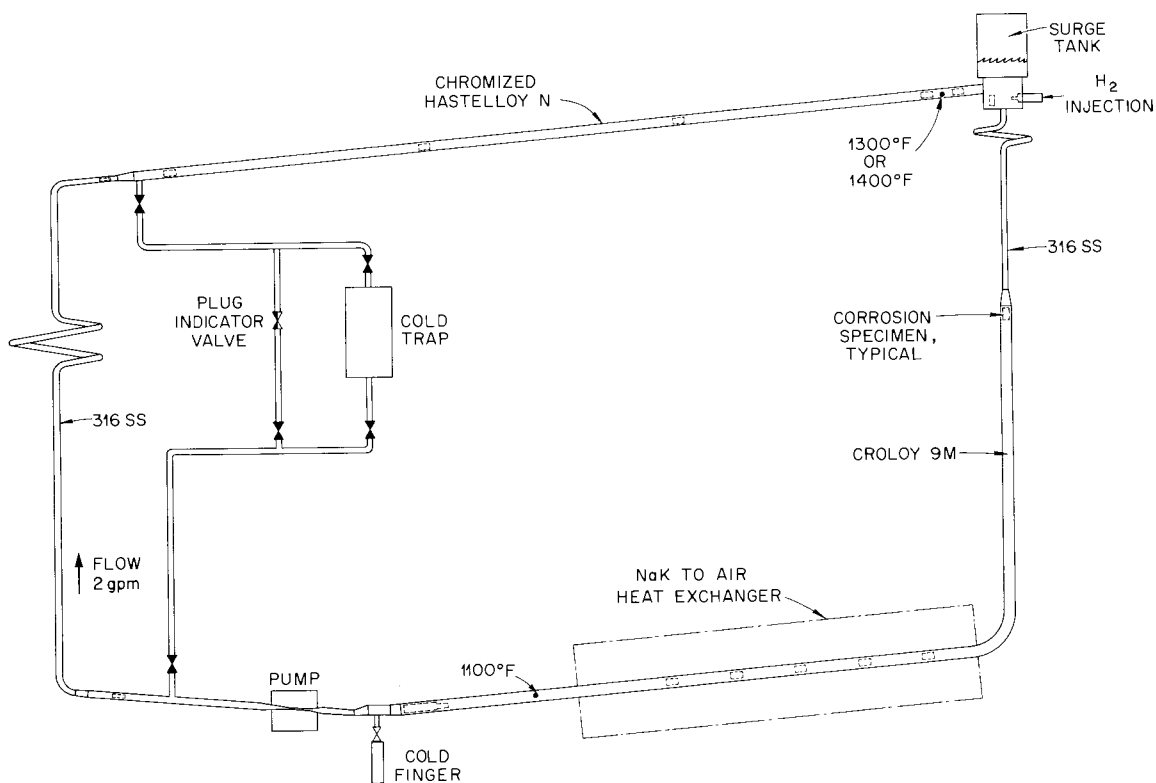


Fig. 2. Diagram of SNAP-8 Corrosion Loop.

perature to 84.1 in. of 1-in.-OD Croloy 9M tubing; this tubing simulated the SNAP-8 mercury boiler, and about one-half of it was finned for cooling purposes. As the NaK left the Croloy 9M heat exchanger, it passed over an insert of Hastelloy C, past the dead-leg cold trap simulating the SNAP-8 pump-shaft annulus, through 4 in. of 1/2-in.-OD type 347 stainless steel tubing, through 24 in. of 1/2-in.-OD type 316 stainless steel tubing, through the type 316 stainless steel cell of a standard General Electric G-3 electromagnetic pump, through 96 in. of 3/8-in.-OD type 316 stainless steel tubing, past an electromagnetic flowmeter, and back into the heater section. A dump tank was connected to the bottom of the loop and isolated from it by a valve.

A bypass between the electromagnetic pump discharge and the inlet to the Hastelloy N heater section provided three individually operable parallel paths with isolation valves. One path included a hot trap containing zirconium foil, the second included an air-cooled finned cold trap, and the third included a pre-cooler and a valve that was used as a plugging indicator. These paths were used to determine and control the oxide concentration in the NaK in the main circulating loop.

Hydrogen was injected into the loop NaK at a rate of 0.6 std cc/hr on certain of the loops (see Table 1) to study the effects of hydrogen which will evolve from the SNAP-8 reactor fuel elements. Monitoring systems were also attached to these loops to observe the permeation of injected hydrogen from within loops to the ambient environment. Details of the design and operation of these and all other auxiliary equipment are covered in the section of this report entitled Design and Operation of Auxiliary Loop Equipment. Detailed schematic flowsheets for loops both with and without hydrogen injection showing thermocouple locations, inert-cover-gas system, flow rates, automatic control points, and valve locations are presented in Appendix A.

Corrosion specimens of Hastelloy N (chromized), type 316 stainless steel, Croloy 9M, type 347 stainless steel, and Hastelloy C were mounted throughout the main loops and were checked metallographically and for weight changes at the end of each test run, at which time the main loop was also cut apart and examined.

Five test stands with associated instrumentation were built to carry out the test program. At the end of a typical 2000-hr run, the main loop piping was removed for examination; however, the instrument control systems were reused with subsequent loops installed in the same test stand, and the bypass oxide-removal systems, surge tanks, and dump tanks were disassembled, cleaned, and then reused.

Data on the SNAP-8 primary system surface areas and temperature distribution which were simulated are presented in Table 3, along with some comparisons of the test loop design. These data reflect the then current information from the reactor and systems designers, Atomics International and Aerojet-General Corporation respectively.

Instrumentation and Controls

Chromel-P/Alumel thermocouples were used on all loop piping temperature measurements. Bare-wire thermocouples of 0.030 in. diameter with ceramic bead insulation were used in most locations; these were attached to the loop piping with a condenser discharge welder. Stainless-steel-sheathed, 1/16-in.-OD, magnesium-oxide-insulated, grounded-junction Chromel-P/Alumel thermocouples were used in thermocouple wells at the plugging indicator and cold traps. The accuracy rating of standard Chromel-P/Alumel thermocouple wire is $\pm 3/4\%$ above 531°F. Thermocouple output was read out on recorders which have a rated accuracy of 1/4% of full scale or 5°F. Periodic checks were made with potentiometers to verify the accuracy of the recorders.

For the more critical loop temperature measurements, a special calibrated wire with an accuracy rating of $\pm 3/8\%$ above 531°F was employed. These higher-accuracy units were used at the heater inlet, heater outlet, and at the outlet of the finned Croloy 9M heat exchanger. The thermocouples used in the plugging indicator were checked in a calibration furnace prior to assembly.

Table 3. SNAP-8 Design Data

Surface	Material	Area (ft ²)	Percentage of Total Area	Temperature Distribution	
				Percentage of Area at 1100-1200°F	Percentage of Area at 1200-1300°F
Reactor core areas	Hastelloy N	45.2			
	Hastelloy C	1.35			
	Type 316 SS	9.63			
	Type 347 SS	5.31			
Other primary NaK system areas					
Piping from reactor to boiler (14 ft of 2-in.-OD, 0.049-in.-wall pipe)	Type 316 SS	7.0			
Boiler tubes	Croloy 9M	72.3			
Boiler shell	Type 316 SS	30.6			
Piping from boiler to reactor (17.3 ft of 2-in.-OD, 0.049-in.-wall pipe)	Type 316 SS	8.65			
Parasitic load heater	Type 316 SS	9.17			

Table 3 (continued)

Surface	Material	Area (ft ²)	Percentage of Total Area	Temperature Distribution	
				Percentage of Area at 1100–1200°F	Percentage of Area at 1200–1300°F
Total areas, SNAP-8 pri- mary NaK system	Type 316 SS	65.05	34.45	59	41
	Hastelloy N	45.2	23.8	50	50
	Hastelloy C	1.35	0.7	100	0
	Type 347 SS	5.31	2.8	50	50
	Croloy 9M	72.3	38.25	50	50
Grand total area		<u>189.21</u> ft ²			
		Area (in. ²)			
Total areas, test loop NaK system	Type 316 stainless steel	213.7	36.0	53.9 ^a	46.1 ^a
	Hastelloy N	148	24.9	50	50
	Hastelloy C	4	0.7	100	0
	Type 347 stainless steel	15.6	2.6	50	50
	Croloy 9M	212.5	35.8	45.8	54.2
Grand total area		<u>593.8</u> in. ²			

^aAll percentages listed for the temperature distribution of the test loop are for those loops which operated at a maximum NaK temperature of 1300°F (i.e., loops 7, 8, 9, and 10).

A test was run on loop 14 to verify that drift of the bare-wire Chromel-P/Alumel thermocouples at 1300°F was indeed small during the lifetime of an average loop. Two reference sheathed Chromel-P/Alumel thermocouples were periodically inserted into a thermocouple well adjacent to three thermocouples at the heater exit (TE Nos. 21, 22, and 34), and the output of the references was read on a potentiometer. Within the accuracy of the readings there was no observable drift between the output of the periodically inserted references and the continuously operated thermocouples attached to the loop during 2200 hr of operation at 1300°F. This test demonstrated that there was no significant drift in the output of the thermocouples during operation of a loop.

All flowmeters used on the loops were of the electromagnetic type. Field strength of the several magnets used varied from about 3600 to 4100 gauss. Field strength of the magnets was checked and the readings were filed for future reference after assembly in the loop, during loop shut-downs, and at the conclusion of each loop run to ensure that significant flux loss did not occur during operation.

No calibration tests were made of these flowmeter designs, and flow curves were based on calculation alone. Therefore, the accuracy of flow indication was of the order of $\pm 5\%$.

The temperature of the NaK leaving the Hastelloy N heater section of the loops was automatically controlled at the design temperatures of either 1300 or 1400°F. The temperature controller was a Wheelco model 407 indicating pyrometer connected to silicon controlled rectifiers which adjusted the power to the radiant-wire clamshell heaters. Day-to-day variations in the NaK heater exit temperature were normally less than 5°F with this system.

The temperature of the NaK leaving the finned Croloy 9M heater section was manually controlled at approximately 1100°F by a butterfly valve on the coolant air blower inlet. Day-to-day variations in NaK cooler exit temperature were normally less than 10°F with this system.

Design of Hot-Spot Loops

Corrosion loops 1 through 10 (Table 1) were of essentially identical configuration and were operated with a constant NaK velocity of 134 fpm in the Hastelloy N section. However, the maximum fuel element cladding temperatures could vary in the SNAP-8 reactor, and hot spots could develop if bowing of the fuel elements should occur. Our loops have been operated at two conditions: (1) a maximum NaK temperature of 1300°F, a condition less severe than the hot spots within the SNAP-8 reactor but identical with all other parts of the SNAP-8 primary loop, and (2) a maximum metal temperature of 1425°F and a maximum NaK temperature of 1400°F, a condition more severe than in the SNAP-8 reactor due to the high velocity at all temperatures and more severe than in all other parts of the SNAP-8 primary loop due to the higher temperatures of the NaK. The premise has been that the actual SNAP-8 corrosion situation should be

considerably less severe than the high-temperature loop cases studied due to (1) the lower NaK velocities at locations of high-temperature cladding and (2) the lower overall NaK temperature gradient (200 instead of 300°F).

During the course of our program, the fuel element cladding temperatures and the velocity characteristics of the NaK adjacent to the fuel elements of the SNAP-8 reactor were under continual study by Atomics International. These studies indicated a possible maximum temperature of 1450°F and NaK velocities adjacent to fuel elements from 0 to 2% of the bulk mean velocity, depending on whether or not adjacent fuel elements are in contact. Studies of flow and temperature profiles of the tricuspid-shaped passage defined by a nest of three adjacent fuel elements indicated that about one-fourth of the fuel element area could be at temperatures greater than 1400°F.

A "hot-spot" loop was designed to test the validity of our premise that the corrosion situation in the SNAP-8 reactor was predictable from the results of loop experiments 1 through 10. The hot-spot loop had the same basic configuration as the other loops, except that the main-flow 1100 to 1300°F heater section was reduced to 75% of the earlier length and the remaining 25% was placed in a low-velocity stream in parallel with the shortened main loop heater. The main loop operated at a maximum NaK temperature of 1300°F, an overall NaK temperature drop of 200°F, and a NaK velocity in the Hastelloy N section of 132 fpm.

The portion of the heater in the bypass line provided a maximum metal temperature of 1460°F and a maximum NaK temperature of 1450°F; the NaK velocity was 3.3 fpm. The two streams from the heaters joined at the loop expansion tank before the NaK entered the loop cooler. We were unable to design an inexpensive heater configuration for this small 1/45-scale loop that would simulate closely the tricuspid-shaped NaK passages of the SNAP-8 reactor; therefore the simple, circular-cross-section hot-spot mockup was used.

A diagram of a hot-spot loop (loops 13 and 14) is presented in Fig. 3, and the detailed flowsheet for this loop is shown in Appendix A. A hot-spot loop is shown during final assembly and prior to insulating in Fig. 4. The bypass stream was taken from the 1100°F portion of the loop downstream of the pump, electrically heated to 1450°F, and then discharged back into the 1300°F portion of the loop at the surge tank. Flow in the bypass line was maintained at 0.05 gpm (18.3 lb/hr) with a throttle valve and was monitored with an electromagnetic flowmeter. Type 316 stainless steel tubing (1/4 in. in outer diameter; 0.035-in. wall) was used to route the 1100°F NaK isothermally to the chromized Hastelloy N hot-spot section inlet. The hot-spot section consisted of a 15-in. length of 3/4-in.-OD, 0.072-in.-wall tubing, within which were mounted five chromized Hastelloy N corrosion specimen tabs. An 11-in.-long, 1/4-in.-OD, 0.035-in.-wall, chromized Hastelloy N tube connected the exit end of the hot-spot section to the loop surge tank. The Hastelloy N heater section of the basic loop was shortened from 70.2 to 52.7 in. so that the total amount of Hastelloy N in the loop would be unchanged. This heater operated at the SNAP-8 reactor outlet temperature of 1300°F with a NaK flow of 0.95 gpm (702 lb/hr).

The hot-spot loop design data are given in Table 4. Parameters of the SNAP-8 system, the original loop design, and the hot-spot loop design are compared in Table 5. A complete list of all mechanical, electrical, and instrumentation drawings for the loops is included in Appendix B.

Design of Duplex Tubing Installation

During the course of this program, duplex tubing (Croloy 9M jacketed with type 316 stainless steel) was considered as a substitute for single-walled Croloy 9M in SNAP-8 boilers. To evaluate duplex tubing for this purpose, a 24-in.-long section of 3/4-in.-OD tubing of this type was installed in loops 13 and 14 at the high-temperature end of the cooler. It was located at a hydrogen-detection annulus (sample point 2) to permit observation of hydrogen permeation characteristics. In loops 13 and 14, the inner Croloy 9M surface of the duplex tube is exposed to NaK, and therefore the direction of hydrogen movement is opposite to that which would occur in a SNAP-8 system. This method of installation was chosen

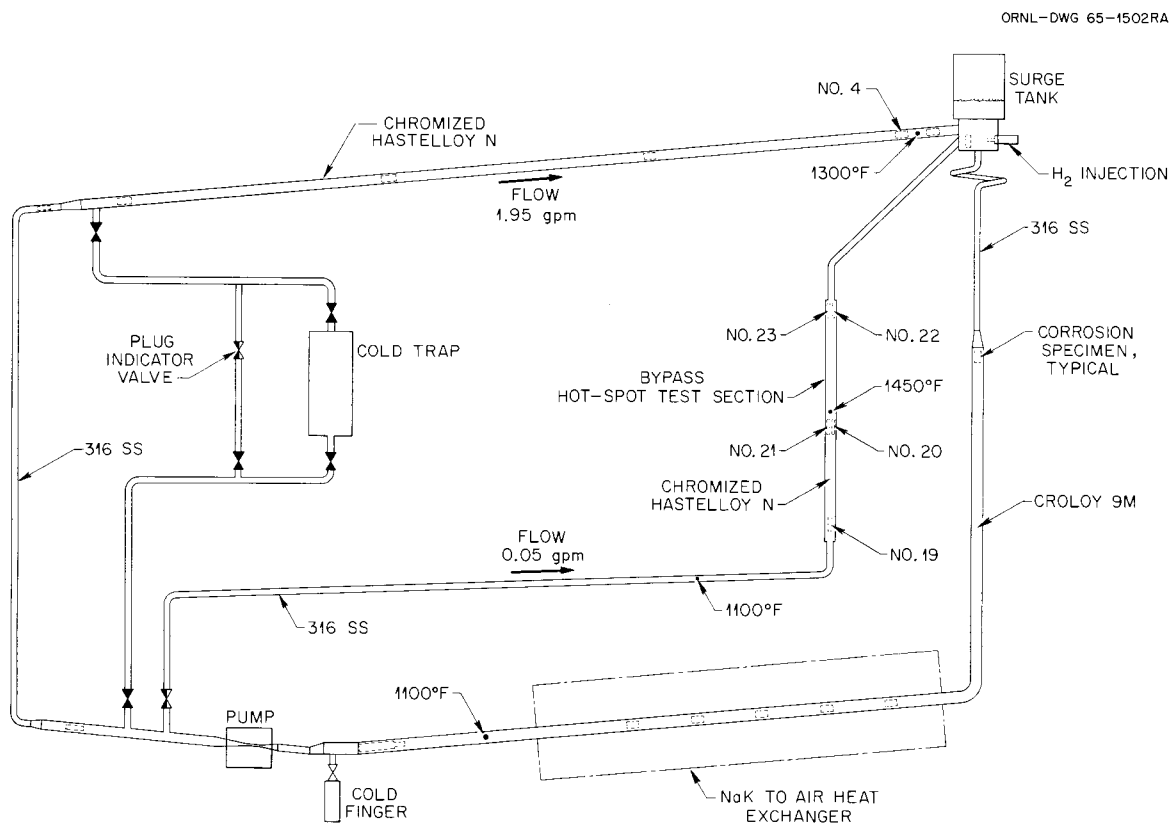


Fig. 3. Diagram of SNAP-8 Hot-Spot Loop.

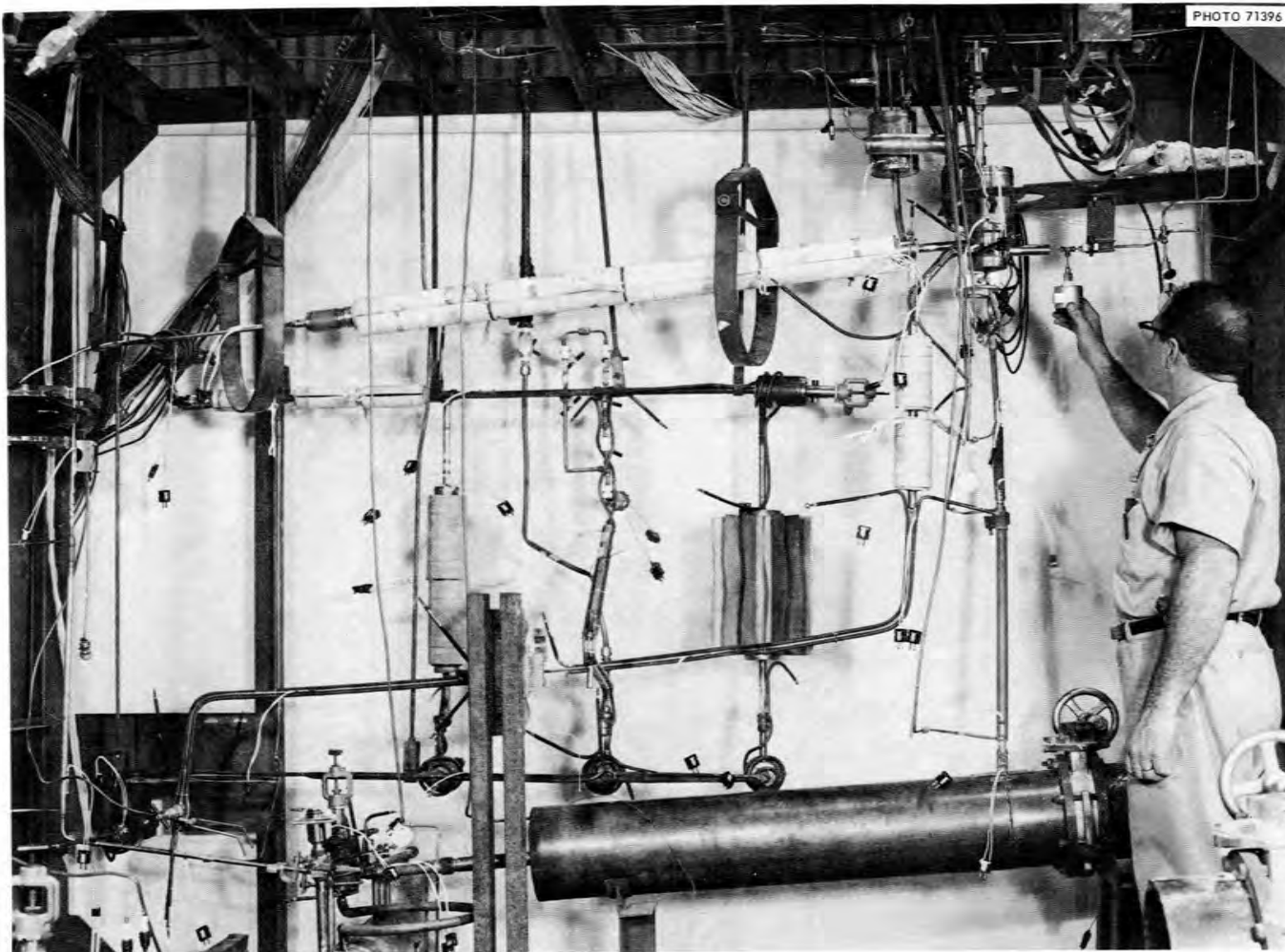


Fig. 4. Loop 13 During Heater and Thermocouple Installation.

Table 4. Summary of Hot-Spot Loop Design Data

Loop Section	Material	Pipe or Specimen Size	Inside Diameter (in.)	Length (in.)	Surface Area (in. ²)	Cross-Sectional Area (ft ²)	NaK Volume (in. ³)	NaK Flow Velocity at Maximum Temperature (fpm)
Heated leg	Hastelloy N	$\frac{3}{4}$ -in.-OD, 0.072-in.-wall tubing	0.606	52.65	100.0	0.0020	15.2	135
	Hastelloy N specimens ^a				10.4			
	Type 347 SS	$\frac{1}{2}$ -in. sched-40 pipe	0.622	4.0	7.8	0.0021	1.2	128.5
Surge tank	Type 316 SS	3-in. sched-40 pipe	3.068	4.45 ^c	58.4 ^c	0.0515	41.8	5.4
		4-in. sched-40 pipe	4.026					
Surge tank baffle and level-indicator tube	Type 316 SS	$\frac{1}{8}$ -in.-thick plate and $\frac{3}{8}$ -in.-OD tubing			8.2 ^c			
Specimen in surge tank ^a	Type 316 SS	$\frac{3}{8}$ -in.-OD, 0.020-in. wall tubing			2.4			
Hot leg from surge tank to heat exchanger	Type 316 SS	$\frac{3}{8}$ -in.-OD, 0.049-in.-wall tubing	0.277	27.75	24.2	0.00042	1.68	660
		$\frac{3}{8} \times 1$ in. adapter		1.44	2.13		0.29	
		$\frac{3}{4} \times 1$ in. adapter		0.625	2.76		0.48	
Heat exchanger	Croloy 9M	1-in.-OD, 0.109-in.-wall tubing	0.782	62.34	156.0	0.00334	29.8	82.5
		$\frac{3}{4}$ -in.-OD \times 0.65 ID tube ^e	0.650	24.0	49.0	0.00231	7.98	120
	Croloy 9M specimen ^a	0.030-in.-thick sheet			5.5 ^b			
	Type 316 SS specimens ^a	0.010-in.-thick sheet and $\frac{3}{32}$ -in. rod			6.9			

Table 4 (continued)

Loop Section	Material	Pipe or Specimen Size	Inside Diameter (in.)	Length (in.)	Surface Area (in. ²)	Cross-Sectional Area (ft ²)	NaK Volume (in. ³)	NaK Flow Velocity at Maximum Temperature (fpm)
Cold leg (1100°F)	Hastelloy C insert ^d		0.415	3.06	4.0	0.00094	0.4	285
	Type 347 SS	1/2-in. sched-40 pipe	0.622	4.0	7.8	0.0021	1.2	128
	Type 316 SS	1/2-in.-OD, 0.065-in.-wall tubing	0.370	24.0	28.0	0.00075	2.6	348
	Type 316 SS	3/8-in.-OD, 0.049-in.-wall tubing	0.277	72.0	62.6	0.00042	4.36	620
Hot-spot line	Type 316 SS	Hoke THY-442 valve and ends		7.5	9.90		0.47	20.4 ^f
		1/4 × 0.035 in. tubing	0.180	83.0	47.00	0.000177	2.11	37.8
		1/4-in.-OD × 3/4-in.-OD S.W. adapters	0.188	1.5	1.29	0.000193	0.042	34.5
		Specimen support wires		3.0	0.33			
	Hastelloy N, chromized	3/4 × 0.072 in. tubing	0.606	15.0	28.5	0.002	4.32	3.56
		3/8 × 1/2 × 0.010 in. specimens ^a				1.03		
		1/4 × 0.035 in. tubing	0.180	10.95	6.22	0.000177	0.28	40.2
Total					630.36		114.2	

^aMetal specimens listed are those that fit loosely inside piping and therefore present added area in contact with flowing NaK.

^bArea of four specimens.

^cBased on 4.45-in. depth NaK in surge tank.

^dLocated at exit of Croloy 9M tubing.

^eDuplex tubing 3/4-in.-OD × 0.050-in. wall; 0.035-in.-thick, type 316 stainless steel on outside of 0.015-in.-thick Croloy 9M.

^fFlow in 3/8-in.-OD × 0.065-in.-wall tubing ends.

Table 5. Comparison of SNAP-8 System and Test Loop Features

	SNAP-8	Original Test Loop Design	Hot-Spot Loop	
			Main Loop Portion	Hot- Spot Portion
NaK velocity, fpm				
In Croloy 9M	22.6 ^a	82.5	82.5 ^b	
In type 316 SS exit line from reactor	684 ^c	660	660	
In type 316 SS surge tank	22.6 ^a	5.4	5.4	
In type 316 SS return line	662	637	620	37.8
In Hastelloy N	134	138.5	135	3.56
In type 347 SS	134	132	128.5	
In Hastelloy C	290 ^d	285	285	
Ratio of Hastelloy N area to Croloy 9M area	0.625	0.695	0.695 ^e	
Ratio of Hastelloy N area to NaK volume, ft ⁻¹	15.8	15.2	15.32 ^e	59.6
Hastelloy N heat flux, w/in. ²	100	100 ^f	88.1	34.6
Reynolds number in Hastelloy N area	18,100	53,700	52,300	1820
Ratio of Hastelloy N area to type 316 stainless steel area	0.695	0.693	0.562	0.612
NaK flow, lb/hr	36,000	720	701.7	18.3
Volume of NaK, ft ³	2.86	0.0675	0.0662 ^e	0.00414
Hydrogen input rate, std cc/hr	60	0.6	0.6	

^aMaximum velocity in SNAP-8 boiler.

^bVelocity was 120 fpm at duplex tubing Croloy 9M.

^cBased on 2-in.-OD, 0.049-in.-wall tubing in SNAP-8.

^dMaximum velocity in SNAP-8 grid plate.

^eFor entire loop, including hot-spot portion.

^fFor loops operated at a NaK exit temperature of 1400°F.

to provide NaK-wetted material area ratios as near as practicable to those of previous loops. Postrun examination of the duplex tubing showed that no separation of the bond between the two metals had occurred due to hydrogen permeation during operation.

FABRICATION OF CORROSION LOOPS AND TEST FACILITIES

Purchase Specifications

All materials used in loop construction were procured in accordance with applicable standard ASTM specifications. All pipe and tubing were specified to be seamless. The carbon content of all stainless steel was specified to be greater than 0.04%. Although application of the materials in the corrosion loop justified the use of the more restrictive ORNL Reactor Material Specifications (RMS series), the latter specifications cannot be met normally by existing warehouse inventories. Since the required special mill orders could not be obtained in a time consistent with the schedule for operating the loops, the material used was taken from existing warehouse inventories; however, it was inspected on site and upgraded to RMS standards by a sorting process. Certified chemical and physical analyses were required of all vendors to show compliance with the purchase order and applicable ASTM specifications, and these were supplemented by check analyses at ORNL. A list of the specifications which served as the final criteria for material acceptance is given in Table 6; the results of the ORNL check analyses are presented in Appendix C, along with the specification requirements and ladle analyses presented in the receiving reports.

Inspection Procedures for Materials

All pipe, tubing, rod, and plate were inspected visually, dimensionally, ultrasonically, and with dye penetrant upon receipt from the vendors. All purchased fittings were similarly inspected, with the exception of ultrasonic testing. All special fittings machined on site from raw stock were dye-penetrant inspected upon completion of machining operations. The ORNL specifications for the nondestructive testing of the materials are also listed in Table 6. All inspection reports and chemical analyses have been kept on permanent file, and the appropriate file number was recorded on each material.

Cleaning and Assembly Techniques

Components for the loops, such as dump tanks, surge tanks, hot traps, cold traps, etc., were fabricated in several machine shops within the Oak Ridge area. However, the final closure weld on all components was made at the test site so that final inspection and proper cleanliness could be

Table 6. Corrosion-Loop Material Specifications

Material	Item	Purchase Specification	Inspection Procedure ^a	Acceptance Specification ^{a,b}
Type 316 SS	Tubing	ASTM A-269	MET-NDT-3, -4	MET-RM-A202
	Pipe	ASTM A-312	MET-NDT-3, -4	MET-RM-A200
	Plate	ASTM A-240	MET-NDT-1, -4	MET-RM-A1
	Rod	ASTM A-276	MET-NDT-2, -4	MET-RM-A102
	Fittings	ASTM A-403	MET-NDT-4	MET-RM-A300
Type 347 SS	Pipe	ASTM A-312	MET-NDT-3, -4	MET-RM-A200
	Rod	ASTM A-276	MET-NDT-2, -4	MET-RM-A102
Croloy 9M	Tubing	ASTM A-213-T-9	MET-NDT-3, -4	
Hastelloy N	Tubing	MET-RM-B167	MET-NDT-3, -4	MET-RM-B167
Hastelloy C	Rod	ASTM B-336-58T	MET-NDT-2, -4	MET-RM-B336

^aORNL specifications.

^bHydrostatic tests, required by MET-RM specifications, will normally not be made in the case of materials purchased to ASTM specifications.

assured. All components were degreased with a perchloroethylene vapor degreaser upon receipt from the machine shops. Acetone degreasing was used on the smaller fittings and subassemblies. Welds were thoroughly inspected using dye-penetrant techniques and radiography. All weld inspection reports have been kept on permanent file. Upon completion of assembly, each loop was evacuated and leak checked with a mass spectrometer helium leak detector. Each weld in the NaK system was required to have an indicated leak rate of less than 5×10^{-10} std cc/sec.

CORROSION-LOOP OPERATION

Filling and Pretest Operation

All loop dump tanks were charged with reactor-grade eutectic NaK directly from the vendor's 30-gal drums. A 10- μ porous metallic filter was installed in the fill line between the drum and dump tank. Typical vendor data on the composition of the NaK and the results of ORNL check analysis have been reported previously.²

All loops were evacuated and then filled with NaK to provide complete filling of the loop piping system. Several of the loops were gradually brought to operating temperature with frequent plugging indicator runs to observe oxygen pickup from the pipe walls. As would be expected, gradual increases in oxygen level of the NaK occurred with increasing temperature. Somewhat surprisingly, the maximum oxygen level found in any of these loops at full temperature and prior to cold trapping was less than 100 ppm. This was considered to be a low initial, non-trapped oxide level for loops having relatively high surface-area-to-volume ratios of about 60 ft⁻¹. The time spent in shakedown operations varied from loop to loop and is given in Table 7, along with a summary of other loop operating conditions. Shakedown periods were generally longer during early loop operation, when procedures for oxygen control and plug indicator interpretation were being developed.

Corrosion-Loop Operating Conditions

Eleven corrosion loops were operated in this program. The loops accumulated a total of approximately 25,000 hr of operation at design conditions. Table 8 is a summary of the average corrosion specimen temperatures and the average NaK velocity at each specimen. The temperatures are based on the average of temperatures which were logged once daily by shift technicians during loop operation. NaK velocities over each specimen are tabulated for the three types of loops - 1300°F maximum temperature, 1400°F maximum temperature, and the 1450°F hot-spot loops. Table 7 is a summary of general loop operating parameters, such as minimum and maximum circulating NaK temperatures, hydrogen input rate, and operating time in shakedown operations and at design conditions.

Table 7. Summary of Loop Operating Conditions

	1400°F Loops				Long-Term Loop	1300°F Loops				Hot-Spot Loops	
	Loop 1	Loop 1A	Loop 2	Loop 4	Loop 5	Loop 7	Loop 8	Loop 9	Loop 10	Loop 13	Loop 14
Maximum NaK temperature, °F ^a	1396	1397	1400	1408	1396	1285	1298	1312	1306	1450	1450
Minimum NaK temperature, °F ^a	1100	1055	1079	1067	1088	1080	1066	1070	1048	1066	1071
Hydrogen input, cc (STP)/hr ^b	0	0	0	0.57	0.50	0.63	0.58	0	0	0.55	0.28 ^c
Time at design conditions, hr	701	2003	2000	2033	5133	2021	2053	2000	2000	2000	2659
Time at design temperature, ^d hr	701	2068	2205	2683	5828	2705	2435	2476	2000	2238	2659
Time in shakedown, hr	175	95	279	682	748	916	448	1003	88	296	360
Time of hot trapping during operation, hr	160	28	0	24	31	0	138	0	170	0	0

^aAverage indicated temperature during the run.

^bAverage from plot of periodic measurements.

^cDeuterium was injected into loop 14 in lieu of hydrogen.

^dRepresents hours at full temperature but with oxygen or hydrogen levels not necessarily at design conditions.

Table 8. Average Specimen Temperatures and NaK Velocities over the Specimens

Specimen No. ^a	Material	Average Specimen Temperatures (°F)											Average NaK Velocities over Specimens (fpm)		
		1400°F Loops				Long-Term Loop	1300°F Loops				Hot-Spot Loops		Loops 7-10	Loops 1-5	Loops 13 and 14
		Loop 1	Loop 1A	Loop 2	Loop 4	Loop 5	Loop 7	Loop 8	Loop 9	Loop 10	Loop 13	Loop 14			
1	Hastelloy N ^b	1100	1055	1079	1067	1088	1080	1066	1070	1048	No specimen	No specimen	133.0	133.0	
2	Hastelloy N	1200	1160	1179	1171	1184	1148	1144	1150	1135	1094	1100	134.5	135.0	130.0
3	Hastelloy N	1306	1285	1294	1300	1296	1217	1220	1235	1221	1208	1205	136.5	138.5	133
4	Hastelloy N	1396	1397	1400	1408	1396	1285	1298	1312	1306	1311	1300	138.5	141.5	135
5	347 SS	1396	1397	1400	1408	1396	1285	1298	1312	1306	1311	1300	124.0	126.0	121.0
6	316 SS	1396	1397	1400	1408	1396	1285	1298	1312	1306	1311	1300	5.4	5.5	5.4
7	Croloy 9M	1380	1361	1367	1360	1369	1266	1273	1283	1278	1285	1260	82.5	84.2	82.5
11	Croloy 9M	1329	1314	1321	1321	1322	1245	1248	1230	1250	1260	1210	82.1	84.0	82.1
16	316 SS	1288	1273	1280	1280	1283	1217	1210	1205	1222	1230	1188	81.7	82.5	81.7
10	Croloy 9M	1250	1230	1237	1240	1242	1190	1182	1180	1193	1200	1167	81.3	81.9	81.3
15	316 SS	1208	1189	1194	1198	1200	1160	1155	1156	1164	1170	1145	81.0	81.5	81.0
9	Croloy 9M	1170	1147	1152	1157	1160	1133	1128	1130	1136	1140	1125	80.7	81.0	80.7
8	Croloy 9M	1121	1098	1101	1109	1110	1103	1098	1108	1093	1108	1104	80.2	80.2	80.2
12	Hastelloy C	1121	1098	1101	1109	1110	1103	1098	1108	1093	1108	1104	285	285	285
13	316 SS	1110	1090	1086	1081	1095	1090	1085	1099	1080	1100	1080	420.0	420.0	409
14	316 SS	1100	1055	1079	1067	1088	1080	1066	1070	1048	1066	1071	655.0	655.0	638
19	Hastelloy N										1113	c			3.34
20	Hastelloy N										1442	1445			3.56
21	Hastelloy N										1442	1445			3.56
22	Hastelloy N										1448	1450			3.56
23	Hastelloy N										1448	1450			3.56

^aSpecimens listed in order of stream position starting at heater inlet.

^bAll Hastelloy N specimens are chromized.

^cThis specimen was operated at 1300°F for first 20 days, then at 1425°F for 20 days; balance of run was at 1100°F.

Oxygen Control During Loop Operation

The major problem in the operation of the corrosion loops was the measuring and maintaining of oxide levels. Oxide measurements were made with plugging indicators. A plugging indicator determination of oxygen level is obtained by slowly cooling a liquid metal stream and then passing it through a flow restriction. Upon reaching saturation temperature the oxides precipitate, plugging the restriction, and a break or decrease in flow is observed. An oxide-saturation curve^{3,4} is used to relate the plugging temperature to the oxygen impurity level. Observations of multi-break plugging indicator curves were made throughout the program, and interpretation of the plugging indicator data was difficult. Details of plugging indicator design and of the three-break plugging indicator curves are discussed later. NaK sampling was also used to measure oxide levels, but correlation between the plugging indicator and the chemical analysis was unsatisfactory, as discussed in the section entitled NaK Sampling.

The level of oxygen for the low-oxide loops in this corrosion program was set at < 30 ppm. Lower levels of oxide are not quoted because they could not be monitored with the specific loop and plugging indicator designs being used. At levels lower than 30 ppm, insufficient oxide material was available to form a flow-restricting oxide plug.

The general operating procedure used on low-oxide loops 1, 1A, 4, 8, and 10 was to initially cold trap the loop NaK at flow rates of 0.025 to 0.050 gpm and at trap exit temperatures of 125 to 250°F (equivalent to saturation temperature for 10 to 19 ppm) for periods of at least 24 hr. This was followed by zirconium foil hot trapping at 1400°F for periods of at least 16 hr to further ensure a low oxide level at startup. Intermittent plugging indicator monitoring and cold trapping were employed during the 2000 hr of operation of all low-oxide loops to further ensure levels of < 30 ppm throughout the loop lifetime. The specific details of plugging indicator performance and of cold and hot trapping for each loop are shown in the individual loop histories, which are included in Appendix F.

Loops 5 and 13, low-oxide loops, were operated with a minimum of cold trapping once initial oxide removal was accomplished. This method of operation was used to simulate a proposed SNAP-8 reactor operating procedure in which initial oxide removal would be done prior to launching, with no further oxygen control in space. Loop 5 was operated in this manner with initial cold and hot trapping and then was not cold trapped during the subsequent 5133 hr of operation. Loop 13 was cold trapped initially, and no further trapping was planned. However, it was necessary to cold trap on two occasions during its 2000 hr of operation because of loop repairs made during loop shutdowns which resulted in oxygen contamination to the NaK system.

The level of oxygen for the high-oxide loops in this corrosion program was set at approximately 80 ppm after several futile attempts to maintain higher levels satisfactorily. Initial operating experience with

loop 9 showed that at oxide levels of several hundred parts per million, day-to-day flow degradation occurred due to mass transfer. It was further found in loops 7 and 9 that at values appreciably above 80 ppm (saturation temperature, 550°F) the initial break (presumably non-oxide) in the plugging indicator curve combined with the oxide break in such a fashion that interpretation of the curve was extremely difficult. Adoption of the 80-ppm oxide level provided a condition that could readily be monitored and distinguished from the initial break.

The general operation procedure for high-oxide loops 2, 7, and 9 consisted of bringing the loop to temperature and then monitoring the oxide level with the plugging indicator. Oxygen pickup from the walls of these loops during initial startup was less than 80 ppm; therefore it was necessary to add oxygen to each loop. Gaseous oxygen was injected above the liquid metal surface in the flow-through surge tanks. This was followed by cold trapping at the saturation temperature, 550°F, corresponding to 80 ppm. The loops were intermittently plugging indicator monitored and cold trapped at 550°F throughout operation to further ensure the proper oxide level. The above procedure was developed during initial operation of loops 7 and 9; therefore the initial portion of the operation of these loops was made at conditions which vary from this procedure, as shown in the loop histories of Appendix D.

EFFECT OF COLD TRAPPING ON HYDROGEN CONCENTRATION IN THE LOOPS

Preliminary Hydride Cold-Trapping Tests in Loop 8

A series of preliminary tests were run on loop 8 to obtain a measure of the reduction in hydrogen concentration of the NaK during cold trapping. Loop 8 operated with a NaK outlet temperature at the heater of 1300°F, a low oxide level of less than 30 ppm, and a hydrogen-injection rate of 0.6 cc (STP)/hr.

Four jacketed hydrogen-monitoring sections were installed on loop 8. Argon sweep gas was passed through each jacketed section by suitable valving, and the hydrogen content of the effluent argon was monitored with a calibrated thermal-conductivity cell. The design and operation of the hydrogen-detection system is described in detail in the section entitled Hydrogen-Detection System. This hydrogen-detection system was used to obtain a measure of the variations in hydrogen pressure within the loop during the cold-trapping tests. Operation of the detection annuli has shown that the hydrogen concentration in the low-flow (6 to 24 cc/min) argon purge stream tends to come to equilibrium with the hydrogen partial pressure in the loop. Therefore the hydrogen concentration in the annuli effluent is a direct measure of the hydrogen pressure within the loop.

The cold-trapping tests on loop 8 were for ascertaining whether the hydrogen level in a typical SNAP-8 primary system could be reduced and thereby lessen the amount of hydrogen that might accumulate in the

secondary mercury system. In these tests the hydrogen input rate to the loop was maintained while cold trapping at 150, 250, 350, 450, and 550°F. The flow rate through the cold trap was about 0.03 gpm during the 150°F run and was increased with each temperature level to about 0.11 gpm during the 550°F run. The volume of the main loop is about 0.5 gal and the main loop flow rate is 2 gpm. A measure of the effectiveness of the cold trap for hydrogen removal was obtained by observing changes in the hydrogen from one of the jacketed detection areas. The results of these runs are shown in Table 9. Values less than 0.020 cc/hr or less than about 25 ppm are not reported in the table because they are below the lower calibration limit of the thermal-conductivity cell used to monitor hydrogen.

A cold-trapping run was repeated at 250°F, with a flow rate through the trap of 0.025 gpm, which was as low as could be measured with existing loop equipment. This cold-trapping temperature was used to more nearly duplicate the SNAP-8 system capability.

Gas samples were taken for mass spectrometer analysis as a check against the thermal-conductivity cell. The gas samples taken at the lower hydrogen levels were of particular interest because the thermal-conductivity cell was not capable of accurate measurement of hydrogen concentrations below about 25 ppm. Before activating the cold trap, the effluent argon had a hydrogen concentration of 132 ppm (by volume). With the cold trap on stream the effluent argon contained 17 ppm of hydrogen. The feed argon flowing at 22.8 cc/min contained 11 ppm in both cases. The reduction in effluent hydrogen at constant argon flow was unique to the annulus in question and was a factor of

$$\frac{132 - 11}{17 - 11} = 20.2 .$$

Assuming equilibration between the hydrogen partial pressure in the loop and in the annulus, the loop partial pressure was decreased by a factor of

$$\frac{132}{17} = 7.75 .$$

The validity of the assumption of equilibration between the annulus and the internal hydrogen pressure has been discussed in detail in a previous report.⁵

The results of the test on loop 8 showed that cold trapping might be a feasible means of reducing the hydrogen flow from the SNAP-8 primary system. Plans were then made to design loop 14, which incorporated a more sensitive hydrogen-detection apparatus and additional cold traps. The cold-trap operating experience on loop 14 is covered in the following section.

Table 9. Hydrogen Flow from Loop 8 as a Function of Cold-Trapping Temperature

Cold-Trapping Temperature (°F)	Date of Test	Hydrogen Flow from Point 2 [cc (STP)/hr]	Total Flow from All Hydrogen-Detection Annuli [cc (STP)/hr]	Total ^a H ₂ Concentration in Effluent Argon on Point 2 (ppm)	Approximate Factor of Reduction of H ₂ Pressure Within Loop
Cold trap isolated for 11 days prior to reading	3-21-64		0.36		
Cold trap isolated for 14 days prior to reading	3-24-64	0.096		~84	
150	3-25-64	< 0.020		< 25	> 3.3
250	4-9-64	< 0.020		< 25	> 3.3
350	4-8-64	0.043		~42	~2
450	4-6-64	0.05		~46	~1.8
550	4-6-64, 4-7-64	0.054 ^b		~49	~1.7
150	4-10-64	< 0.020		< 25	> 3.3
Cold trap isolated for 6 days prior to reading	4-16-64	0.091	0.35	~79	

^aThis column is the sum of the thermal-conductivity cell reading plus the hydrogen content of the inlet argon, which was determined by prior analysis of the argon supply.

^bAverage of five runs.

Deuteride Cold Trapping in Loop 14

Loop 14 was the second hot-spot loop to be operated. It was similar to previously operated loop 13 except that deuterium was injected to the NaK circuit in place of hydrogen and nearly continuous cold trapping was employed. These modifications in the test procedure were aimed at (1) evaluating the effectiveness of cold trapping in reducing the hydrogen level of the SNAP-8 primary system and (2) defining the differences in corrosion and mass transfer that may result from a continuous cold trapping. Deuterium was used in this test to avoid the problem of extraneous hydrogen detected in previous tests, as described in a later section entitled Extraneous Hydrogen Measurements. Two cold traps were provided for the primary purpose of collecting hydrides and deuterides during the course of the test. These traps were approximately 1 in. in outside diameter by 10 in. long and were filled with wire mesh. In addition, a larger cold trap was used primarily for removal of oxides from the system following startup. The loop operating history is shown graphically in Appendix D.

Deuterium was injected into the loop at a rate of 0.3 std cc/hr. This rate of injection was expected to produce a deuterium partial pressure within the loop similar to the equilibrium hydrogen partial pressure in a SNAP-8 primary system in space. Deuterium outflow from the loop was monitored with a mass spectrometer attached to a jacketed portion of the loop. Deuterium background from the jacket was $< 10^{-8}$ cc (STP)/sec prior to D_2 injection. The D_2 outflow gradually increased when injection started and reached an equilibrium value of about 10^{-5} cc (STP)/sec after three days of operation. The time to attain equilibrium in loop 14 was much shorter than the nine- to ten-day periods observed in two previous loops in which hydrogen was injected at a rate of 0.6 std cc/hr. The reasons for this considerable variation in equilibration time have not been determined. The time to reach equilibrium was rechecked in loop 14-4 just prior to loop termination. For this test the loop was cold trapped at 100 to 115°F to remove deuterides from the NaK, injection was started, and the buildup time was again observed. The loop reached equilibrium in approximately two days.

After a steady-state level of deuterium had been obtained in the loop (with no cold trapping), a series of gas samples were taken by flowing argon sweep gas through one of the three annuli which are not attached to the on-line mass spectrometer. Gas samples were removed downstream of the sleeves and were analyzed with another mass spectrometer. These samples provide a means of determining deuterium levels in the loop NaK because the deuterium pressure in the slow-moving argon purge flow in the annulus tends to equilibrate with the deuterium pressure in the loop.

The argon flows through the detection annuli at atmospheric pressure. Therefore, the deuterium concentration of the effluent argon is approximately a direct measure of the deuterium partial pressure expressed in atmospheres; for example, if the deuterium content of the effluent argon

was 30 ppm, the partial pressure in the NaK was approximately 30×10^{-6} atm. The data from the sampling are given in Table 10. The source of hydrogen which increases the hydrogen level of the argon above the original value is undefined. The deuterium data, although scattered, indicate the equilibrium D_2 pressure in the loop was similar to the previously calculated hydrogen partial pressure of 2.4×10^{-5} atm for a SNAP-8 primary NaK system in space.⁶

The deuterium-injection system in loop 14-4 and the accompanying mass spectrometer detection system which can identify H_2 , HD, and D_2 have proven very useful in observing the performance of cold traps in the loop. Extraneous hydrogen was observed throughout the operation, but this was readily distinguishable from the deuterium outflow, which was of prime interest.

A series of cold-trapping tests were made to determine the reduction of deuterium flow from the loop as a function of cold-trap temperature. The loop was first allowed to reach equilibrium at design temperature with no cold trapping and with a D_2 injection rate of about 0.3 cc (STP)/hr. Deuterium flow from the loop was monitored by the mass spectrometer leak detector. Prior to cold trapping, the D_2 flow from the jacketed portion of the loop was 2.5×10^{-5} cc (STP)/sec. Cold trapping with the large trap at a flow rate of 0.5 gpm and at 115 to 125°F reduced the D_2 outflow to a value of about 10^{-8} cc (STP)/sec or a reduction by a factor of 2500. Flow was later directed from the large trap to the second small cold trap at a flow rate of 0.05 gpm and at a trap exit temperature of 260°F to more nearly simulate cold trapping which might be available on a SNAP-8 reactor in space. The loop reached a new equilibrium value in about 40 hr of operation, and the D_2 outflow at this time was about 4×10^{-6} cc (STP)/sec. This represents a reduction in D_2 outflow by a factor of 6 over the untrapped level of 2.5×10^{-5} cc (STP)/sec. Typical D_2 output data of the mass spectrometer attached to the loop are shown in Fig. 5. Areas of the

Table 10. Analysis of Gas Samples Removed from Loop 14 Detection Sleeves During Deuterium Injection and Prior to Cold Trapping

Date	Sample No.	Annulus No.	Argon Purge Flow (cc/min)	Original H_2 Content of Argon (ppm)	Sample Analysis (ppm)			Approx. Equivalent D_2 Partial Pressure in the NaK (atm)
					H_2	HD	D_2	
3/25/65	109	1	10	6	10	30	30	30×10^{-6}
3/29/65	110	1	10	6	20	30	10	10×10^{-6}
3/31/65	111	1	10	6	40	30	<10	$<10 \times 10^{-6}$
3/31/65	112	1	10	6	40	40	10	10×10^{-6}
3/31/65	113	4	10	6	20	20	30	30×10^{-6}

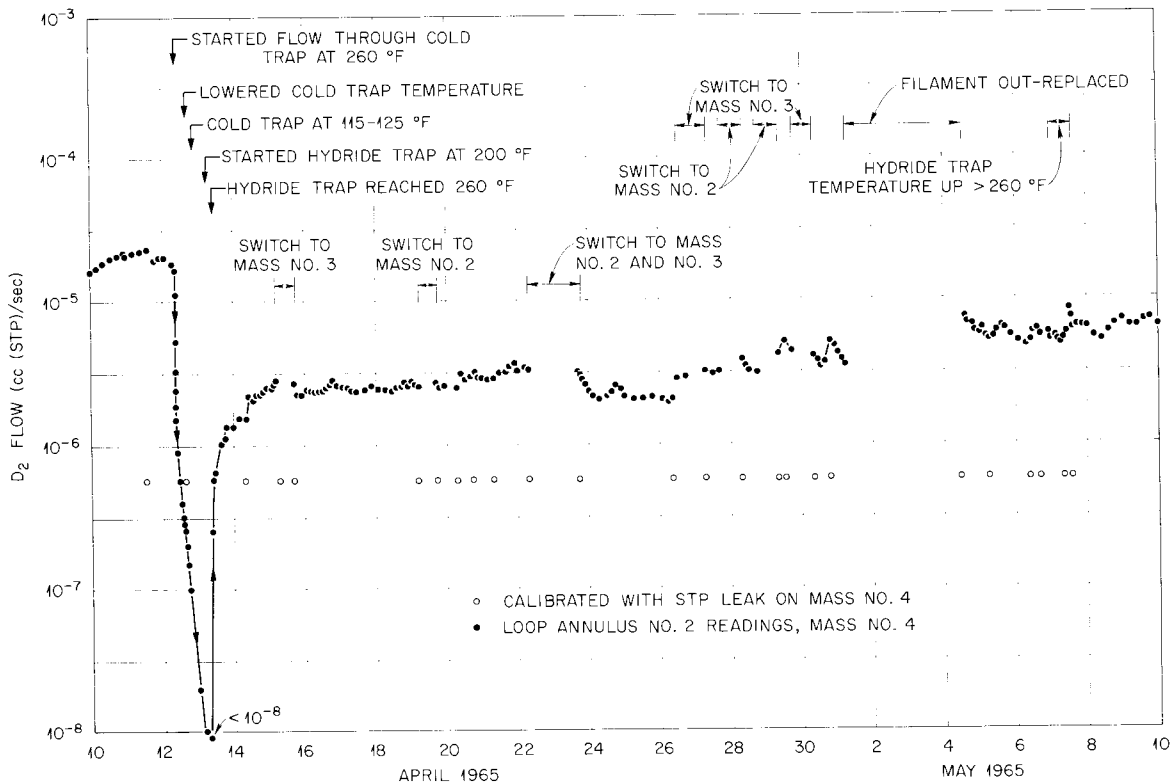


Fig. 5. D_2 Flow from Annulus 2, Loop 14-4, as Observed with Mass Spectrometer. Measurements made with mass spectrometer attached to annulus around NaK piping.

graph in which no data are presented generally represent times when data were being taken on masses 2 and 3 (H_2 and HD). The instrumentation was not designed to give simultaneous output readings for the three masses. The cause of the general rise in the D_2 outflow in the period extending from April 15 in Fig. 5 is not definitely known. However, post-run examination of the outer surface of the NaK-containing piping within the detection annulus showed a considerable oxide film which is believed to have accumulated during early operation of the argon-sweep-gas system in this annulus. It is probable that this oxide film was being gradually reduced by the deuterium flow through the metal wall, and this is thought to account for the increasing D_2 flow rate at the annulus.

The D_2 partial pressure in the test loop prior to cold trapping was measured, as shown in Table 10, and found to be similar to the estimated hydrogen partial pressure in a SNAP-8 primary system in space - about 2.4×10^{-5} atm. Therefore, the reduction in D_2 outflow observed at the loop as a function of cold-trap temperature is a reasonable approximation of the reduction of hydrogen flow which might be accomplished in the

SNAP-8 machine if attempts were made to reduce by cold trapping the amount of hydrogen permeating into the mercury boiler.

ARGON GAS TRANSFER IN LOOPS DUE TO DIFFERENTIAL TEMPERATURE SOLUBILITY IN NaK

The economizer in the oxide-removal bypass system in loop 14 and the vertical pipe runs leading to it provided volumes where gas could be trapped; these did not exist in previous loops. During shakedown operation, this piping configuration served as a means for observing that argon could be transferred by differential temperature solubility from the flow-through surge tank through the NaK to cooler regions. Some gas transfer and resultant trapping were noted on all previous loops as variations in the liquid level at the surge tank and as flow disturbances when the trapped bubbles were released and swept by the electromagnetic flowmeter; but these variations were much smaller than in loop 14 due to different bypass piping configurations. Loop 14 was vacuum filled originally and was free of trapped gas, as observed by varying the loop pressure from 2 to 20 psig with no indicated level change at the surge tank. After a few hours of operation at temperature, the system was observed to be "soft," in that the NaK liquid level would vary with changes in cover-gas pressure.

A test was run to show that the rate of argon transfer into the trapping areas of the bypass system was proportional to the temperature difference in the NaK. This was done to demonstrate that gas was being transferred by solubility and not by simple gas entrainment at the flow-through surge tank. The first run was made with 10 psig of argon cover gas on the surge tank, with a bypass flow rate of 0.07 gpm, and with a 200°F temperature difference between the surge tank surface and the bypass exit. The gas accumulation was observed by a gradual increase of the surge tank level as the argon collected in the trapped volumes of the bypass; it was calculated to be 0.2 in.³ (STP) of argon per hour. The second run was made with the same cover-gas pressure and NaK flow rate, but with a 1100°F temperature difference between the surge tank surface and the bypass exit; the gas accumulated at a rate of 1.5 in.³ (STP) of argon per hour, or about seven times as fast.

A further test was made to establish that the gas accumulating in the cooled regions of the bypass system was indeed argon. The NaK flow was directed through the bypass NaK sampler and through a valved sample bomb containing an enlarged cross section for gas accumulation. The bomb was evacuated at room temperature, filled with NaK by opening isolation valves leading to the loop, and then x rayed to determine the degree of filling. While the loop was operating at design conditions, NaK at 1100°F was directed isothermally through the bypass and bomb for 30 min at 0.1 gpm. The flow was then blocked by the inlet valve, and the bomb was cooled to room temperature. A second x ray showed that no noticeable amount of gas had accumulated. Flow was restarted through the bomb for

30 min at 0.1 gpm, the NaK being cooled from 1100 to 200°F. Flow was again stopped, and a third x ray showed that the enlarged portion of the bomb had filled with gas. The bomb was removed from the loop, and the mass spectrometer analysis of the gas trapped above the NaK surface within the bomb was as follows:

<u>Gas</u>	<u>Volume (%)</u>
Ar	98.9
O ₂	0.008
N ₂ + CO	0.88
H ₂ O	0.12
H ₂	0.05

LOOP SHUTDOWN AND REMOVAL PROCEDURE

At the completion of a loop run the heaters were deenergized and the NaK was immediately dumped while at elevated temperatures. The isolation valves in the cold fingers which simulated the SNAP-8 pump shaft annulus were closed prior to NaK dumping. After draining from the loop, the NaK was isolated in the dump tank by a manual valve. The loop was then cooled, stripped of instrumentation, and sectioned with tubing cutters and saws. The entire main loop was then cleaned with butyl alcohol and flushed with water to remove the reacted products. The loop was then submitted for analysis, described in a later section. Bypass purification piping and components such as the cold traps and plugging indicators were steam cleaned, flushed with water, and disassembled for inspection. The hot traps were rinsed with alcohol prior to steaming, due to the zirconium foil configuration, which prevented complete NaK drainage. If the hot- or cold-trap shells were to be reused, new filler materials were installed. The NaK charge in the dump tank was discarded at the end of each loop test. The loop surge tank and dump tank were cleaned out and usually reused in subsequent tests.

DESIGN AND OPERATION OF AUXILIARY LOOP EQUIPMENT

Bypass Oxide-Removal System

A bypass oxide-removal system was attached to each loop for oxide removal and control. The system piping was 3/8-in., sched 40, type 316 stainless steel. The NaK flow entered this system through a valve which was used for both throttling and isolation of the bypass system; it then

passed through an electromagnetic flowmeter and could be directed to either the cold trap, plugging indicator, or hot trap by valving. After leaving the traps or plugging indicator, the flow passed through a manually controlled electric clamshell heater section, where the NaK temperature was adjusted to main loop temperature. The flow then returned to the main loop through an isolation valve. All bypass piping was traced with electric tubular heaters in the event that inadvertent oxide or hydride plugs might occur during operation. In addition, the tubular heaters were used to heat the lines leading from the main loop to the isolation valves. When the bypass system was not operating, the isolation valves were closed, and these heaters were used to prevent inadvertent cold trapping in these static lines leading from the main loop. Schematic drawings of the bypass system are shown in the loop flowsheets of Appendix A.

Hot-Trap Design and Operation

The hot trap consisted of a 17-in. length of 2-in., sched 80, type 316 stainless steel pipe, within which was coiled about 7.2 ft² of alternate layers of plain and corrugated 0.004-in.-thick zirconium foil. The trap was vertically mounted and heated with an electric clamshell heater. The NaK entered the bottom of the trap at about 1000°F and was heated to 1400°F. Flow through the trap was 0.025 gpm; so the delay time in the trap was about 8.7 min. The ratio of zirconium surface area to volume of NaK in the loop and bypass was 2072 in.²/357 in.³, or about 5.81 in.⁻¹.

The hot trap was operated on the low-oxide loops to ensure oxygen levels less than 30 ppm, as required by the corrosion-loop experiment plan. The normal procedure was to hot trap the loop for periods of at least 16 hr after initial cold-trapping operations were completed. The total time of hot trapping for each loop is shown in Table 11. The specific periods of operation of the hot traps were intermittent in some of the loops and are shown in the operating histories of each loop in Appendix F. No hot trapping was necessary to obtain desired oxide level for the high-oxide loops (2, 7, and 9). No hot trapping was employed on the two hot-spot loops (13 and 14) because these loops simulated proposed operating procedures of the SNAP-8 primary system in which no initial hot trapping was being planned.

Cold-Trap Design and Operation

The cold trap consisted of a 13-1/2-in. long, 3-in., sched 40, type 316 stainless steel shell, within which was packed type 316 stainless steel, 0.010-in.-diam wire mesh at a density of about 20 lb/ft³. The cold trap was mounted vertically with the inlet at the bottom, and axial fins were welded to the exterior of the shell for cooling. The ratio of

Table 11. Total Time of Operation of Hot Traps for Each Loop

Loop No.	Type of Loop	Total Hot-Trapping Time (hr)
1	Low oxide	160
1A	Low oxide	28
2	High oxide	0
4	Low oxide	24
5	Low oxide	31
7	High oxide	0
8	Low oxide	138
9	High oxide	0
10	Low oxide	170
13	Hot spot	0
14	Hot spot	0

the total volume of the loop and bypass system to the cold trap volume was $357 \text{ in.}^3/100 \text{ in.}^3$, or 3.57/1.

A cold trap of the above design was installed on each of the 11 loops operated in this program. The minimum NaK exit temperature attainable was about 115°F at NaK flow rates of 0.025 gpm. At a flow rate of 0.025 gpm, the delay time in the trap was about 17.3 min. Operating experience showed that cold-trapping periods as short as 1/2 hr would alter the loop oxide level such that the plugging indicator would plug at the approximate cold-trap exit temperature. The total amount of cold trapping varied with each loop. The specific times and NaK exit temperature of cold-trap operation are shown in the individual loop histories of Appendix F.

Hydrogen-Injection System

A hydrogen-injection system was designed for certain of the corrosion loops. The purpose of this system was to mock up the hydrogen input which will occur in the SNAP-8 primary NaK system due to the permeation of hydrogen from the reactor fuel elements into the NaK coolant. Loops were operated both with and without hydrogen injection to obtain a measure of the effect on corrosion behavior and loop performance.

A bench test was built and operated for determining the performance of the hydrogen-injection system prior to use on the loops. Hydrogen was injected into the NaK through a Hastelloy N diffusion tube located in a typical loop surge tank. The system consisted of a Hastelloy N diffusion tube (0.123 in. OD, 3/8 in. long, 0.030 in. wall thickness) mounted in a static NaK-filled surge tank, a hydrogen supply, a palladium-diaphragm hydrogen purifier, appropriate valving and tubing, and a 0- to 200-psig pressure transducer. An argon cover-gas pressure of 30 psig was maintained in the surge tank, while the tank temperature was held at 1425°F. Hydrogen diffusion rates were determined by measuring the pressure decay in a known volume of gas between a close-off valve and the upstream surface of the diffusion tube. The leak tightness of this supply volume was checked by reducing the diffusion tube temperature (thereby lowering the permeability of the tube) and by lowering the supply pressure upstream of the close-off valve and then observing the pressure. A constant pressure indicated leak tightness.

After the initial 144 hr of operation of the bench test, it was noted that the diffusion rate of hydrogen into the NaK-filled surge tank had dropped to about 75% of the initial rate. While the original rate could be reestablished by increasing hydrogen pressure, use of this technique to maintain a uniform hydrogen-injection rate to a loop was not considered completely satisfactory. Repeated overriding of the injection rate decreases by hydrogen pressure increases was possible only at pressures below the upper limit of 200 psig on diffusion-tube supply-pressure measuring equipment.

Following the diffusion rate decrease in the bench test, the input side of the diffusion tube was evacuated to remove any large molecules from air inleakage or residual inert gas which might have accumulated on the input side of the diffusion surface. Hydrogen was again introduced into the tube, and the diffusion rate was noted to nearly equal the original rate. Provisions were made for this operation on the loop test stands, and the evacuation procedure was used numerous times during subsequent operation of the loops.

Hydrogen was injected into the NaK in five of the corrosion loops through a Hastelloy N diffusion tube located in the flow-through surge tank. The injection rate was 0.6 cc (STP)/hr to mock up the predicted SNAP-8 maximum input rate of 60 cc (STP)/hr. The injection rate was calculated by comparing the diffusion characteristics of the SNAP-8 and corrosion-loop circuits in an attempt to produce a hydrogen concentration in the loop equivalent to that for the SNAP-8 circuit.

Measurements taken on all loops with hydrogen injection showed that the effluent argon from the hydrogen-detection sleeves which were attached to the exterior of the main loop piping had from 90 to 150 ppm of hydrogen at equilibrium conditions. Therefore, the hydrogen partial pressure within the loop was at least equally as high, or 0.9×10^{-4} to 1.5×10^{-4} atm. The final estimate of the SNAP-8 hydrogen partial pressure was made late in the corrosion program as more-exact data became available, and the steady-state hydrogen pressure was calculated to be about

2.4×10^{-5} atm.⁷ No attempts were made to reduce the hydrogen level in the remaining loops, since the bulk of the loop operation was completed and no adverse effects had been observed in the loops from hydrogen injection. Therefore, the hydrogen partial pressure in the corrosion loops was about four times that now expected in the SNAP-8 system in space. The hydrogen partial pressure and concentration are related in accordance with Sieverts' law ($S = X/P^{1/2}$), and therefore the concentration of hydrogen in the loop NaK was about twice that now expected in the SNAP-8 system.

During loop operation the hydrogen input rates were calculated at least once a week for each loop. A review of these periodically calculated inputs for the five loops which incorporated hydrogen injection (4, 5, 7, 8, and 13) show that the reproducibility of the hydrogen-injection measuring system readings was generally ± 0.05 cc/hr.

Gas samples taken from the hydrogen-detection sleeves of several loops prior to injection of hydrogen into the loops showed an unexplained hydrogen content. The source of this hydrogen was not discovered. The level of this extraneous hydrogen was low compared to the normal equilibrium level of 90 to 150 ppm in loops in which hydrogen was being injected and was not of significance on loops 4, 5, 7, 8, and 13. However, on loop 14 studies were to be made of the effect of cold trapping on hydrogen removal, and the extraneous hydrogen was significant at the predicted lower hydrogen levels in this loop. Therefore, deuterium was injected into loop 14 in lieu of hydrogen to preclude confusion with the extraneous hydrogen source. The deuterium would, of course, act chemically the same as hydrogen.

Bench tests were run and reported⁸ which verified that the permeation of deuterium in lieu of hydrogen through a metal diaphragm such as the loop injection nozzle would vary as the square root of the atomic weight ratio of $1/\sqrt{2}$. Therefore the standard hydrogen-injection system was used for the deuterium injection with appropriate adjustment of the supply pressure to obtain the desired rate of permeation.

Hydrogen-Detection Systems

Thermal-Conductivity Cell Hydrogen Monitoring System

This system was provided on all loops in which hydrogen was injected to monitor changes in the loop hydrogen partial pressure. Four jacketed areas, representing about 18% of the total main loop surface area, were monitored for hydrogen effluent. The four areas monitored are shown schematically in the simplified schematic diagram in Fig. 6. Purified argon sweep gas was passed through an annulus around the selected segments of the loop piping, and the gas was monitored for hydrogen content by Gow-Mac Instrument Company model 9199 thermal-conductivity cells. The cells were calibrated with known mixtures of gases such that full-scale output was

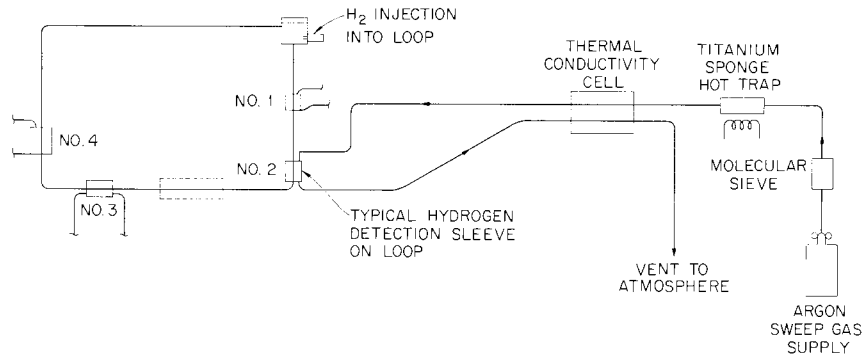


Fig. 6. SNAP-8 Corrosion Loops - Thermal-Conductivity Cell H₂ Monitoring.

obtained with argon containing 200 ppm of hydrogen. Argon flow was provided at all times to carry away hydrogen diffusion through the wall and to prevent oxidation of the pipe wall.

The argon sweep-gas supply system consisted of argon supply bottles, pressure regulators, room-temperature molecular sieve beds, titanium-sponge hot traps, and a pressure regulator ahead of the jacketed areas on the loops. The molecular sieve bed and hot trap were used to remove water vapor and residual oxygen respectively. A dual-path system was used so that traps could be regenerated or replaced as required without interrupting the argon sweep flow. The majority of the low-temperature tubing in the system was copper (0.250 in. in outside diameter; 0.065-in. wall). The argon sweep gas was directed to the thermal-conductivity cells, then to the jacketed areas of the loops, back to the thermal-conductivity cells for hydrogen measurement, and then vented. The system was designed so that any of 12 jacketed areas on three different test loops could be monitored by either of two thermal-conductivity cells, and the output reading of one cell could be checked with that of the other cell.

The four annuli were attached so that high- and low-temperature portions of the 1-in.-OD Croloy 9M and 3/8-in.-OD type 316 stainless steel tubing could be monitored for hydrogen effluent. The length of the annuli varied, as loop geometry permitted, from 11 to 26 in. The cross-sectional flow area in the annuli for the argon sweep gas varied from 0.087 to 0.134 in.², so that at the design flow rate of 24 cc (STP)/min, the delay time ranged from 14 to 45 sec.

Operation of the hydrogen-detection system showed a consistent zero shift of the thermal-conductivity cell that monitored the argon sweep gas for hydrogen effluent. However, acceptable results were obtained by zeroing the instrument prior to each series of readings. About 40 gas samples were taken from the argon sweep gas of the hydrogen-detection system for mass spectrometer analysis to check the hydrogen output reading

of the thermal-conductivity cell. Agreement within 10 ppm was normally obtained on samples containing from 20 to 130 ppm of hydrogen and taken at the design flow rate of the thermal-conductivity cell, which was 24 cc/min.

Typical hydrogen flow rates from the annuli during loop operation have been reported previously.⁹ In general, about one-half to two-thirds of the 0.6 cc/hr of hydrogen injected into the loop was recovered at the annuli. The high percentage of hydrogen recovered at the annulus detection sleeves, which represented about 18% of the loop surface area, was due to the relatively oxide-free surfaces in the jacketed areas. These surfaces had much less resistance to hydrogen permeation than the heavily oxidized surfaces elsewhere in the loop that were exposed to atmosphere. Visual post-run inspection of the outer surface of the loop tubing in hydrogen-detection areas of several loops revealed very light oxidation after 2000 hr of operation. The degree of oxidation, as indicated by discoloration, decreased along the tubes going from the gas inlet end to the gas exit end. The decrease in oxidation was probably due to depletion of oxidants as the argon gas stream traversed the length of the hot metal. On loop 8, metallographic examinations failed to reveal the presence of an oxide film at the gas exit ends of any of the tubes or at the inlet end of the coolest type 316 stainless steel tube. However, examination of the inlet ends of both the Croloy 9M tubes and the hottest type 316 stainless steel tubes revealed very thin oxide films; each was less than 0.1 mil thick.

The gradual accumulation of slight oxide films on the exterior of the NaK containment piping within the detection sleeves prevented any realistic comparison of the permeation characteristics of the four jacketed regions. In addition, the hydrogen concentration in the argon purge stream created a significant back pressure compared with the equilibrium hydrogen partial pressure in the loop. This served to block additional hydrogen movement through the wall into the argon. Recognition of the importance of the back pressure in the annuli led to their use for direct measurement of the loop hydrogen pressure. The argon flow was reduced to about 10 cc/min to better allow the hydrogen partial pressure in the loop to come into equilibrium with the slow-moving argon purge flow. Observation of the hydrogen content of the argon effluent from the sleeves therefore provided a sensitive method of determining the hydrogen partial pressure and concentration in the loop NaK. A theoretical analysis of this method of determining loop hydrogen partial pressure was reported previously.¹⁰

Mass Spectrometer Hydrogen Monitoring System

A mass spectrometer hydrogen- and deuterium-detection system was used on the final corrosion loop test. This system was used in lieu of the thermal-conductivity cell detection system used on all previous loops which had hydrogen injection. The mass spectrometer was used to: (1) monitor deuterium (or hydrogen) levels during cold-trapping tests which would be at levels below the sensitivity of the thermal-conductivity cell

and (2) to provide identification of D_2 , HD, and H_2 levels so that extraneous hydrogen observed on previous loops could be accounted for while injecting deuterium into the loop. A simplified schematic drawing of the mass spectrometer detection system is shown in Fig. 7. The mass spectrometer was adjusted to monitor masses 2, 3, and 4 and could be calibrated with standard leaks of H_2 , HD, and D_2 attached to the apparatus by suitable valving. The purge flow of argon in the remaining three annuli was stopped to provide only a static inert atmosphere on these annuli. The flow of argon was stopped to preclude supplying hydrogen to the loop from the residual hydrogen in the argon, which usually is in the 6- to 20-ppm (by volume) range.

The mass spectrometer hydrogen- and deuterium-detection system was used during three months of operation and proved to be a reliable, trouble-free instrument. Typical output data for the D_2 measurements are shown in a previous section, Effect of Cold Trapping on Hydrogen Concentration in Loops.

Extraneous Hydrogen Measurements

Extraneous hydrogen was observed with both the thermal-conductivity cell and mass spectrometer hydrogen-detection systems. This hydrogen was observed with the loops at design temperature and at times prior to injection of hydrogen or deuterium into the loops. The source of this extraneous hydrogen is not known. The moisture content of the inlet argon of the thermal-conductivity cell hydrogen-detection system was periodically checked with an on-stream monitor downstream of the molecular sieve in the gas supply train, and consistent values of 1 ppm or less were found. This is consistent with values shown by mass spectrometer analysis of the gas in each argon cylinder prior to use and would appear to rule out water vapor in the argon supply as a major source of H_2 in the effluent from the high-temperature annuli.

ORNL-DWG 65-1500A

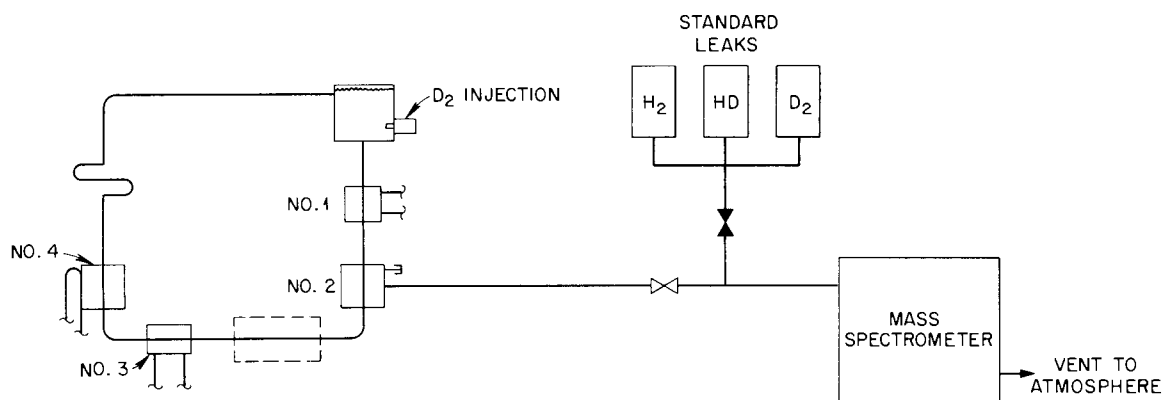


Fig. 7. SNAP-8 Corrosion Loops - Mass Spectrometer H_2 and D_2 Monitoring.

The hydrogen content of the atmosphere was measured at the test site to determine if this was the source of the extraneous hydrogen being observed in the loops. A gas chromatograph was modified to monitor the air at various locations around the test area. Calibration of the chromatograph was done with gas from a cylinder of air known to contain 200 ppm of hydrogen and also with specific dilutions of this known mixture. Air samples were taken from over the hydrogen control panel, inside a loop operation enclosure, and in the general loop area, with no measurable amount of hydrogen being detected. Since the calibration indicated a lower limit of sensitivity of less than 5 ppm for the chromatograph, it was concluded that the hydrogen content of the ambient air is less than 5 ppm and probably less than 2 ppm. Based on these results, the increase in hydrogen concentration of the annulus purge on the loops prior to hydrogen injection cannot be attributed to the hydrogen level in the atmosphere. It is speculated that at least part of the extraneous hydrogen evolves from the Croloy 9M heat exchanger section, which is heat treated in a hydrogen atmosphere during fabrication, but this has not been demonstrated as a fact; so the source of the hydrogen remains unexplained.

Extraneous hydrogen measurements made with the thermal-conductivity cell on loop 14 were reported in detail in a previous report.¹¹ These tests were made to verify the evidence of extraneous hydrogen which had been observed in previously operated loops. In summary, the sweep argon entered the detection annuli with a hydrogen content of 7 to 10 ppm, and the hydrogen content of the effluent ranged from 11 to 16 ppm. After 635 hr of loop operation at design temperatures, during which continuous argon flow had been maintained at 25 cc/min through the detection annuli, loop 14 was shut down for attachment of the mass spectrometer to annulus 2. This 23-in.-long annulus was normally operated at about 1270°F and had a NaK containment wall of 0.050-in.-thick Croloy 9M-type 316 stainless steel duplex tubing, through which hydrogen and deuterium permeate from the loop NaK. Static argon was maintained in the remaining three annuli for the balance of the test to preclude any hydrogen addition to the loop from the residual hydrogen in the sweep argon, which usually is in the 6- to 20-ppm range.

Measurable amounts of hydrogen were observed by the mass spectrometer when the loop was brought up to temperature with no hydrogen injection into the loop and with the cold trap operating continuously at 260°F. Initial values of hydrogen flow from the annulus averaged approximately 1×10^{-5} cc (STP)/sec and gradually lowered to an average of approximately 2×10^{-6} cc (STP)/sec in a 30-day period. The hydrogen outflow remained at this lower level of 2×10^{-6} cc (STP)/sec for the final two months of operation. During this period, the hydrogen flow rate from the annulus was also observed several times with the loop cooled to room temperature and was found to be at least a factor of 200 less [$<10^{-8}$ cc (STP)/sec]. The higher hydrogen flow rate returned when the loop was reheated to design temperature. The background levels of HD and D₂ in the annulus prior to D₂ injection into the NaK were also measured and were found to be much less [10^{-7} to 10^{-8} cc (STP)/sec] than the hydrogen flow.

One of the small, 1-in.-diam by 10-in.-long hydride traps on loop 14 was operated for 500 hr at 260°F in an attempt to collect hydrogen from

extraneous sources during a period in which no deuterium was being injected. The trap was then isolated from the loop by valving and kept isolated at room temperature during the remainder of the test. The analysis of the total contents of this hydride trap are shown in Table 12. Separate analysis was done on (1) the NaK drained from the trap, (2) the remaining NaK and residue on a 4-in.-long portion of wire mesh at the trap inlet, and (3) the remaining NaK and residue on a 5-1/2-in.-long section of wire mesh at the exit end. Approximately 80% of all Na₂O and K₂O was found in the 5-1/2-in.-long mesh. This was probably concentrated in a faintly visible accumulation observed when the trap was disassembled in a dry box in the downstream 1/2 to 3/4 in. of the wire mesh.

The analysis indicated that only 0.44 cc (STP) of extraneous hydrogen was collected in the trap during the 500-hr period; about 5 cc (STP) of extraneous hydrogen was removed from the loop during the same period with the mass spectrometer attached to the 23-in.-long jacketed hydrogen-detection annulus at the inlet to the Croloy 9M heat exchanger section. The 500-hr cold-trapping test demonstrated that the quantity of the extraneous hydrogen is small.

NaK Sampling Equipment

A bucket-type NaK sampler was designed for removal of samples through a ball valve on a riser above the loop surge tank. A hydrogen-fired nickel bucket with a capacity of about 2 g of NaK could be lowered on an O-ring-sealed push rod below the liquid metal surface for filling. By suitable valving and argon purging operations, the NaK-filled bucket was raised and transferred to an evacuated Pyrex test tube, and the test tube was then fused off with a torch under vacuum to encapsulate the bucket for

Table 12. Analysis of Contents of Hydride Trap from Loop 14^a

	Hydride Trap
Date of operation	2/18/65-3/11/65
Time of operation, hr	500
Total weight of NaK in trap, g	119
Total weight of Na ₂ O in trap, g	5.708
Total weight of K ₂ O in trap, g	1.913
Equivalent oxygen, ppm by weight	15,420
Total H ₂ in trap, cc (STP)	0.44

^aLoop was operated with no deuterium injection; no HD or D₂ was observed in the trap.

transfer to the analytical laboratory. The sampling apparatus was later modified to permit transfer of the NaK-filled bucket into an argon-filled, valved container in lieu of the evacuated Pyrex tube.

Approximately 90 NaK samples were taken with the bucket sampler for oxygen analysis during the loop program. No direct correlation could be made between the plugging indicator and the analytical oxide determinations. Analytical oxide results varied randomly from about 50 to 200 ppm on loops which were believed to be at <30 ppm based on cold- and hot-trapping operations and plugging indicator readings prior to sampling. The difficulty may have been in the sampling technique, the handling of the sample between the loop and the chemical analysis laboratory, or in the techniques used in analysis. Resolution of the problem was not sought further, and this type of sampling was discontinued at about the midpoint of the program.

A flow-through NaK sampling device was incorporated in the bypass system of loops 4, 13, and 14. The system was provided to obtain samples of the NaK for oxide analysis and to attempt to isolate and identify the materials other than oxide which were causing the multibreak plugging indicator curves discussed in the following section.

The sampling system consisted of a valved header to which a valved sample container of about 3-1/2 g capacity could be attached by means of Swagelok mechanical compression fittings. The NaK flow could be measured and directed through the sampler at $\sim 1200^\circ\text{F}$ or less for any desired time. The sample was isolated by valving, cooled to room temperature, and then removed by loosening the mechanical fittings.

Nine NaK samples were taken for oxygen analysis from three loops with the flow-through NaK samplers. The analysis data are presented in Table 13, along with data from the plugging indicators and pertinent notes on the loop operation. The analytical data were always higher than would be expected based on plugging indicator data and cold-trapping temperatures. However, with the exception of sample 7, the data were less scattered than those obtained with the bucket sampling technique discussed previously.

Flow-through samplers were used on loops 4 and 13 in attempts to obtain samples of unknown materials (not believed to be oxides) that have caused flow degradation during plugging indicator runs in previous tests. These unknown materials have consistently resulted in plugging-indicator flow reductions in the 400 to 600°F range, which was above the oxide precipitation temperatures for the low-oxide loops in this program. The NaK sampler was a flattened 1/4-in.-OD tube with isolation valves at each end. The NaK flowed through the flattened area of the tubing and was cooled until a plug occurred; the isolation valves were then closed, and the sampler was then removed for analysis of its contents.

Six samples were taken from loops 4 and 13 over a four-month period. Mercury amalgamation was used in analyzing the tube contents. Dilute HCl treatment of the amalgamation residue was used to determine the presence of carbon compounds, and no significant amounts were found. Mass spec-

Table 13. NaK Oxide Analysis Data for Samples Removed with Flow-Through NaK Sampler

NaK Analysis Data				Plugging Indicator Data		Notes
Sample No.	Loop No.	Date of Sampling	Oxygen [ppm (wt)]	Plugging Temperature (°F)	Equivalent Oxide Level [ppm (wt)]	
5	13	8/18/64	31	< 200	< 15	Cold trapped loop at 150°F prior to sampling
7	4	8/22/64	303	< 250	< 19	
8	4	9/21/64	110	< 225	< 16	
9	13	9/22/64	84	350	30	
12	4	10/1/64	155			Cold trapped loop at 200°F 2 hr prior to sampling
13	4	10/13/64	107	560	82	
14	13	11/5/64	75	< 250	< 19	Cold trapped at 150°F prior to sampling
15	13	12/4/64	80	< 250	< 19	
16	14	1/14/65	38	< 200	< 15	Cold trapped overnight at <150°F prior to sampling

trometer checks of the amalgamation residue showed no significant traces of corrosion products such as iron, chromium, or nickel. In two samples a small amount of HCN was observed by mass spectrography in the gas liberated by addition of acid to the residue; however, the amount was small. All analyses indicated that the only major contaminants in the flattened-tube NaK samples were Na_2O and K_2O . In these samples the ratio of K_2O to Na_2O was high. The data for K_2O and Na_2O for all the samples are listed in Table 14, along with other analytical observations. The plugging-indicator readings taken just prior to each sampling are also listed. No further flattened-tube NaK samples were taken after September 25, 1964, when it became apparent that the materials other than oxide which caused plugging-indicator breaks could not be identified by this technique.

Oxide Plugging Indicators

The original plugging indicator was fabricated from a modified 1/2-in. sched 40, bellows-sealed valve. The plugging orifices were machined into the valve poppet and consisted of four grooves at 90° whose cross section was half circular with a 0.0185-in. radius. The NaK velocity through the four orifices with the valve poppet closed and at the design flow rate of 0.1 gpm was 16.7 fps. A 1/8-in.-OD, stainless-steel-sheathed Chromel-Alumel thermocouple was inserted through the valve body such that the NaK temperature immediately upstream of the plugging orifices could be measured. The pre-cooler upstream of the plugging indicator valve was a vertically mounted 16-ft-long coil of 1-in. sched 40, type 316 stainless steel pipe which was cooled by natural convection.

The original design of plugging indicator was used successfully on the first low-oxide loop (No. 1) which was operated. However, the design was not adequate for the high-oxide loops because it was difficult to pre-heat the uninsulated natural-convection-cooled pre-cooler to a high temperature prior to a plugging run and because the NaK volume in the pre-cooler was large compared to the loop and created a large dilution effect when the plugging indicator circuit was operated.

A small (2-in.³ volume) forced-convection plugging indicator and pre-cooler was designed for use on the initial high-oxide loop (No. 9); this design of plugging indicator was used on all subsequent loops. The plugging orifice sizes were the same as the original design. Two 1/16-in.-OD, type 316 stainless-steel-sheathed Chromel-Alumel thermocouples were inserted and furnace brazed in place upstream of the orifices for temperature indication.

Normal operating procedure for the plugging indicator consisted in initially flowing through the circuit at about 0.16 gpm with the poppet of the plugging valve open and with electric trace heaters energized such that the temperature of the valve was raised to 1100°F . The plugging valve was then closed, which reduced the NaK flow to about 0.09 gpm, and trace heaters were turned off. Forced-air cooling was manually introduced to the pre-cooler to maintain a cooling rate of the NaK of about $40^\circ\text{F}/\text{min}$.

Table 14. Analytical Data Obtained from the Flattened-Tube Flow-Through NaK Sampler

Sample No.	Loop No.	Date Sample Taken	NaK Sample Data			Notes	Plugging Indicator Data ^a			
			Weights of Sample Constituents				Temperature (°F)		Complete Plug Occurred	Notes
			NaK (g)	Na ₂ O (mg)	K ₂ O (mg)		First Break in Flow Rate	Second Break in Flow Rate		
1	4	6/22/64	0.27	1.09	4.34	No CO ₂ produced from acid treatment of residue	950	675	Yes	Data taken prior to any cold trapping of loop
2	4	6/25/64	0.32	0.81	1.64	Insignificant H ₂ and CO ₂	1050	None	No	Data taken after cold trapping of loop
4	4	7/1/64	0.36	1.17	5.30	24 µg of CO ₂ and 270 µg of HCN	950	595	Yes	Data taken 5 days after hot trapping of loop
6	13	8/20/64	0.48	0.32	1.8	Insignificant H ₂ and CO ₂	1000	475	No	Data taken 2 days after cold trapping of loop
10	13	9/25/64	0.38	0.43	1.78	Solution of amalgamation residue examined with mass spectrometer; no significant traces of corrosion products	900	560	Yes	Data taken 20 days after cold trapping of loop
11	4	9/25/64	0.35	0.47	1.4	Solution of amalgamation residue examined with mass spectrometer; no significant traces of corrosion products	900	570	Yes	Data taken 43 days after cold trapping of loop

^aPlugging indicator runs were made prior to NaK sampling.

Approximately 500 plugging-indicator runs were made throughout the operation of the corrosion loops.

Observations of multiple breaks in flow through the plugging indicator have been made throughout this corrosion study program. The first observations reported¹² were for loop 10, where indications of a precipitate other than oxide were noted at plugging-indicator temperatures of 400 to 500°F. This precipitate could not be completely removed by cold trapping at temperatures as low as 100°F, but the initial point of precipitation could usually be lowered to a plugging-indicator temperature of about 300°F. If no further trapping was employed, this breakpoint would increase again in two to four days to levels between 400 and 500°F. At lower temperatures a second and more rapid break in flow was observed that was consistent with cold-trapping temperatures and presumably reflected the oxide level. This oxide break could be eliminated completely in loop 10 (and all subsequent loops) by cold trapping at low temperatures. The absence of a break in the flow curve corresponding to these low cold-trapping temperatures is due to insufficient oxygen being available in the limited NaK volume (115 in.³) of the loops to form a plug.

In later loops of higher oxide content (loops 9 and 7), it was normal to preheat the plugging indicator to higher temperatures (1100 to 1200°F) than those of loop 10 prior to the plugging-indicator cooling run. In these two loops an additional break in the plugging-indicator flow rate was observed in the range from 800 to 1100°F. This preheat procedure was adopted as a standard technique and was applied to all subsequent plugging runs. Throughout the course of the test program, two breaks consistently continued to occur at levels above the oxide break and above the cold-trap operating temperature. A typical three-break plugging-indicator trace is shown in Fig. 8.

Observations of the initial plugging break (800 to 1100°F) were reported earlier.^{13,14} A brief summary of the previous observations and of the more recent experience follows:

1. In a new system the initial break occurs in the temperature range 900 to 1100°F.
2. Random variations of $\pm 100^\circ\text{F}$ are observed in the initial break temperature after cold trapping at temperatures as low as 110°F.
3. Hot trapping with zirconium foil at 1400°F has no effect on the initial break.
4. Injection of hydrogen at a rate of 0.6 cc (STP)/hr into five different loops had no effect on the characteristics of the initial plugging indicator break or on subsequent breaks. This lack of effect is probably due to the low equilibrium hydrogen level in the loops, which is estimated to be less than 2 ppm by weight.
5. Replacing the charge of NaK in the loop has no effect on the temperature at which the initial break occurs.

6. The temperature at which the initial break occurs usually decreases about 100°F during the first month of operation. Loop 5 was an exception in that the initial point decreased 450°F during the first month.
7. The rate of flow decrease with a constant cooling rate is more gradual for the initial break than for subsequent breaks.

ORNL-DWG 65-4024

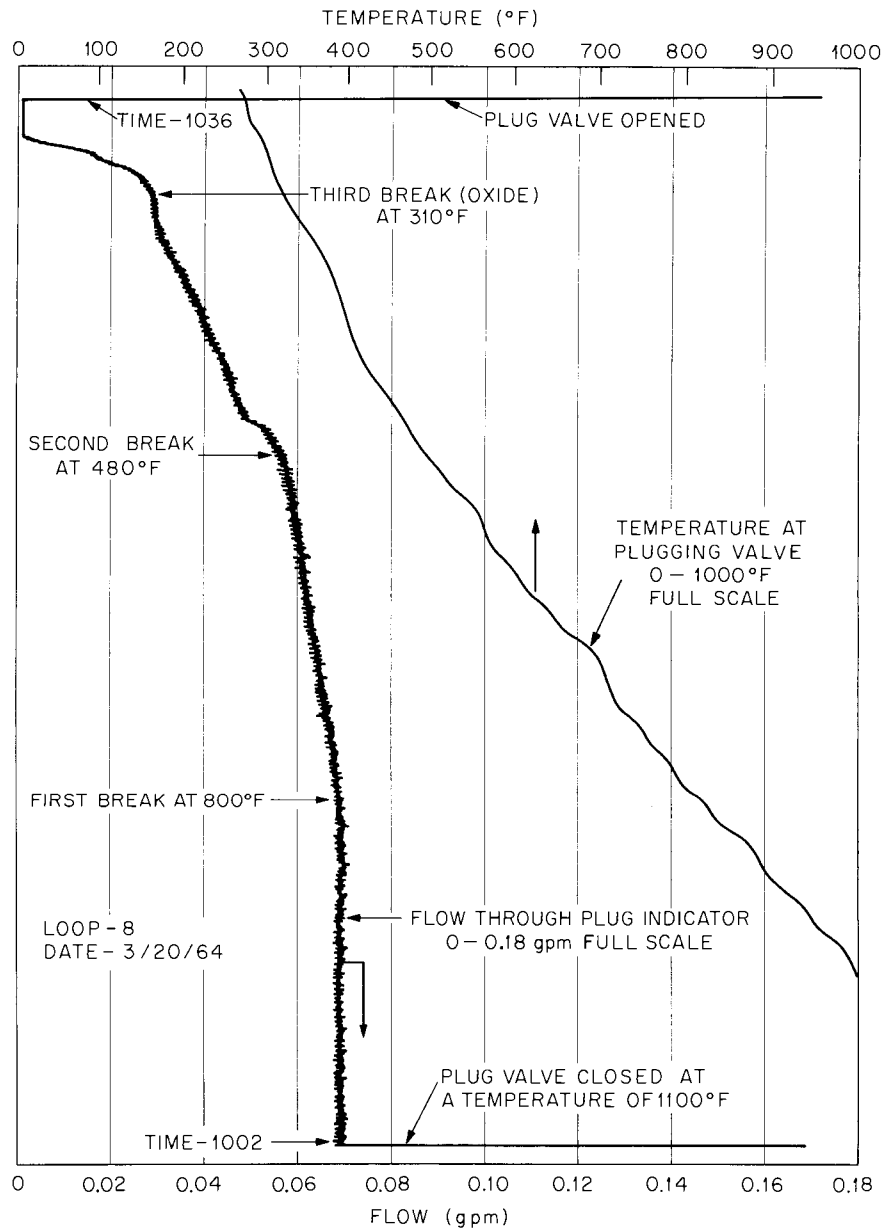


Fig. 8. Typical Three-Break Plugging-Indicator Curve.

As mentioned in an earlier section of this report, an observable amount of argon was being transferred throughout loop 14 by differential temperature solubility in the NaK. A series of tests were therefore run on the loop 14 plugging indicator to demonstrate that argon coming out of solution during cooling was the cause of the initial break in flow. For these tests the NaK flow path was normal. The bypass stream passed through the economizer, through a cooler, and into the plugging valve, where it flowed through four small orifices in the plug-seat combination. By the use of external heaters, the tendency of the economizer to cool the incoming stream could be controlled, and the temperature at the inlet of the plugging-indicator cooler could be adjusted as desired.

Three runs were made with inlet temperatures to the cooler of 1000, 800, and 625°F. Care was taken that temperatures significantly lower than these did not exist upstream. When cooling air was started through the precooler, initial breaks occurred at 800, 600, and 325°F respectively. The fact that the initial break could consistently occur 200 to 300°F below the inlet temperature combined with the demonstrated solubility of argon in NaK is believed to demonstrate that argon coming out of solution in the NaK as it passes through the cooler is the cause of the initial break. In addition, the presence of argon seems consistent with earlier observations made about the initial break. It is obvious that argon must also be coming out of solution as a result of any required cooling process upstream of the cooler; however, argon released at the economizer is trapped in the low-velocity downcomer that leads to the plugging indicator. Prolonged operation has shown that the vertical downcomer eventually fills with argon, and bubbles are then released in bursts.

Previous operation of loop 5 had shown that the temperature level of the initial break changed with accumulated operating time to a much greater degree than in the other loops. Postrun examination of six plugging-indicator valves showed that a marked degree of erosion had occurred at the type 316 stainless steel valve seat of the loop 5 unit as compared with the others. This change in orifice configuration on loop 5 is believed to be the reason for the difference in the observed characteristic of the initial break.

Plugging runs were attempted on loop 14 with different argon cover-gas pressures in the surge tank in an attempt to affect the behavior of the initial break and to further demonstrate that argon was a factor. This series of tests proved inconclusive because the argon pressure required to suppress boiling in the loop was apparently adequate to cause the plugging indicator initial break. No change in the initial break temperature was observed with the argon cover pressure maintained at levels of 8.8, 14.1, 19.7, and 24.7 psia. The loop could not be operated under a complete vacuum at the surge tank without modifications, which were not feasible.

The cause of the second break (400 to 600°F) phenomenon in the plugging indicator is unknown. Some observations on the second break are that:

1. The material responsible does not form as tenacious a plug as oxide and sometimes sweeps partially away.
2. Reheating runs made after partial plugging occurred showed that the material flushed away at about the same temperature that precipitation occurred.
3. This second plugging break is affected moderately by cold trapping, but is not as readily affected as the oxide break.
4. The rate of plugging from the second break is more gradual than from oxide precipitation.
5. Hot trapping at 1400°F with zirconium foil on loops 1A and 8 did not remove the second break, although the break temperature was reduced to the 410 to 460°F range.
6. The second break consistently became more pronounced in all low-oxide-content loops when either the hot traps or cold traps were isolated from service for two or more days.
7. Postrun examination of low-oxide-content (<30 ppm) loops 1A, 5, 8, 10, and 13 showed low corrosion rates of the 300 series stainless steels as compared with high-oxide-content loops 2, 7, and 9. All the above-listed low-oxide-content loops had pronounced second breaks in the 400 to 600°F range. The corrosion results imply that the second break is caused by a material other than oxide.

OTHER OPERATING EXPERIENCE

Cold Finger Design and Analysis

The cold finger was attached to the loops to mock up the small flow passage along the SNAP-8 primary pump shaft and the low-temperature, 300°F, NaK volume within the pump. The purpose of this device was to determine if large amounts of oxide or hydrides might accumulate by diffusion into this static region, which was maintained at 300°F during operation. The cold finger was attached to the loop piping downstream of the heat exchanger in the 1100°F portion of the loop.

The original cold finger design consisted of a section of 1/2-in. sched 40 pipe containing 2.6 in.³ of NaK to simulate the approximately 50/1 volume ratio of the SNAP-8 main loop to the volume within the SNAP-8 pump. This small volume was connected to the main loop by two 0.062-in.-diam holes in a 1/4-in.-thick bulkhead to simulate the restricted passage along the pump shaft. The cold finger was oriented so that it would not drain as the main loop NaK was dumped. This design of cold finger was installed on loops 1, 7, 9, and 10. At the conclusion of a 2000-hr test run the cold finger was cut from the loop for analysis of its contents.

Postrun removal of the first cold fingers proved difficult because there was no positive means of preventing oxide contamination of the cold

finger NaK contents during removal operations. An isolation valve was added between the 2.6-in.³ NaK volume and the two 0.062-in.-diam holes in the bulkhead. This cold finger design was designated modification 1, and was used on loops 1A, 2, 4, 5, and 8. At the end of a loop run the isolation valve was closed prior to cutup of the loop to preclude oxidation of the cold finger NaK, and the device was then removed for analysis.

A second modification of the cold finger design was made for use on the final two loops in the program (13 and 14). The annular area of the pump shaft was scaled down to the 1/45 scale of the loops and was simulated by a 1-3/4-in.-long piece of 1/8-in.-OD by 0.032-in.-wall stainless steel tubing. The temperature at the outboard end of the 1/8-in. tubing was maintained at 400°F to match the temperature expected at the end of the annular region in the pump. The 2.6-in.³ volume of NaK in the remainder of the cold finger was again maintained at 300°F. This cold finger design is shown in Fig. 9 after the cold finger had been removed from loop 14 at the end of its operation.

The results of the chemical analysis of the cold fingers are presented in Table 15. It will be noted that on all high-oxide loops (2, 7,



Fig. 9. Modification 2 Cold Finger After Removal from Loop 14.

Table 15. Cold Finger Analysis Data
 Sequence of analysis: 10, 9, 8, 7, 1A, 2, 4, 5, 13

Loop No.	Average Cold Finger Temperature (°F)	Cold Finger Design	Weight of NaK (g)	Total Na ₂ O (mg)	Total K ₂ O (mg)	Weight of Hydrogen (mg)	Total Oxygen in Cold Finger (mg)	Equivalent Oxygen in Cold Finger [ppm (wt)]	Oxygen Level of Loop During Operation	Hours of Loop Operation at Design Conditions	H ₂ Injected into Loop	
1		Original	Not analyzed								701	No
1A	290	Mod-1	32.96	7.45	8.915	0.057	3.44	104.5	Low	2003	No	
2	650-850	Mod-1	35.92	9.17	6.97	0.096	3.55	98.8	High	2000	No	
4	300	Mod-1	34.51	7.44	7.33	0.069	3.17	91.8	Low	2033	Yes	
5	310	Mod-1	32.96	8.17	40.38	0.190	8.95	271.5	Low	5133	Yes	
7 ^a	670-800	Original	24.79	117.7	54.7	0.098	39.70	1600.0	High	2021	Yes	
8	900 1st 380 hr; 300 remainder	Mod-1	36.75	5.19	5.26	0.270	2.23	60.7	Low	2053	Yes	
9 ^{a,b}	800-1000	Original	13.74	316.4	20.48		85.18	6200	High	2000	No	
10 ^a	300	Original	26.57	6.75 ^c	78.45 ^c		17.04	642.0	Low	2000	No	
13 ^d	320	Mod-2	35.3	10.31	4.34	0.144	3.40	96.3	Low	2000	Yes	
14	300	Mod-2	Excess weld penetration on $\frac{1}{8}$ -in. tube prevented filling with NaK							Low	2659	No

^aOriginal cold fingers on these loops were subject to indeterminate oxide contamination during removal.

^bCorrosion products found in orifices.

^c2 mg of oxygen as K₂O and Na₂O also found in liquid; data listed are for walls alone.

^d46% of total oxygen found on walls.

59

and 9), the cold fingers were operated at elevated temperatures of 650 to 1000°F. Maintenance of known, elevated oxide levels was of primary importance in these three loops, and the cold fingers were kept at high temperature to preclude gradual oxide reduction in the loop NaK by static-leg cold trapping. Therefore, the oxide and hydride accumulations in the cold fingers of loops 2, 7, and 9 are not indicative of the accumulations which might occur in a SNAP-8 pump.

The most realistic set of conditions were obtained with the cold fingers on loops 5 and 13. In the case of loop 13 the final design of cold finger was used, and the loop was operated with a minimum of cold trapping after initial loop oxide cleanup at startup and after later loop repair operations. Loop 5 operated for 5133 hr, a longer period than any other loop, and no cold trapping was done after initial loop cleanup at the start of the run. Cold trapping was minimized specifically in loops 5 and 13 to more nearly simulate proposed SNAP-8 reactor system operating procedures. The small amount of hydrogen found in all the cold fingers seems to indicate that hydride accumulation in the pump region would not be a problem. The oxide accumulation in the cold finger was much larger than the hydrogen accumulation, and the effects of the oxide within the pump secondary NaK coolant circuit are problematical.

Corrosion of Hastelloy N Underneath Lava Bushings

Several instances of excessive corrosion were noted on the exterior of "chromized" Hastelloy N tubing underneath lava bushings. The first instance noted was on loop 1 after 552 hr of operation at design temperature. The corrosion was found during replacement of heaters. No NaK leakage had occurred. Exterior pitting was found on the chromized 3/4-in.-OD, 0.072-in.-wall Hastelloy N tubing under the lava bushings (grade A, unfired) used to space the electric heaters from the tubing. The attack was noticeable on the tube wall at the location where the temperature was estimated to have reached 1250°F, and the attack increased toward the high-temperature end of the tubing, where the temperature was calculated to have been approximately 1445°F. The maximum attack found near the hottest end of the tube was 0.037 in. deep, as determined by external measurements and x rays of the area. While the exact nature of this attack was not determined, it was attributed to oxidation-inducing volatile material driven out of the lava bushings. Subsequent to this, all lava bushings were fired at 2000°F prior to installation.

The second instance of exterior corrosion on chromized Hastelloy N occurred late in the program on loop 13. The exterior corrosion occurred on the 3/4-in.-OD, 0.072-in. wall of the hot-spot section, which was operating at ~1450°F. A NaK leak developed after 1300 hr of operation. Visual inspection of the failed area showed that the Hastelloy N piping had been excessively oxidized in very localized areas under the fired lava insulator bushing in the heater section. The failed region, pictured in Fig. 10, shows the hole through which the leak occurred and an adjacent area with accelerated oxidation that had not quite penetrated the wall.¹⁵ A section taken through the area adjacent to the hole is shown in Fig. 11.¹⁵ Metallographic examination revealed a mixture of metal and oxides

PHOTO 71696

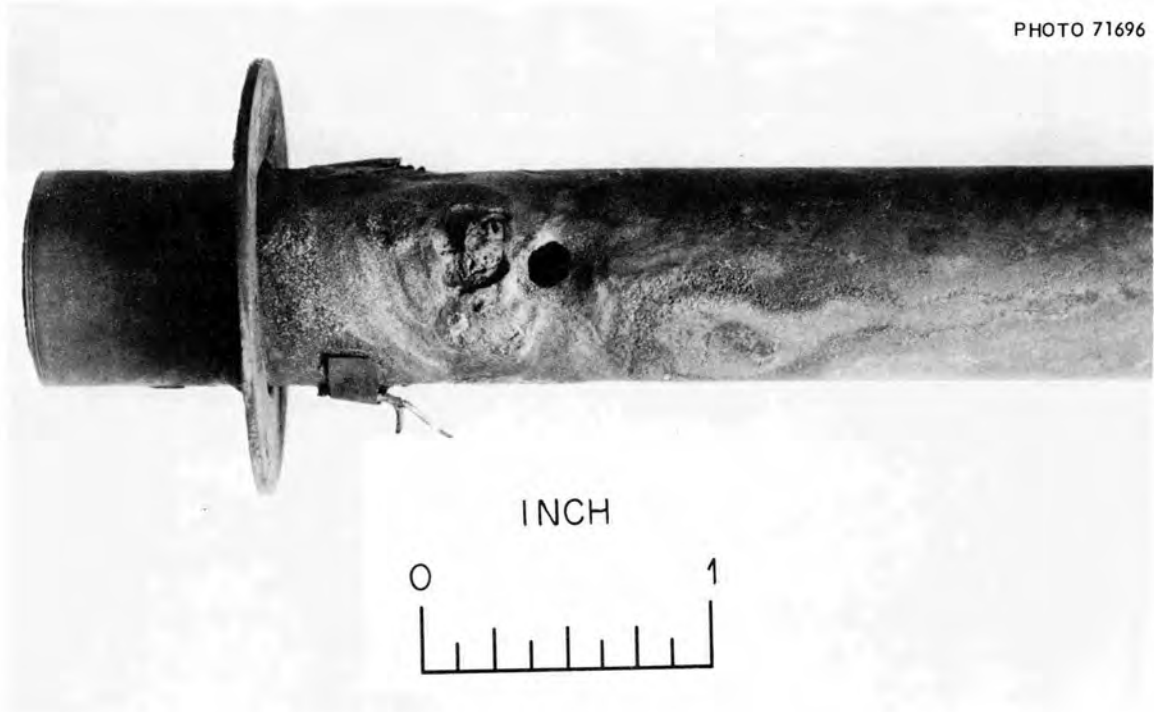


Fig. 10. Failure Region of Loop 13-3 Hot-Spot Piping.

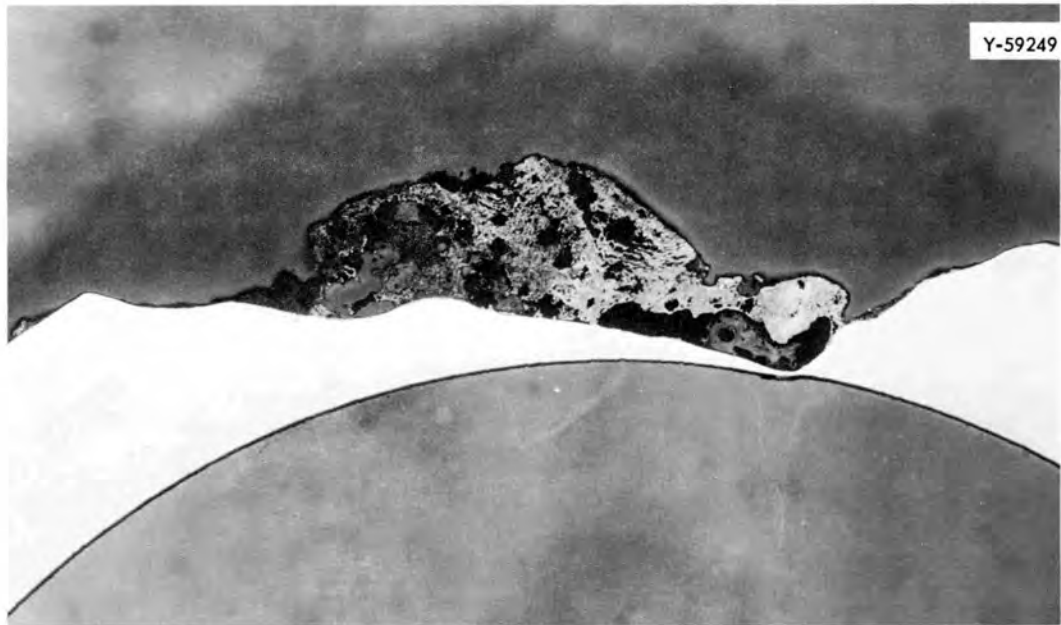


Fig. 11. Cross Section of Oxidized Region Adjacent to Hole in Failed Section of Loop 13-3. $\sim 14\times$.

in the corrosion products, which proved to be mostly nickel and NiO by x-ray-diffraction analysis.

The circumstances surrounding this incidence of catastrophic oxidation suggest that breakdown of the normally protective oxide layer on the pipe exterior surface was attributable either to contamination from some unknown element or compound in the lava bushing or to oxygen starvation in the stagnant area under the bushing. An Inconel shim was placed between the lava bushings and the tubing to eliminate these conditions in the remaining loops.

ANALOG STUDY OF HYDROGEN CONCENTRATION IN THE LOOPS

An analog study was made of the hydrogen concentrations in a typical corrosion loop as a function of various modes of loop operation. The purpose of the study was to better understand the variations in hydrogen outflow which were being monitored with the thermal-conductivity cell hydrogen-detection system on the loops.

The following symbols are used in this analog study:

- N = cc (STP) of hydrogen,
- X = hydrogen concentration, cc (STP) of hydrogen per gram of NaK,
- A = area, cm^2 ,
- θ = thickness, cm,
- ρ = density, g/cm^3 ,
- S = Sieverts' hydrogen solubility constant, $\text{cc (STP) g}^{-1} \text{atm}^{-1/2}$,
- Y = function denoting degree of hydrogen saturation of argon in annuli;
 $Y = 1$ for saturation to same pressure as loop NaK,
- V = volume of gas space, cm^3 at 1 atm,
- T_g = temperature of gas space, $^{\circ}\text{K}$,
- K = permeability coefficient for metal, $\text{cc (STP) cm cm}^{-2} \text{hr}^{-1} \text{atm}^{-1/2}$,
- P_{H_2} = pressure of hydrogen, atm,
- $P_{\text{H}_2\text{a}}$ = partial pressure of hydrogen in argon, atm,
- P_a = pressure of argon, atm,
- Q/R = flow rate of argon, $\text{cc (STP)}/\text{hr}$,
- β = flow rate through cold trap, g/hr ,
- X_T = hydrogen concentration in NaK at cold trap exit, $\text{cc (STP)}/\text{g}$.

The hydrogen capacitance of the loop was defined as the summation of the storage capacities of the NaK, the oxidized piping and NaK jacketed

heater, the hydrogen-detection sleeve metal, the surge tank metal above the liquid surface, and the gas space in the surge tank, that is,

$$N = W_{\text{NaK}} (X) + \sum_{\substack{\text{piping and} \\ \text{NaK jacket}}} A\theta\rho \left(\frac{S_{\text{met.}}}{S_{\text{NaK}}} \right) X + \sum A\theta\rho \left(\frac{S_{\text{met.}}}{S_{\text{NaK}}} \right) \left(\frac{1+Y}{2} \right) X \\ + \sum_{\substack{\text{gas space} \\ \text{metal}}} A\theta\rho \left(\frac{S_{\text{met.}}}{S_{\text{NaK}}} \right) X + \left(\frac{V273}{T_g S_{\text{NaK}}^2} \right) X^2 .$$

The capacitance term for a 1400°F corrosion loop reduces to:

$$N = (1311.11 + 1685.57 + 15.43 + 42.2X) X .$$

For the expected range of X of about 0.03, the final term within the parentheses for the amount of hydrogen in the surge tank vapor phase is small and becomes 42.2 (0.03) or ~1.26 and the capacitance, $N = \sim(3013)X$.

The hydrogen concentration within a loop as a function of time was defined as follows:

$$\frac{dN}{dt} = \frac{KA}{\theta} \sqrt{P_{\text{H}_2}} \quad (\text{input at injection nozzle}) \\ - \left(\frac{KA}{\theta S_{\text{NaK}}} \right) X \quad (\text{back pressure at injection nozzle}) \\ + \sum \frac{KA}{\theta} \sqrt{P_{\text{H}_2}} \quad (\text{input from atmosphere through oxidized pipe}) \\ - \sum \left(\frac{KA}{\theta S_{\text{NaK}}} \right) X \quad (\text{losses to atmosphere through oxidized pipe}) \\ + \sum \left(\frac{Q}{R} \right) \left(\frac{P_{\text{H}_2 a}}{P_a} \right) \quad (\text{input from H}_2 \text{ in argon sweep gas of H}_2 \text{ detection annuli}) \\ - \sum \left(\frac{Q}{R} \right) \frac{Y^2}{S^2} X^2 \quad (\text{losses of H}_2 \text{ carried away in sweep gas}) \\ + B X_T \quad (\text{input for saturated NaK from cold trap}) \\ - B X \quad (\text{loss from loop NaK to cold trap}).$$

The assumptions that were used in the analog solution of the above equation were as follows: The input at the injection nozzle was set at 0.6 cc (STP)/hr, which was the standard injection rate for the hydrogen.

For the expected values of X , the back pressure at the nozzle was negligible, and this term was eliminated. It was assumed that the NaK in the jacket around the heated section of the loop had no resistance to hydrogen flow and that there was zero lag between the jacketed section and the main loop. It was assumed that three of the detection sleeves were operating at an argon flow rate of 7.82 cc (STP)/min and the fourth was operating at a purge flow three times this value. The argon at the inlet to the sleeves was assumed to contain 11 ppm (by volume) of hydrogen. The assumptions regarding the detection sleeves were based on past loop operating experience. The slow-moving argon flow was assumed to be saturated with hydrogen at the annuli exit to the same pressure as the hydrogen within the loop. The value of parameter Y for saturated conditions is 1. An analytical treatment of flow through these annuli, with a discussion of the reasons for assuming hydrogen saturation of the argon at the annuli exit, was given in an earlier progress report.¹⁶ The value of flow through the cold-trap circuit was set at 4967 g/hr, or about 0.025 gpm, which was the lowest flow which could be measured with existing flow measuring equipment on the loops. The concentration of hydrogen in the NaK at the cold trap exit, X_T , was assumed to be 1×10^{-3} cc (STP)/g.

During the test program measurements were made with a gas chromatograph to determine the amount of hydrogen in the atmosphere at the loop

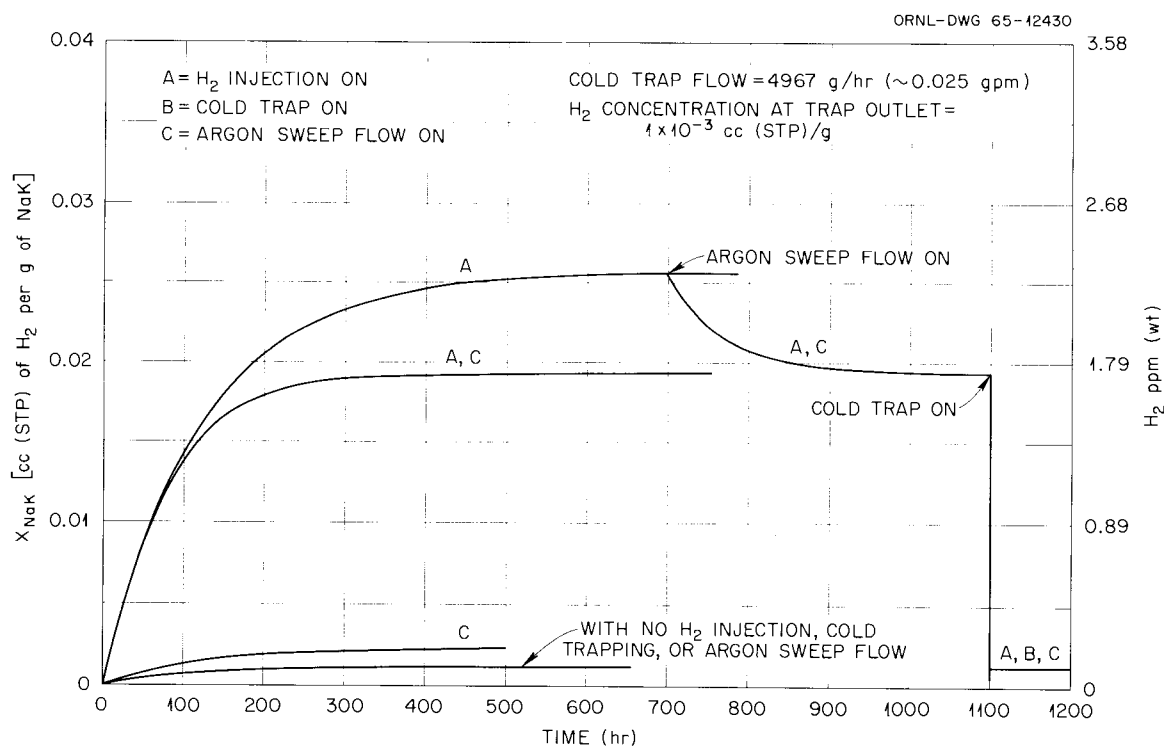


Fig. 12. Results of Analog Study of Hydrogen Concentration vs Time for SNAP-8 1400°F Corrosion Loop Without Hot Spot. H₂ in atmosphere = 5 ppm.

test area. This is, of course, an important parameter in determining the final equilibrium level of hydrogen in the loops. These measurements for hydrogen showed that the hydrogen content of the air was definitely less than 5 ppm and perhaps lower than 2 ppm. The analog studies were run for hydrogen concentrations at two levels, 5 and 0 ppm, and the effects of this choice are shown in equilibrium values attained in the analog outputs shown in Figs. 12 and 13.

Comparison of Analog Study with Loop Performance

The model of the loop demonstrated that the operation of the argon sweep gas of the hydrogen-detection system could make a considerable effect on the loop hydrogen concentration. The effect of cold trapping at the assumed conditions ($\sim 1.25\%$ of main loop flow) is shown to be very large and rapid. The analog simulation appears to be reasonable in that the time to reach initial equilibrium with H_2 injection, no cold trapping, and with argon sweep gas flowing (curves AC) is consistent with the nine- to ten-day periods observed in actual operation for loops 4 and 5. In the analog simulation, the equilibrium hydrogen concentration in the NaK for normal operation of the loops without cold trapping (curves AC) was

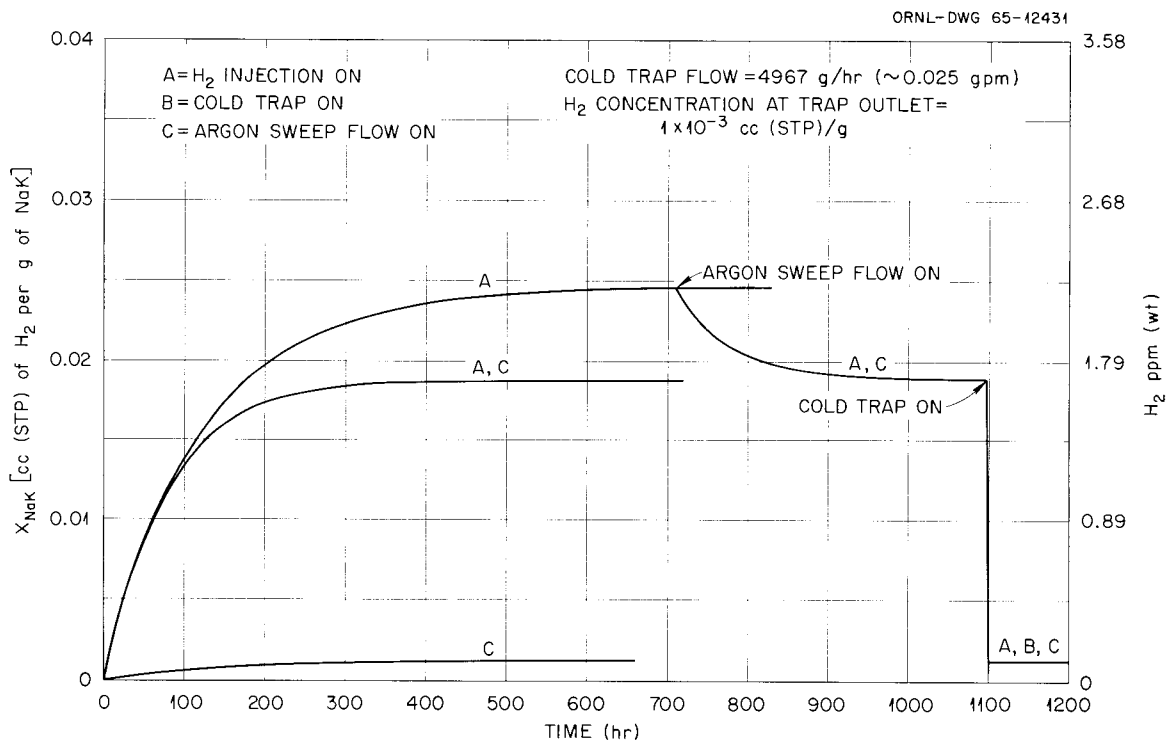


Fig. 13. Results of Analog Study of Hydrogen Concentration vs Time for SNAP-8 1400°F Corrosion Loop Without Hot Spot. H_2 in atmosphere = 0 ppm.

about 0.02 cc (STP)/g. Using the equation for the solubility of hydrogen in NaK which was determined in this program at ORNL,

$$\log_{10} \frac{X}{P^{1/2}} = 0.0756 + \frac{274}{T} ,$$

one can calculate an equivalent pressure of 8.3×10^{-5} atm in the 1400°F portions of a test loop for this concentration of 0.02 cc/g. This pressure value of 8.3×10^{-5} atm is also consistent with the pressures observed in the argon-swept hydrogen detection annuli on the loops during periods of no cold trapping.

REFERENCES

1. ORNL-3730, p. 50.
2. ORNL-3604, p. 9.
3. R. R. Miller, D. D. Williams, and J. A. Grand, *J. Phys. Chem.* 63, 68-71 (1959).
4. D. D. Williams, Solubility of Oxygen in Potassium Metal and Sodium-Potassium Alloys, NRL-3894 (Dec. 19, 1951).
5. ORNL-3730, p. 44.
6. ORNL-3730, p. 36.
7. ORNL-3730 (Aug. 31, 1964).
8. ORNL-3823, p. 30.
9. ORNL-3671, pp. 11-12.
10. ORNL-3730, p. 40.
11. ORNL-3823, p. 10.
12. W. R. Huntley et al., SNAP-8 Corrosion Program Quart. Progr. Rept. Feb. 29, 1964, ORNL-3618, p. 7.
13. W. R. Huntley et al., SNAP-8 Corrosion Program Quart. Progr. Rept. May 31, 1964, ORNL-3671, p. 6.
14. Op. cit., ref. 7, p. 17.
15. ORNL-3784.
16. ORNL-3730, p. 44.

Corrosion-Loop Materials Studies

B. Fleischer

A. Taboada

INTRODUCTION

All corrosion mass-transfer phenomena in a heat transfer system such as the SNAP-8 system are ascribable to the chemical potential gradients existing in the system. These gradients are the result of differences in temperature, compositions, and concentrations, or combinations of the three. Since heat transfer systems must involve parameters which result in these gradients, mass transfer will occur, and successful operation of a given system will therefore depend on the nature of the transfer, the rate at which transfer occurs, and the effect of the transfer on the properties of the affected materials. These, in turn, depend on the magnitude of the above-mentioned parameters and other engineering properties of the system.

At present, there exists no universal equation incorporating the engineering properties of a system that will allow reliable prediction of the above information. It is, therefore, necessary that a system be mocked up or simulated in order to determine this. This was done for the SNAP-8 primary system in a series of forced-flow corrosion loop tests.

The test plan was also formulated to enable an evaluation at several levels of oxygen, hydrogen, hot-leg temperature, and time. The data generated in the test program indicate several important materials compatibility phenomena that may be expected in the SNAP-8 reactor. Extensive migration of carbon from Croloy 9M indicates that considerable loss of strength will occur at the hot end of the boiler tubes. Migration of carbon to other surfaces in the system will result in some loss of ductility. Phase changes occurring in types 347 and 316 stainless steel at 1300°F will also result in some loss of ductility in these areas.

Metal migration from the chromized¹ Hastelloy N fuel elements at the 1300°F end of the core should involve somewhat less than 15 mg/cm² metal loss in 10,000 hr. This should result in not more than 0.0015 in. of intergranular penetration. This does not include effects of irradiation, which may aggravate or be superposed on the nonnuclear corrosion results. Metal being deposited in cold regions of the system can be expected to accumulate in the vicinity of flow disturbances where eddy currents are expected. The sensitivity of the iron-base alloys to oxygen contamination requires that adequate care be exercised in maintaining low oxygen during startup and operation.

The data upon which the findings are based are discussed in detail in the following sections. Data are also presented concerning the effect of decarburization on the mechanical properties of Croloy 9M and a modified Croloy 9M alloy. The methods of analysis are described in Appendix F.

GENERAL PATTERN OF MIGRATION OBSERVED IN CORROSION LOOPS

To interpret and understand the data from the corrosion loops, it is helpful to first discuss the general pattern of material migration in a loop. The schematic of a typical loop is depicted in Fig. 1, showing the materials of construction, sample points, and basic temperature profile. As the NaK passes through the piping, the various elements present in the piping surfaces are dissolved into the NaK stream. The concentration of each element increases until the rate of entrance into the stream is balanced by the rate of removal from the stream. The driving forces producing this material migration are the chemical potential gradients caused by thermal gradients and/or dissimilar materials in the system. The chemical potential gradients cause transfer of mass from one solid surface to another through the liquid phase. This transfer of mass may be manifested as diffusion alloying into the metal walls and/or deposition and growth of

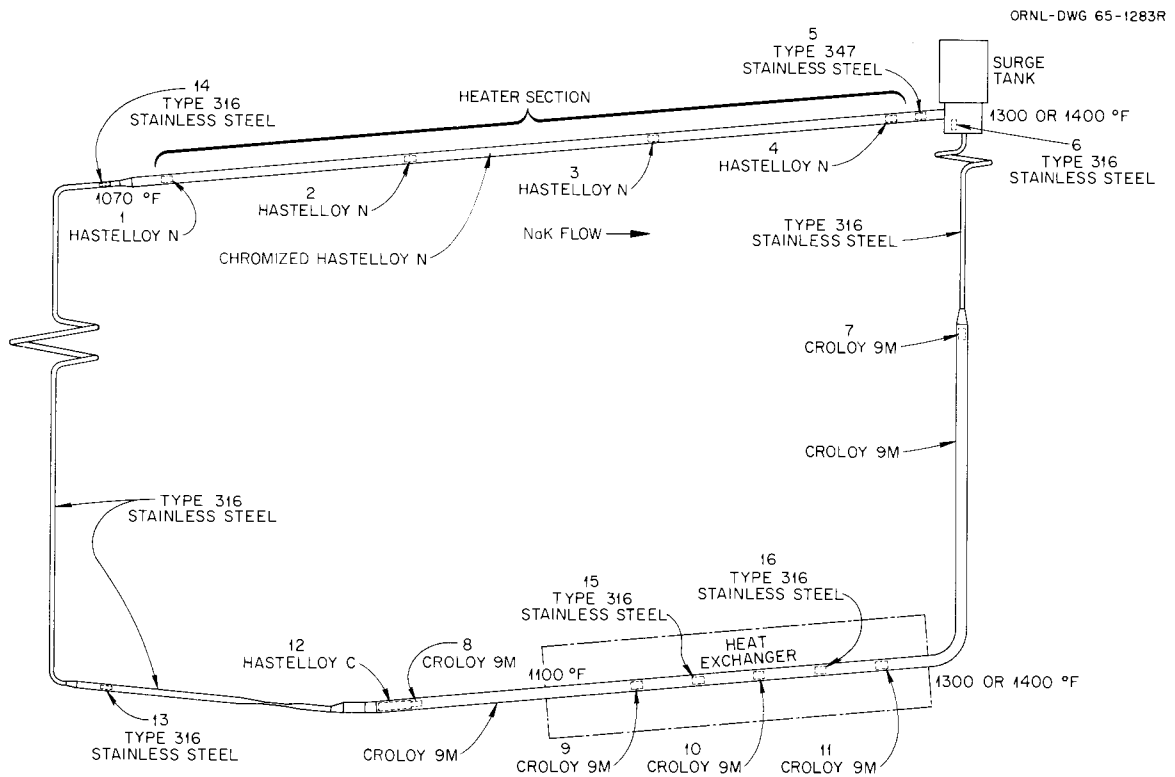


Fig. 1. Diagram of SNAP-8 Corrosion Loop, Showing Location of Insert Specimens.

particulate matter on the metal walls or in the NaK. Growth of particulate matter occurs only when the concentration of a particular species in solution exceeds its solubility limit at a particular temperature.

Material migration in the SNAP-8 loops involved both manifestations of mass transfer. The general patterns present in all loops involved the migration of metallic elements from the hot to the cold regions (see Figs. 2-12) in the form of particulate matter and diffusion alloying. Carbon migrated from the hot end of the Croloy 9M section and was diffusion alloyed into all other surfaces, including colder portions of Croloy 9M itself in the 1400°F loops. In low-oxygen loops, weight losses were usually observed starting with specimen No. 2 (Hastelloy N) in the heated section and extending around to specimen No. 6 (316 stainless steel) in the surge tank. This specimen always showed significantly less corrosion than specimen No. 5 (347 stainless steel) located at the end of the heated section. This difference is believed to be attributed to the differences in NaK velocity at the two locations rather than alloy content. Specimen No. 7 (Croloy 9M) usually showed very little weight change and, on several occasions, gained a small amount of weight which was probably associated with nickel pickup stemming from the dissimilar materials in the system. The remainder of the specimens located in the heat exchanger and cold leg usually gained weight, including specimen No. 1 (Hastelloy N) at the upstream end of the heated section.

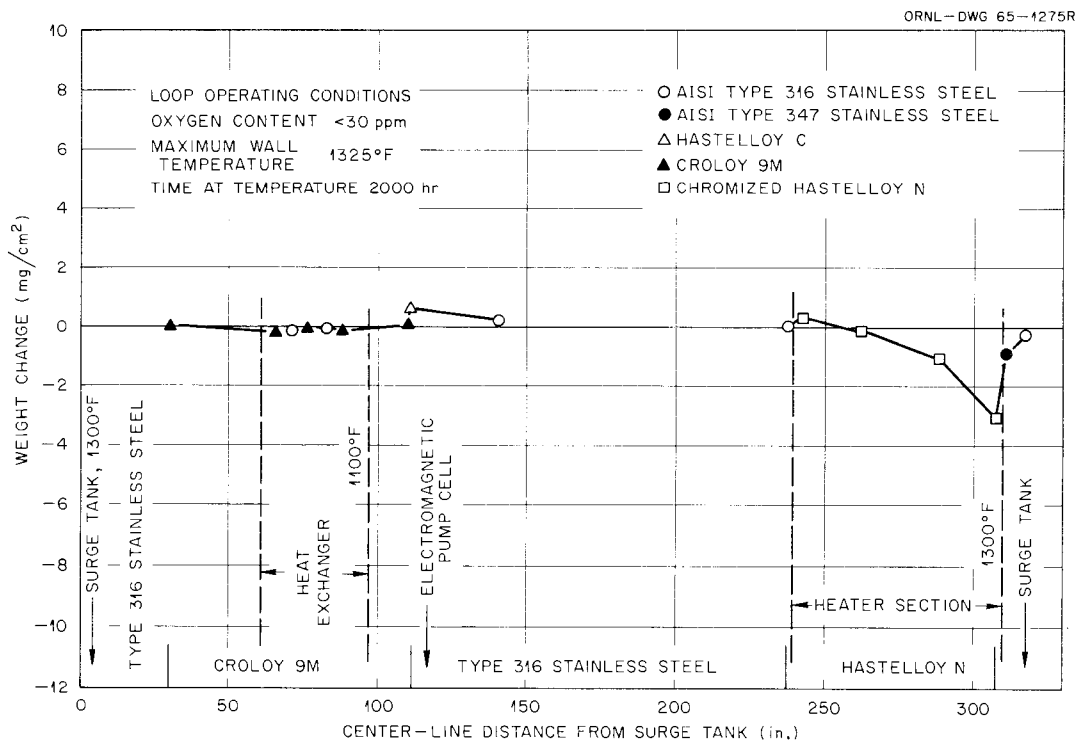


Fig. 2. Mass-Transfer Profile of Loop 10.

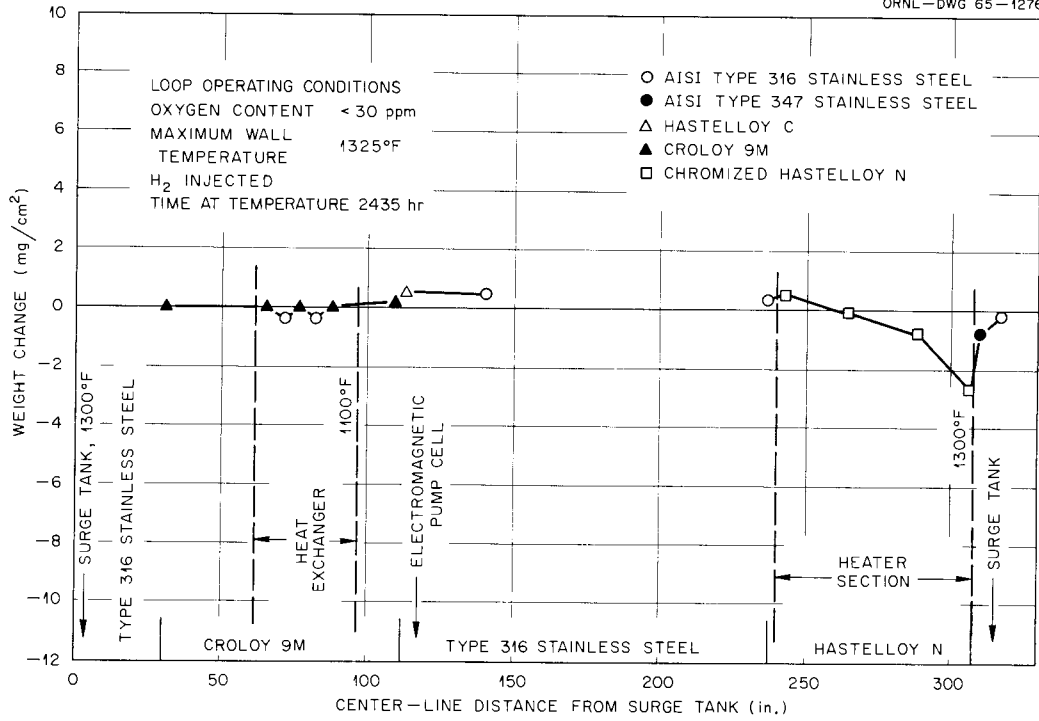


Fig. 3. Mass-Transfer Profile of Loop 8.

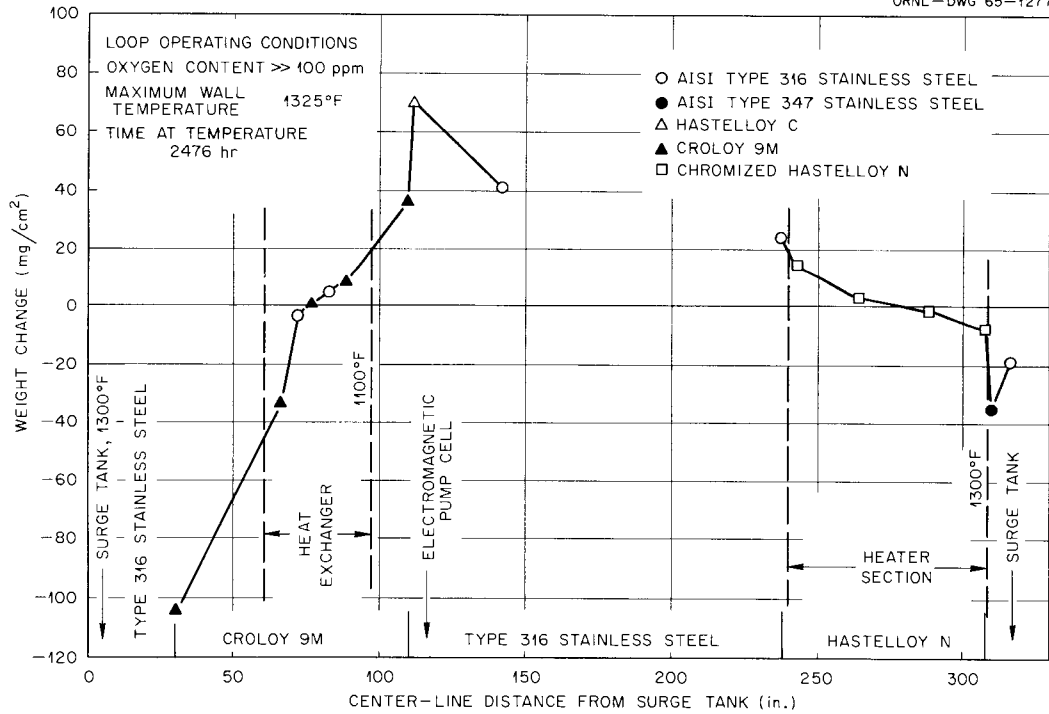


Fig. 4. Mass-Transfer Profile of Loop 9.

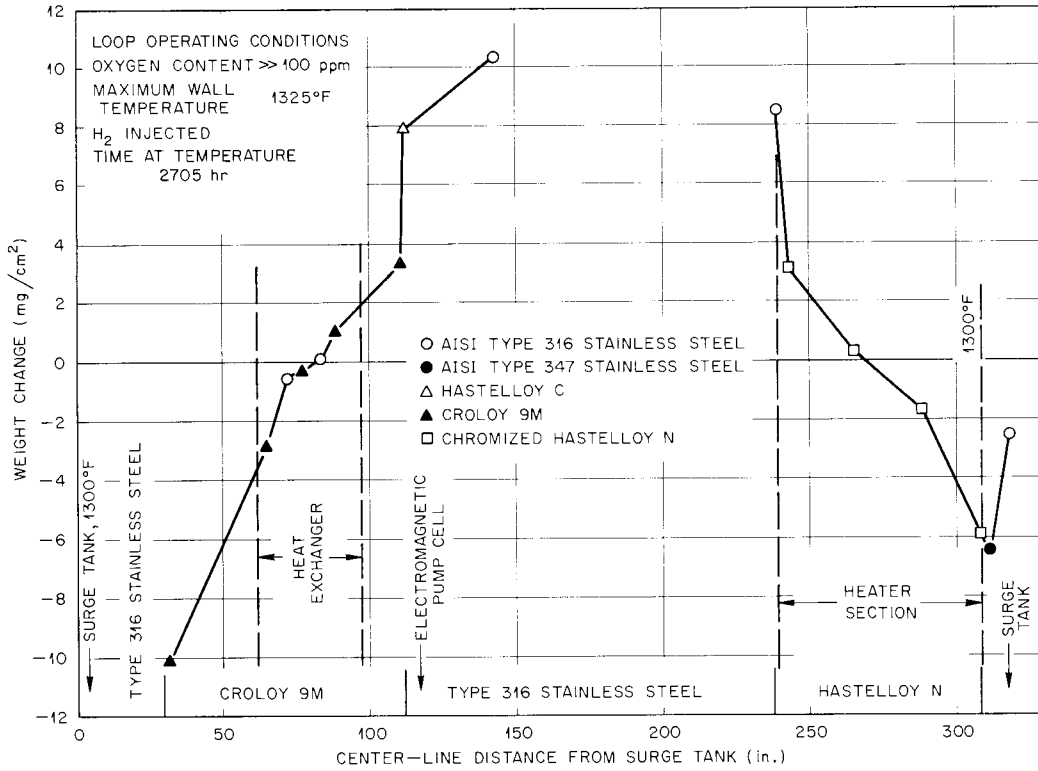


Fig. 5. Mass-Transfer Profile of Loop 7.

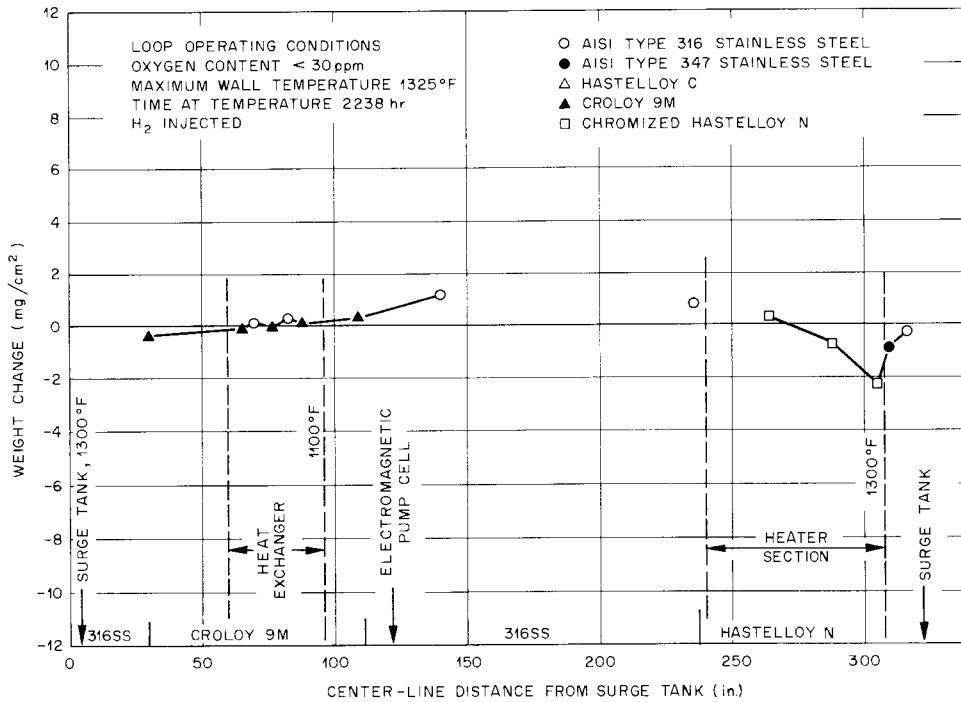


Fig. 6. Mass-Transfer Profile of Loop 13.

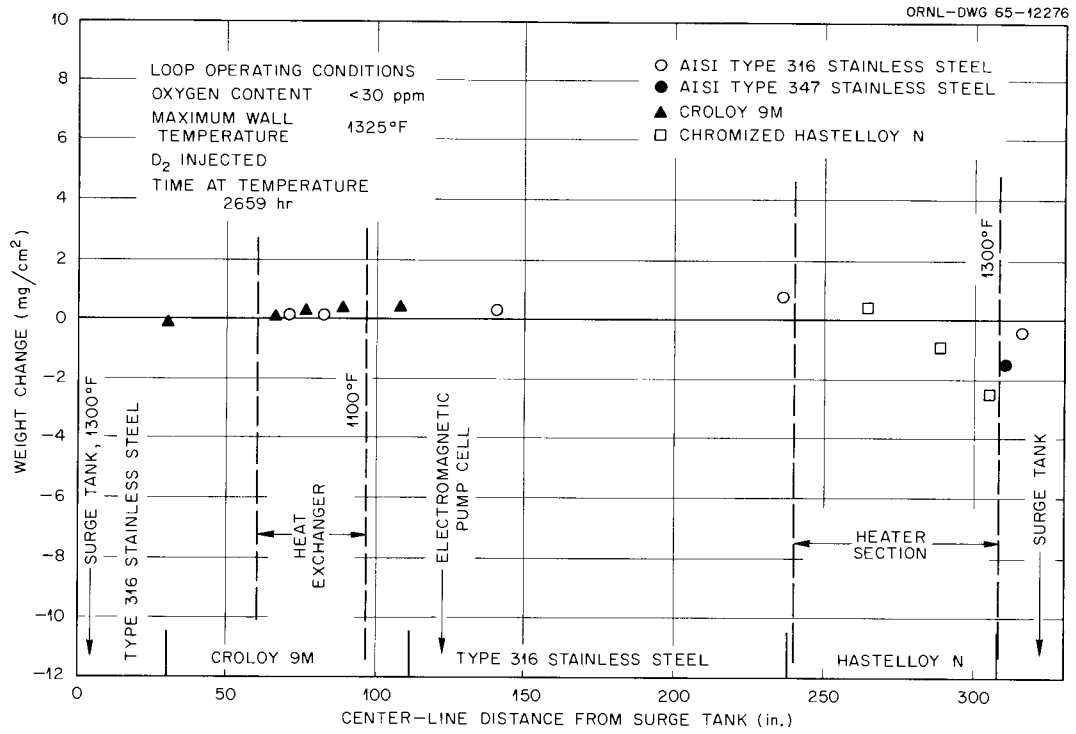


Fig. 7. Mass-Transfer Profile of Loop 14.

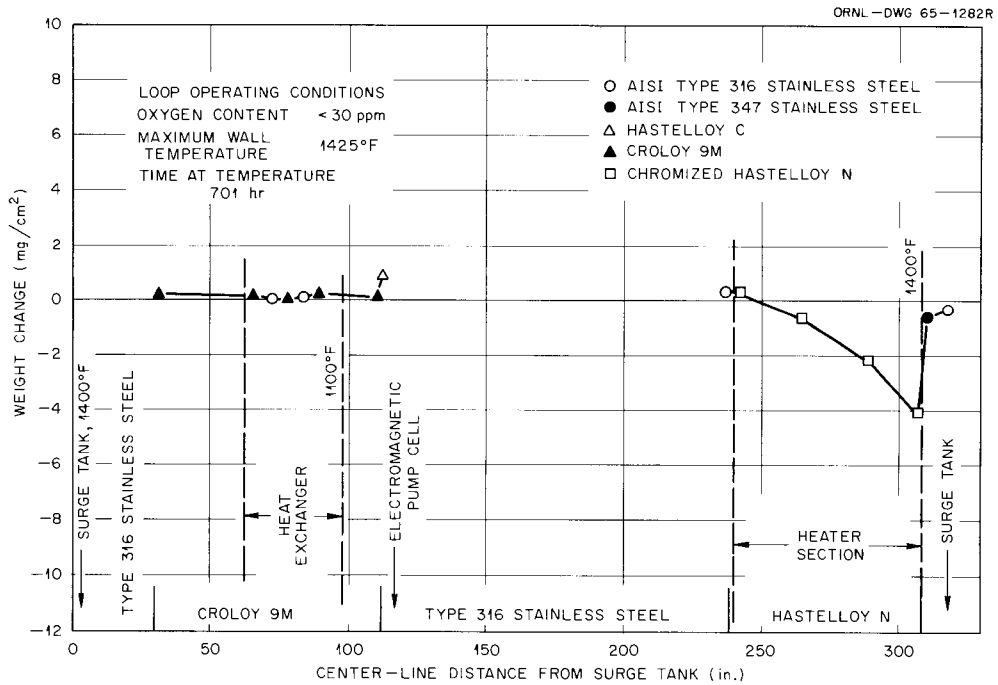


Fig. 8. Mass-Transfer Profile of Loop 1.

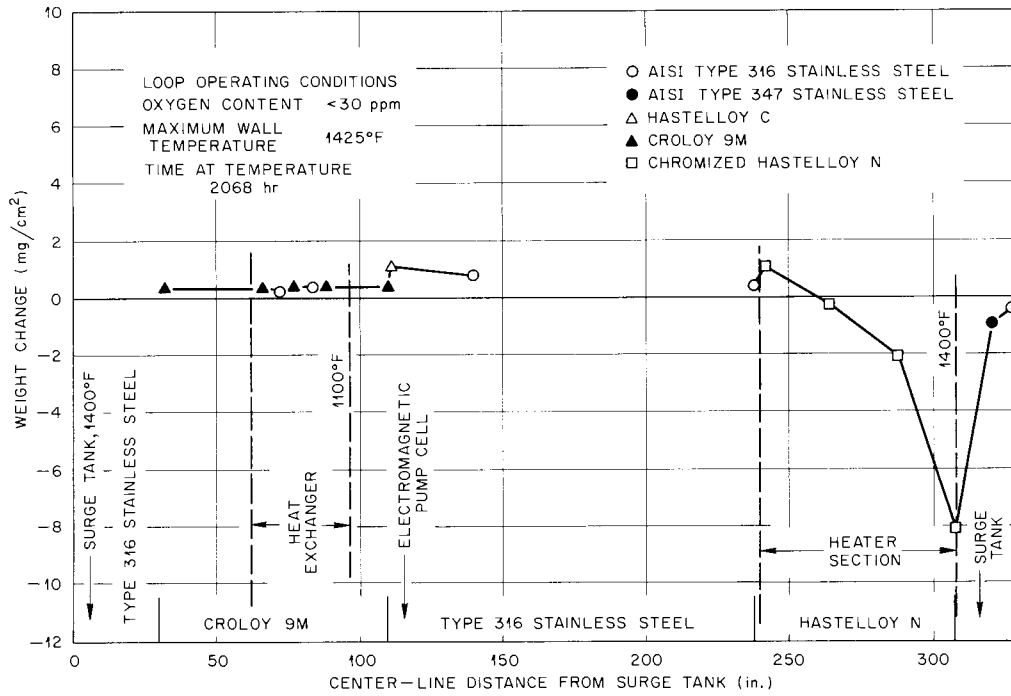


Fig. 9. Mass-Transfer Profile of Loop 1A.

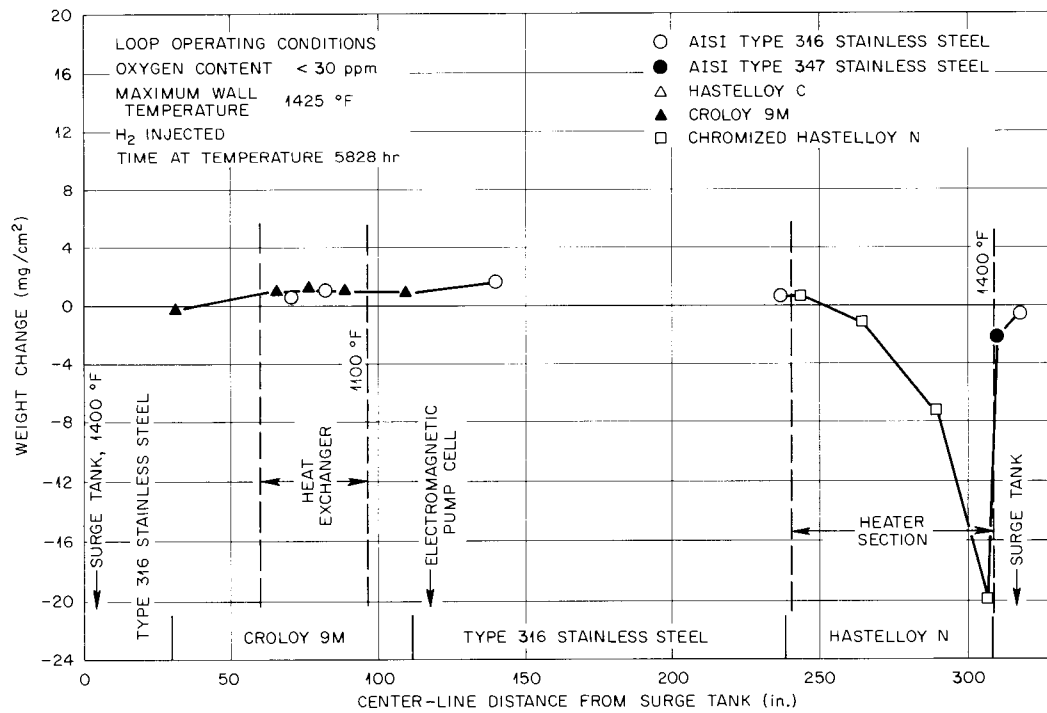


Fig. 10. Mass-Transfer Profile of Loop 5.

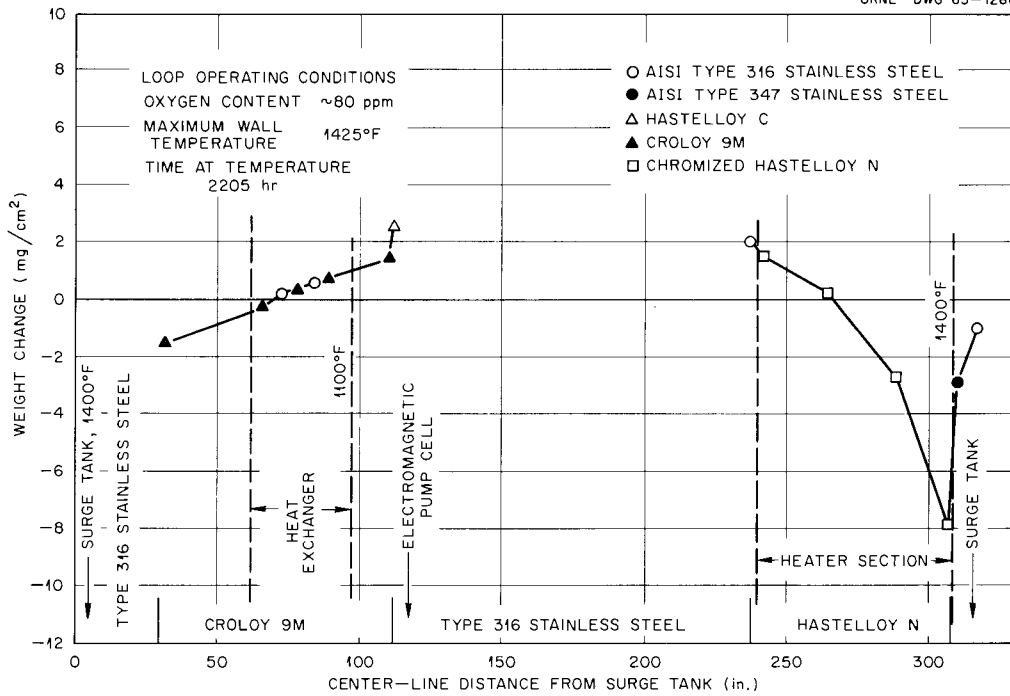


Fig. 11. Mass-Transfer Profile of Loop 2.

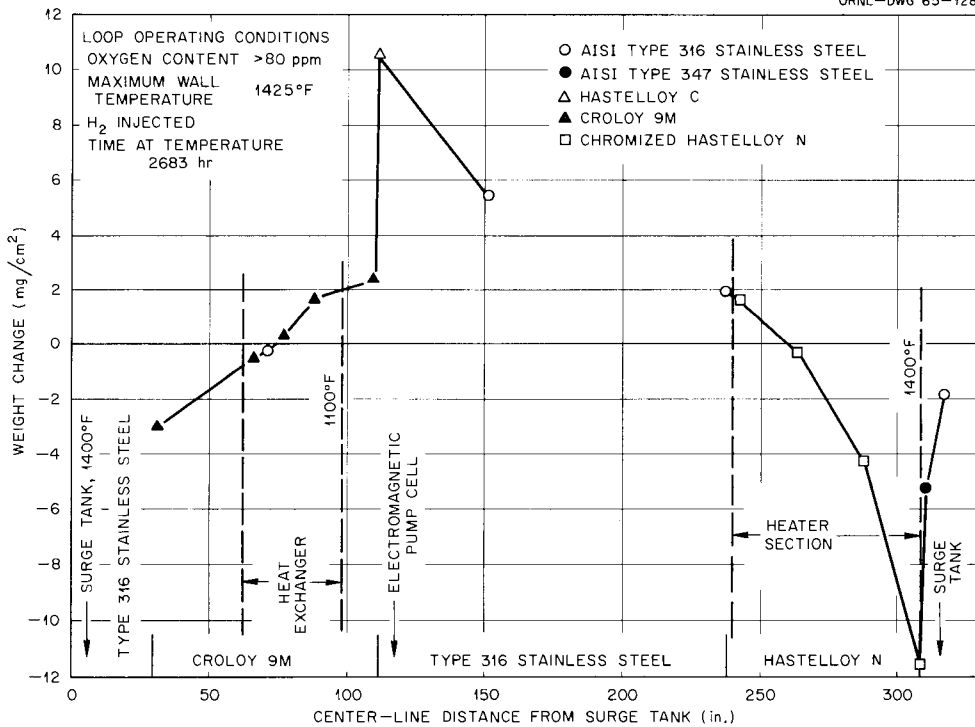


Fig. 12. Mass-Transfer Profile of Loop 4.

In high-oxygen loops the general pattern remained the same except that specimen No. 2 gained weight and the iron-base alloy specimens in the heated section, including specimens No. 11 (Croloy 9M) and No. 16 (316 stainless steel) in the heat exchanger, showed significant weight losses.

More detailed information regarding extent, character, and effects of variables on metallic element and carbon transfer will be discussed in the following sections.

METAL MIGRATION

The extent of metal migration was determined in all 11 loop tests that operated at several levels of temperature, oxygen concentration, hydrogen, and time. The corrosion and loop operating data for each loop are summarized in Table 1 (and Tables 7 and 8 in the section on "Forced-Flow Corrosion-Loop Experiments"). The effects of the variables are presented separately. Following these presentations is a section describing the identification of the migratory species and interpretations of the general pattern of migration.

Effect of Hydrogen

The effect of hydrogen addition on corrosion was investigated by comparing similar loops both with and without hydrogen injection. The injection rate of $0.6 \text{ cm}^3 \text{ (STP)/hr}$ resulted in an observed hydrogen partial pressure of approximately $9 \times 10^{-5} \text{ atm}$ of hydrogen under steady-state conditions.

Corrosion rate data presented for comparable specimens are shown in Table 2. These data indicate that the corrosion behavior of the various materials is not deleteriously affected at this level of hydrogen. The variations of the data are believed to be extraneous scatter.

Effect of Time

The effect of time on the corrosion rates of the various materials was evaluated by comparing three low-oxygen loops operated at 1425°F maximum hot-leg temperature. One loop (loop 5) also had hydrogen injection, but its use in establishing effect of time is considered reasonable since the data presented in the previous section indicated no adverse effects associated with hydrogen injection.

The weight-change data from these tests (Fig. 13) suggest that the corrosion rate of both Hastelloy N and 347 stainless steel steadily decreases with increasing time until the corrosion rate becomes approximately linear. The higher corrosion rate behavior initially would be

Table 1. Summary of Insert Specimen Weight-Change Data^a
Weight change (mg/cm²)

No. ^b	Specimen Material	1400°F				Long-Term 1400°F Loop	1300°F Loops				Hot-Spot Loops		
		Loop 1	Loop 1A	Loop 2	Loop 4	Loop 5	Loop 7	Loop 8	Loop 9	Loop 10	Loop 13	Loop 14	
1	Hastelloy N ^c	+0.28	+1.13 ^d	+1.55	+1.70	+0.47	+3.19	+0.39	+13.67	+0.31	+0.25	+0.43	
2	Hastelloy N	-0.60	-0.24	+0.23	-0.35	-1.21	+0.28	-0.11	+2.35	-0.14			
3	Hastelloy N	-2.17	-2.17	-2.68	-4.31	-7.33	-1.55	-0.84	-1.66	-1.08	-0.74	-0.90	
4	Hastelloy N	-4.08	-8.11 ^d	-7.91	-11.50	-20.00	-5.99	-2.64	-7.63	-3.08	-2.24	-2.50	
5	Type 347 stainless steel	-0.66	-0.97	-2.99	-5.22	-2.30	-6.28	-0.82	-35.14	-0.76	-0.97	-1.46	
6	Type 316 stainless steel	-0.27	-0.35	-0.98	-1.84	-0.69	-2.49	-0.18	-16.22	-0.25	-0.36	-0.34	
7	Croloy 9M	+0.20	+0.32	-1.46	-3.01	-0.38	-10.24	-0.03	-104.6	+0.11	-0.40	-0.13	
11	Croloy 9M	+0.11	+0.29	-0.22	-0.46	+0.89	-2.84	+0.05	-33.1	-0.14	-0.16	+0.01	
16	Type 316 stainless steel	+0.09	+0.20	+0.11	-0.21	+0.63	-0.49	-0.33	-3.52	-0.12	+0.07	+0.10	
10	Croloy 9M	+0.08	+0.44	+0.38	+0.32	+1.03	-0.35	+0.03	+1.36	0	-0.03	+0.18	
15	Type 316 stainless steel	+0.12	+0.37	+0.55	+0.74	+0.98	+0.10	-0.37	+4.08	-0.03	+0.24	+0.17	
9	Croloy 9M	+0.17	+0.39	+0.74	+1.77	+0.90	+0.99	+0.04	+9.77	-0.07	+0.07	+0.27	
8	Croloy 9M	+0.04	+0.38	+1.44	+2.38	+0.77	+3.99	+0.05	+36.0	+0.05	+0.29	+0.39	
12	Hastelloy C	+0.93	+1.16	+2.64	+10.49	+1.50	+7.94	+0.44	+70.3	+0.57	+1.27	+1.18	
13	Type 316 stainless steel		+0.76		+5.54	+1.56	+10.37	+0.46	+41.2	+0.28	+1.10	+0.38	
14	Type 316 stainless steel	+0.18	+0.41	+2.12	+1.90	+0.45	+8.49	+0.26	+24.0	0	+0.66	+0.79	
											Hot-Spot Specimen No.		
											19	+0.07	+0.02
												+0.09 ^e	
											20	-1.7	-0.62
											21	-1.45	-0.34
											22	-1.64	-1.71
											23	-1.94	-1.64

^aAdjusted for carbon migration.

^bSpecimens are listed in order of stream position starting at inlet to heater section.

^cAll Hastelloy N specimens were chromized.

^dSpecimen damaged during removal; weight change reported is based on estimate derived by weighing and measuring a portion of the specimen.

^e+0.07 for first 1300 hr; +0.09 for last 700 hr on a new specimen.

expected with both materials if preferential leaching of chromium occurred. Evidence that this happened was suggested by the analysis of corroded surfaces and deposition products as discussed in a later section of this report. This initial transient period has also been reported for 316 stainless steel in sodium at 1200°F (ref. 2) and at 1575°F in sodium and potassium.³

Table 2. Effect of Hydrogen on Corrosion in 1300°F Low-Oxygen Loops

Specimen No.	Material	Corrosion Rate (mg/cm ²)		
		Control Loop Without Hydrogen Injection	Loops with Hydrogen Injection	
		Loop 10	Loop 13	Loop 8
4	Hastelloy N	-3.08	-2.24	-2.64
5	347 stainless steel	-0.76	-0.97	-0.82
7	Croloy 9M	+0.11	-0.40	-0.03
Exposure time, hr		2000	2238	2435

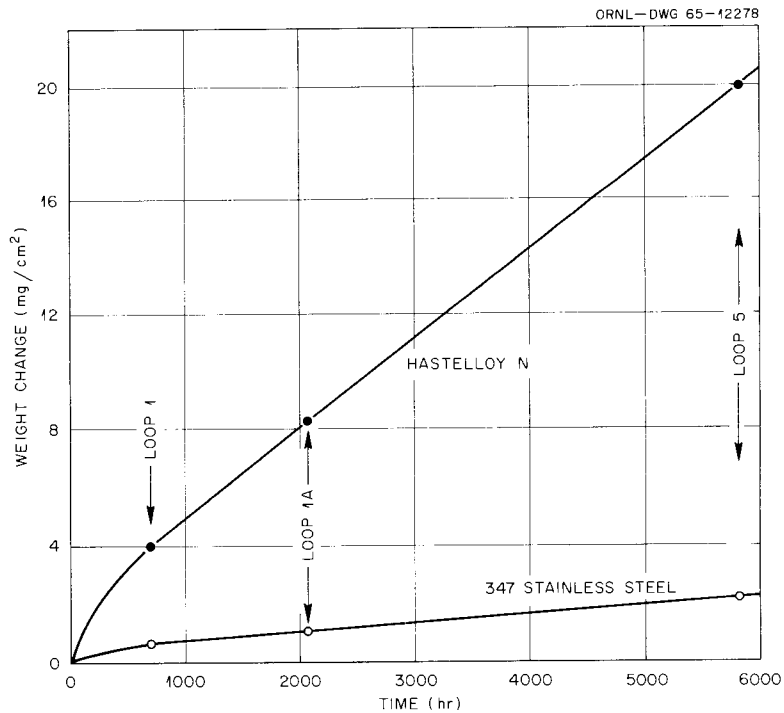


Fig. 13. Effect of Time on Corrosion of Hastelloy N and 347 Stainless Steel at ~1400°F.

The extent of damage resulting from metal migration was also evaluated by metallographic observation. Examinations of the 347 stainless steel specimens from the longest test failed to reveal any corrosion damage; however, a considerable number of microstructure changes occurred. These changes are discussed in a later section.

Metallographic examination of Hastelloy N specimens from various loops revealed the occurrence of corrosion damage as a function of time as illustrated in Fig. 14. The depth of attack resulting from selective corrosion in 5828 hr was approximately 1.5 mils as revealed in this figure. The weight-change data for this specimen, when converted to uniform metal removal, indicated only 0.9 mil of corrosion. These data show that the use of weight-change data could lead to considerable error when extrapolating and estimating extent of corrosion damage. The relationship between weight change and degree of corrosion damage could not be established from the few test points available.

Effect of Oxygen

Oxygen was found to be very influential on the corrosion behavior of the iron-base alloys 316, 347, and Croloy 9M, but did not affect Hastelloy N except at very high oxygen levels. These conclusions are drawn from the data presented in Tables 3 and 4. Loops 1A and 2 (Table 3), which operated at a maximum NaK temperature of 1400°F, reveal that the corrosion of Hastelloy N is not deleteriously affected when the oxygen concentration is varied from <30 to ~80 ppm. The corrosion of 347 and Croloy 9M, however, readily shows the effects of variation in oxygen within this range. Several loops which operated at 1300°F with very high oxygen levels also revealed the effects on the iron-base alloys and, furthermore, revealed an effect of oxygen on the corrosion rate of Hastelloy N. These data are presented in Table 4. The oxygen levels in loops 9 and 7 are not definable but were known to be much higher than 100 ppm during several periods of operation. During these periods of very high oxygen, corrosion and deposition took place very rapidly, as indicated by rapid degradation of the NaK flow.

Effect of Temperature

The behavior of the various materials with respect to temperature was also very dependent on the alloy content. The effect of temperature on the corrosion of the nickel-base alloy, Hastelloy N, was found to be very significant. A plot of the logarithm of weight change vs $1/T$ is presented for this material in Fig. 15.

The data in this plot are from specimens 3 and 4 from loops that operated with and without hydrogen injection and with oxygen levels 80 ppm or less. Data points from specimen No. 2 in the various loops were not included because the corrosion behavior at this location was obviously being affected by some transient such as the hysteresis that might be as-

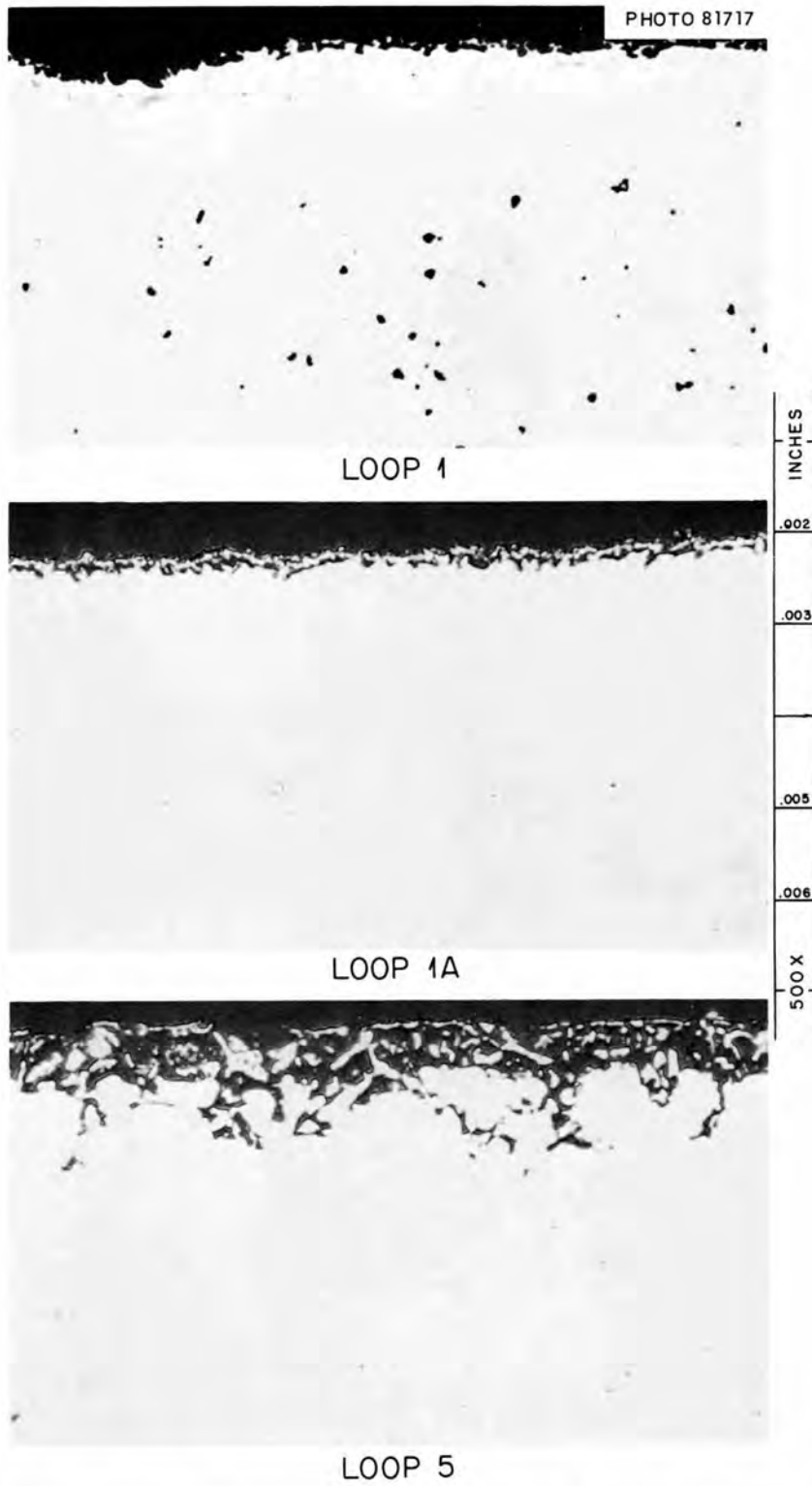


Fig. 14. Cross Sections of Hastelloy N Specimen 4 from Various Loops, Showing Corrosion Damage and Effect of Time at 1400° F.

Table 3. Effect of Oxygen on Corrosion in 1400°F Loops

Specimen No.	Material	Temperature (°F)	Loop 1A	Loop 2
			Corrosion (mg/cm ²)	
4	Hastelloy N	1400	-8.11	-7.91
5	347 stainless steel	1400	-0.97	-2.99
7	Croloy 9M	1364	+0.32	-1.46
Oxygen concentration, ppm			<30	~80
Time at temperature, hr			2068	2205

Table 4. Effect of Very High Oxygen Level on Corrosion in 1300°F Loops

Specimen	Material	Temperature (°F)	Loop 10	Loop 7	Loop 9
			Corrosion (mg/cm ²)		
4	Hastelloy N	1300	-3.08	-5.99	-7.63
5	347 stainless steel	1300	-0.76	-6.28	-35.14
7	Croloy 9M	1275	+0.11	-10.24	-104.6
Oxygen concentration, ppm			<30	>>100	>>100
Time at temperature, hr			2000	2705	2476

sociated with supersaturation or the change from precipitation processes to solution processes. This condition resulted in an unduly low corrosion rate for this specimen in comparison with No. 3 and No. 4 specimens from the same loop and was noted in every loop. An example of the extent of deviation is indicated by the data from loops 1A and 10 presented in Fig. 16. The numbers by the data points identify the specimens.

In contrast to the behavior of Hastelloy N, virtually no effect of temperature was noted for the iron-base alloys 316, 347, and Croloy 9M, as seen by the data in Table 5. The low corrosion rates of these materials plus the scatter of the data were sufficient to mask out any small effects that could be ascribed to temperature effects. This result is rather startling since the data available in the literature suggest that the corrosion of iron-base alloys in liquid metals in this temperature

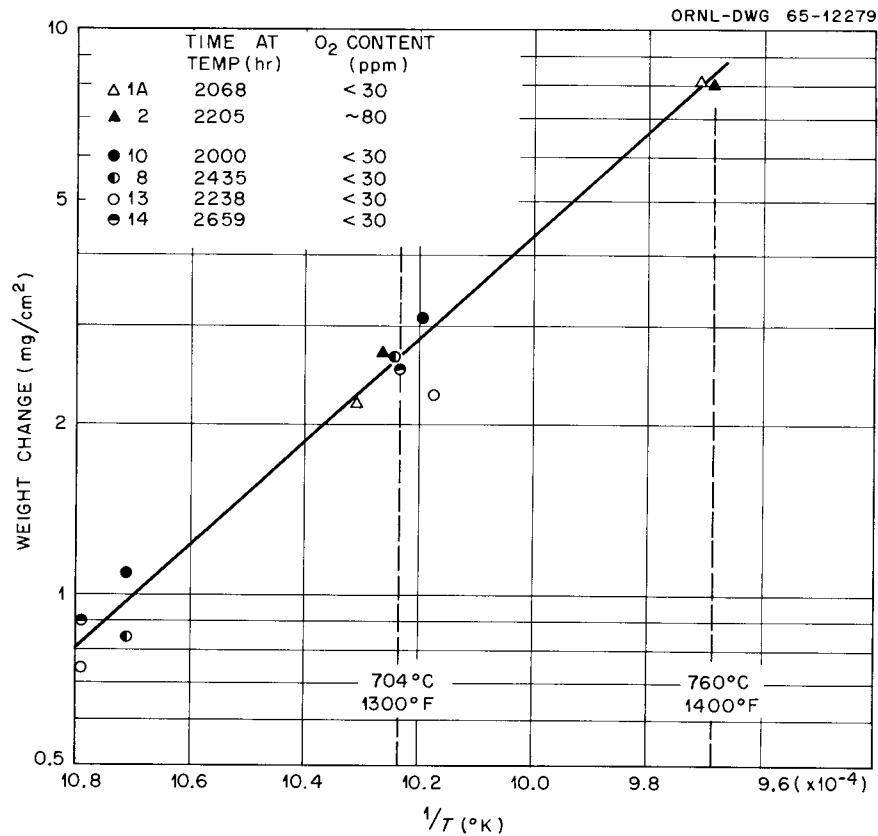


Fig. 15. Effect of Temperature on Corrosion Rate of Hastelloy N.

Table 5. Effect of Temperature on Corrosion of Iron-Base Alloys in Low-Oxygen Loops

Loop No.	Time (hr)	Temperature (°F)	Weight Change (mg/cm ²)		Temperature (°F)	Weight Change (mg/cm ²), Specimen No. 7 Croloy 9M
			Specimen No. 5 347 Stainless Steel	Specimen No. 6 316 Stainless Steel		
8 ^a	2435	1298	-0.82	-0.18	1273	-0.03
10 ^a	2000	1306	-0.76	-0.25	1278	+0.11
13 ^a	2238	1311	-0.97	-0.36	1285	-0.40
14 ^a	2659	1300	-1.46	-0.34	1260	-0.13
Av.	2333	1304	-1.00	-0.28	1274	-0.11
1A ^b	2068	1397	-0.97	-0.35	1361	+0.32
5 ^{b,c}	2000	1396	-1.05			
Av.	2034	1396	-1.01	-0.35	1361	+0.32

^a1300°F loops.

^b1400°F loops.

^cCorrected to 2000 hr using curve in Fig. 13.

range should show almost as strong a dependence on temperature as that of the nickel-base alloys. One possible explanation for the behavior of the iron-base alloys in this system is that the presence of nickel and chromium in the NaK may have a depressive effect on the temperature coefficient of solubility of iron in NaK. In support of this explanation, it was observed by Weeks⁴ that chromium depressed the solubility of iron in liquid bismuth at about 1100°F.

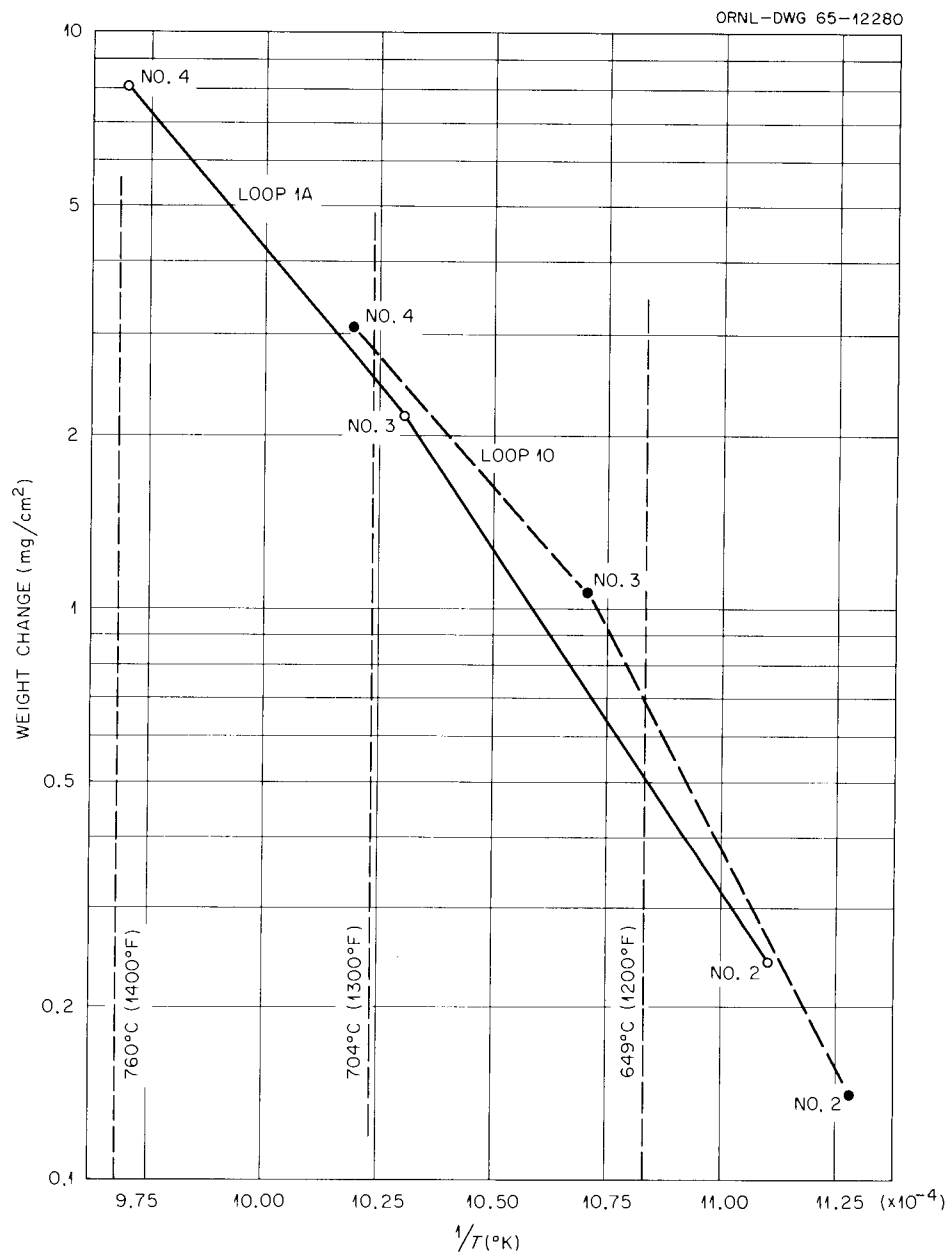


Fig. 16. Effect of Hot-Leg Temperature and Stream Position on Corrosion of Hastelloy N.

Identification of Mass-Transfer Deposits and
Interpretation of Migration Pattern

Mass-transfer deposits identified in several of the loops revealed that the elements present depended largely upon the oxygen level present during operation. In loop 5, a long-time low-oxygen loop, the deposits consisted mostly of nickel, chromium, and manganese, and relatively small quantities of iron, as revealed by the data shown in Table 6. The elements were present as Cr_7C_3 , M_6C , and alloys of Ni-Mn as indicated by x-ray diffraction analysis. The small amount of iron and the large amount of manganese present are especially significant when considering the relative availability of these elements in the hot part of the system. If the product of the surface area of the various alloys times the percentage of the various elements present in the alloys is used to approximate the availability of each element, the relative amounts present would be those shown in column 1 of Table 6. These values when compared to the analytical data clearly show that the elements present did not transfer in proportion to the amounts present.

In loop 9, a loop with very high oxygen during operation, the bulk analysis of the deposits removed from specimens 8, 12, and 13 showed mostly iron and chromium and relatively small amounts of nickel and manganese, as revealed by the data reported in Table 7. Metallographic examination of deposition areas, however, revealed the presence of two

Table 6. Analysis of Mass-Transfer Deposits from
Loop 5 - Low-Oxygen Loop
Values in weight percent

Element	Relative Availability of Element ^a	Sample No. 1 ^b	Sample No. 2 ^b	Sample No. 3 ^b
Fe	47	1.1	0.9	4.0
Ni	31	53.2	46.1	34.5
Cr	12	18.3	15.2	14.0
Mo	7	<0.1	<0.4	<0.8 ^c
Mn	3	10.2	11.7	6.9
C		0.8	0.5	0.1

^aSee text for description of this index.

^bSample No. 1 taken just upstream of EM pump cell; sample No. 2 taken from EM pump cell; sample No. 3 taken from piping in vicinity of specimen No. 13.

^cIncreasing uncertainty in Mo analysis is result of decreasing sample size.

basically different types of deposit, a grayish oxide-like constituent predominantly adhering to the surface, and bright metallic crystals, as seen in Fig. 17. When both were removed from the metal surfaces, they

Table 7. Analysis of Mass-Transfer Deposits from Loop 9 - Very-High-Oxygen Loop

Values in weight percent

Element	Specimen 8 ^a	Specimen 12 ^a	Specimen 13 ^a	Magnetic Deposit	Nonmagnetic Deposit
Fe	94.53	78.30	62.20	64.6	3.4
Cr	0.90	5.35	14.90	15.4	39.0
Ni	3.31	4.16	2.68	<1	<1
Mo	1.09	1.03	1.09	0.8	<1
Mn	0.28	0.37	0.87	0.8	2.3
Na		1.31	2.61	0.39	1.38
K		<0.1	<0.2		
C	0.282	0.209	0.301		

^aDeposits were scraped from these specimens.



Fig. 17. Cross Section of Deposits on Croloy 9M Piping at Cold End of Heat Exchanger in Loop 9. 500X.

could be partially separated by vigorous agitation in water and extraction of the metallic particles with a magnet. Analysis of each portion revealed the nonmagnetic gray material to be mostly chromium and the magnetic metallic material to be primarily iron, as shown in Table 7. The presence of some of the chromium in the metallic material is believed to be the result of some gray oxide-like material that was not removed during the separation process. X-ray diffraction studies of the materials indicated the presence of iron and a complex oxide of the type MNO_2 , where N could be Na or K and M could be Cr, Ni, or Fe. The presence of sodium and the relatively high concentration of chromium in the gray material indicate that the complex oxide compound present was probably $NaCrO_2$, sodium chromite. Electron microprobe analysis of the deposits in situ also showed the gray material to be principally chromium, while the metallic particles were principally iron. These results are reported in Table 8 for the areas indicated in Fig. 18. Electron microprobe analysis also showed the existence of the sodium chromite compound in a stagnant region on the back side of specimen No. 5 (347 stainless steel) in the heated section. The compound occurred in the grain boundaries, as revealed by Fig. 19. The electron microprobe results are indicated in Table 9 and Fig. 20. Analysis of the corroded surfaces of the Hastelloy

Table 8. Electron Microprobe Analysis of Deposits on Specimen 1 - Loop 9

Area of Analysis	Ni (wt %)	Fe (wt %)	Cr (wt %)	Mo (wt %)
1	0.7	1.8	47.9	0.8
2	0.1	0.7	36.5	0.0
3	25.2	73.2	0.6	1.0
4	21.2	73.3	1.1	1.1
5	69.9	4.2	6.6	14.1

Table 9. Electron Microprobe Analysis of Oxide Product on OD of Specimen 5, Loop 9

Area of Analysis	Ni		Fe		Cr	
	Intensity Ratio	Weight Percent	Intensity Ratio	Weight Percent	Intensity Ratio	Weight Percent
1	0.0055	0.6	0.0501	6.2	0.3832	37.6
2	0.0180	2.2	0.1655	20.1	0.3620	35.1
3	0.0727	10.2	0.5751	63.2	0.1903	17.6

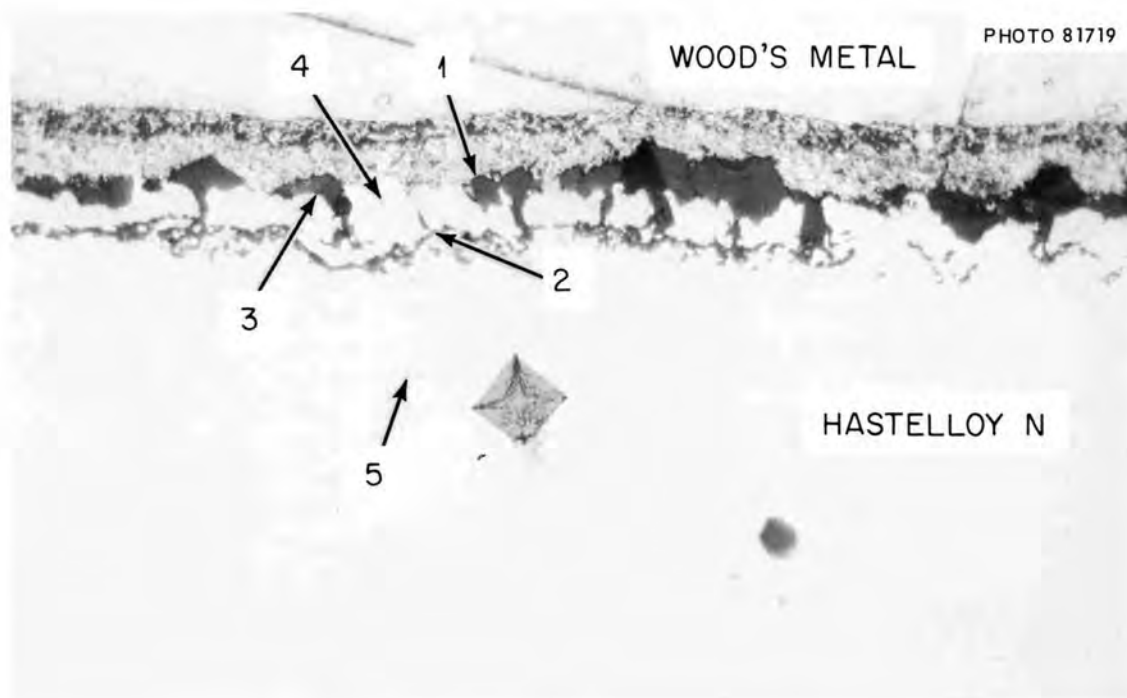


Fig. 18. Cross Section of Specimen 1, Loop 9. 500X.

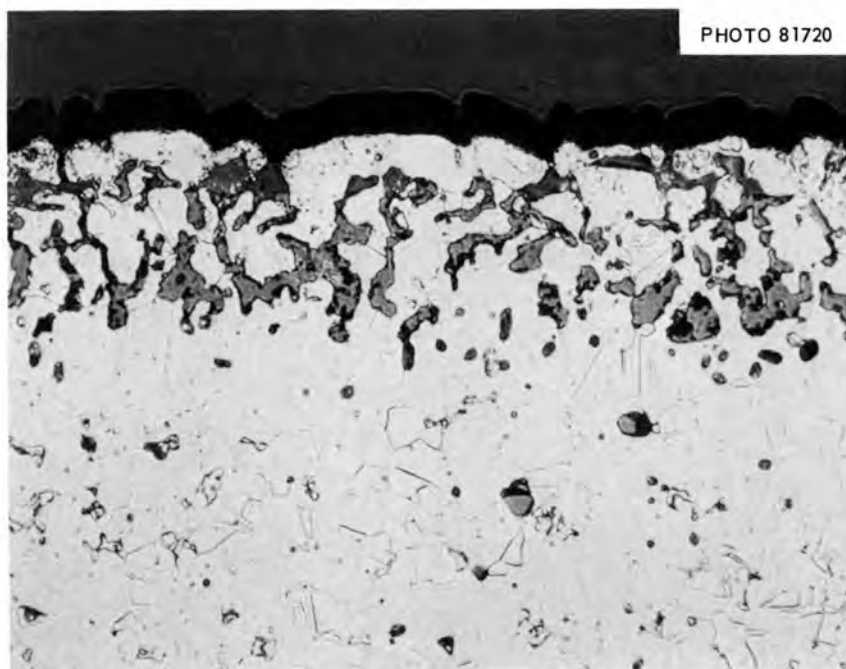


Fig. 19. Intergranular Deposits on OD of Specimen 5, Loop 9. 500X.

N, 347 stainless steel, and Croloy 9M showed that chromium had been selectively removed in each case, thus indicating that the driving force for chromium removal was significantly greater than that of nickel or iron.

In addition to the above, electron microprobe analysis also revealed that nickel was transferred to Croloy 9M in the form of diffusion alloying. The concentration profile for the nickel diffusion zone of specimen No. 7 (Croloy 9M) from loop 9 is shown in Fig. 21. The change in composition in the nickel-rich layer is believed to have caused a phase transformation from bcc to fcc structure at loop temperatures, which returned to bcc upon cooldown. These transformations were believed to be responsible for the surface microstructure, shown in Fig. 22.

The above information as to the migrating species, together with operation data and weight-change data, infers several important phenomena regarding corrosion in this liquid-metal system that may also apply to other NaK, Na, and K systems where Fe, Ni, Mo, and Cr are the principal elements present in the construction materials. The most important variable affecting both the magnitude and character of corrosion is the oxygen availability and concentration in the system. The element having the greatest affinity for oxygen is chromium. (Manganese, which is normally present in minor amounts in most alloys, has more affinity for oxygen than

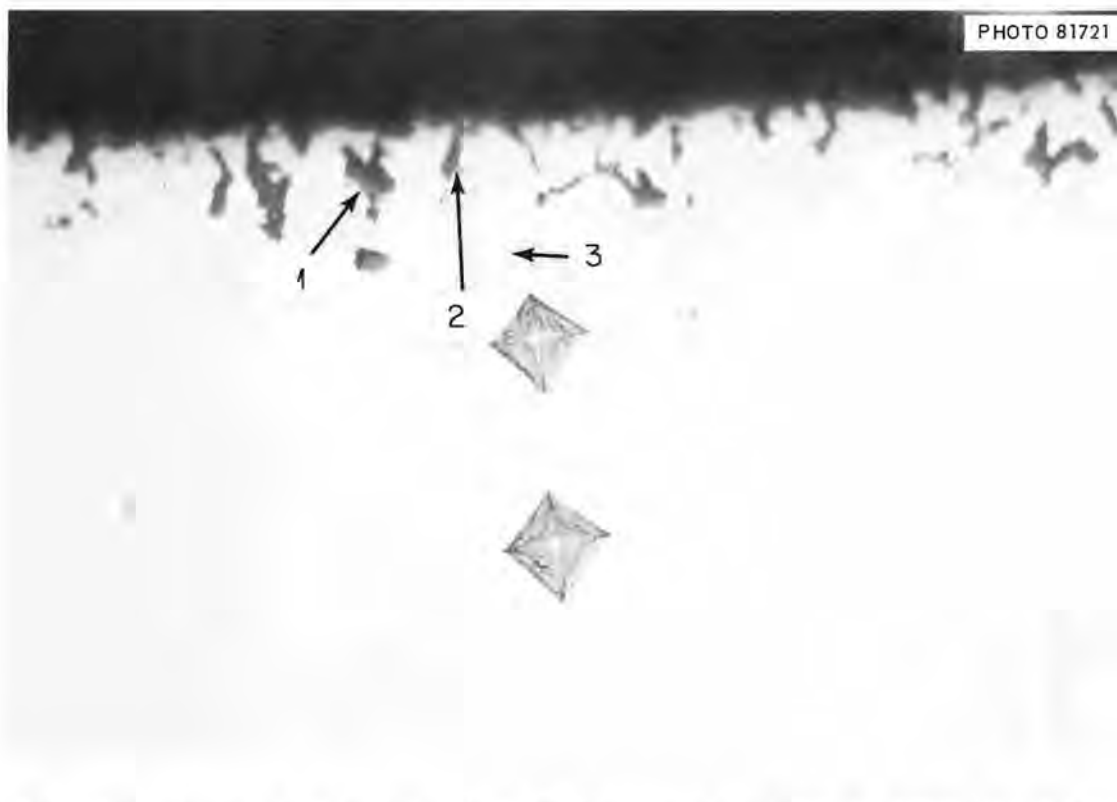


Fig. 20. Cross Section Showing OD Edge of Specimen 5, Loop 9. 500x.

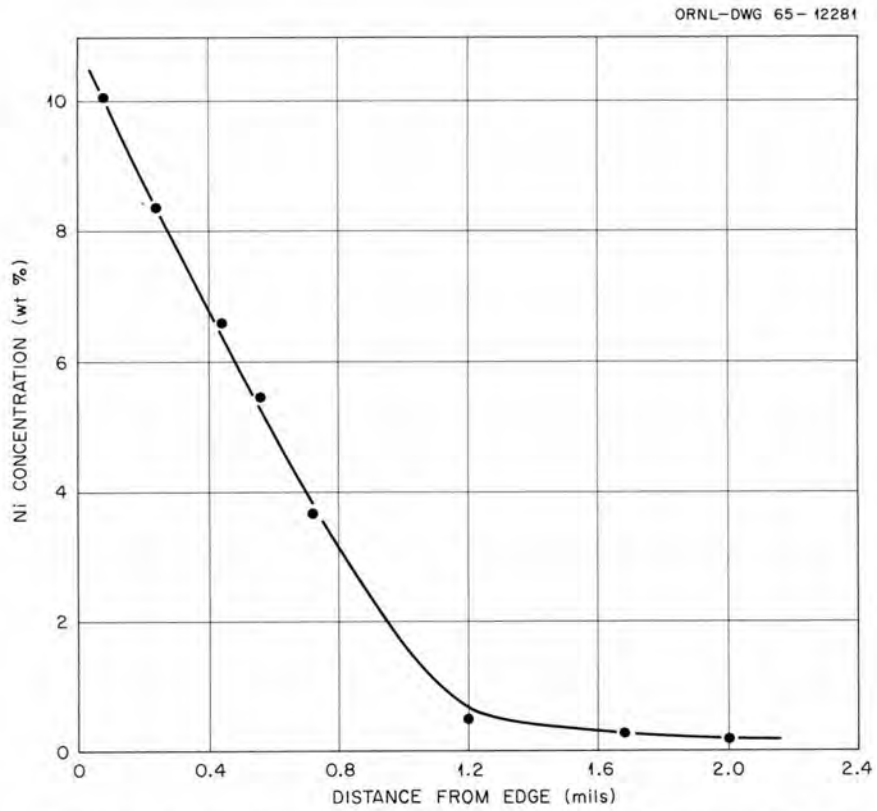


Fig. 21. Nickel Diffusion Layer on Specimen 7 (Croloy 9M) from Loop 9.

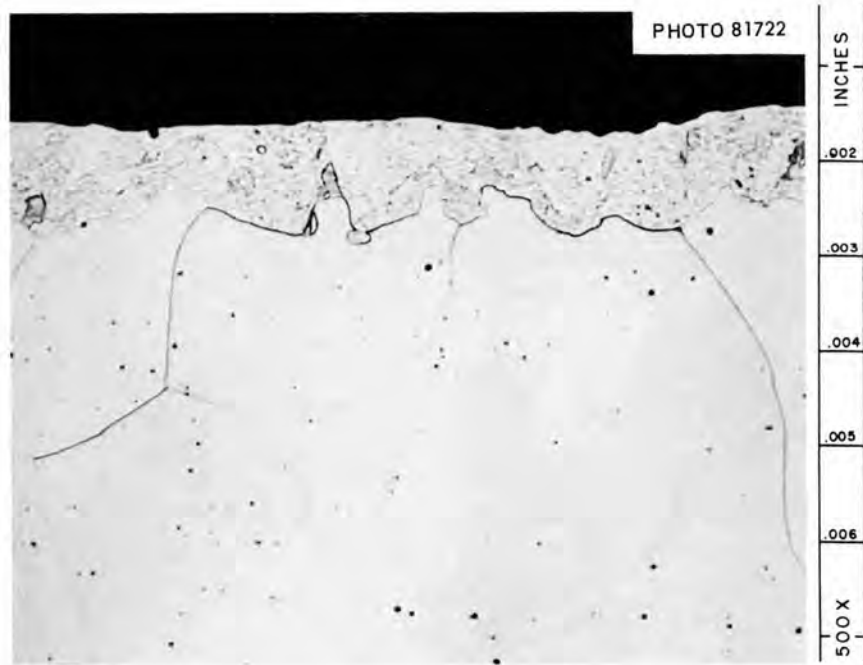


Fig. 22. Microstructure Associated with Nickel Diffusion Layer on Surface of Croloy 9M. Etched 4% picral, 1% HCl.

chromium and probably would behave similarly.) Oxygen residing in or entering a system containing chromium will be gettered as a complex oxide of chromium. Where chromium is available as an alloying agent, it will serve to keep the oxygen concentration down in proportion to the transfer rate of chromium from the bulk solid to the NaK. If the oxygen feed rate to the NaK is greater than the supply rate of chromium, then the oxygen concentration of the system will increase. As the oxygen concentration of a system increases, the transfer rate of iron then becomes very significant and may grossly exceed that of chromium transfer because of the relatively high availability of iron. The mechanism for the very gross effect of oxygen concentration on iron transfer is not clear at present. This could result from an increase in the solubility or temperature coefficient of the solubility of iron in NaK, or, perhaps, through development of an unstable complex oxide of iron, sodium, and oxygen as suggested by Wilkinson, Yaggee, and Kelman.⁵ Either mechanism could result in very high corrosion rates without depletion of the oxygen available in the NaK. However, more chromium would eventually become available as the iron corroded, and this would continue to getter the oxygen from the system. If there were not a continuously high oxygen supply to the NaK, the chromium would eventually lower the oxygen level, thus reducing the transfer rate of iron.

Within the range of oxygen from <30 to ~80 ppm, the transfer rate of the nickel-base alloy, Hastelloy N, did not appear to be significantly affected by the oxygen concentration of the NaK. However, when the oxygen level was very high (much greater than 100 ppm), there was an increased transfer rate of the Hastelloy N material. It is not certain whether this was a result of increased nickel transfer or transfer of other elements present, such as molybdenum and chromium.

One further point should be made regarding the effect of oxygen on corrosion. The operating data from loops 9 and 7 (very-high-oxygen loops) indicated that the mechanism for transfer of material under high oxygen conditions results in a very rapid transfer. Degradation of flow in these loops closely followed additions of oxygen to the NaK. This information suggests that corrosion damage occurring under a short-time intermittently high oxygen condition might exceed that encountered in long-time low-oxygen exposures, thus significantly affecting interpretation of corrosion results.

Effect of Hot-Spot Conditions

Several test loops were modified to evaluate the effect of simulated hot-spot conditions on corrosion of Hastelloy N. The modification involved the insertion of a bypass line in which slow-flowing (~3.56 fpm) NaK was heated from 1100 to 1450°F over a 6-in. length of Hastelloy N piping. A schematic of the system is shown in Fig. 3 in the previous section. Specimens placed in the 1450°F low-flow hot-spot section showed even less weight change than the 1300°F specimens exposed to the full flow of NaK in the main flow channel. The data for these specimens are presented in Table 10. Data for specimen No. 4, located in the main loop, are also

Table 10. Results of Hot-Spot Test Loops

Specimen No.	Temperature (°F)	Velocity (fpm)	Weight Change (mg/cm ²)	
			Loop 13 (2238 hr)	Loop 14 (2659 hr)
20	1445	3.56	-1.70	-0.62
21	1445	3.56	-1.45	-0.34
22	1450	3.56	-1.64	-1.71
23	1450	3.56	-1.94	-1.64
4	1300	121	-2.24	-2.50

included for comparative purposes. These data demonstrate that hot-spot areas at 1450°F involving very low flow rates will not be corroded excessively.

CARBON MIGRATION

Character of Carbon Migration

Carbon migration followed the same general pattern in all the test loops. The pattern of migration is indicated by the carbon profile curves made at various points around the loop as shown in Fig. 23. These curves show that carbon was removed from the hot end of the Croloy 9M section and transferred to the 316 surfaces at all temperatures. Analysis of insert specimens confirmed this and also showed that carbon was transferred to the Hastelloy N, as is indicated by the posttest carbon contents reported in Table 11. In the 1400°F loops, carbon was also transferred to the cold end of the Croloy 9M section, thus revealing the large effect of temperature on the activity of carbon in NaK. Exceptions to the general pattern were noted only in the surge tank of loops 1, 10, and 14. In these loops the surge-tank insert specimens were slightly decarburized. Analysis of the 316 stainless steel piping leaving the surge tank of loop 1, however, showed carburization, as revealed by the carbon profile shown in Fig. 23. The reasons for the anomalies and the opposing results are not apparent.

The extent of carbon transfer along the hot vertical section of the Croloy 9M piping decreased significantly, as is shown by the carbon profiles in Fig. 23 and in the profiles and photomicrographs shown in Figs. 24 through 32. This was evident in every loop and, therefore, is believed to be representative of the behavior pattern. The maximum conceivable temperature difference between the upstream and downstream locations was about 10°F. It seems unlikely that this temperature differential or the carbon activity change in the NaK along this short

Table 11. Carbon Analysis of Insert Specimens

Specimen No.	Material	As-Received Carbon Content (%)	Posttest Average Carbon Content (%)							
			Loop 10	Loop 8	Loop 13	Loop 14	Loop 1	Loop 1A	Loop 5	Loop 2
1	Hastelloy N	0.028	0.042	0.042	0.048	0.071	0.070	0.063	0.075	0.059
2	Hastelloy N	0.028	0.051	0.045			0.081	0.071	0.077	0.093
3	Hastelloy N	0.028	0.060	0.046	0.034	0.058	0.088	0.081	0.107	0.078
4	Hastelloy N	0.028	0.052	0.084	0.040	0.049	0.087	0.120	0.148	0.090
5	347 stainless steel	0.035	0.049	0.059	0.051	0.042	0.067	0.117	0.146	0.120
6	316 stainless steel	0.054	0.029	0.073	0.065	0.030	0.050	0.123	0.234	0.120
7	Croloy 9M	0.11	0.002	0.004	0.005	0.008	0.013	0.004	0.002	0.003
11	Croloy 9M	0.11	0.048	0.041	0.061	0.072	0.004	0.004	0.005	0.006
16	316 stainless steel	0.054	0.127	0.260	0.096	0.058	0.211	0.260	0.430	0.275
10	Croloy 9M	0.11	0.077	0.090	0.082	0.088	0.056	0.088	0.030	0.120
15	316 stainless steel	0.054	0.107	0.280	0.076	0.080	0.208	0.203	0.360	0.203
9	Croloy 9M	0.11	0.103	0.102	0.096	0.107	0.115	0.157	0.225	0.120
8	Croloy 9M	0.11	0.100	0.099	0.103	0.113	0.170	0.160	0.201	0.130
13	316 stainless steel	0.054	0.084	0.063	0.071	0.060		0.100	0.203	
14	316 stainless steel	0.054	0.088	0.069	0.053	0.059	0.136	0.107	0.183	0.131
Maximum NaK temperature, °F			1325	1325	1325	1325	1425	1425	1425	1425
Oxygen level, ppm			<30	<30	<30	<30	<30	<30	<30	~80
Time at temperature, hr			2000	2435	2238	2659	700	2068	5828	2205

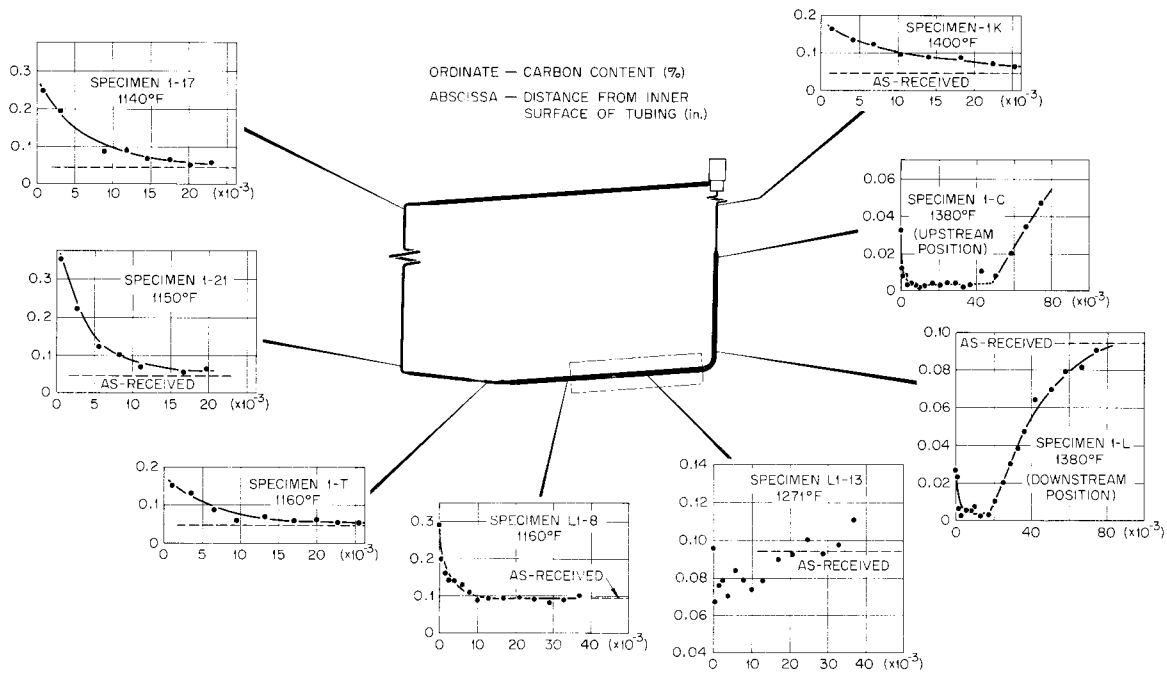


Fig. 23. Carbon Survey of Loop 1 Piping, Showing Pattern of Migration.

section could either separately or in combination account for the rather large differences in degree of decarburization. It should be noted, however, that the carbon transfer in the solid is rather unusual in itself. C. Wagner^{6,7} has treated a similar diffusion problem regarding the transfer of carbon in a two-phase alloy consisting of α -Fe and Fe_3C , in which it is assumed that the decomposition rate of the carbide is a much faster process than the diffusion rate of carbon through the α -Fe. This type of behavior would result in the carbon profile curve depicted in Fig. 33. The obviously different behavior of the Croloy 9M in our tests suggests that perhaps the carbon transfer rate is significantly affected by both the diffusion of carbon in the matrix and the decomposition rate of the carbide phase. Since the carbon transfer process in the solid is radically different from the normal case, it is not possible to estimate the effects of a small change in temperature on the extent of carbon transfer.

One further point of interest is noted from the carbon profile curves. Uphill diffusion of carbon occurred, as is shown by the increased carbon content near the ID surface in all the carbon profiles. This was presumably brought about by the infusion of nickel into the surface. The nickel alloying served to change the thermodynamic activity of carbon in this material, thus resulting in a free-energy gradient sufficient to cause the carbon to flow from the low-carbon-concentration material to the higher-carbon-alloyed material.

ORNL-DWG 65-12282

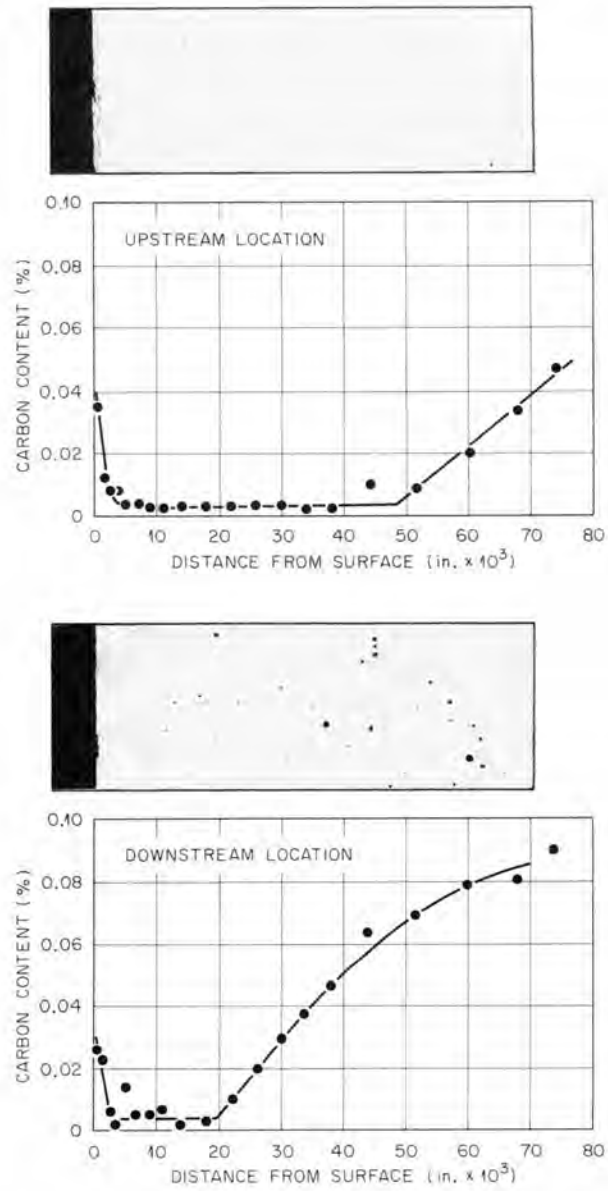


Fig. 24. Carbon Profile Curves for Croloy 9M from Loop 1. 1380°F; 701 hr.

ORNL-DWG 65-42283

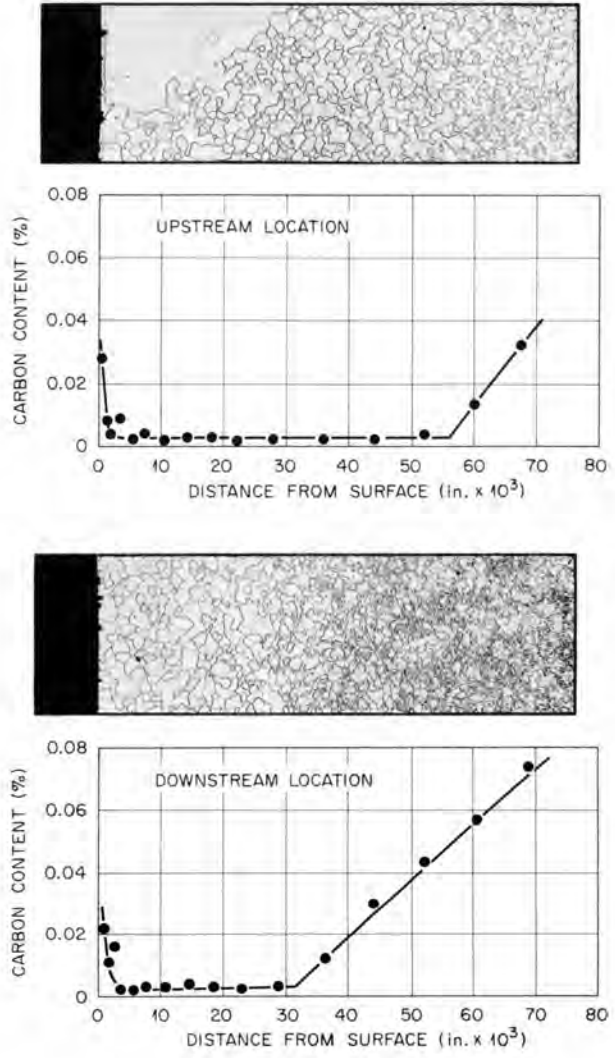


Fig. 25. Carbon Profile Curves for Croloy 9M from Loop 1A. 1361°F; 2068 hr.

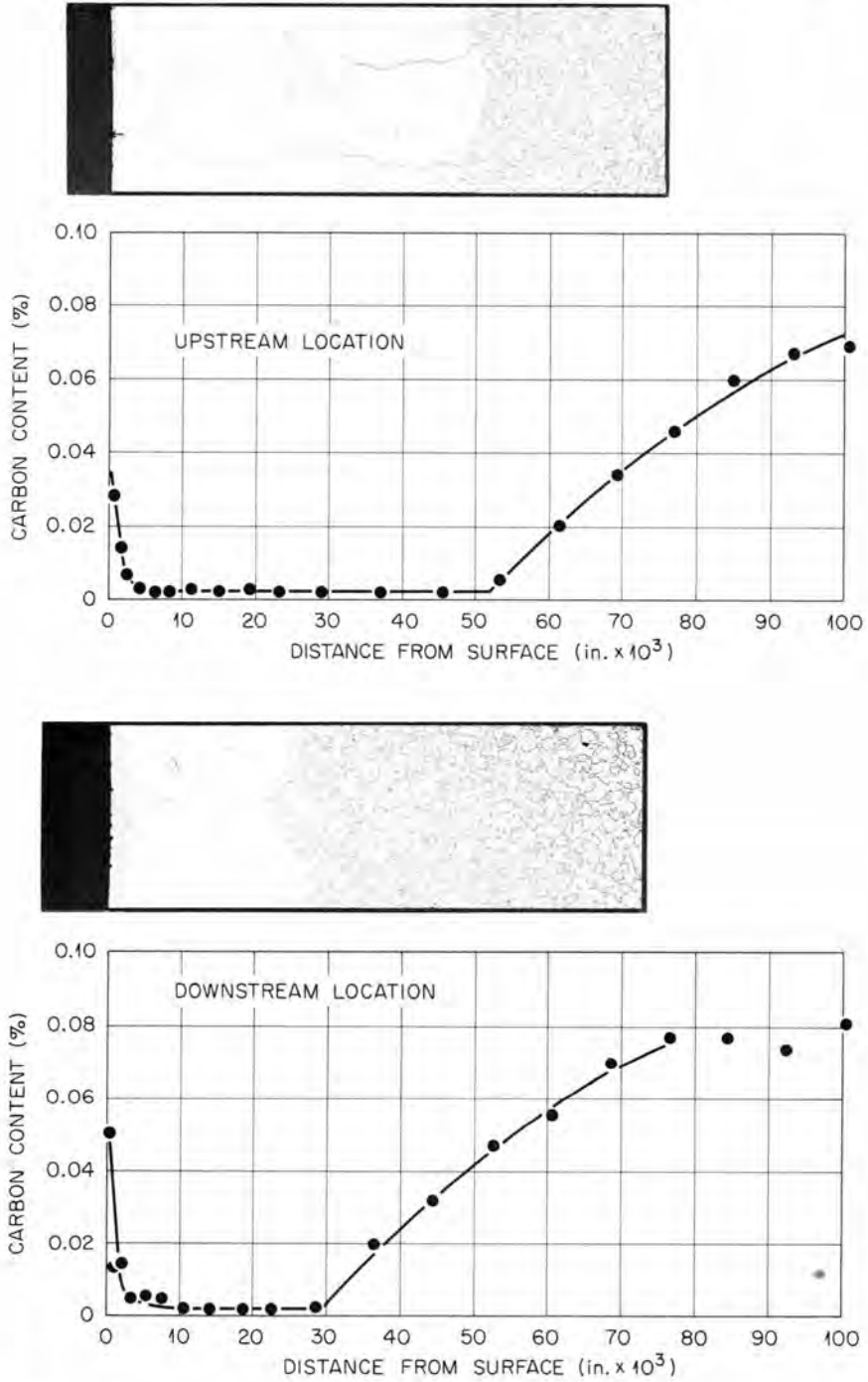


Fig. 26. Carbon Profile Curves for Croloy 9M from Loop 2. 1367° F; 2205 hr.

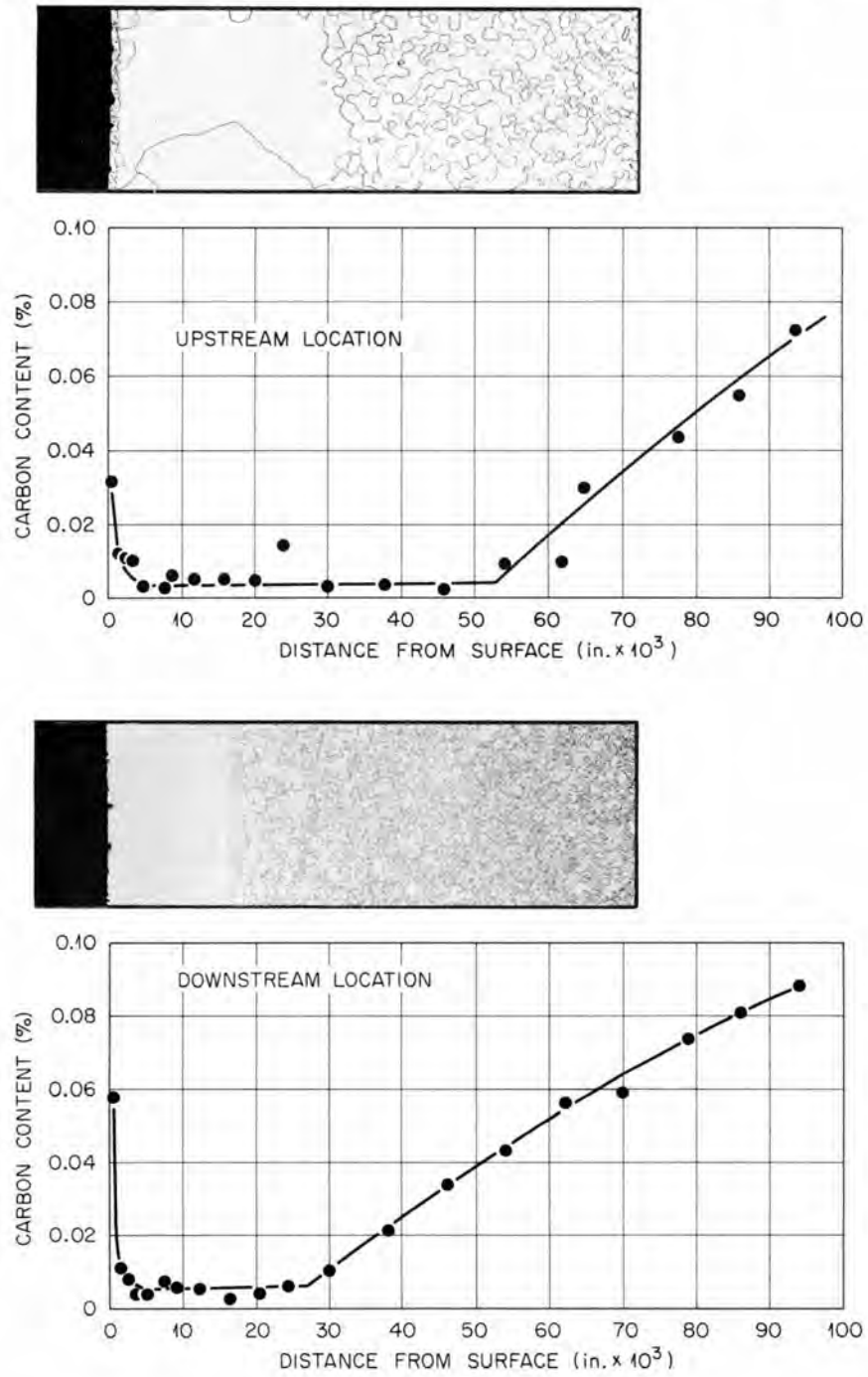


Fig. 27. Carbon Profile Curves for Croloy 9M from Loop 4. 1360° F; 2683 hr.

ORNL-DWG 65-12286

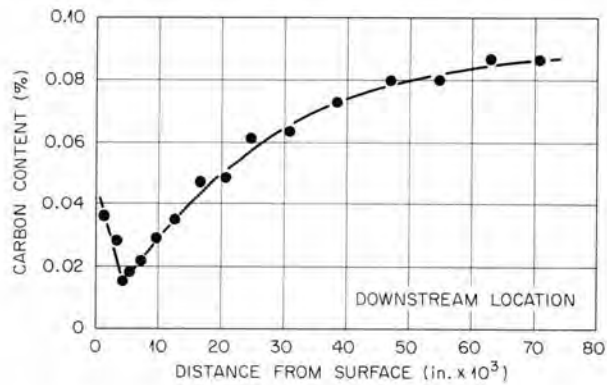
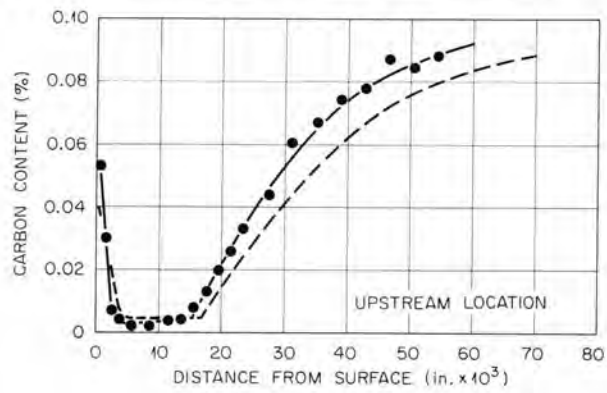


Fig. 28. Carbon Profile Curves for Croloy 9M from Loop 10. 1278° F; 2000 hr.

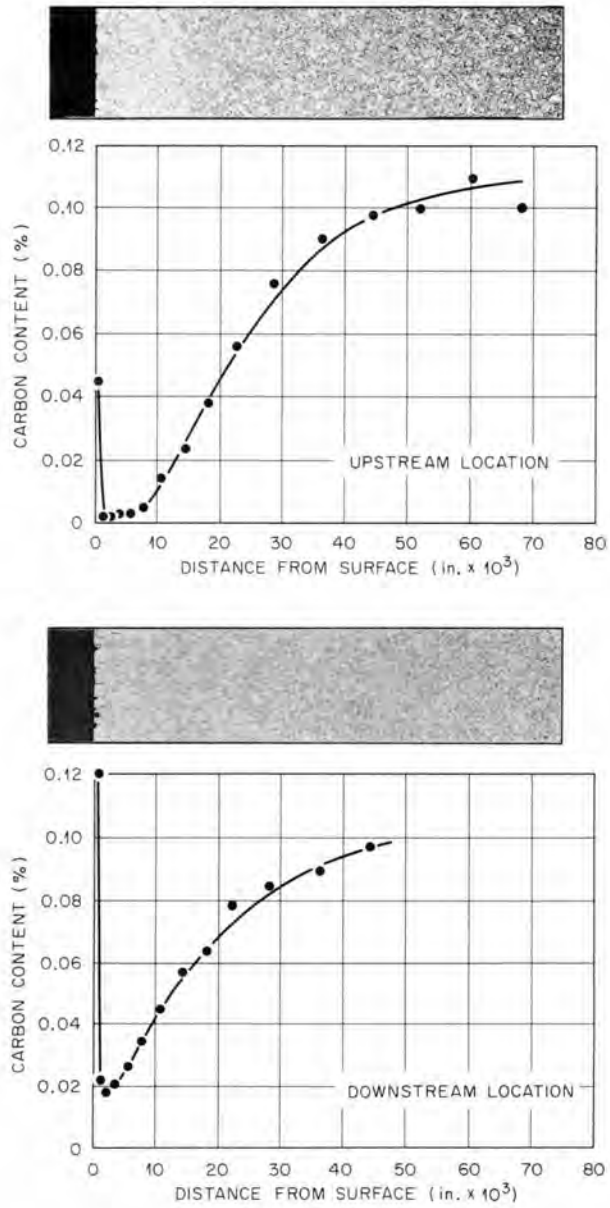


Fig. 29. Carbon Profile Curves for Croloy 9M from Loop 8. 1273°F; 2435 hr.

ORNL-DWG 65-12288

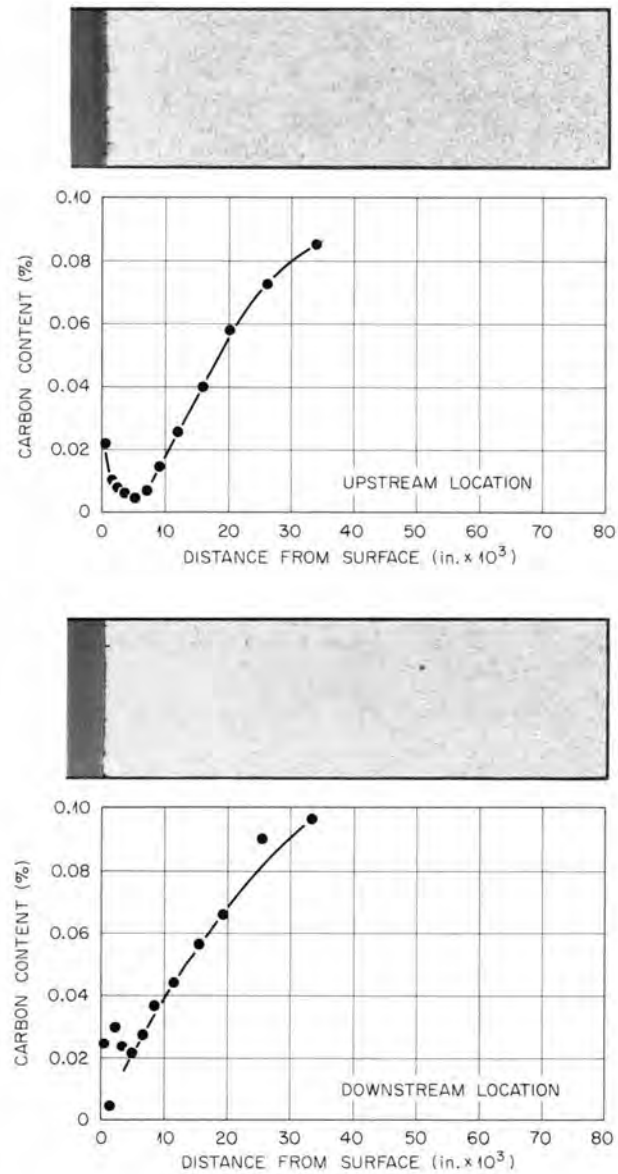


Fig. 30. Carbon Profile Curves for Croloy 9M from Loop 13. 1285°F; 2238 hr.

ORNL-DWG 65-12289

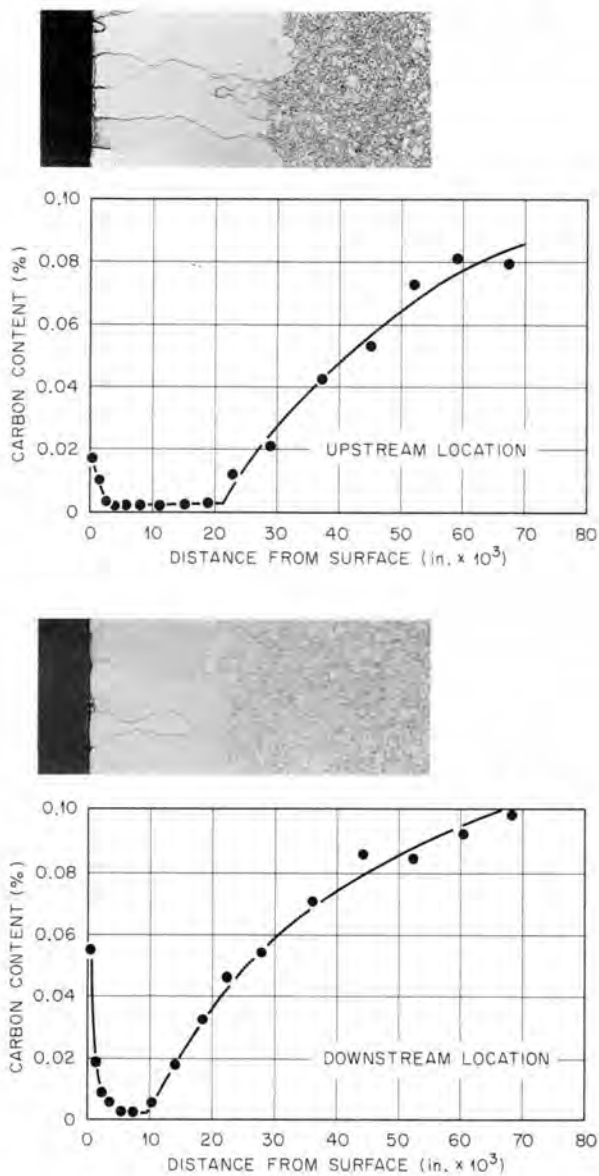


Fig. 31. Carbon Profile Curves for Croloy 9M from Loop 9. 1283°F; 2476 hr.

ORNL-DWG 65-12290

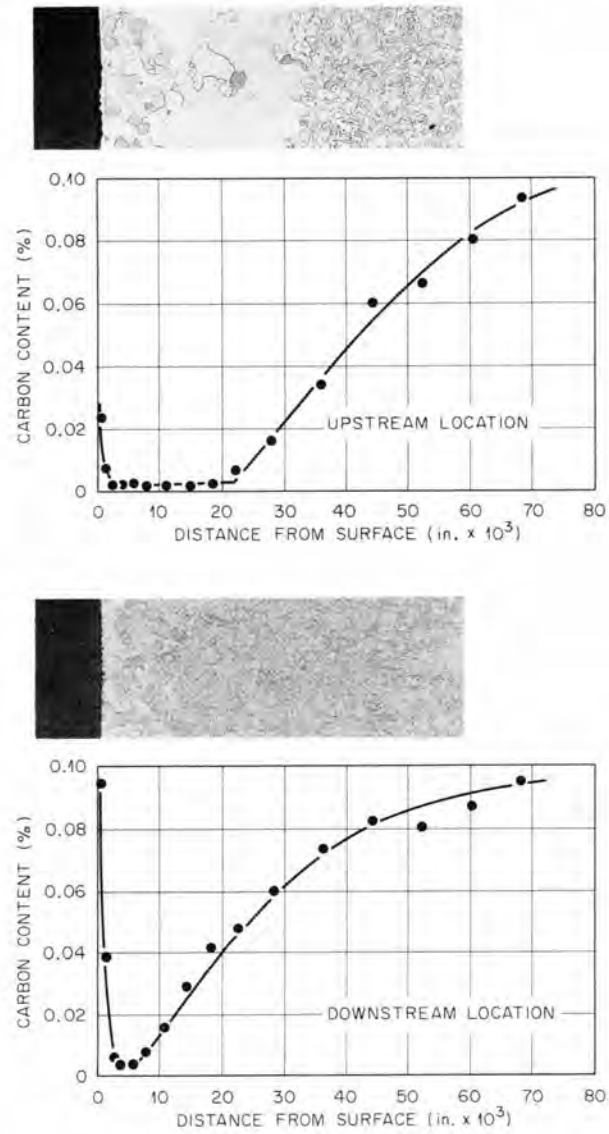


Fig. 32. Carbon Profile Curves for Croloy 9M from Loop 7. 1266° F; 2705 hr.

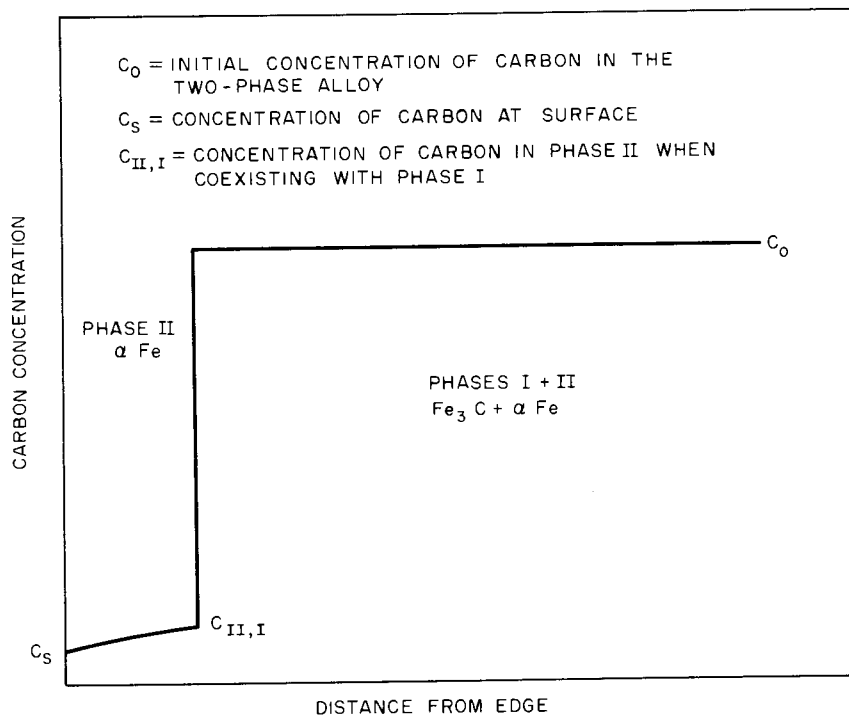


Fig. 33. Decarburization in Two-Phase Fe-C Alloys.

Within the scatter of the carbon analysis data it is possible to show that the extent of decarburization was very dependent on temperature and time of exposure. Furthermore, the extent of carbon migration does not appear to be increased by the injection of hydrogen into the loop. These effects can be seen by comparison of the various carbon profile curves presented in Figs. 24 through 32 and the posttest carbon analysis data reported in Table 11. It is not clear whether or not oxygen exerted any significant influence on either the character or extent of carbon transfer. The method of analysis and the control of extraneous variables, such as the as-received carbon content, were not sufficiently sensitive to justify any definite conclusions regarding this variable.

Effect of Carbon Transfer on Material Properties

The transfer of carbon around the system has various effects, depending on both the direction and extent of migration. Materials receiving carbon - Hastelloy N, Hastelloy C, 347 stainless steel, and 316 stainless steel - become stronger but less ductile with increasing carbon concentration. The hot regions of the Croloy 9M that lose carbon lose strength and become more ductile. The degree of change in properties associated with the materials receiving carbon has not been ascertained,

but considering the large amount of ductility normally present in these materials and the low stresses normally encountered in design, it seems unlikely that serious damage would result. The very large loss of carbon and the rather drastic effects on the microstructure of the decarburized Croloy 9M, however, suggested significant mechanical property deterioration. Accordingly, a test program was initiated to determine the magnitude of damage resulting from the decarburized conditions imposed by the loop exposure. As part of this program, a modified grade of Croloy 9M was also included, since this material was being considered as a backup material for the standard Croloy 9M. In general, these tests showed that significant loss of strength occurred for both grades of material as a result of decarburization. However, the modified Croloy 9M appeared to have significantly better properties after decarburization than the standard Croloy 9M. The data and a description of the test program are presented in the section entitled "Mechanical Properties of Decarburized Croloy 9M."

Effect of Decarburization on Microstructure of Croloy 9M

The rather extensive decarburization occurring in Croloy 9M produced considerable changes in the microstructure of this material. The most pronounced effect was the growth of tremendously large grains, such as depicted in Fig. 26. In some instances, very mixed grain sizes occurred, as revealed by the microstructure in Fig. 32; and in several cases, a relatively uniform small amount of grain growth occurred, as indicated in Fig. 28. The smaller grains and mixed grains appeared to be more associated with instances of relatively milder degrees of decarburization, such as that occurring at 1285°F, as compared with that occurring at 1385°F; however, there were exceptions to this. In general, the area of grain growth extended to depths where decarburization had reduced the carbon concentration from 0.11 to 0.02-0.06%. High magnification (500X) examination of the large-grain regions showed a complete absence of carbide particles except in the areas near the region of transition from large to small grains. Grain growth occurred in this region even though some carbide particles still remained within the grains. The preferential removal of carbides from the grain boundaries probably accounts for this, since the carbon would be removed more rapidly along grain boundary paths than across the grains. Once the carbides were removed from the grain boundaries, grain growth could proceed.

PHASE IDENTIFICATION STUDIES

Metallographic examination of the types 347 and 316 stainless steel insert specimens exposed 2000 hr at 1300°F or higher in all the loops has revealed the presence of several metallurgical phases not originally present in the as-received microstructures. It is generally known that long-time exposure at 1300°F can cause reduction of ductility resulting from precipitation of such phases as sigma, chi, and metal carbides. The occurrence of these phases would depend on the existing chemical balance

in the alloy. To ascertain the presence of these structures, several identification methods were employed, such as selective etching and selective extraction of precipitates. The etchant technique involved the use of dilute and concentrated solutions of Murakami's reagents, as described by Emmanuel.⁸ These reagents indicated the presence of both carbide and sigma-phase structures in types 347 and 316 stainless steel exposed at 1400°F. In type 347 stainless steel specimens (see Fig. 34), the phase indicated as carbides occurred in the portion of the specimen nearest the surface that had been exposed to NaK, and the phase indicated as sigma occurred in the other portion. Since the specimens were undergoing carburization through the surface exposed to NaK, the apparent separation of phases indicated that carbon enrichment was causing decomposition of sigma-phase material. This is consistent with the general theory regarding sigma phase in austenitic stainless steels. The carbon acts as an austenite stabilizer. It also removes the chromium from the matrix by formation of chromium carbides, and thus it further affects the matrix composition in favor of sigma-phase decomposition.

The selective extraction technique used for identification of the phases present in type 347 stainless steel involved the use of an electrolytic solution of FeCl_3 , as described by Barnett.⁹ A sample of metal was dissolved, and the particulate phases were collected by centrifuge separation. X-ray diffraction analysis of the extracted phases showed



Fig. 34. Carbides (Dark Particles) and Sigma Phase (Light-Gray Particles) in Type 347 Stainless Steel Exposed to NaK at 1400°F for 5828 hr. Specimen 5, loop 5. Surface exposed to NaK is at right side of photograph.

the presence of austenite, Cr_7C_3 , $(\text{Fe,Cr})_{23}\text{C}_6$, and sigma phase. Similar analysis of type 316 stainless steel failed to reveal the presence of sigma phase, but showed both carbides. There was also a weak unknown structure apparent in both alloys.

MECHANICAL PROPERTIES OF DECARBURIZED CROLOY 9M

The primary objective of this work was to determine qualitatively and inexpensively if the mechanical properties of Croloy 9M deteriorate significantly due to the decarburization encountered in the corrosion loop tests. Additional objectives included: (1) determining if prior heat-treat condition had any effect on the properties of the decarburized material, and (2) determining if modified Croloy 9M offered any advantage over standard Croloy 9M in the decarburized condition.

Procedure

Materials

The materials evaluated (compositions reported in Table 12) were received as sheet stock 0.060 in. thick (standard 9M) and sheet stock 0.090 in. thick (modified 9M), which were subsequently cold rolled to

Table 12. Chemical Compositions of Materials Used in Decarburization Studies

Element	Standard Croloy 9M (wt %)	Modified Croloy 9M (wt %)
Chromium	9.10	8.65
Molybdenum	0.86	1.03
Niobium		0.045
Zirconium		
Vanadium		0.25
Manganese	0.53	0.55
Nitrogen		0.053
Boron		
Silicon	0.90	0.47
Phosphorus	0.014	0.012
Sulfur	0.005	0.011
Carbon	0.14	0.14

a thickness of 0.030 in. After the appropriate heat treatments, the materials were cut into specimen blanks which were either exposed to the decarburizing environment or to the same thermal environment in argon for use as control material. Some specimen blanks were also used to determine the tensile properties of the as-heat-treated materials.

The carbon analysis data for the decarburized specimens are reported for each specimen in Table 13. The carbon content of specimens given the control exposure was unchanged from that reported in Table 12 for the as-received materials.

Method of Decarburization

Decarburization was performed by exposing the specimen blanks (5 × 0.75 × 0.030 in.) in a small-volume (85-in.³) isothermal NaK loop at 1425°F for 400 hr. The loop had a 316 stainless steel-to-Croloy 9M surface area ratio of about 3:1, and contained an in-line zirconium hot trap. The specimen holder accommodated 20 specimen blanks arranged in a matrix of five evenly spaced columns with 4 specimen blanks per column.

Table 13. Carbon Content of Decarburized Test Specimens

Standard Croloy 9M				Modified Croloy 9M			
Prior Heat-Treat Condition	Type of Test	Temperature (°F)	Carbon Content (%)	Prior Heat-Treat Condition	Type of Test	Temperature (°F)	Carbon Content (%)
Annealed	Tensile	78	0.008	1700°F-normalized	Tensile	78	0.005
Annealed	Tensile	500	0.007	1700°F-normalized	Tensile	1100	0.008
Annealed	Tensile	1100	0.005	1700°F-normalized	Tensile	1300	0.005
Annealed	Tensile	1300	0.004	1700°F-normalized	Tensile	1300	0.005
Annealed	Tensile	1400	0.004	1700°F-normalized	Strain rate	1100	0.007
Annealed	Strain rate	1100	0.007	1700°F-normalized	Strain rate	1300	0.005
Annealed	Strain rate	1300	0.004	1700°F-normalized	Strain rate	1400	0.004
Annealed	Strain rate	1400	0.003	1700°F-normalized	Creep rupture	1325 (2250) ^a	0.007
1700°F-normalized	Strain rate	1100	0.005	1700°F-normalized	Creep rupture	1325 (3500)	0.006
1700°F-normalized	Strain rate	1300	0.003	1700°F-normalized	Creep rupture	1325 (6000)	0.006
1700°F-normalized	Strain rate	1400	0.005	2000°F-normalized	Strain rate	1100	0.005
2000°F-normalized	Strain rate	1100	0.004	2000°F-normalized	Strain rate	1300	0.007
2000°F-normalized	Strain rate	1300	0.004	2000°F-normalized	Strain rate	1400	0.007
2000°F-normalized	Strain rate	1400	0.003	2000°F-normalized	Strain rate		

^aNumbers in parentheses represent stress levels used during creep-rupture tests.

Flow straighteners 5 in. long and fabricated from 316 stainless steel were placed at each end of the specimen holder to ensure a uniform flow of 90 fpm over all surfaces of the specimen blanks.

A new loop was constructed for each of the two batches of specimen blanks that were processed. The only portion of the first loop reused in the second loop was the specimen holder.

Tensile Tests

Tensile test specimens of 2 in. gage length and 1/4 in. gage width were made from the specimen blanks after they were given the treatments described above. These tests were performed in a standard Instron machine at a strain rate of 0.6 in. in.⁻¹ hr⁻¹. All tensile tests were done in air, the specimen being heated to the test temperature by a resistance-wound tube furnace.

Strain Rate Tests

The stresses to produce strain rates of 0.06, 0.15, 0.6, and 1.5 in. in.⁻¹ hr⁻¹ were determined at 1100, 1300, and 1400°F by changing the strain rate during tensile tests and observing the stress level associated with each particular strain rate. These tests were also performed in air in a standard Instron machine using the same specimen configuration.

Creep-Rupture Tests

Stress-rupture tests using tensile-type specimens were performed in a static argon environment at 1325°F. Zirconium getters were used to remove any oxygen present in the argon.

Results of Mechanical Property Tests

Tensile Tests

The results of tensile tests are reported in Tables 14 and 15. These data show that the tensile strength of both modified and standard Croloy 9M is significantly lowered at all temperatures as a result of decarburization. The data at 78°F in Table 15 also show that a significant reduction in tensile strength occurs as a result of the thermal exposure itself (compare as-heat-treated to control specimen).

The data for both alloys are also presented in Table 16 for comparison. There appears to be no significant difference in the tensile properties of the materials except at room temperature, where the data indicate somewhat lower strength for modified 9M.

Table 14. Tensile Properties of Fully Annealed^a Standard Croloy 9M Showing Effect of Decarburization

Test Temperature (°F)	Material Condition	Ultimate Strength (ksi)	0.2% Yield Strength (ksi)	Elongation (%)
78	Control ^b	71.2	45.3	27.8
78	Decarburized ^c	51.1	35.5	28.9
500	Control	64.9	34.6	19.6
500	Decarburized	48.9	24.5	22.0
1100	Control	27.6	19.1	63.0
1100	Decarburized	22.0	16.3	30.5
1300	Control	10.2	9.6	80.7
1300	Decarburized	8.1	7.8	53.2
1400	Control	6.1	5.8	90.0
1400	Decarburized	4.3	3.9	72.3

^a1500°F anneal followed by 50°F/hr cool to 1300°F, plus air cool to room temperature.

^bExposed 400 hr at 1425°F in argon.

^cExposed 400 hr at 1425°F in NaK/316 stainless steel loop.

Table 15. Tensile Properties of Normalized^a Modified Croloy 9M Showing Effect of Decarburization

Test Temperature (°F)	Material Condition	Ultimate Strength (ksi)	0.2% Yield Strength (ksi)	Elongation (%)
78	As heat-treated	118.5	96.5	12.8
78	Control ^b	92.1	65.7	13.0
78	Decarburized ^c	39.5	29.2	30.6
1100	Control	41.1	37.0	33.5
1100	Decarburized	22.4	13.4	31.0
1300	Control	14.5	11.9	34.0
1300	Decarburized	7.4	7.0	54.0

^aNormalized at 1700°F, tempered at 1350°F.

^bExposed 400 hr at 1425°F in argon.

^cExposed 400 hr at 1425°F in NaK/316 stainless steel loop.

Strain Rate Tests

The data from the strain rate tests for each material are presented in Figs. 35 through 39. These data clearly show that decarburization significantly reduces the strength of both materials regardless of prior heat-treat condition. Cross plots of these data were also made to determine if prior heat treatment affected the degree of strength reduction. The data for modified 9M, Fig. 40, indicated that material normalized at 1700°F was superior at all temperatures to that normalized at 2000°F. However, the data for standard 9M, Fig. 41, indicated that the 2000°F-normalized was superior to both the 1700°F-normalized and the fully annealed material. Material normalized at 1700°F was superior to fully annealed material at 1100 and 1400°F, but the reverse occurred at 1300°F.

Table 16. Comparison of Modified 9M and Standard 9M Tensile Strength After Decarburization

Temperature (°F)	Ultimate Strength (ksi)		0.2% Yield Strength (ksi)	
	Standard 9M ^a	Modified 9M ^b	Standard 9M	Modified 9M
78	51.1	39.5	35.5	29.2
1100	22.0	22.4	16.3	13.4
1300	8.1	7.4	7.8	7.0

^aFully annealed.

^bNormalized at 1700°F, tempered at 1350°F.

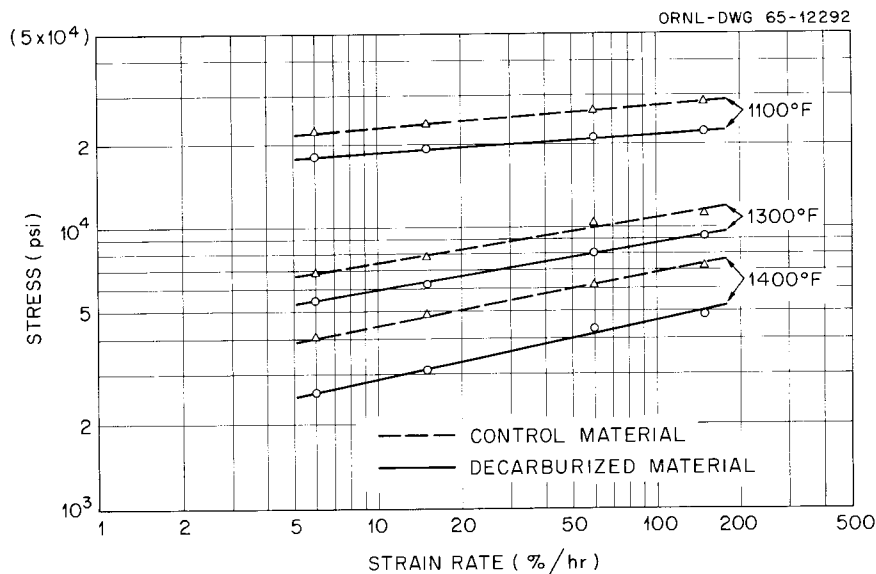


Fig. 35. Effect of Decarburization on Strain-Rate Properties of Standard Croloy 9M - Fully Annealed.

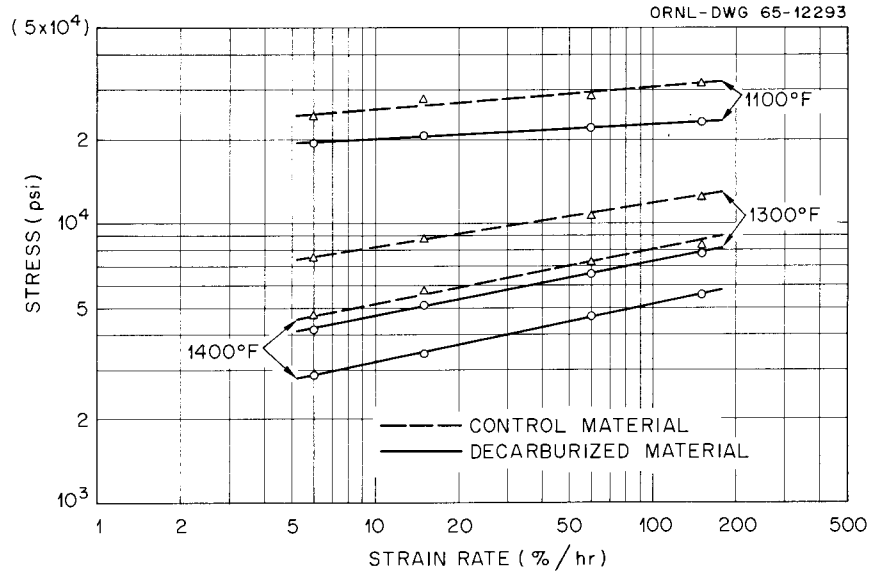


Fig. 36. Effect of Decarburization on Strain-Rate Properties of Standard Croloy 9M - Normalized at 1700°F.

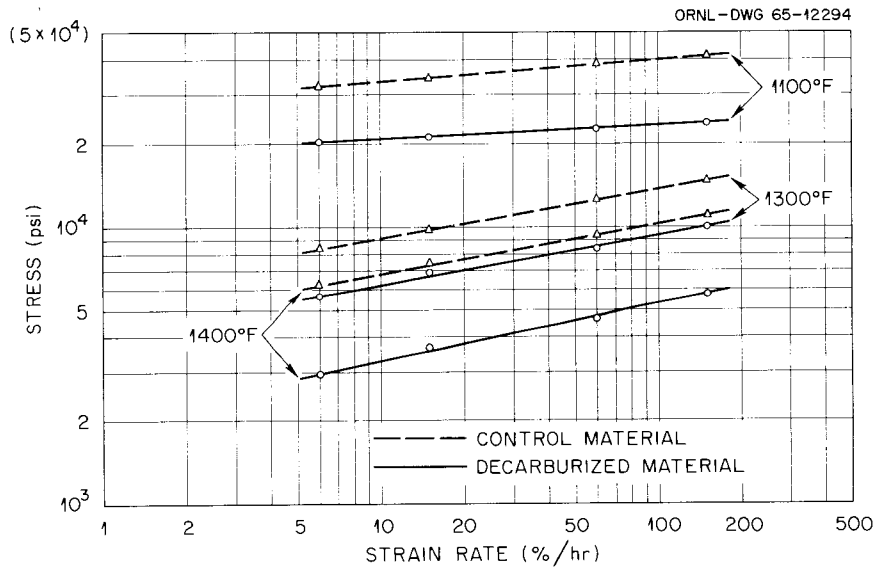


Fig. 37. Effect of Decarburization on Strain-Rate Properties of Standard Croloy 9M - Normalized at 2000°F.

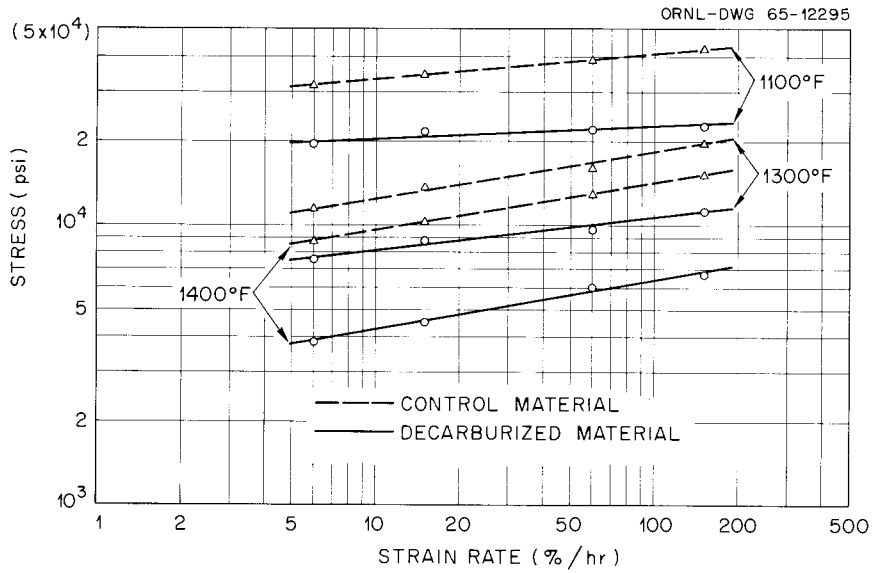


Fig. 38. Effect of Decarburization on Strain-Rate Properties of Modified Croloy 9M — Normalized at 1700°F.

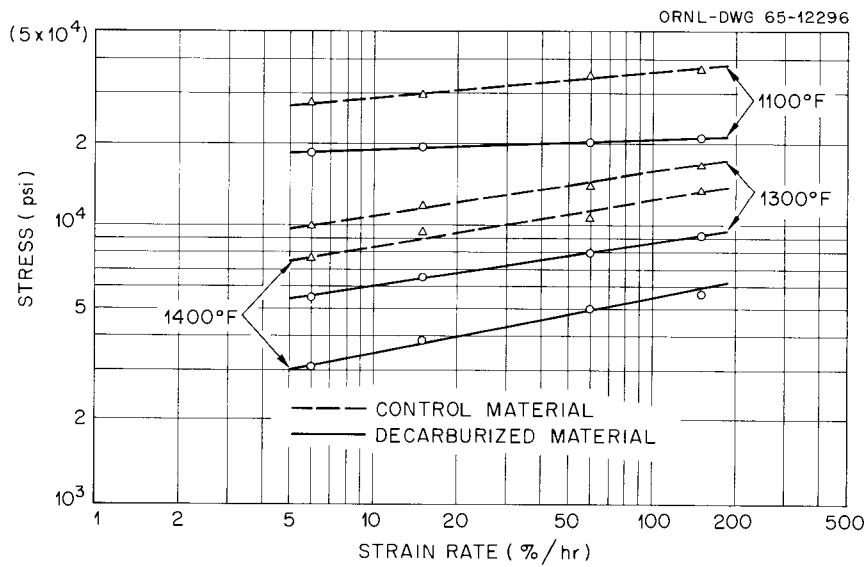


Fig. 39. Effect of Decarburization on Strain-Rate Properties of Modified Croloy 9M — Normalized at 2000°F.

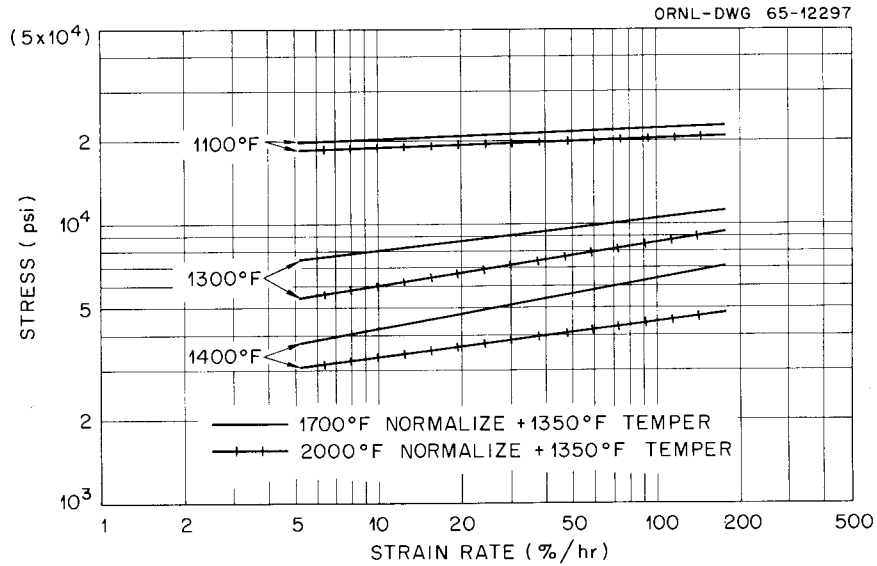


Fig. 40. Effect of Prior Heat Treatment on Strain-Rate Properties of Decarburized Modified Croloy 9M.

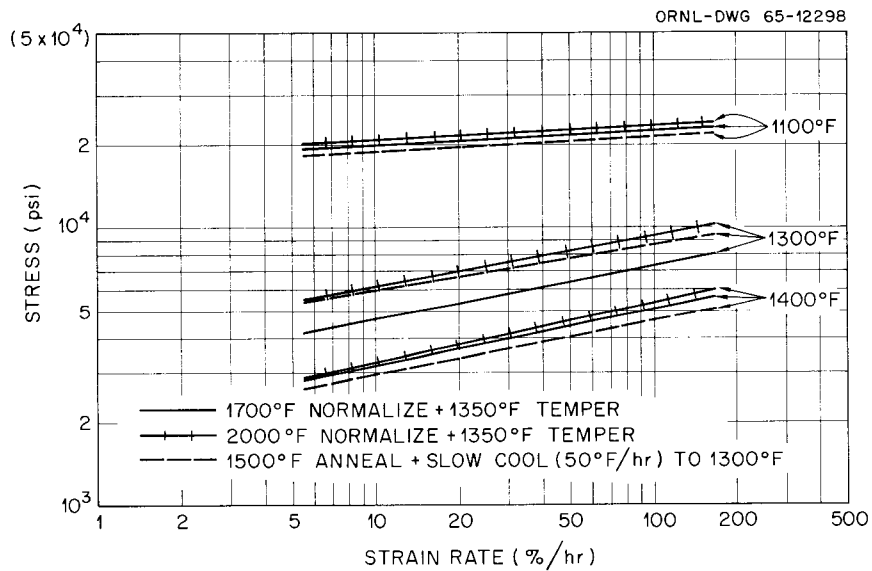


Fig. 41. Effect of Prior Heat Treatment on Strain-Rate Properties of Standard Croloy 9M - Decarburized.

Comparison of the decarburized alloys presented in Fig. 42 shows that modified Croloy 9M (normalized at 1700°F) offers some advantage over standard Croloy 9M (normalized at 2000°F) at both 1300 and 1400°F. At 1100°F there appears to be no significant difference between the materials.

In addition to the above, minimum creep-rate data from creep-rupture tests were determined for modified 9M normalized at 1700°F and standard 9M fully annealed. The data are presented in Table 17. These data plus those from the strain-rate tests were used in constructing the Dorn parameter curves presented in Figs. 43 through 45. Agreement between the strain-rate data and creep-rate data is very good in all cases except for the decarburized modified 9M. The two data points which fall below the curve in Fig. 45 were from rather short creep-rupture tests in which the measurement of the minimum creep rate was considered to be subject to error. The minimum creep rate determined from the long-time (728 hr) creep-rupture test agreed very well with the rest of the strain-rate data.

It should be noted that the apparent activation energies for creep of these materials varied from 54,000 cal/mole to about 135,000 cal/mole. This result is somewhat unusual, since it would seem reasonable that the same activation energy would prevail for all the materials because of their basic similarities.

Creep-Rupture Tests

The data from these tests are presented in Table 17 and in Fig. 46. These results also show that decarburized modified 9M has somewhat greater rupture strength than decarburized standard 9M under creep conditions.

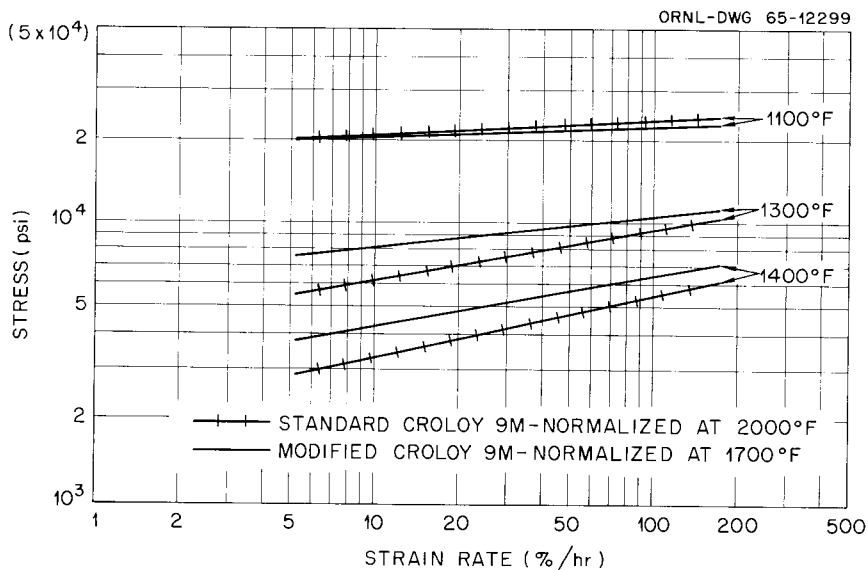


Fig. 42. Comparison of Alloys Based on Strain-Rate Properties of Decarburized Materials.

Table 17. Creep-Rupture Test Data at 1325°F

Material	Condition	Stress (psi)	Rupture Life (hr)	Minimum Creep Rate (in. in. ⁻¹ hr ⁻¹)
Modified 9M	Control	10,000	4.6	
Modified 9M	Control	6,500	41.9	2.3×10^{-3}
Modified 9M	Control	4,000	519	1.4×10^{-4}
Modified 9M	Decarburized	6,000	2.7	2.3×10^{-4}
Modified 9M	Decarburized	3,500	42.5	7.2×10^{-3}
Modified 9M	Decarburized	2,250	728	1.4×10^{-1}
Standard 9M	Control	2,500	750	2.0×10^{-4}
Standard 9M	Control	2,000	2400	1.3×10^{-4}
Standard 9M	Decarburized	2,500	135	3.4×10^{-3}
Standard 9M	Decarburized	2,100	100	
Standard 9M	Decarburized	2,000	250	1.4×10^{-3}
Standard 9M	Decarburized	1,000	2000	1.4×10^{-4}

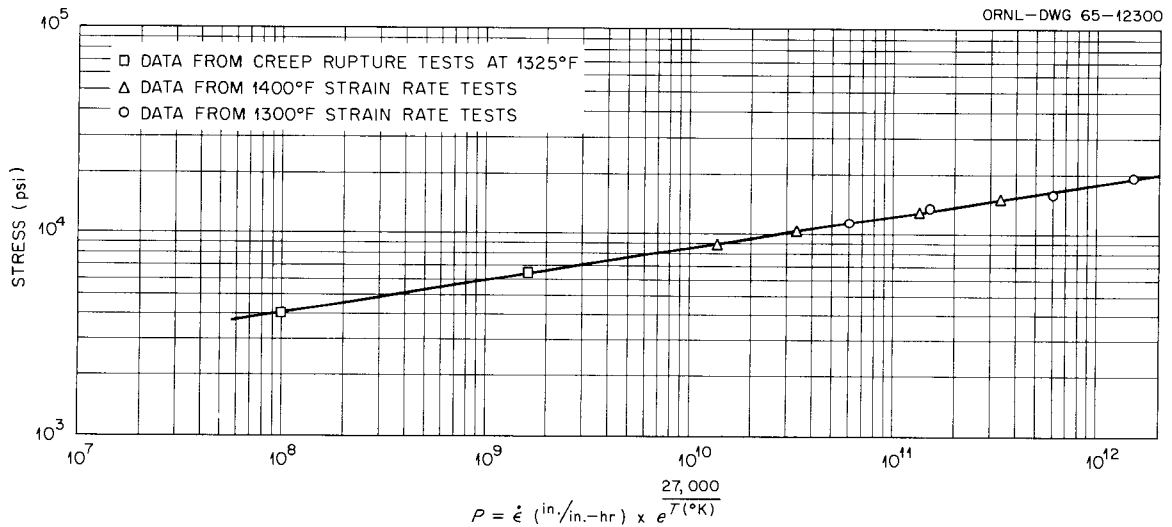


Fig. 43. Dorn Parameter Curve for Strain-Rate Properties of Modified Croloy 9M Control Material - Normalized at 1700°F.

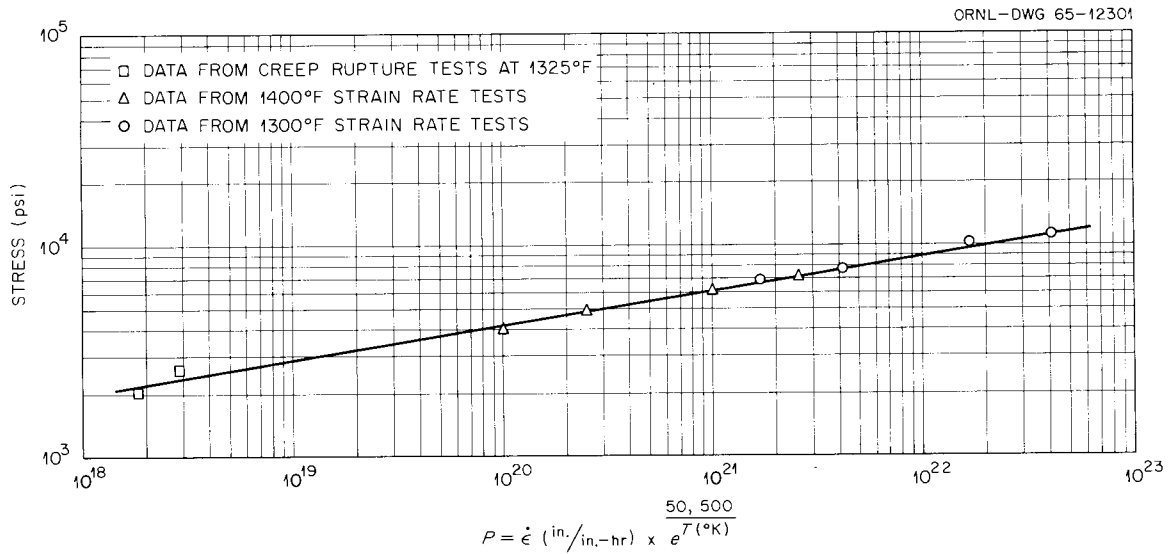


Fig. 44. Dorn Parameter Curve for Strain-Rate Properties of Standard Croloy 9M Control Material -- Fully Annealed.

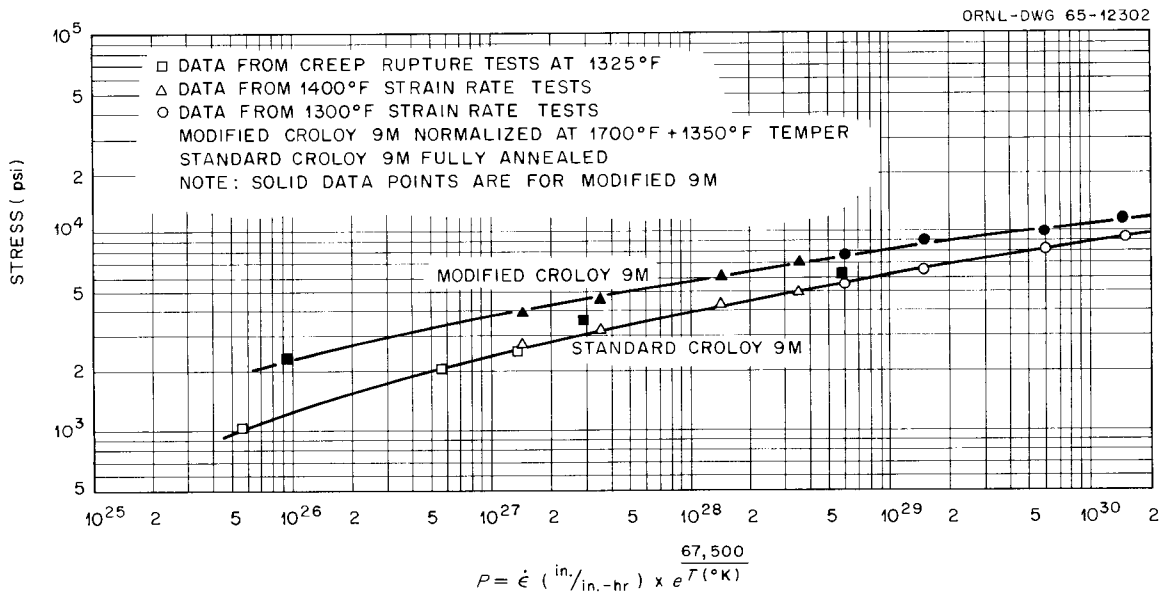


Fig. 45. Dorn Parameter Curves for Strain-Rate Properties of Decarburized Modified and Standard Croloy 9M.

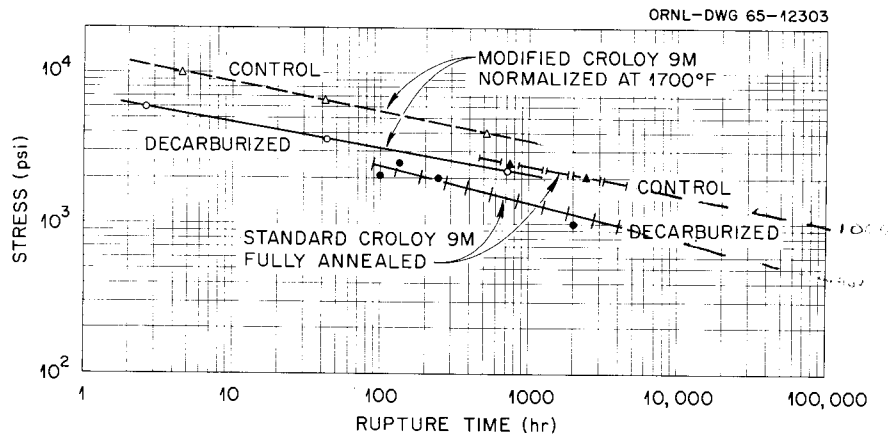


Fig. 46. Effect of Decarburization on Stress-Rupture Properties of Standard and Modified Croloy 9M at 1325°F.

DISCUSSION AND CONCLUSIONS

The relatively small number of data (no duplicate test points) gathered on just one heat of each material necessarily imposes limits on the validity of conclusions reached. It is believed, however, that the foregoing data firmly establish that decarburization to 0.002–0.008% carbon content causes a rather marked deterioration in both the tensile strength and creep strength of modified and standard Croloy 9M. With less certainty, the data also suggest that modified Croloy 9M retains more creep resistance after decarburization than standard Croloy 9M does.

The scatter of the data is believed to be too large to justify any definite statements regarding the effect of prior heat-treat conditions on the strength subsequent to decarburization.

REFERENCES

1. Hereafter, this will be referred to as Hastelloy N. A discussion of the chromizing effects on mass transfer can be found in Appendix E.
2. Paper presented by R. W. Lockhart and K. S. Young, General Electric Co., San Jose, Calif., at the AEC Sodium Components Development Program Information Meeting at Chicago, June 16, 1965.
3. Proceedings of the NASA-AEC Liquid Metals Corrosion Meetings, Oct. 2-3, 1963, vol. I, NASA SP-41 (Oct. 23, 1963), pp. 214-15.
4. Proceedings of the NASA-AEC Liquid Metals Corrosion Meetings, Oct. 2-3, 1963, vol. I, NASA SP-41, pp. 22-26.
5. L. R. Kelman, W. D. Wilkinson, and F. L. Yaggee, ANL-4417.
6. Private communications, 1955.
7. W. Jost, Diffusion in Solids, Liquids, and Gases, pp. 68-78, Academic, New York, 1960.
8. G. M. Emmanuel, Metal Progr. 53, 78-79 (1947).
9. W. J. Barnett, Metal Progr. 53, 366-67 (1948).

Chemistry Studies

E. L. Compere J. E. Savolainen
H. C. Savage T. H. Mauney
 J. M. Baker

INTRODUCTION

The anticipated entry of hydrogen from uranium-zirconium hydride fuel elements into the NaK circulating in the SNAP-8 reactor primary coolant circuit introduces a number of questions concerned with the fate of the hydrogen and the effects to be anticipated from its presence. Preliminary analysis indicates that much of the hydrogen will be lost through the walls containing the primary coolant, including loss into the mercury boiler system.

A hydrogen steady state will be established in the primary coolant system after a short time. In the absence of bubbles or precipitates, the hydrogen will be entirely in dissolved form in the NaK. Bubbles may be prevented by sufficient overpressure. Precipitation, as alkali metal hydride, will depend on the temperature and on the concentration of dissolved hydrogen. Precipitation is not anticipated at mainstream NaK temperatures of 1100 to 1300°F; however, it might occur in cold traps, cold dead legs, or in cooled internal regions of the pump. Therefore, in order to establish the nature and limits of the problem of hydrogen in SNAP-8 NaK, it is necessary to determine phase equilibria in the hydrogen-sodium-potassium system over relevant ranges of temperature, pressure, and associated composition.

Since the hydrogen of the primary system is expected to be dissolved in NaK, we need to know if this will affect its permeation characteristics. The dissolved species, which could be hydrogen atoms or alkali metal hydride, might find that entry into the solid metal is controlled by factors different from those affecting entry from the gas phase. The only permeation data available have been with hydrogen from the gas phase. Consequently, measurements comparing permeation of gaseous hydrogen and hydrogen dissolved in NaK are indicated.

In the permeation studies described below, the first studies considered the permeation of hydrogen through Hastelloy N from the gas phase, and in the presence of NaK in a tilting cell, at 1 atm upstream pressure and temperatures as low as 660°F and as high as 1425°F. Both tilting and the improved iron thimble cells were used for Croloy 9M, with gas-phase

hydrogen pressures from 1 atm down to 23 mm and with temperatures of 1000, 1100, and 1300°F.

The studies were conducted using both type I (tilting) and especially the iron thimble (type II) cell, in the presence and absence of NaK. A pressure range from 1 atm to below 1 mm was covered, at temperatures of 1000, 1100, and 1300°F. The permeation rate of deuterium was compared with that of hydrogen. Observations of the transient effect on permeation rate of brief downstream oxidation of the permeation cell were made.

In the solubility studies described below, the amounts of hydrogen absorbed by NaK at various pressures were observed at temperatures of 1300, 1100, 1000, 752, 626, and 572°F. Pressures ranging from a few millimeters to 1 atm were employed. At 1000°F and higher, only unsaturated solutions were encountered, while at 752°F and below, precipitation of alkali metal hydride was indicated as saturation pressures were exceeded. Exploratory studies of NaK solutions containing small proportions of lithium metal, added to reduce terminal hydrogen solubility, were conducted. Calculations, based on inventory, were verified in each experiment by chemical analysis.

Calculations of hydrogen effects in the SNAP-8 primary coolant were made concerning steady-state pressure and the possibility of reducing the dissolved hydrogen concentration by cold trapping, hydrogen permeable windows, or solid or soluble getters.

MATERIALS AND GENERAL FACILITIES

Hydrogen

Hydrogen was obtained from commercial cylinders of high-purity hydrogen, and was further purified by passage through the heated palladium alloy diaphragm of a model HPD 0-50 hydrogen purifier made by Englehard Industries, Inc. A typical analysis by mass spectrograph showed the following impurities: N₂ + CO, 320 ppm; H₂O, 430 ppm; CO₂, 50 ppm; O₂, <5 ppm; hydrocarbons, 130 ppm; Ar, not detected. In the solubility experiments and in the permeation experiments using the iron thimble cell, the hydrogen may have been further purified by passage through 0.020 in. or more of pure Armco iron.

Croloy 9M

Croloy 9M was used to fabricate permeation cells of both type I and the iron thimble design. A forging blank 7 in. in diameter by 2-1/4 in. thick of 9 chrome and 1 moly steel was furnished by the Thompson Ramo Wooldridge Corporation from stock understood to be obtained from the

Aerojet-General Corporation SNAP-8 program. Chemical analysis of this material (%) was as follows:

<u>Fe</u>	<u>Cr</u>	<u>Mo</u>	<u>Mn</u>	<u>C</u>	<u>Si</u>	<u>P</u>	<u>S</u>
Bal	8.55	0.97	0.5	0.12	0.68	0.015	0.17

Spectrographic analysis (%) showed:

<u>Al</u>	<u>Ni</u>	<u>Cu</u>	<u>Mn</u>	<u>V</u>	<u>Si</u>	<u>Co</u>
0.03	0.5	0.1	0.2	0.02	0.7	0.05

Hastelloy N

Hastelloy N was used to fabricate permeation cells for early studies. In order to avoid "stringer" problems associated with rod material, items were machined from forging blanks of heat Ni-5093 which originated from Haynes Stellite Company, Kokomo, Indiana. Analyses of the blanks are given below (%):

<u>Ni</u>	<u>Mo</u>	<u>Cr</u>	<u>Fe</u>	<u>Mn</u>	<u>V</u>	<u>W</u>	<u>B</u>	<u>Cb + Ta</u>
Bal	15.71	7.64	3.70	0.62	0.37	0.25	0.004	Nd
Bal	15.31	7.71	3.80	0.60	0.41	0.35	0.002	Nd
<u>Si</u>	<u>C</u>	<u>P</u>	<u>S</u>	<u>N</u>	<u>Al</u>	<u>Ti</u>	<u>Cu</u>	
0.68	0.07	0.001	0.008	Nd	0.01	0.01	0.02	
0.44	0.06	0.011	0.008	Nd	0.01	0.01	0.02	

Nd = none detected.

Type 316 Stainless Steel

This material was obtained as bar stock from the local supply. Metallographic examination revealed normal amounts of stringers, characteristic of this material, parallel to the extrusion axis. Consequently, when this material was used to fabricate permeation cells of either type, the diffusion disk was machined so that its plane was parallel to the extrusion (and stringer) axis. The stringers in consequence were across rather than through the disk and should not contribute unduly to the passage of hydrogen. Analysis of the type 316 stainless steel (%) is as follows:

<u>Fe</u>	<u>Cr</u>	<u>Ni</u>	<u>Mo</u>	<u>Mn</u>	<u>Si</u>	<u>C</u>	<u>S</u>	<u>P</u>
Bal	17.45	12.17	2.60	1.82	0.34	0.054	0.018	0.02

Armco Iron

The capsules for containing the NaK and some components of type II permeation cells were made of Armco iron obtained from the Corey Steel Company, Chicago, Illinois. All the 3/4-in. rod material was from a single heat, No. 3056, which had the following certified analysis (%):

<u>Fe</u>	<u>C</u>	<u>Mn</u>	<u>P</u>	<u>S</u>	<u>Si</u>	<u>Cu</u>
Bal	0.021	0.036	0.005	0.014	0.004	0.080

NaK-78

The NaK used was part of a 550-lb batch of eutectic sodium-potassium alloy obtained from MSA Research Corporation, Callery, Pennsylvania. Analysis of this batch as shipped was:

<u>%</u>		<u>ppm</u>							
<u>Na</u>	<u>K</u>	<u>C</u>	<u>O</u>	<u>Li</u>	<u>Cs</u>	<u>Rb</u>	<u>Mg</u>	<u>Ca</u>	<u>Si</u>
Bal	77.3	29	3	0.1	<20	3	2	10	15
	77.9	31	10				1	3	<10
		46	7				<1	5	<10
							10		

(Fe, B, Co, Al, Pb, Cr, Ti, Ni, Mo, V - each <10 ppm; Zr <10; Ba <3; Cu <2; Mn, Sn, Be, Ag, Sr - each <1 ppm).

The NaK was blown, using an inert gas, by siphon into a stainless steel tank. It was kept there at room temperature under helium pressurization. Lines led from the tank through sintered stainless steel filters of nominal 20- and 5- μ pore sizes to an outlet in an inert-atmosphere glove box. The filters served to keep the delivered liquid free of any precipitated oxide or hydride or other solids.

When NaK was to be used, the line was first flushed and some NaK placed in a wide dish. It was required that NaK in the dish retain a bright surface during the period in which any operations involving exposure of NaK to the box atmosphere were conducted.

Lithium

Lithium was obtained from the Metals and Ceramics Division from a large-volume supply which originated from the Maywood Chemical Works. A typical analysis of this metal supplied by the manufacturer is Na, 0.015-0.015; K, 0.06-0.07; Ca, 0.0001; Fe, 0.0005; Al, 0.0005; Si, 0.001; Cl, 0.04; N, 0.012; and Li, 99.88%.

Lithium was withdrawn without contact with the atmosphere from the large-volume supply into stainless steel tubes, which were sealed by crimping and welding. The tubes were opened in the inert-atmosphere glove box, and lithium from the middle sections was transferred into an extrusion chamber. A length of the approximate desired mass could be extruded as a wire into a weighed metal capsule containing NaK, which was then weighed again, plugged, and welded closed.

Inert-Atmosphere Glove Box

All operations involving the handling of alkali metals were conducted in a large (25 ft³) inert-atmosphere glove box. This box was constructed of stainless steel. Windows were covered with safety glass. Four apertures in the box were fitted with butyl rubber gloves and could be covered with metal plates when not in use.

The box wall was penetrated by connections for Heliarc welding apparatus. The box also had standard electrical outlets. To one end of the box was attached a 13-in.-diam by 2-ft vacuum loading port. All items put into the box were normally subjected to overnight (16-hr) vacuum with a final steady pressure of 15 μ in the loading port before being passed into the glove box.

It was possible to recirculate the box atmosphere through drying columns, displacing the box atmosphere approximately every 1-1/2 hr. Columns of heated calcium chips, cold traps using molecular sieves or charcoal at liquid-nitrogen temperature, and other devices were used to maintain the box atmosphere at very low moisture content.

The original air in the box was displaced by inflating in it a large plastic bag and then replacing the air with very dry helium. The lowest moisture content values were obtained when the helium was bubbled through a beaker of NaK and then through a layer of fiber glass.

A bubbler maintained a moderate positive pressure on the box and permitted a slight continuous purge of the box atmosphere by incoming helium.

In addition, during NaK-handling operations, the brightness of the surface of a dish of NaK served as a direct monitor of the inertness of the box atmosphere.

At 20 ppm moisture, as determined on a Beckman electrolytic hygrometer, an initially bright NaK surface became coated with a heavy scum in a few minutes. At a moisture level of 1 ppm, as determined by mass spectrographic analysis of the box atmosphere, a fresh exposed NaK surface remained bright for at least 15 min. During actual operations, the moisture level was such that the NaK pool remained bright for half an hour or more. Thus sufficient time was available to permit such operations as loading NaK, weighing, and welding the experimental apparatus closed.

EXPERIMENTAL COMPARISON OF PERMEATION THROUGH METALS OF
HYDROGEN FROM THE GAS PHASE AND HYDROGEN DISSOLVED IN NaK

As indicated in the introduction, a primary purpose of these studies was to determine whether the presence of NaK affected the permeation rate of hydrogen at relevant temperatures through metals of interest to the SNAP-8 program. Previous estimates of the diffusion rate have been based on literature values of permeation coefficients which were obtained for the diffusion of gaseous hydrogen through pure metals, usually with upstream pressures of the order of 1 atm and a Toepler pump vacuum ($\sim 10^{-5}$ atm) downstream. No information was available from the literature as to what effect the dissolution of hydrogen in the NaK would have on diffusion rates.

The permeation of hydrogen through clean metal at the design temperatures, without considering the presence of NaK, may be expressed as follows:

$$\frac{d(H_2)}{dt} = \frac{KA}{d} (P_1^{1/2} - P_2^{1/2}) ,$$

where $d(H_2)/dt$ is the hydrogen permeation rate [$\text{cm}^3(\text{STP})/\text{hr}$], A is the area (cm^2) of metal through which diffusion occurs, d is the metal thickness (mm), P_1 is the interior or upstream hydrogen pressure (atm), P_2 is the exterior or downstream hydrogen pressure (atm), and K is the permeability of the metal to hydrogen at a given temperature expressed in the above units. Values of K are available for the metals of the SNAP-8 system.¹⁻³

According to Barrer, the diffusion of hydrogen through metal oxides usually varies directly with the pressure difference, while hydrogen diffusion through pure metals is found to vary as the difference of the square roots of the respective upstream and downstream pressures. It follows that at low hydrogen partial pressures, oxide films may control the rate of diffusion. Such films should not persist in the SNAP-8 primary system; on the inside they would be reduced by the sodium-potassium alloy and on the outside by the diffusion of hydrogen.⁴ Only Cr_2O_3 might remain. During the interval of persistence of any oxide film, the hydrogen partial pressure in the SNAP-8 primary coolant system would be higher than when the metals were unoxidized. Precautions were taken in the experimental work to minimize the development of such films.

Our experimental work was aimed at comparing permeation characteristics of hydrogen in the absence and presence of NaK, through Hastelloy N, Croloy 9M, and type 316 stainless steel at temperatures of interest to the SNAP-8 system. In the original (type I) permeation cell, NaK was caused to be in contact with the diffusion diaphragm or separated from it by tilting the cell. Measurements were made using this type of cell in the presence and absence of NaK, with cells fabricated of Hastelloy N, Croloy 9M, and type 316 stainless steel. However, some distillation of NaK into hydrogen inlet lines was observed. To relieve this problem, a cell other-

wise similar but with a thin soft iron barrier between the diffusion diaphragm and the hydrogen inlet was fabricated. This iron thimble (type II) cell was used for measurements on type 316 stainless steel, both without NaK and with NaK in contact with the diaphragm contained between it and the iron thimble barrier. Measurements were also made without NaK in such a cell fabricated of Croloy 9M.

PERMEATION CELLS AND EXPERIMENTAL METHOD

The apparatus for measurement of the rate of permeation of hydrogen through metal diaphragms is shown in Figs. 1 to 4. This equipment closely resembled that used by other investigators in the field.^{2,3} However, provision was made for the system to contain liquid NaK, samples of which could be removed at the completion of the experiment.

Type I Cell

The permeation cell consisted of three parts: a central cylindrical section with the separating diaphragm and two end caps. The normal dia-

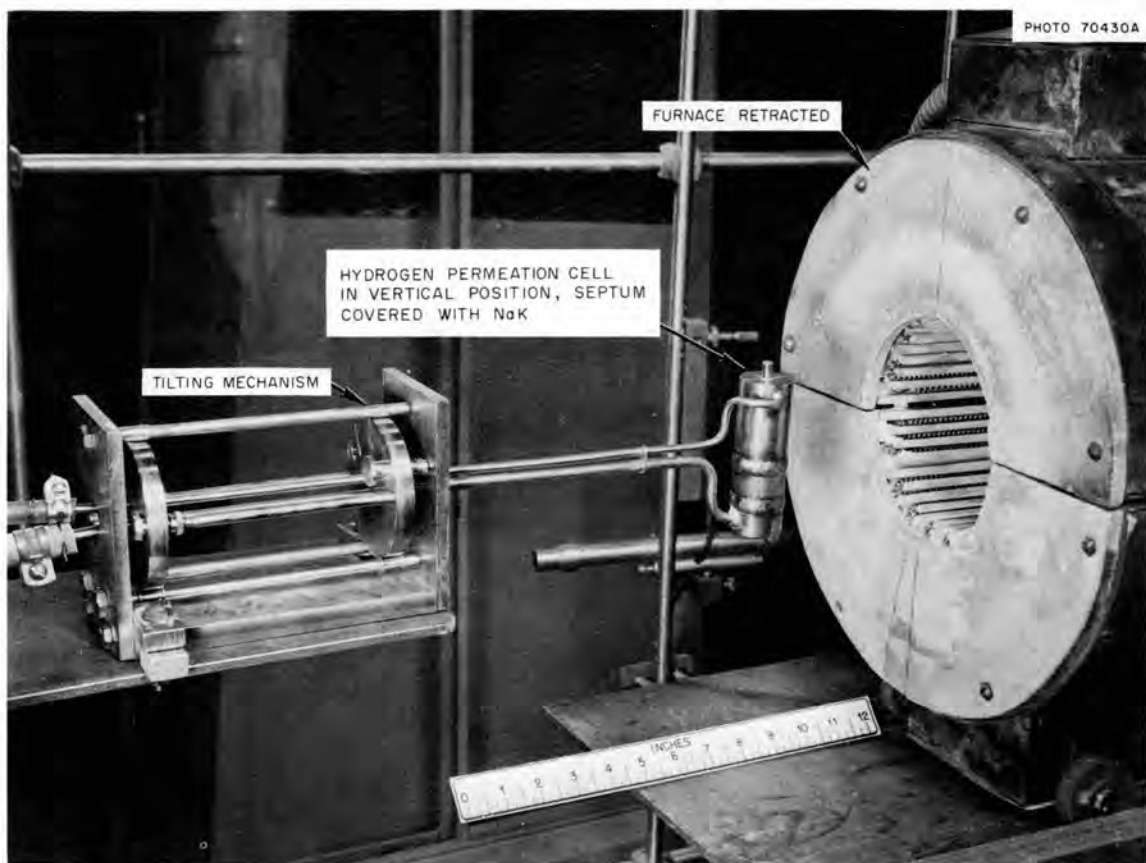


Fig. 1. Hydrogen Permeation Cell and Furnace.

phragm was 0.75 in. in diameter and 0.125 in. thick. The parts were machined from forgings when possible. In the case of type 316 stainless steel, the plane of the diaphragm was cut parallel to the direction of extrusion of the bar stock. The end caps, each with an attached tube, were welded to the central section. An additional short tube, which was welded closed, provided access for loading and removing NaK from the high-pressure side of the cell. During operation the cell, supported by the attached tubes, could be rotated 120° from the vertical position with the NaK completely covering the diaphragm to an inclined position with the diaphragm exposed only to the gas phase.

An experiment was conducted by appropriately cleaning and evacuating on both sides of the apparatus. Subsequently, the heated cell was alternately pressurized with a hydrogen atmosphere on both sides and evacuated to remove oxide films on the diaphragm as much as possible. After this had been done, the permeability of the diaphragm at various temperatures could be measured by placing a suitable pressure (about 1 atm) of hydrogen on the upstream side and a vacuum on the downstream side. In the case of type 316 stainless steel and also Croloy 9M, measurements were also made at several upstream pressure levels below 1 atm, in some cases of the order

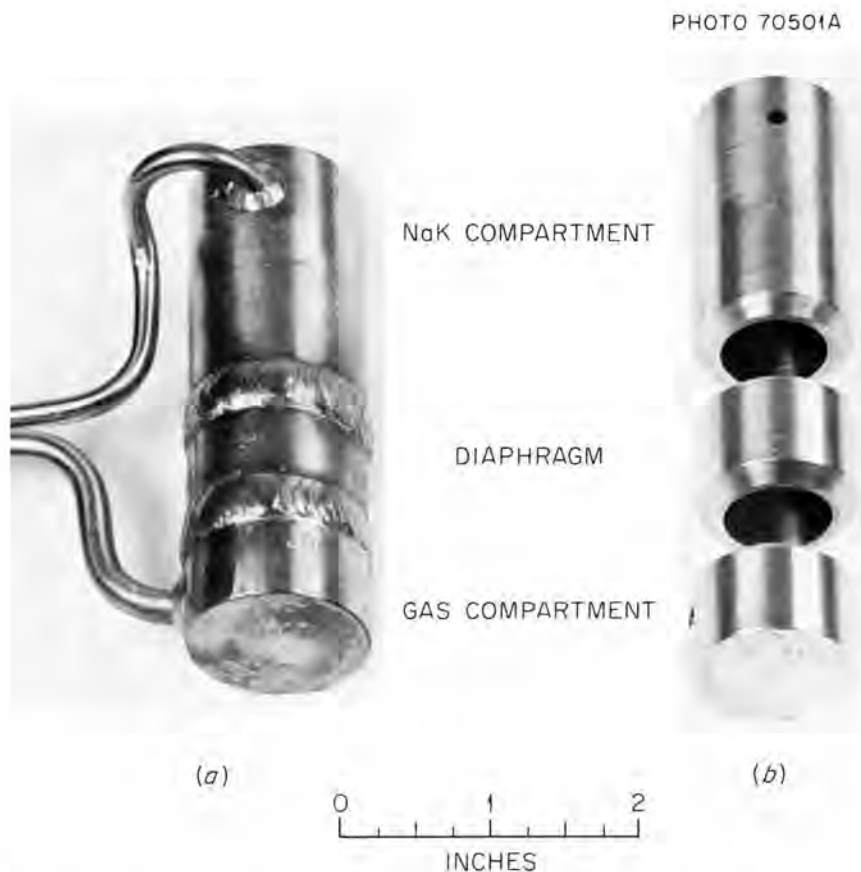


Fig. 2. (a) Welded Hydrogen Permeation Cell. (b) Components Before Welding.

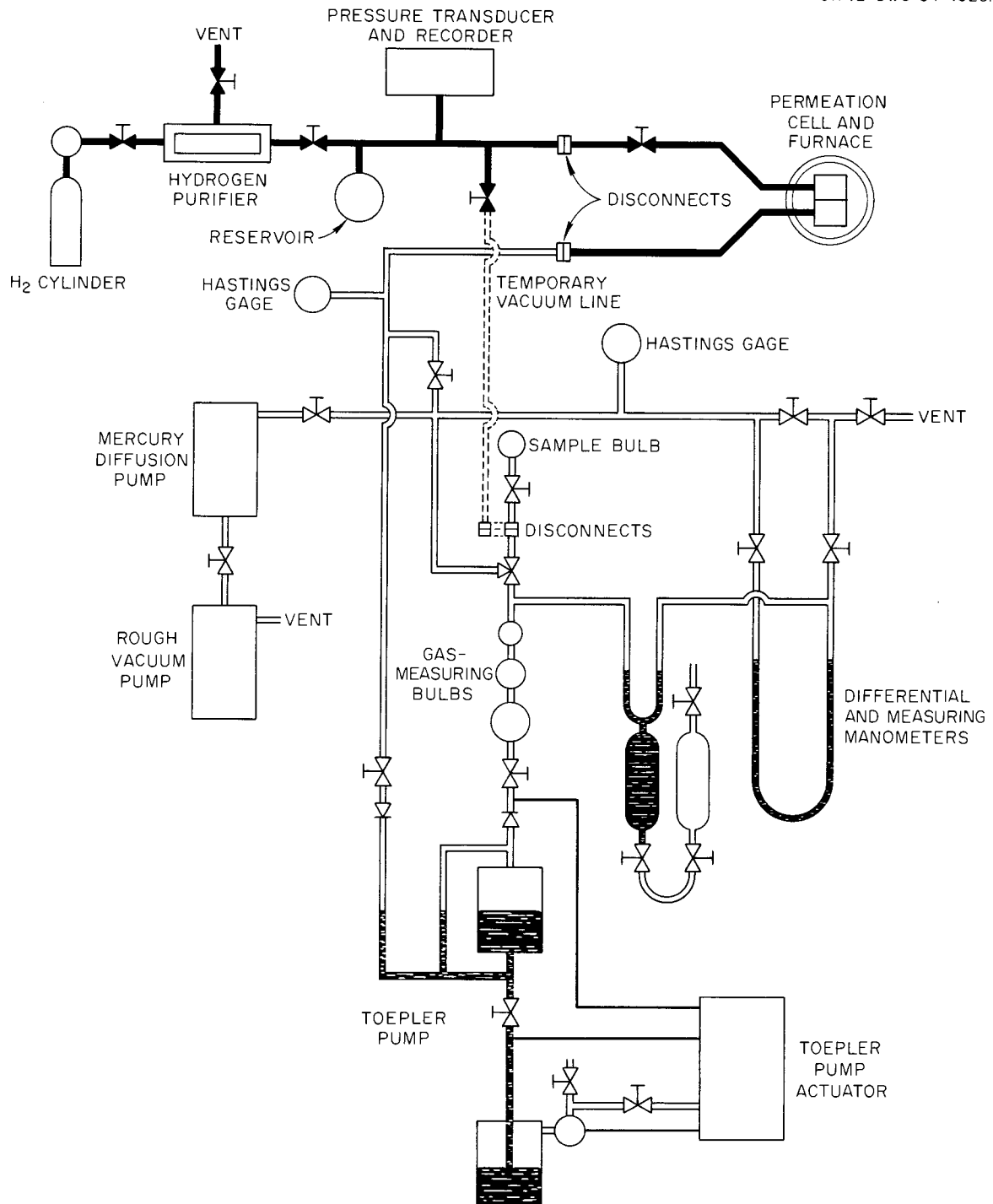


Fig. 3. Diagram of Apparatus for Measuring Hydrogen Permeation Through Metal Diaphragms.

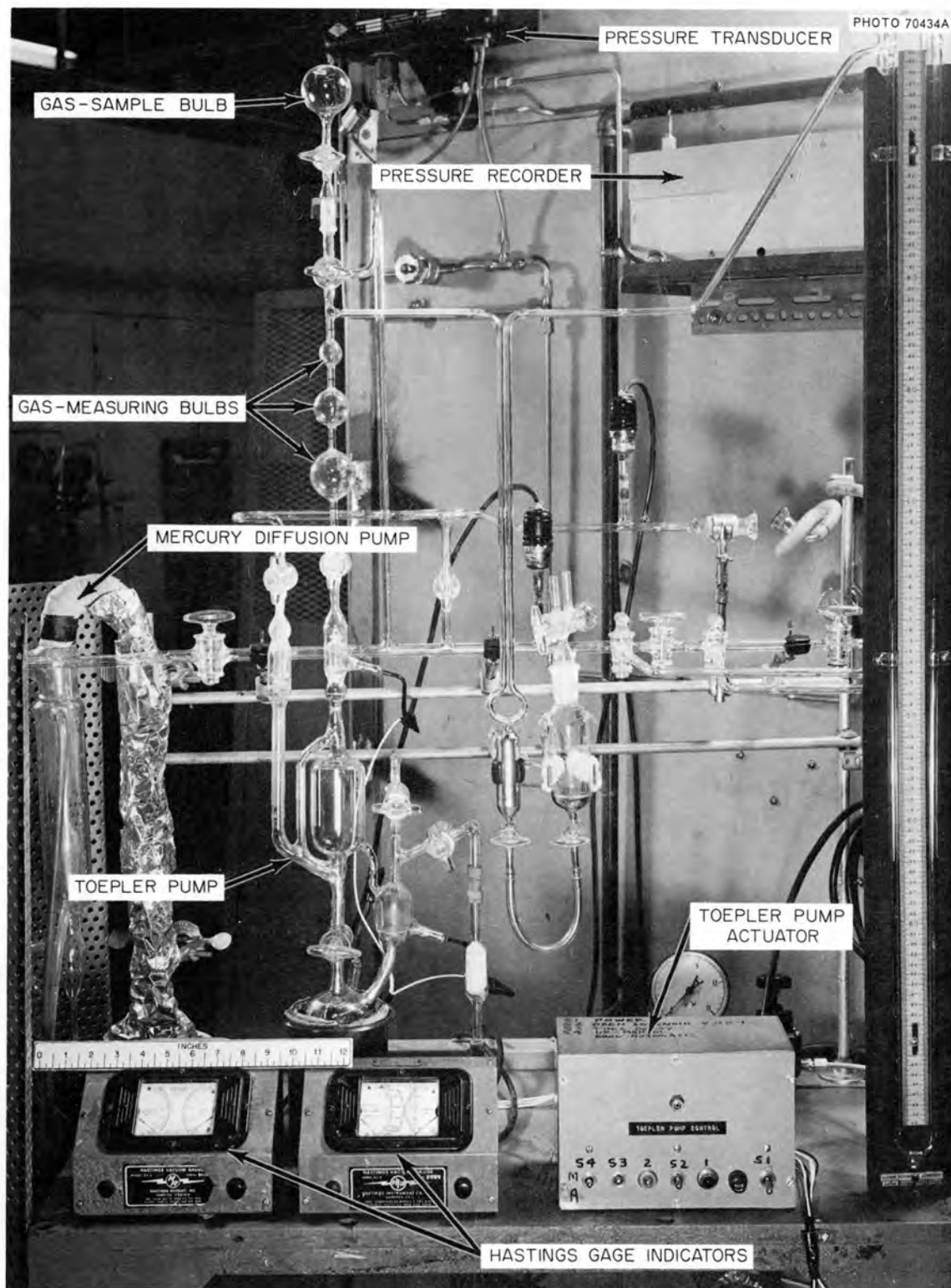


Fig. 4. Pumping, Measuring, and Sampling System of Hydrogen Permeation Apparatus.

of 1 mm. The hydrogen passing through the test cell diaphragm was removed immediately by a continuously operating Toepler pump, and the gas was stored for measurement in a series of bulbs. From time to time, the amount of hydrogen which had passed through was measured manometrically. Samples of the gas collected from the downstream side of the diaphragm could be removed for mass spectrographic analysis.

The system was filled with hydrogen at room temperature after a shut-down and transferred to the inert-atmosphere glove box. Purified NaK was introduced after an evacuation of the upstream side. The system was then sealed again, welded shut on the upstream side, and a hydrogen atmosphere was placed over the NaK. The device was then operated either with the cell in a vertical position, which caused the diaphragm to be covered by about 1 cm of NaK, or it was operated in the inclined position, in which the NaK flowed away from the diaphragm and left the diaphragm exposed only to gas. In both positions, measurements were made of the permeation rate; so repeated series of measurements permitted a determination of whether the presence of NaK resulted in any appreciable changes in the permeation rate.

Tilting to drain NaK away from the diaphragm was employed only with the type I cells.

Type II, Iron Thimble Permeation Cell

The design of the type I hydrogen permeation cell was later modified to eliminate the problem of NaK losses into the hydrogen feed line. A thimble of Armco iron was placed within the cell separating the hydrogen inlet line and the central chamber with the diaphragm to be tested. The components of the new cell before welding are shown in Fig. 5. The diaphragm of the cell and the components other than the thimble and its internal supporting spider, which were made of Armco iron, were made of type 316 stainless steel. The thimble, which had a high permeability and a large area-to-thickness ratio, was set into the body of the cell in such a way that its enlarged open end protruded from the body into the head end cap. The body, thimble, and end cap were welded together at this junction. The hydrogen inlet tube was welded into the opening in the head end cap. The diaphragm section was welded to the body, and the outlet end cap to the diaphragm section. The Toepler pump was connected to the cell through a tube welded to the outlet end cap. The cell was carefully hydrogen fired after fabrication to remove any surface oxides from the central portion of the cell, and the nozzle was seal welded.

In operation, hydrogen was fed into the cell through the tube welded to the head end cap. The hydrogen permeated the thin thimble wall into the isolated intervening chamber between the thimble and the body, where it then permeated the diaphragm located in the chamber. Because hydrogen passed far more freely inward through the thimble than outward through the diaphragm, the hydrogen pressure in the region between the thimble and the diaphragm was essentially the same as the hydrogen inlet pressure after a very brief lag. The gas diffusing through the diaphragm was re-



Fig. 5. Components of Modified Permeation Cell.

moved from the apparatus by the Toepler pump and recovered for measurement and analysis. A loading nozzle was welded into the body so that NaK could be placed in the region above the diaphragm.

The permeation characteristics of this cell were determined at 1300, 1100, and 1000°F at various hydrogen inlet pressures. When these measurements were completed, the cell was removed from the furnace to prepare for loading NaK. The loading nozzle was opened and the cell transferred to the helium-filled glove box, where the NaK was charged and the loading nozzle seal welded.

A similar cell was made with a Croloy 9M diaphragm section. The other components of this cell were of type 316 stainless steel, except for the thimble and supporting spider of Armco iron. This cell was hydrogen fired. On cooling, it was carefully annealed through the 1600 to 1400°F temperature region. The loading nozzle opening to the inner chamber of the cell was then seal welded in a helium-filled glove box.

HYDROGEN PERMEATION THROUGH HASTELLOY N (TYPE I CELL ONLY)

First Cell (A)

The initial measurements of hydrogen permeation were made in a type I cell of Hastelloy N without NaK. These measurements were made in increasing temperature steps from 660 to 1020°F. At each temperature, the permeation cell was outgassed by evacuating both sides of the system sufficiently to detect any major leak. The high-pressure side of the cell was then pressurized with 1 atm of hydrogen, while the low-pressure side was maintained at a pressure of less than 100 μ with the Toepler pump. When a sufficient amount of gas had accumulated downstream, it was measured and sampled for analysis by mass spectrometry. Results of the permeation experiments on two Hastelloy N cells in the absence and presence of NaK, at various temperatures, are shown in Table 1.

As indicated by analyses of the diffused gases obtained from runs 1 to 3, the gas-recovery system had an air leak. It is possible that such

Table 1. Permeation of Hydrogen Through Hastelloy N in the Absence and Presence of NaK in Two Type I Cells
Upstream hydrogen pressure: 1 atm

Cell and Sequence No.	Diaphragm Covered	Temperature (°F)	Permeation Coefficient (std cc H ₂ hr ⁻¹ cm ⁻² atm ^{-1/2})	Comments
<u>First Cell (A): No NaK Present</u>				
A-1	No	660	0.0054	Downstream air leak
A-2	No	750	0.0055	Downstream air leak
A-3	No	806	0.0030	Downstream air leak
A-4	No	920	0.072	
A-5	No	1020	0.215	
<u>First Cell (A): NaK Added to Cell</u>				
A-6	No, tilted	1020	0.099	
A-7	Yes	1020	0.080	
A-8	Yes	1020	0.106	
A-9	No, tilted	1020	0.075	
<u>Second Cell (B): No NaK Present</u>				
B-14	No	1100	0.33	
B-15	No	1100	0.30	
B-13	No	1300	0.89	
B-16	No	1300	0.71	
B-18a	No	1300	0.79	
B-18b	No	1300	0.60	
B-10	No	1425	2.39	
B-11	No	1425	1.08	
B-12	No	1425	0.82	
B-17a	No	1425	0.40	
B-17b	No	1425	1.06	
<u>Second Cell (B): NaK Added to Cell</u>				
B-19	Yes	1425	0.81	NaK distilled into hydrogen entry line

an air leak led to surface oxides, which may account for the low rates of diffusion shown in tests 2 and 3. An improved vacuum coupling was made for the low-pressure side of the cell by drilling an axial hole through a valve stem. The valve packing permitted rotation of the permeation cell about the valve stem without loss of vacuum. After eliminating the various causes of air leaks, comparatively pure gas was obtained in the diffusion experiments. The permeability coefficients for runs 1, 4, and 5 are consistent with extrapolations of such coefficients for Inconel, as reported by Flint.⁵

A measured amount of NaK (6.3 cm^3) was then introduced into the high-pressure side of the cell under vacuum. Since the dry, inert-atmosphere glove box was not yet in operation, a temporary rig was used to introduce the NaK through the gas inlet line. A gamma radiograph of the loaded cell showed that the NaK level was about 1 cm above the diaphragm.

The hydrogen permeability was measured at 1020°F when the NaK was tilted away from the diaphragm and also when the cell was rotated to the vertical position so that the NaK covered the diaphragm. The values of the permeability were approximately 40% of the values obtained at 1020°F before the introduction of the NaK. However, no significant difference was shown for permeation rates with or without NaK covering the diaphragm. In general, samples of the diffused gas seemed to show a greater quantity of methane, although small, than the feed gas, with considerable regularity. Since this may be of interest at a later time, it is recorded. The somewhat erratic behavior of the hydrogen permeability is consistent with reported effects⁶ of impurities absorbed on the metal surface. A more effective outgassing treatment of the metal was indicated.

Second Cell (B)

A second Hastelloy N cell was operated without NaK at 1100, 1300, and 1425°F . To make sure that the cell was clean, it was first heated to 1425°F , while under vacuum, to remove occluded gases. Then, while the temperature was maintained, both cell compartments were treated with purified hydrogen at atmospheric pressure and evacuated several times to remove any volatile materials (i.e., water) which might form in the cell because of the presence of hydrogen.

The temperature sequence of the runs was irregular to permit separation of the time and temperature effects on the diffusion rate. The results are consistent with those previously obtained with the first cell at lower temperatures. Each sample of the diffused gas analyzed more than 98% hydrogen, indicating that errors had not been introduced by air leaks.

The data obtained with the first and second diffusion cells are reasonably consistent, both between the two cells and with the literature, and appear high enough to represent the behavior of clean metal. Representative data from other investigations^{3,5} for nickel and for clean and oxidized type 303 stainless steel support the validity of the present data.

Second Cell (B), with NaK Present

After the initial hydrogen permeability determinations were completed, the cell was prepared for loading with NaK. The welded closure of the cell was pierced with a 1/16-in. drill while the cell compartment was pressurized slightly with helium to reduce exposure to air and to remove chips when the drilling was completed. The cell was placed in the glove box vacuum lock immediately after the drilling was completed.

Since the conditions of the dry, inert-gas glove box had been improved, the diffusion cell was loaded by a direct method. The NaK was loaded into the cell with a hypodermic syringe, and the amount was determined by weighing the syringe. The hole in the nozzle was closed by welding. The loading and the welding were completed in less than 15 min, during which time a freshly exposed pool of NaK in the cell remained bright, demonstrating the inertness of the atmosphere.

Measurement of the hydrogen permeation of Hastelloy N (INOR-8) in the presence of NaK was initiated at 1425°F (774°C) with about 1 atm total pressure (NaK + H₂) in cell B. When the cell was removed from the apparatus, the hydrogen inlet tubing was found to contain a deposit of 320 mg of NaK and some solid material. The solid material consisted of 19 mg of potassium and 0.7 mg of sodium as hydrides, with a negligible amount of oxide. The NaK vapor apparently had diffused and condensed in the hydrogen inlet tube during the high-temperature operation. On cutting the loading nozzle of the cell open, the inside surfaces of the cell were found to be completely wet by the NaK.

The cell was subsequently cleaned with butyl alcohol and then sectioned axially for examination. The upstream surface that had been exposed to the NaK was silver bright; the downstream surface was less silvery, but it was lustrous and had no visible film.

Because of the condensation of NaK in the inlet line during the course of the experiment, there is some doubt as to the exact hydrogen partial pressures. As a result, only the first measurement of several made with this capsule is considered valid. With the diaphragm covered by NaK, a permeation rate of 0.283 cc (STP)/hr through the 0.75-in.-diam, 0.132-in.-thick diaphragm was measured at a total upstream pressure of 771 mm Hg. This yielded a specific permeation rate of 0.334 cc (STP) mm cm⁻² hr⁻¹. To obtain a permeability coefficient, K, this value is divided by the square root of the hydrogen pressure in atmospheres. Using an interpolation of data from the Liquid Metals Handbook, a value of 642 mm Hg is estimated for the NaK vapor pressure. Based on this value, the hydrogen permeability coefficient K is calculated to be 0.81 cc (STP) mm cm⁻² hr⁻¹ atm^{-1/2}. In prior tests at this temperature, this cell had exhibited hydrogen permeability coefficients of 0.4 to 2.4 cc (STP) mm cm⁻² hr⁻¹ atm^{-1/2} in the absence of NaK. The wetting of all interior surfaces of the upstream compartment by NaK requires that the effect of NaK on permeation be established by comparison with tests in the absence of NaK, rather than by tilting the cell to expose the diaphragm surface.

The difficulties which resulted from the distillation of NaK into the hydrogen entry line of this type I cell thus led to the design and fabrication of the type II iron thimble permeation cell.

In the SNAP-8 system the most important permeation regions involved type 316 stainless steel and Croloy 9M. Consequently, type II iron thimble permeation cells were fabricated of these alloys. The program was terminated without conducting any further studies in Hastelloy N cells of either design.

CROLOY 9M IN THE ABSENCE OF NaK (TYPE I CELL)

The permeability of Croloy 9M to hydrogen at elevated temperatures was determined in the absence of NaK. The type I permeability cell was machined from the Croloy 9M forging obtained from Thompson Ramo Wooldridge Corporation that was understood to be from material supplied by Aerojet-General Corporation for SNAP-8 studies. The end caps were also of Croloy 9M, while the inlet and outlet tubing were of nickel. The diffusion diaphragm was 3/4 in. in diameter and 1/8 in. thick. The cell was prepared for operation by outgassing both sides of the diaphragm and then hydrogen firing. These operations, covering a period of 20 hr, were conducted at 775°C.

Permeation measurements were made at 775°C (1425°F), 704°C (1300°F), and 593°C (1100°F) with an upstream hydrogen pressure of about 1 atm. One hour was allowed for development of steady-state conditions before beginning measurements. The results are given in Table 2. Average values of the permeation coefficient at the respective temperatures were 0.77, 0.55, and 0.28 cc (STP) mm hr⁻¹ cm⁻² atm^{-1/2}. Corresponding average values for Hastelloy N, reported in a preceding section, were 1.3, 0.75, and 0.32. It is reasonable for the permeability of the iron-based Croloy 9M to be moderately below that of the nickel-based Hastelloy N.

Table 2. Hydrogen Permeability of Croloy 9M

Temperature		Permeability ^a [cc (STP) mm hr ⁻¹ cm ⁻² atm ^{-1/2}]
(°C)	(°F)	
775	1425	0.79, 0.75
704	1300	0.53, 0.57
593	1100	0.29, 0.27

^aData obtained in the absence of NaK and with ~1 atm of hydrogen upstream; Toepler pump vacuum downstream.

CROLOY 9M IRON THIMBLE CELL WITHOUT NaK

A type II permeation cell with an Armco iron entrance thimble similar to that of the stainless steel cell but with a Croloy 9M diaphragm was operated in the absence of NaK to determine the characteristics of the cell. The data were obtained after extended hydrogen permeation to obtain a steady state across the cell for each temperature and pressure condition. The results were obtained in pairs to verify that a steady state had been reached by the second reading matching the first. Table 3 presents the results in the sequence in which they were obtained, along with comparative data from a previously reported determination on another cell of the same material.

The paired values obtained agree fairly well with each other. Replicate determinations at 1300°F at the end of the series gave higher values

Table 3. Permeability to Hydrogen of Croloy 9M in the Absence of NaK
Values given in the sequence obtained

Pressure (mm Hg)	Permeability [cc (STP) mm hr ⁻¹ cm ⁻² atm ^{-1/2}]		
	At 1000°F	At 1100°F	At 1300°F
<u>Type II Iron Thimble Cell</u>			
760			0.590
760			0.588
199			0.359
196			0.342
28.5			0.374
23			0.374
760		0.263	
760		0.263	
137		0.225	
112		0.226	
39		0.170	
36.5		0.166	
760	0.178		
760	0.180		
760			0.656
760			0.664
196			0.612
<u>Type I Cell</u>			
760 ^a		0.29	0.53
760 ^a		0.27	0.57

^aResults reported in previous section for type I Croloy 9M cell.

at 1 atm and 196 mm than were obtained at the start of the series, indicating that the continued permeation of hydrogen over a period of three weeks may have resulted in a moderate increase in permeability. However, the first points at 199 and 196 mm are somewhat inconsistent with the remainder of the data. The permeabilities at 1 atm obtained at 1100 and 1300°F agree fairly well with data from the previous type I Croloy 9M cell. Lower permeability coefficients were obtained at the lower pressures, both at 1100 and at 1300°F, which indicates that a surface oxide effect might be of significance.

The program was terminated before the planned experiments in the presence of NaK could be conducted.

PERMEATION OF HYDROGEN THROUGH TYPE 316 STAINLESS STEEL IN THE ABSENCE AND PRESENCE OF NaK

Determinations of the permeability of type 316 stainless steel to hydrogen were conducted in both type I and type II (iron thimble) cells. The use of the iron thimble cell became necessary because NaK at elevated temperatures was found in other experiments to condense in the hydrogen entry line, which made the measurement of upstream hydrogen partial pressure uncertain. As will be seen below, the iron thimble cell gave somewhat higher results in the absence of NaK, as compared with the type I cell. It is thought that this may have been due to the formation of a slight oxidation film on the upstream surface of the type I cell diaphragm during heatup. In the case of the iron thimble cell, such an oxide film was prevented from forming on the diaphragm.

Type I Cell

A series of determinations of the permeability of type 316 stainless steel to hydrogen at several pressures was made in a type I cell in the absence of NaK at temperatures of 1000, 1100, and 1300°F. The components of the stainless steel permeation cell were machined from bar stock and welded together. The part containing the diaphragm was machined so that the plane of the diaphragm was parallel to the axis of the rod to prevent stringers from causing channels between the high- and low-pressure sides of the cells. The hydrogen pressures were maintained at 760, 100, and 10 mm Hg on the high-pressure side of the diaphragm, while the low-pressure side was evacuated.

To eliminate the influence of transient conditions on the lower diffusion rates occurring at the lower pressures and temperatures, only those observations are reported that were preceded by a preliminary permeation period of 20 hr or more to allow the hydrogen permeation rate through the diaphragm to attain a steady value. The data obtained are given in Table 4. As shown in the table, the values of the permeability coefficient did not vary much with age, exhibiting only a moderate downdrift at any particular temperature.

Table 4. Permeation of Hydrogen Through Type 316 Stainless Steel (Type I Cell)
at Temperatures of 1300, 1100, and 1000°F and Several Pressures

Diaphragm area: 2.85 cm²
Diaphragm thickness: 3.48 mm

Run No.	Temperature (°F)	Pressure Upstream (atm)	Test Period (hr)	Specific Permeation Rate [cc (STP) mm hr ⁻¹ cm ⁻²]	Permeation Coefficient at Given Pressure Level [cc (STP) mm hr ⁻¹ cm ⁻² atm ^{-1/2}]		
					0.1 atm	0.12 atm	0.013 atm
23	1100	1.02	5.0	0.0650	0.064		
25	1100	0.132	7.0	0.0191		0.053	
26	1100	0.132	7.0	0.0191		0.053	
28B	1100	0.013	23.5	0.0054			0.047
29B	1100	1.03	5.5	0.0468	0.047		
29C	1100	1.03	18.0	0.0504	0.050		
Cell Hydrogen Treated and Reevacuated Four Times on Both Sides at 1100°F							
30A	1100	1.01	40.0	0.0532	0.053		
30B	1100	1.01	24.1	0.0545	0.054		
31A	1100	0.132	24.0	0.0133		0.037	
31B	1100	0.132	24.0	0.0117		0.032	
Both Sides of Cell Hydrogen Treated and Reevacuated Twice at 1425°F After a Power Outage							
32A	1100	0.013	24.0	0.0072			0.055
32B	1100	0.013	43.5	0.0024			0.019
Temperature Lowered to 1000°F							
33A	1000	0.96	7.5	0.0267	0.027		
33B	1000	0.93	16.0	0.0292	0.030		
34A	1000	0.124	45.0	0.0077		0.022	
34B	1000	0.121	67.5	0.0065		0.019	
Temperature Increased to 1300°F							
35A	1300	0.93	2.5	0.259	0.27		
35B	1300	0.93	2.5	0.288	0.30		
36A	1300	0.129	6.0	0.087		0.24	
36B	1300	0.132	18.0	0.081		0.22	
37A	1300	0.015	24.0	0.030			0.25
37B	1300	0.014	24.0	0.027			0.23
38A	1300	0.94	2.5	0.260	0.27		
38B	1300	0.94	2.5	0.269	0.28		

The constancy of the coefficient at the various pressures indicates that the permeation was proportional to the square root of pressure, as assumed. There does appear to be a relatively great scatter in values obtained at the lower pressures, and it is possible that at the lower pressures and at temperatures of 1100°F or lower, dependence on the square root of pressure no longer holds completely. The temperature dependence appears to be normal.

After completing the hydrogen studies in the absence of NaK, 5.8 cc of NaK was placed in the cell, and the NaK entry aperture was rewelded closed. Experiments with the Hastelloy N cell containing NaK had indicated that at the higher temperatures, NaK would distill into the hydrogen inlet tubing. Efforts to find alternate modes of operation to avoid this difficulty were not successful. It was decided therefore that the cell using an internal iron thimble could prevent the distillation of NaK while still affording adequate access of hydrogen to the diaphragm. Such a cell was fabricated of type 316 stainless steel and used in the tests described below.

Type 316 Stainless Steel Iron Thimble Cell With and Without NaK

Studies were conducted of hydrogen permeation in a type 316 stainless steel cell of the second design in the absence and in the presence of NaK. The cell has an Armco iron barrier in the form of a thimble of large area-to-thickness ratio to permit easy diffusion of hydrogen into the NaK while preventing the transport of NaK vapor into the hydrogen feed line.

The results obtained with no NaK in the cell are listed in Table 5. The data obtained at the higher pressures are in quite good agreement at each temperature. In the absence of NaK, data obtained at the lower pressures showed a moderate dropoff in the permeability coefficient with pressure at the lower temperatures. The present permeability data are somewhat higher at 1100 and 1000°F than the data from the type I cell, but the two sets of data coincide at 1300°F. The present data agree almost exactly with the data for type 316 stainless steel reported by Flint⁵ and are higher than the data for type 304 stainless steel reported by Flint⁵ and by Steigerwald.³

After concluding the determinations in the absence of NaK, the cell was removed to the inert-atmosphere glove box, and the chamber was opened. A charge of 2.6 cc of NaK was then loaded into the chamber between the thimble and the upstream side of the diaphragm, and the opening was seal welded.

Subsequent hydrogen permeability measurements were made at a series of pressures from 1 atm downward to a pressure of 42 mm at 1300°F, to below 1 mm at 1100°F in two series, described below, and at 1 atm at 1000°F. The results are listed in Table 5 in the sequence obtained. They are plotted as the logarithm of the permeation rate [$\text{cc (STP) mm cm}^{-2} \text{ hr}^{-1}$] vs the logarithm of the pressure (mm) in Fig. 6.

In the first determinations after NaK was present at 1100°F, the permeation rate was slightly higher than in the absence of NaK. This was attributed to the possible removal by the NaK of slight oxide films from the interior surfaces between the thimble and diaphragm contacted by the NaK. Subsequent receipt of feed-gas analyses indicated slight air contamination and the possibility of some oxidation of the upstream thimble surfaces. Consequently, the system was charged with hydrogen at 1300°F and the feed-gas region evacuated, thereby reversing the hydrogen flow for a time, with the intent of reducing any surface oxides and removing the associated moisture. When measurements were again made at 1100°F, following those at 1300 and 1000°F, the rates appeared to be about one-third higher than the original measurements. They were also more consistent (linear) with the 1000 and 1300°F data when the logarithm of the permeability coefficient was plotted vs the inverse of the absolute temperature (see Fig. 7).

There is no particular effect of time (aging) on the permeability coefficient that appears clearly indicated by the data, although it is

Table 5. Permeability of Type 316 Stainless Steel to Hydrogen in the Absence and Presence of NaK at Various Pressures and Temperatures^a

Pressure (mm Hg)	Permeability [cc (STP) mm hr ⁻¹ cm ⁻² atm ^{-1/2}]		
	At 1000°F	At 1100°F	At 1300°F
	<u>In the Absence of NaK</u>		
760		0.096 0.094 0.098	
68		0.084	
63		0.084	
760			0.278
			0.284
175			0.265
170			0.288
23			0.223
16			0.214
13			0.200
760	0.060		
	0.060		
	<u>In the Presence of NaK</u>		
760		0.100 ^b 0.095 ^b	
216		0.105 ^b 0.101 ^b	
39		0.100 ^b 0.096 ^b	
(Hydrogen feed system evacuated at 1300°F to remove possible impurities)			
760			0.288
			0.294
206			0.297
204			0.292
47			0.300
42			0.314
760	0.070		
	0.070		
747		0.132 0.132	
		0.135	
216		0.134	
55		0.127	
50		0.132	
8		0.126	
6		0.140	
6-3		0.136	
3		0.143	
2.8-1.2		0.134	
1.2-0.8		0.157	
0.8-0.6		0.145	

^aPermeability determined with the same diaphragm, first in the absence of NaK and then after loading the cell with NaK; results are listed in chronological sequence.

^bSlight impurities (nitrogen, air) noted in feed gas may have resulted in increased resistance to flow. Experiment repeated after 1300°F hydrogen charge and evacuation to remove possible oxide from thimble surface.

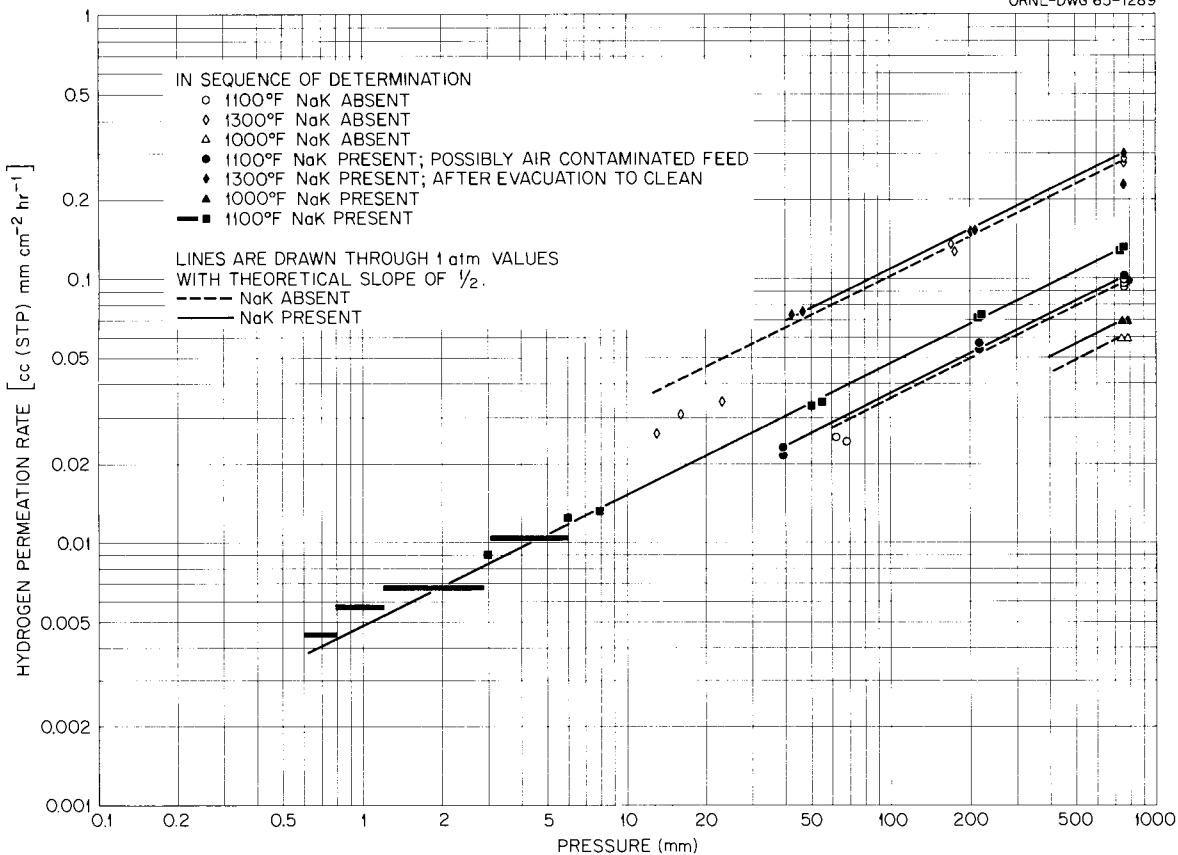


Fig. 6. Permeability of Type 316 Stainless Steel to Hydrogen in the Absence and in the Presence of NaK at Various Pressures and Temperatures.

not easy to separate such effects from others acting concurrently. Certainly any such effect is not great.

It is believed to be demonstrated by these experiments that the presence of NaK has no adverse effect on the permeation of hydrogen through type 316 stainless steel at SNAP-8 temperatures. Indeed, rates may be moderately increased in the presence of NaK as a result of the reduction of resistance to hydrogen passage at the NaK-metal interface. This may be largely due to dissolution of slight oxide films. It could also be affected by easier entry into the structural metal of hydrogen atoms from the liquid metal as compared with hydrogen from molecules of the gas phase.

Deuterium Permeation of Type 316 Stainless Steel

The injection of deuterium instead of hydrogen into loop 14-4 was considered in order to relieve problems arising from traces of normal

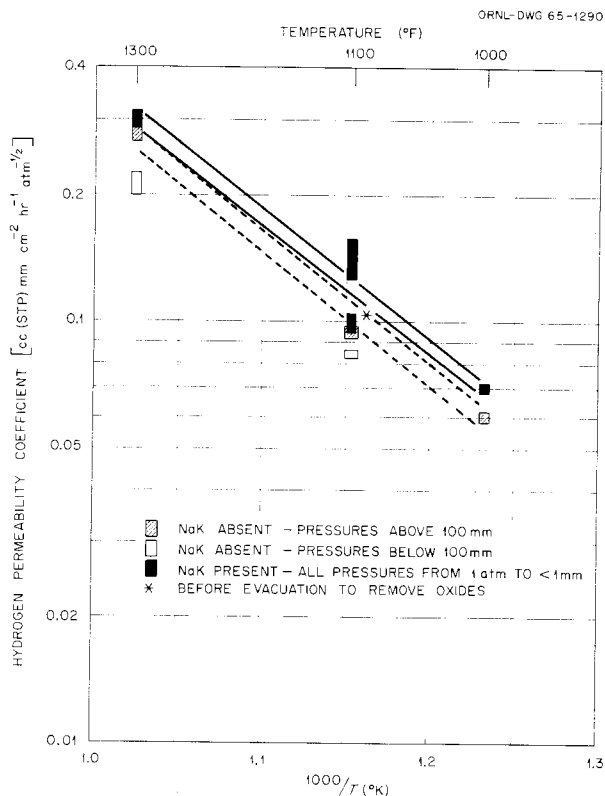


Fig. 7. Permeability of Type 316 Stainless Steel to Hydrogen in the Absence and in the Presence of NaK Plotted as a Function of the Inverse of the Absolute Temperature.

hydrogen in the atmosphere and in the argon as a sleeve sweep gas. It was desirable therefore to verify the anticipated drop in permeability, which was expected to be the square root of the atomic weight ratio, or $\sqrt{1/2}$. For the necessary measurements, hydrogen was replaced with deuterium in the type 316 stainless steel iron thimble cell containing NaK, which was used to obtain the extensive hydrogen permeation data reported above.

Performing the permeation measurements in the same cell provided for direct comparison of the hydrogen and deuterium results.

Deuterium permeation data were obtained at 1100 and 1300°F and at pressures of approximately 1 atm and 200 mm. The data are listed in Table 6, along with those of previous tests in the same cell with normal hydrogen at comparable temperatures and pressures. The deuterium results, which are listed in the sequence in which the measurements were made, were obtained after carefully evacuating both sides of the permeation cell for one day. Mass spectrometric analysis of the feed gas showed 99.95% D₂, and only one permeated gas sample was slightly less than 99.0% deuterium.

Table 6. Permeation of Hydrogen and of Deuterium Through Type 316 Stainless Steel in the Presence of NaK at 1100 and 1300°F

Pressure (mm Hg)	Hydrogen Permeability Coefficient [cc (STP) mm hr ⁻¹ cm ⁻² atm ^{-1/2}]		Pressure (mm Hg)	Deuterium Permeability Coefficient [cc (STP) mm hr ⁻¹ cm ⁻² atm ^{-1/2}]	
	At 1100°F	At 1300°F		At 1100°F	At 1300°F
	760			0.288 0.294	731
206		0.297	213	0.0918	
204		0.292	203	0.0924	
747	0.132 0.132		178		0.210
216	0.135 0.134		700		0.219 0.224
Average	0.133	0.293	Average	0.0910	0.218

The ratio of permeabilities of deuterium and hydrogen was 0.68 at 1100°F and 0.74 at 1300°F. These values compare satisfactorily with the anticipated ratio of 0.71.

Hydrogen Permeation After Oxidation of Stainless Steel

Subsequent to the deuterium tests, the stainless steel cell was purged of deuterium, and tests with hydrogen were continued. Studies were made of the effects on hydrogen permeation of air oxidation of the downstream surface of the type 316 stainless steel diaphragm. Prior to oxidation the system was operated at temperature in order to attain steady-state hydrogen permeation in the cell. The feed gas contained 99.91 mole % hydrogen. Permeation coefficients were determined for comparison with those reported in the previous section (Table 6) and for comparison with values to be obtained after oxidation. The hydrogen permeation coefficient of the diaphragm at various pressures was independent of pressure, as shown in the first part of Table 7. The values ranged from 0.114 to 0.129 cc (STP) mm hr⁻¹ cm⁻² atm^{-1/2}, in fair agreement with the value of 0.133 from Table 6.

First Oxidation Experiment (1100°F)

Before admitting air to the downstream chamber of the cell, hydrogen was supplied at a pressure of 1 atm to the upstream side of the cell, and permeation was continued for 23 hr with a downstream vacuum to establish a steady state. Ambient air (at 1 atm pressure) was then admitted to the downstream chamber for 10 min. In this experiment the downstream side was then evacuated for 15 min, and the gases were discarded. Collection and measurement of the permeating gas by means of the Toepler pump were then resumed. Data from this experiment are shown in Table 7. Collection of gas over four periods, totaling 28.6 hr, with the first three gas samples being analyzed, showed that the earlier samples contained a substantial

Table 7. Effect of Air Oxidation on Permeation of Hydrogen Through a Type 316 Stainless Steel Diaphragm

Experiment No.	Conditions	Postoxidation Time (hr)	Pressure of Feed (mm)	Volume of Gas Collected [cc (STP)]	Sample Collection Time (hr)	Permeation Rate [cc (STP)/hr]	Hydrogen Permeation Coefficient ^a	Analysis (mole %)																	
								H ₂	H ₂ O	CO ₂	O ₂	N ₂													
0	Preoxidation determination at 1100°F	0	733				0.124																		
			731				0.122																		
			224				0.129																		
			224				0.125																		
			55				0.114																		
			49				0.128																		
1	Downstream chamber at 1100°F; exposed to air for 10 min and evacuated for 15 min	4.3	742	0.163	4.0	0.040	0.047	83.97	14.18	0.55	0.01	1.24													
		6.8	742	0.193	2.0	0.096	0.116	97.54	1.80	0.08	0.02	0.40													
		26.0	733	0.198	2.0	0.099	0.121	99.52	0.05	0.04	0.01	0.34													
		28.6	731	0.201	2.0	0.100	0.123		Not analyzed																
2	Downstream chamber at 1100°F; exposed to air for 10 min; air recovered																								
														Air recovered by Toepler pump after 10 min oxidation	0.25	723	12.301	0.25		0.04	0.40	0.04	18.04	80.46	
														Hydrogen collected	2.8	723	0.149	2.5	0.060	0.050	25.62	43.13	1.02	3.66	26.19
															4.8	721	0.193	2.0	0.096	0.117	63.02	35.21	0.35	0.04	1.33
															6.8	719	0.206	2.0	0.103	0.126	75.02	23.82	0.15	0.03	0.92
															71.8	682	7.047	65.0	0.108	0.136	96.80	2.56	0.04	0.01	0.47
3	Downstream chamber at 1300°F; exposed to air for 10 min; air recovered																								
														Preoxidation determination		723	0.240	1.0	0.240	0.293	99.25	0.17	0.03	0.02	0.45
														Air recovered by Toepler pump after 8 min oxidation	0.2		11.934				0.10	0.39	0.04	1.67	96.55
														Hydrogen collected	1.9	717	0.294	1.75	0.168	0.197	42.72	52.21	1.51	0.16	3.26
															2.7	717	0.212	0.75	0.282	0.342	76.03	22.13	0.24	0.08	1.41
3.2	717	0.130	0.50	0.261	0.317	14.96	14.96	0.15	0.08	1.40															

^aPermeation coefficient, cc (STP) mm hr⁻¹ cm⁻² atm^{-1/2}; both H₂ and H₂O are included in the calculation.

proportion of water, which decreased in the subsequent samples. This is presumed to be the product of reaction between permeating hydrogen and metal oxide.

The permeation coefficient for the first period (4 hr) was less than 40% of the value before oxidation. However, as permeation continued, the permeation coefficients approached the preoxidation values.

Second Oxidation Experiment (1100°F)

After completion of a total of two days of hydrogen permeation at 1100°F after the first oxidation, ambient air was again permitted to enter the downstream region of the permeation cell, where it remained for 10 min. In this experiment, the air was recovered by the Toepler pump. Collection and measurement of the permeating gas by means of the Toepler pump were continued for a period of almost 72 hr, with four samples being taken. Data from this experiment are also given in Table 7. It may be observed from the data that the major portion of the atmospheric oxygen was recovered unreacted at 1100°F. However, appreciable portions (which diminished in successive samples) of the permeating hydrogen were found in the form of water. The permeation rate, less than 40% of the preoxidation value, increased in successive samples to equal preoxidation levels.

Third Oxidation Experiment (1300°F)

After completion of about 72 hr of hydrogen permeation after the second oxidation, the temperature was increased to 1300°F, and hydrogen permeation was continued for approximately two days with 1 atm of pressure upstream and a diffusion pump vacuum downstream. Permeating gas was then collected for a preoxidation determination of the permeation coefficient, which agreed with the values at this temperature given in Table 7.

Ambient air was permitted to enter and remain in the downstream chamber of the permeation cell for a period of 8 min, after which it was collected with the Toepler pump for measurement and analysis. Most of the oxygen was consumed in this sample. Collection of the permeating gases was continued for a period of 3 hr, and three samples were obtained. The permeation coefficient for the earlier (1.75-hr) period was about 65% of the preoxidation value. The two subsequent determinations somewhat exceeded the preoxidation value. Substantial portions of the hydrogen were found in the form of water in these samples. Data for this experiment are presented in Table 7.

These experiments indicate that brief air oxidation of type 316 stainless steel resulted in an appreciable reduction in hydrogen permeability. The reduction in permeability was a transient condition and after an extended period of time the permeability attained its original steady-state rate. Observation of the permeation rate during this transient period showed generally increasing, but fluctuating, values of the rate and instances when the observed rate was higher than the final steady-state rate. These rate fluctuations are presumed to be caused by the manner of destruction of the oxide surface layers by hydrogen reduction. Further studies of these transient effects and of the effects accompanying more substantial oxidation were not authorized.

SOLUBILITY OF HYDROGEN IN NaK-78

In the SNAP-8 reactor the eutectic sodium-potassium mixture (78 wt % K, or "NaK-78") serves as coolant, entering the reactor core at 1100°F (593°C) and leaving at 1300°F (704°C). Hydrogen lost from the zirconium-uranium hydride fuel can permeate both cladding and system walls, thereby developing a steady-state concentration in the NaK primary coolant.

From this solution the hydrogen may be lost by permeation through the system walls, it may be removed by precipitation in cooler regions of the system or cold traps, or it may react with hydride-forming metals in the system (getters). In the elucidation of all these mechanisms, a knowledge of the pressure-concentration-temperature equilibrium relationships for hydrogen in the various gas, liquid, and solid phases is required.

In general, it is to be expected that more hydrogen will dissolve in a liquid alkali metal, as the pressure is increased, until the precipitation of a solid phase occurs. At this point the addition of more hydrogen will result only in further precipitation, while the pressure will remain constant, as required by the phase rule. In systems having more than one metal, the pressure can gradually alter as a metal hydride precipitates and the relative proportion of metal changes. An excellent summary of the chemistry of metal hydrides is given by Gibb.⁷

A number of studies have reported the plateau decomposition pressures of alkali metal hydride systems.⁸⁻¹³ Both sodium and potassium have been studied separately.

Williams¹⁴ has reported the solubility of sodium hydride in sodium as a function of temperature.

Engineering-scale studies^{15,16} related to the Dounreay reactor used a cold-trapping technique to determine the solubility of solid hydride in NaK-30 (30 wt % K) at various temperatures.

Studies of the solubility of hydrogen in sodium in the absence of precipitate have been reported using laboratory gasometric techniques.^{17,18} In general, in the various papers cited above the values of plateau decomposition pressure are consistent. However, agreement between the respective authors as to the solubility of either gaseous hydrogen or solid hydride is poor; although about the same solubility is found at 1 atm (and 400°C), the findings as regards temperature coefficient and the effect of pressure on solubility do not agree well.

These discrepancies are readily understood. The plateau pressure measurement is not sensitive to losses; however, the quantitative accounting for hydrogen is troublesome. If the liquid metal is directly contained in glass or quartz and is not protected from various contaminating reactions, one kind of error results. If the liquid metal is enclosed in a metal container, diffusion is slow, especially at low temperature. Also, reaction may be slow at low temperatures, below 400°C. At temperatures above 400°C, diffusion losses may be high, particularly from metal systems.

The type of isotherm to be expected is indicated in Fig. 8.

The pressure is expected to rise as hydrogen is added, at first forming an unsaturated solution. The functional relationship between pressure and temperature has not been defined, but Sieverts' law, which applies for solutions of hydrogen in many metals, indicates that the concentration should vary with the square root of pressure. When the solution becomes saturated, the pressure ceases to rise rapidly, and solid hydride, doubtless of a single metal, begins to precipitate. This knee is indicated as point A on the diagram. As precipitation of a single metal hydride continues in our system of mixed metals, the liquid metal composition will drift, as will the decomposition pressure, until a composition B is reached at which two metal hydrides begin to precipitate. The pressure will then remain constant until the liquid phase disappears and two solid phases of metal hydride saturated with metal in solid solution remain.⁷ As even more hydrogen is added, the pressure rises rapidly and the solid phase composition approaches that of pure metal hydride.

As the temperature is lowered, the decomposition pressure becomes lower, as also does the terminal solubility. The terminal solubility may

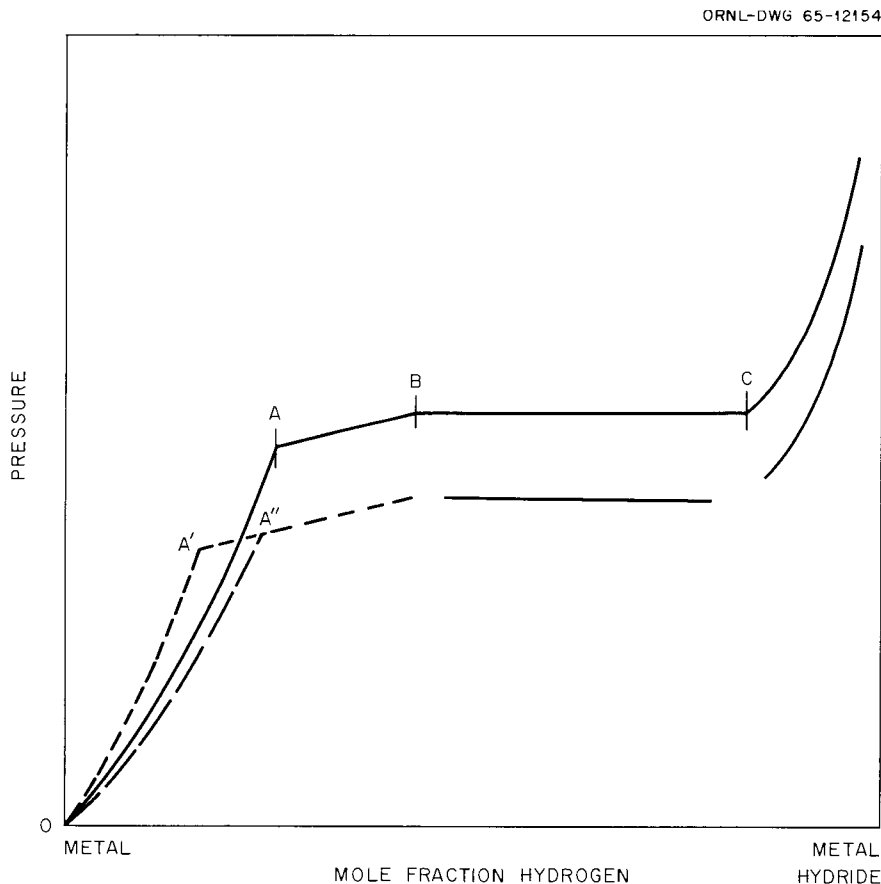


Fig. 8. Possible Isotherms in a Hydrogen-Alkali-Metal Mixture System.

fall to the left or the right of line OA. The literature is inconsistent in this respect for the sodium-hydrogen system. If, for example, the sodium-hydrogen system terminal solubility data of Williams, Grand, and Miller¹⁴ are used along with sodium hydride decomposition pressure data of Herold,⁹ then the terminal solubility at lower temperature (A') lies to the left of line OA. If solubility data of McClure and Halsey¹⁸ are used, it (A'') will lie to the right of OA, though not to the right of A. This relationship is quite important in considering unintentional or intentional (cold trapping) precipitation and other phenomena involving hydrogen in liquid metal systems for reactors.

It is our purpose to determine the relationship between pressure, composition, and temperature for unsaturated solutions of hydrogen in eutectic sodium-potassium mixture (78% K) and to determine the terminal solubility (A) and associated saturation pressure as a function of temperature.

We also conducted some hydrogen solubility experiments in which several atom percent of a third alkali metal, lithium, was added. These experiments permit us to suggest a tentative model for the chemistry of hydrogen in liquid alkali metal solutions.

The apparatus used is shown in Figs. 9 and 10. A thin-walled capsule of Armco iron contained the liquid metal. The capsule fitted closely into a quartz jacket or envelope which was plugged by a closely fitting quartz core tube and sealed by a standard taper joint, outside the furnace.

The capsule was $5/8$ in. in diameter by 5 in. long with 0.020-in.-thick walls. It was hydrogen fired at 1040°C to remove oxide films and was stored in the helium-filled glove box without air contact until used.

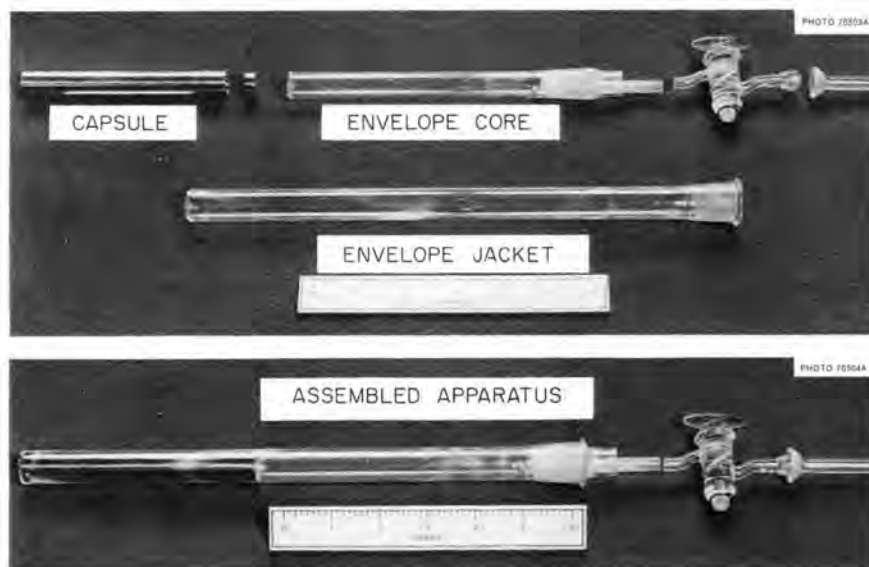


Fig. 9. Hydrogen Solubility Capsule and Envelope.

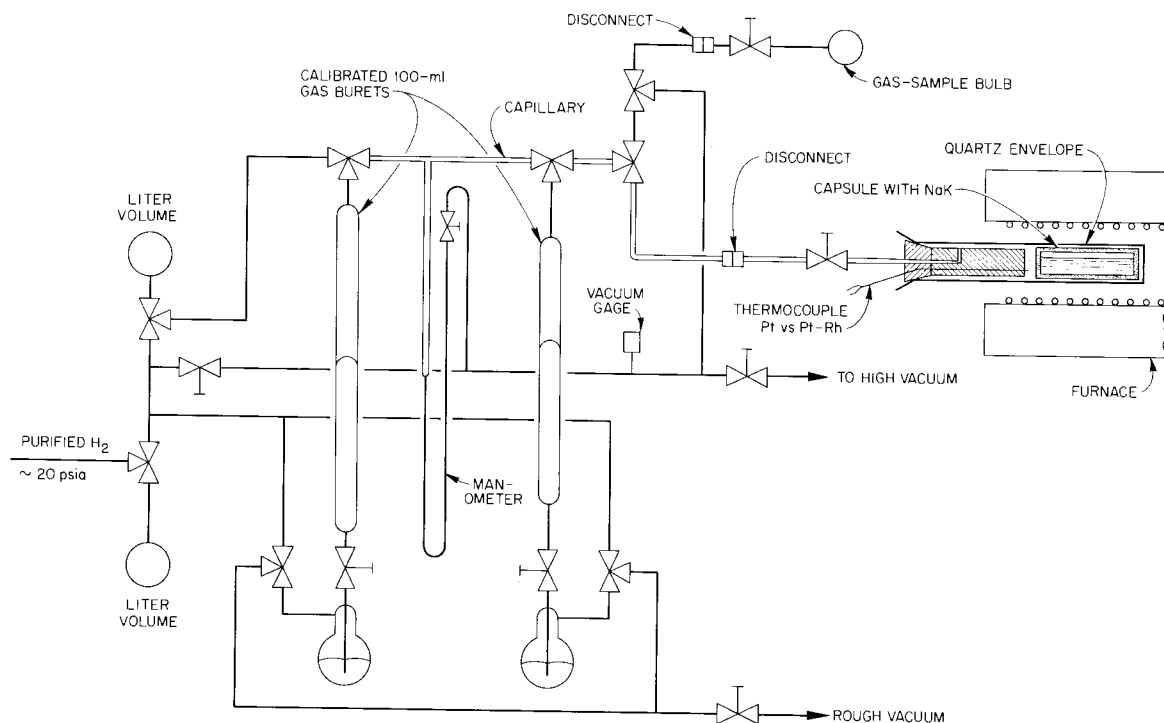


Fig. 10. Diagram of Apparatus for Measuring the Solubility of Hydrogen in NaK.

In a top end a small tapered plug was fitted. After the NaK was injected into the capsule and weighed, the plug was welded in and the end machined flat.

The empty quartz envelope was placed in the furnace and taken to the temperature at which solubility experiments were to be conducted. Hydrogen was admitted from the gasometry apparatus, and hydrogen loss rates were determined at several pressures at levels anticipated for the experiment. Calculated hydrogen inventory was later corrected for such loss on the basis of such calibration of each envelope.

The sealed iron capsule containing about 10 g of liquid metal was put in the quartz envelope, which was placed in the furnace and attached to the gasometry system. The dead space outside the capsule in the envelope, up to the stopcock, was calibrated using pure nitrogen gas, both at room temperature and at experiment temperature. Nitrogen was used, rather than helium, argon, or hydrogen, because it did not react with or permeate significantly through either quartz or iron at the experiment temperature.

Hydrogen was measured in terms of the manometric pressure in small calibrated volumes, mostly consisting of the manometer manifold and associated lines. Usually a fixed quantity of gas would be placed in the manifold, and then the envelope stopcock would be opened, permitting the gas to enter the envelope. As it permeated the capsule wall, the pressure would decrease until pressure equilibrium was reached, as shown by lack of pressure change over a substantial period of time. It was then possible either to make another addition or to evacuate the system up to the envelope stopcock and thereby on opening the stopcock to cause hydrogen to permeate out of the capsule. When the solubility-pressure values obtained in this way were plotted, they usually fell on the same line regardless of the side from which equilibrium was approached. Consequently, it appears demonstrated that the pressure values represented true equilibrium and that the slight time drift of the hydrogen inventory due to permeation of the quartz envelope was adequately accounted for. At temperatures of 548, 593, and 704°C, hydrogen pressures were increased in steps to about 1 atm. After additions and removals were completed, the envelope stopcock was closed at temperature, and analyses were made to determine the hydrogen contained within the envelope for comparison with the inventory value. Hydrogen was determined in the three possible regions. The hydrogen outside the capsule was measured after cooling, using the gasometric apparatus. A sample was analyzed by mass spectrometry. The capsule was then placed on a special puncturing device. The hydrogen gas in the capsule dead space was removed by a Toepler pump and measured, and a sample was analyzed by mass spectrometry. Hydrogen associated with the liquid and solid phases of the capsule was determined as follows.

The punctured capsule was removed from the puncturing device in the helium glove box, and the capsule and entire contents were placed and sealed in the glass container to be used in the amalgamation analysis of the alkali metal by the method of Goldberg.¹⁹ In this analysis mercury was added, and the liquid metals, but not the oxides or hydrides, dissolved in it and were removed. The system was refluxed, and the quantity of hydrogen evolved was determined by gas chromatography. The amount and identity of oxides were determined by titration and flame spectrophotometry of the water-soluble residue.

In eight experiments the recovery of hydrogen was compared with that shown by inventory figures as shown in Table 8. The recovery values ranged from 88 to 142%, with a median of 95 to 98%. One of the values above 100% involved quite low quantities of hydrogen. The remaining two of the values above 100% recovery involved lithium hydride precipitates, which were difficult to decompose. The entire mass of these precipitates was taken as being lithium hydride. These values are consequently less certain than the others.

It is believed that the above recovery values, as determined by chemical analysis, verify the inventory values adequately and support the view that solubility can be determined with adequate accuracy from calculations based on envelope inventory.

To calculate the solubility from envelope inventory, the amount of hydrogen contained in the envelope dead space was calculated using the

Table 8. Total Hydrogen Found vs Inventory in All Solubility Experiments

Liquid Metal	Temperature (°C)	Final Pressure (mm)	Net Hydrogen Charged [cc (STP)]	Total Hydrogen Found [cc (STP)]	Percent "Recovered"
NaK-78	704	284	16.3	15.5	95
	605	552	24.4	21.4	88
	543	659	27.5	27.3	99
	400	288	21.2	20.1	94
	330	23	4.2	6.0	142
NaK-78					
With 1.4 at. % Li	538	54	32.3	40.5 ^a	125 ^a
With 2.2 at. % Li	593	447	77.1	99.2 ^a	129 ^a
With 4.6 at. % Li	593	727	155.0	146.5 ^a	94 ^a

^aLithium in insoluble residue is assumed to be LiH.

earlier calibration. The amount of hydrogen dissolved in the capsule iron was calculated using the solubility coefficients reported by Armbruster.²⁰ The internal gas volume of the capsule was calculated, taking into account the thermal expansion of the capsule material and the liquid metal contained in it. This gas space was regarded as containing hydrogen at the equilibrium pressure and temperature (as well as helium).

The remainder of the hydrogen was taken as being dissolved in the liquid metal. The solubility at the indicated pressure and temperature was expressed variously as std cc of H₂ per gram of liquid metal, parts of hydrogen by weight per million parts of solution (ppm H), or, on occasion, atoms of hydrogen per atom of metal in solution (atom % H/metal). In performing conversions among the above units, it is useful to note that 1 kg of our eutectic sodium-potassium mixture contained 224 g of Na (9.74 gram-atoms of Na or 32.9 at. % Na) and 776 g of K (19.85 gram-atoms of K or 67 at. % K) or 29.59 gram-atoms of metal, with a consequent average atomic weight of 33.8.

Examples of the hydrogen-recovery balance in several solubility experiments are shown in Table 9. A similar calculation of the solubility is made from the net inventory figure.

Experimental Results for Solubility of Hydrogen in NaK-78

Results of experiments at several temperatures are shown in Figs. 11 to 13, in which hydrogen solubilities at various successive equilibrium hydrogen pressure values are shown for each temperature.

Solubility in std cc of H₂ per gram of liquid metal is plotted against the square root of pressure, resulting in straight lines, in agreement with Sieverts' law. The successive pressure values are numbered consecutively.

Table 9. Hydrogen Final Inventory and Recovery Balance in NaK Solubility Experiments

Experiment temperature, °C	330	400	573	605	704
Weight of original NaK, g	9.083	9.222	9.024	9.208	9.366
Weight of recovered NaK, g	8.55	8.90	8.58	8.89	8.96
Pressure at run termination, mm Hg	22.6	288	659	552	284
Final inventory, cc (STP)					
Hydrogen measured into envelope	4.70	23.05	28.27	24.62	16.77
Cumulated permeation loss	0.52	1.83	0.74	0.22	0.51
Net final inventory	4.18	21.22	27.53	24.40	16.26
H ₂ distribution at temperature and pressure					
Envelope dead space	0.29	2.40	2.73	2.85	1.59
Capsule vapor space	0.01	1.45	2.34	1.43	0.75
Dissolved in iron of capsule	0.01	0.19	0.28	0.73	0.34
Total tare	0.31	4.04	5.35	5.01	2.68
Balance dissolved in NaK	3.87	17.18	22.18	19.38	13.58
Solubility at temperature and pressure, cc (STP) per gram of NaK	0.426	1.863	2.458	3.105	1.450
Sieverts' solubility coefficient, cc (STP) g ⁻¹ atm ^{-1/2}	2.47	3.03	2.63	2.47	2.37
Hydrogen recovered (after isolating envelope and cooling), cc (STP)					
Envelope dead space	0.07	1.21	2.68	3.36	1.61
Capsule vapor space	0.08	0.04	0.84	0.02	0.40
Analyzed in recovered NaK	5.8	18.8	23.8	18.0	13.50
Total recovered	5.95	20.05	27.33	21.38	15.51
Percentage of net hydrogen inventory	142.3	94.5	99.2	87.6	95.4
Losses, including H ₂ in iron and lost NaK (apparent gain)	[+1.77]	1.17	0.21	3.02	0.75
Dissolved in NaK (recovered, less tare)	5.64	16.01	21.97	16.37	12.83
Solubility, cc (STP) per gram of original NaK	0.660	1.736	2.435	1.778	1.370
Sieverts' solubility coefficient, cc g ⁻¹ atm ^{-1/2}	3.83	2.82	2.61	2.09	2.24

Thus it is evident that pressure observed when hydrogen had been removed fell on the same line as when hydrogen was added. This confirms that the pressure values did indeed represent equilibrium values. The value of the solubility as determined by hydrogen recovery and analysis is also shown and, in general, agrees well with the gasometric value. In the experiment at 400°C, precipitation of solid began. The break in the pressure-solubility plot is evident.

From these data the value of Sieverts' coefficient for the unsaturated solution, the terminal solubility of hydrogen in the liquid metal, and the saturation pressure can be determined; two of the three constants are independent.

The data may be represented by the following empirical equations (any two of which are independent): For the unsaturated solution,

$$\log_{10} (S \text{ ppm}/P^{1/2} \text{ atm})_{\text{unsat}} = 2.06 + 240/T \text{ (}^\circ\text{K)} ;$$

for terminal solubility,

$$\log_{10} (S^* \text{ ppm})_{\text{terminal}} = 6.69 - 2900/T \text{ (}^\circ\text{K)} ;$$

for the saturation pressure (at knee),

$$\log_{10} (P_{\text{atm}})_{\text{decomp}} = 9.26 - 6280/T (\text{°K}) .$$

All the data obtained are shown on Fig. 14, in which the logarithm of solubility is plotted against the logarithm of the hydrogen pressure.

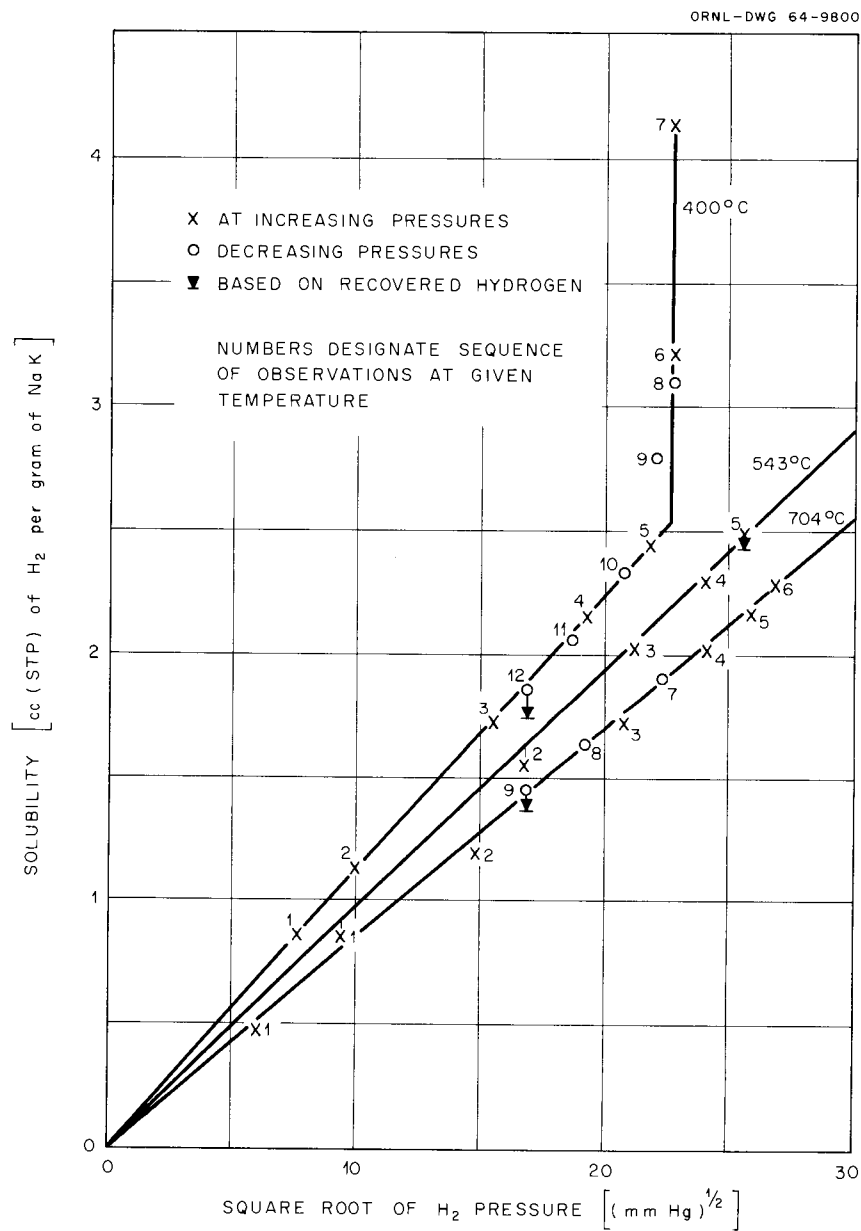


Fig. 11. Solubility of Hydrogen in NaK as a Function of the Square Root of the Hydrogen Pressure at 400, 543, and 704°C.

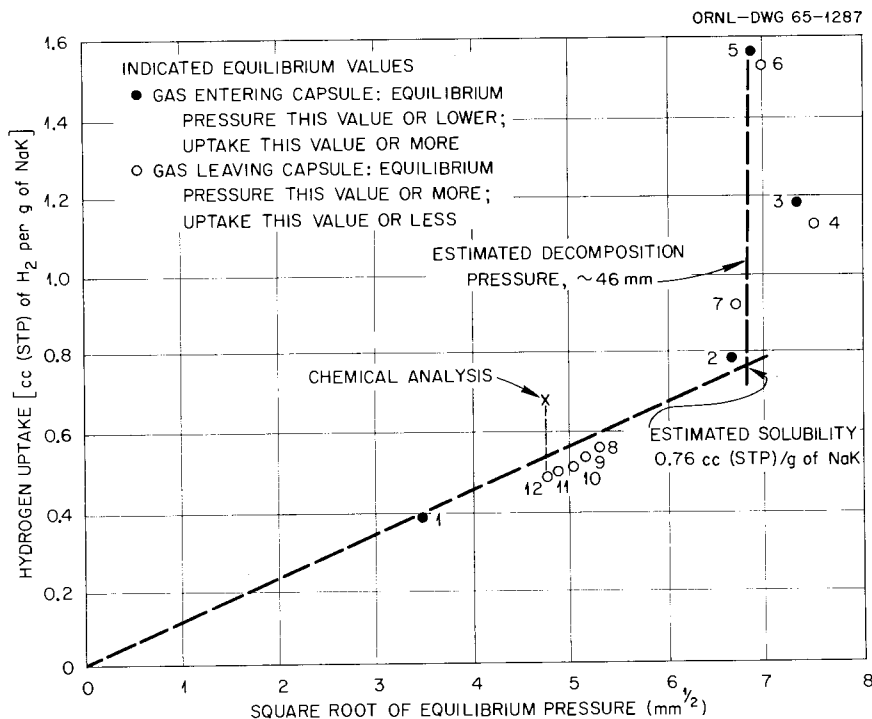


Fig. 12. Solubility of Hydrogen in NaK-78 at 330°C.

In the unsaturated regions, lines of slope 1/2 are found. At temperatures of 400°C and below, precipitation of solid hydride at pressures below 1 atm is indicated by the observed break in the curve.

These lines representing the data are also shown in the left-hand section of Fig. 15, where the logarithm of the equilibrium hydrogen uptake expressed as parts per million is plotted against the logarithm of hydrogen partial pressure, expressed in atmospheres. The hydrogen terminal solubility at 300, 330, and 400°C is plotted on the same scale in the right-hand part of the diagram, against the reciprocal of absolute temperature at which precipitation was observed. The three solubility points do fall in a straight line, as expected, permitting reasonable extrapolation of the temperature-terminal-solubility relationships.

As an example of one application of the diagram of Fig. 15 to a reactor design problem, it had been estimated that the steady-state hydrogen partial pressure for certain SNAP-8 reactor conditions under consideration was 2×10^{-5} atm. From Fig. 15, it may be estimated that the concentration of dissolved hydrogen would be approximately 1 ppm. The liquid metal containing hydrogen at this concentration could be cooled — intentionally in a cold trap or possibly in low-temperature regions of the system — to a temperature of about 300°F before precipitation of metal hydride begins.

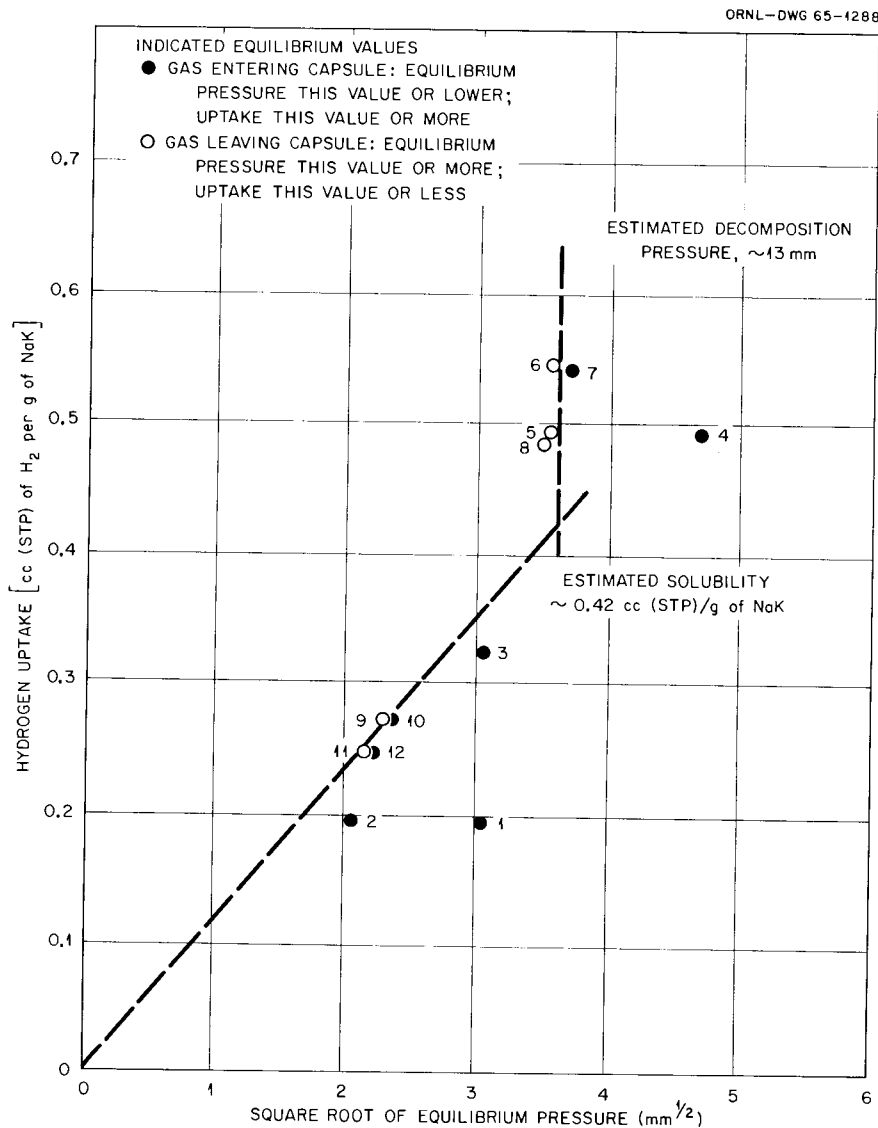


Fig. 13. Solubility of Hydrogen in NaK-78 at 300°C.

Comparison of NaK Data with the Literature

The saturation pressures observed at 300, 330, and 400°C may be compared with decomposition pressures for sodium and potassium hydrides, respectively, using the equations presented by Herold,⁹ as shown in Table 10.

Herold's equations for the decomposition pressures are: for KH, $\log_{10} P_{\text{mm}} = 11.69 - 6175/T$ (°K) and for NaH, $\log_{10} P_{\text{mm}} = 11.66 - 6100/T$ (°K).

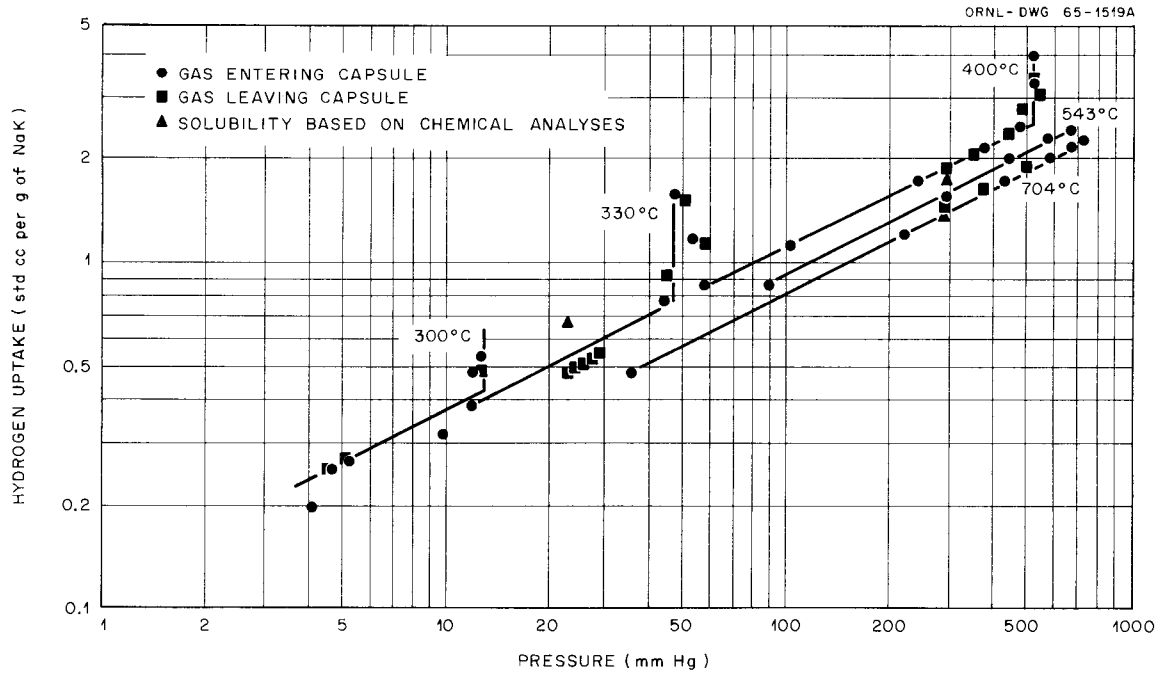


Fig. 14. Solubility of Hydrogen in NaK-78.

ORNL-DWG 65-42155

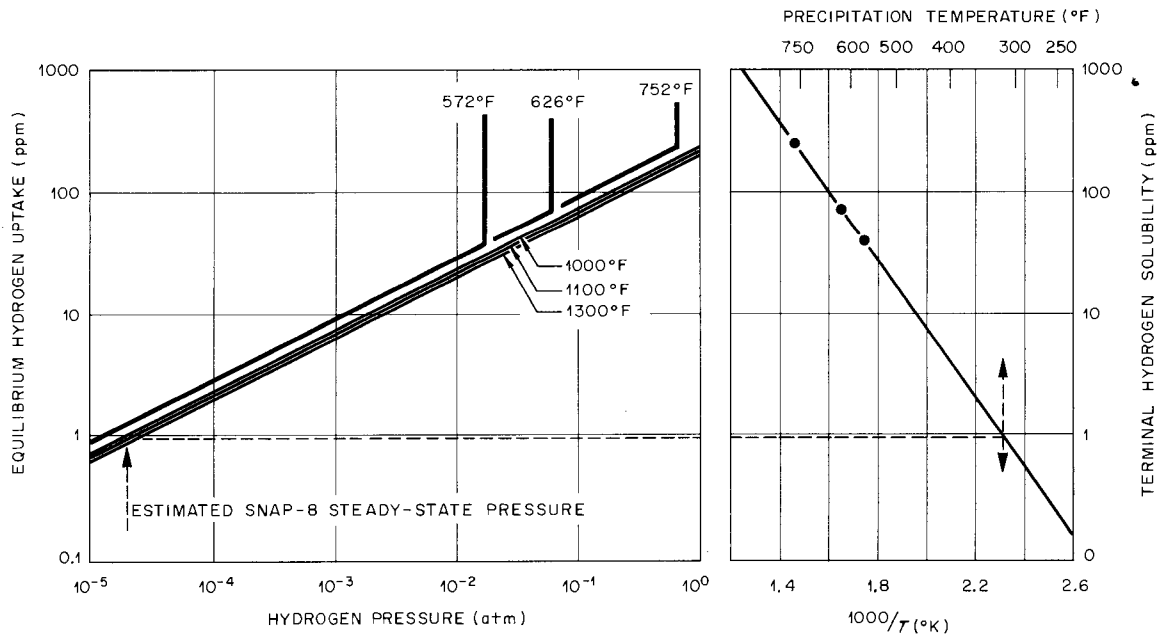


Fig. 15. Dissolution of Hydrogen Gas in NaK-78 and Precipitation of Solid Hydride.

Table 10. Saturation Pressures and Calculated Activity Coefficients Assuming KH or NaH Precipitate

Temperature, °C	300	330	400
Saturation pressure, mm	13	46	517
KH decomposition pressure, ⁹ mm	8.2	28.3	328
Calculated ^a γ_K (KH assumed)	1.18	1.17	1.19
NaH decomposition pressure, ⁹ mm	10.4	35.2	396
Calculated ^a γ_{Na} (NaH assumed)	2.71	2.66	2.66

^aCalculated activity coefficients for a given metal in hydrogen-saturated liquid are obtained from the following equation:

$$\gamma_m = \frac{1}{X_m} \cdot \left(\frac{P^\circ}{P}\right)^{1/2} \cdot \frac{a_M^\circ}{a_{MH}^\circ} \cdot a_{MH} \approx \frac{1}{X_m} \left(\frac{P^\circ}{P}\right)^{1/2} .$$

For our liquid metal mixture:

$$X_{KH} = 0.6705 ,$$

$$X_{NaH} = 0.5295 .$$

If the precipitate is KH, then activity coefficients of ~ 1.2 for potassium in the hydrogen-saturated liquid metal solution are indicated. If the precipitate is NaH, then the sodium activity coefficient is indicated to be about 2.7. Obviously, since at saturation only one precipitate first appears, only one of these calculated activity coefficients is real. Since appreciable departure from ideal behavior by the liquid metal mixture is not indicated by any other considerations, we expect the precipitate to be KH.

Our temperature coefficient for "NaK hydride" agrees well with those reported by Herold⁹ for the pure metal hydrides.

In the unsaturated solutions, the activity coefficient of the dissolved metal hydride appears to be unity, as evidenced by the linearity of the plot of dissolved hydrogen concentration against the square root of pressure and the plot of the logarithm of concentration against the logarithm of pressure. Thus, for $1/2 H_2(g) + M(l) = (MH)(d)$, we may compare hydrogen-saturated and unsaturated solutions.

$$K = \frac{a_{MH}}{P^{1/2} a_M} = \left(\frac{a_{MH}}{P^{1/2} a_M} \right)_{\text{sat'd}} .$$

Doubtless the activity of the metal in either solution is essentially the same. Thus we may obtain

$$\log X_{\text{MH}} - 1/2 \log P_{\text{H}_2} = \log \left(\frac{X_{\text{MH}}}{P^{1/2}} \right)_{\text{sat'd}} + \log \frac{(\gamma_{\text{MH}})_{\text{sat'd}}}{\gamma_{\text{MH}}} .$$

The first term on the right is constant. However, this is the equation of a straight line only if $(\gamma_{\text{MH}})_{\text{sat'd}}/\gamma_{\text{MH}}$ (and thereby γ_{MH}) is also constant over the entire concentration range to saturation. The linearity of such a plot as shown in Fig. 14 shows that γ_{MH} is constant and may be taken as unity by using the saturated solution as a standard state. Stated more simply, we find the unsaturated solutions to be ideal with respect to Sieverts' law.

These findings do not agree with those reported by Addison, Pulham, and Roy,¹⁷ who reported substantial positive deviations from Sieverts' law in the temperature region 300 to 330°C for unsaturated solutions of hydrogen in liquid sodium. Although it is likely that the precipitated solid in our case was potassium hydride, it is doubtful that our mixed sodium-potassium system should be notably more ideal than the pure sodium system.

Thereby the discrepancy between the two sets of data as regards Sieverts' law in the unsaturated region would appear to be real. Some substantiation of our findings was indicated by the studies of McClure and Halsey¹⁸ on solutions of hydrogen in sodium at similar temperatures; agreement with Sieverts' law was reported.

The temperature coefficient of solubility of solid hydride is of considerable significance with respect to the temperature at which solids may inadvertently be deposited in cooler regions and at which they may be removed in cold traps.

Data of Addison, Pulham, and Roy,¹⁷ of Williams, Grand, and Miller,¹⁴ and of McClure and Halsey¹⁸ on the sodium-hydrogen system agree generally as to the solubility level at about 400°C; however, temperature coefficients are quite different, and extrapolation of the data is consequently dubious. Addison, Pulham, and Roy¹⁷ also cited data obtained by Tyzack, of the British Downreay Reactor Project.

Our data on the sodium-potassium-hydrogen system appear to be in agreement as regards temperature coefficient with those of McClure and Halsey, and of Tyzack, on the sodium-hydrogen system. The solid hydride appears to be considerably more soluble at temperatures below 400°C than would be indicated in the widely cited data of Williams, Grand, and Miller for the sodium-hydrogen system. Since the work of those investigators appears to have been carefully done, the difference should merit further attention.

Hydrogen Solubility in NaK Containing Added Lithium

The consideration of possible means of hydrogen removal from SNAP-8 primary coolant is discussed in another section. One of the means of removing dissolved hydrogen from the liquid which appeared promising was the use of a soluble getter, which could be removed in a cold trap at temperatures considerably higher than would be required without it. Lithium appeared to be the most attractive candidate. As a result, several exploratory experiments were conducted to evaluate the effect that small additions of lithium would have on the solubility relationship of hydrogen in NaK. These experiments also lead to a simple model for the mechanism of hydrogen solubility in alkali metals.

The experimental program was halted after the four experiments reported below. However, some insight into hydrogen behavior in alkali metal solutions containing lithium can be obtained from them.

Three experiments were conducted at 1100°F. Hydrogen uptake data from these, as well as a fourth experiment at 1000°F, are shown in Fig. 16. Lithium concentration in the first experiment was 4.4 metal atom percent (or 1.354 gram-atoms of Li per kilogram of NaK). At 16.0 mm hydrogen pressure the system took up 0.776 gram-atom of hydrogen. In the absence of lithium, 0.016 gram-atom of hydrogen would be taken up by 1 kg of NaK. At 727.5 mm hydrogen pressure the system had taken up 1.492 gram-atoms of hydrogen. One kilogram of pure NaK would take up 0.104 gram-atom of hydrogen at this pressure. Such behavior is explainable if most of the hydrogen is combined with the lithium. Doubtless, a solid phase was present at all times in this experiment.

The second experiment, at 2.15 metal atom percent lithium (0.650 gram-atom of Li per kilogram of NaK), involved hydrogen uptakes from 0.259 gram-atom of H per kilogram of NaK to 0.731 gram-atom of H per kilogram of NaK. Here also a solid phase was present.

In order to study unsaturated solutions, the lithium concentration was reduced to 1.16 metal atom percent (0.347 gram-atom of Li per kilogram of NaK). Hydrogen increments were also reduced, the first being only 0.014 gram-atom of H per kilogram of NaK at 1.6 mm. At this pressure the solubility of hydrogen in NaK is 0.010 gram-atom of H per kilogram of NaK. Twelve hydrogen additions were made. The uptake was in proportion to the square root of the hydrogen pressure, in agreement with Sieverts' law, up to about 25 mm. This experiment was terminated because of mechanical problems before substantial LiH precipitation had been developed.

The experiment at 1000°F appears to have been conducted principally in the presence of precipitated lithium hydride and cannot be used thereby to measure the terminal solubility of LiH in NaK.

The discussion to follow will thereby consider only the three experiments at 1100°F in the H-Li-NaK system. The unsaturated solution

follows Sieverts' law, and hydrogen is more soluble in solutions containing lithium than in NaK alone. The uptake data indicate that precipitation of LiH occurred, and it followed a mass-action behavior. Such equilibria are consistent with the data without requiring the assumption of "nonideal" behavior.

Treatment of data in the H-NaK-Li system is shown in Table 11. In this formulation, lithium and hydrogen atoms combine to form dissolved, undissociated LiH. At a given pressure hydrogen is consequently more soluble in solutions containing lithium than in NaK alone. At a particular concentration of the undissociated LiH, precipitation of solid LiH begins.

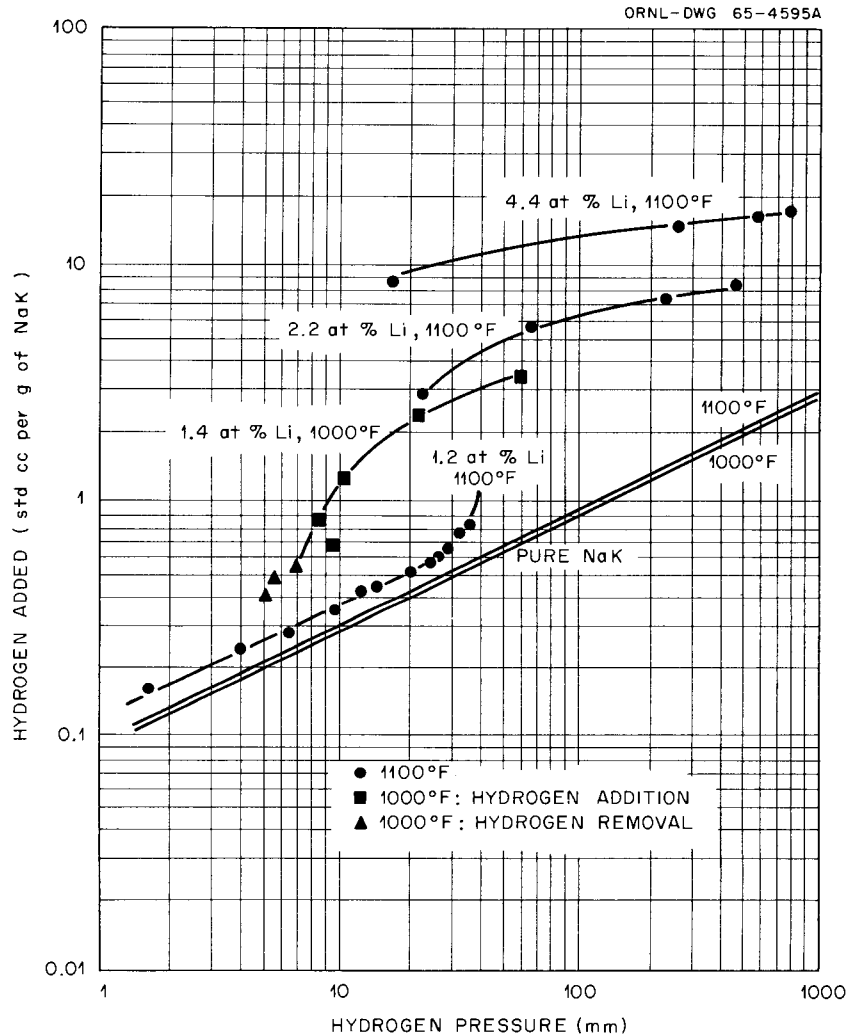


Fig. 16. Absorption of Hydrogen by NaK Containing Added Lithium.

Table 11. Solubility of Hydrogen in NaK-78 Containing Lithium at 1100°F

Data reported in sequence of hydrogen additions

Nominal Lithium Concentration (at. %)	Mass of NaK (g)	Mass of Li (g)	Hydrogen Uptake by NaK		Indicated Concentration of Given Species (gram-atoms per kilogram of NaK)				Free-Atom Product, [Free Li]·[Free H]
			Pressure (mm)	Volume [cc (STP)]	Total H	Free H ^a	Total LiH ^b	Free Li ^c	
4.4	9.192	0.087	16.0	78.8	0.7758	0.0320	0.7438	1.3438 ^c	0.01984
			266.0	135.3	1.3321	0.1303	1.2018	0.1620	0.02111
			556.5	146.2	1.4394	0.1885	1.2509	0.1129	0.02128
			727.5	151.5	1.4916	0.2154	1.2762	0.0876	0.01887
2.15	9.310	0.042	22.0	26.6	0.2586	0.0375	0.2211	0.6500 ^d	0.01608
			64.5	51.0	0.4957	0.0641	0.4316	0.2184	0.01400
			224.5	64.7	0.6289	0.1249	0.5040	0.1460	0.01824
			447.0	75.2	0.7310	0.1689	0.5621	0.0879	0.01485
1.16	9.146	0.022	1.6	1.41	0.0138	0.0101	0.0037	0.3466 ^d	0.00346
			3.8	2.04	0.0199	0.0156	0.0043	0.3423	0.00534
			5.9	2.44	0.0238	0.0194	0.0044	0.3422	0.00664
			9.5	3.03	0.0296	0.0246	0.0050	0.3416	0.00840
			12.1	3.65	0.0356	0.0278	0.0078	0.3388	0.00942
			14.5	3.88	0.0379	0.0281	0.0098	0.3368	0.00946
			19.7	4.52	0.0441	0.0354	0.0087	0.3379	0.01196
			25.6	5.16	0.0504	0.0404	0.0100	0.3366	0.01360
			24.2	5.07	0.0495	0.0393	0.0102	0.3364	0.01322
			28.1	5.59	0.0546	0.0424	0.0122	0.3344	0.01418
32.3	6.45	0.0629	0.0454	0.0175	0.3291	0.01494			
35.2	6.99	0.0682	0.0474	0.0208	0.3258	0.01544			

^aFree hydrogen is based on Sieverts' coefficient for NaK at 1100°F: ~ 0.00797 gram-atom of H per kilogram of NaK per $\text{mm}^{1/2}$.

^bLiH total includes both dissolved undissociated LiH and precipitated LiH, calculated as total H minus free H.

^cFree Li is calculated as original Li minus total LiH.

^dLithium in NaK prior to hydrogen additions.

If the hydrogen associated with the NaK in such solutions is measured by the Sieverts relationship determined previously for solutions without added lithium, stoichiometric relationships permit the concentrations of "free H," "free Li," and "total LiH" to be calculated.

Data calculated in this form are shown in Table 11.

If we plot the logarithm of the free-atom product, $[\text{Li}]_{\text{NaK}} \cdot [\text{H}]_{\text{NaK}}$, vs the logarithm of $[\text{LiH}]_{\text{tot}}$, two lines should ensue. In the absence of precipitate,

$$[\text{LiH}]_{\text{NaK}} = [\text{LiH}]_{\text{tot}} ,$$

$$\log [\text{Li}][\text{H}] = \log K_1 + \log [\text{LiH}]_{\text{NaK}} ,$$

$$\text{slope} = 1 .$$

In the presence of solid,

$$\log [\text{Li}] \cdot [\text{H}] = \log K_2 ,$$

$$\text{slope} = 0 .$$

Such a plot of the three experiments is shown in Fig. 17. As may be seen, the data may be fitted by a line of 45° slope, followed by a line of slope = 0. Deviations from the lines are much below a factor of

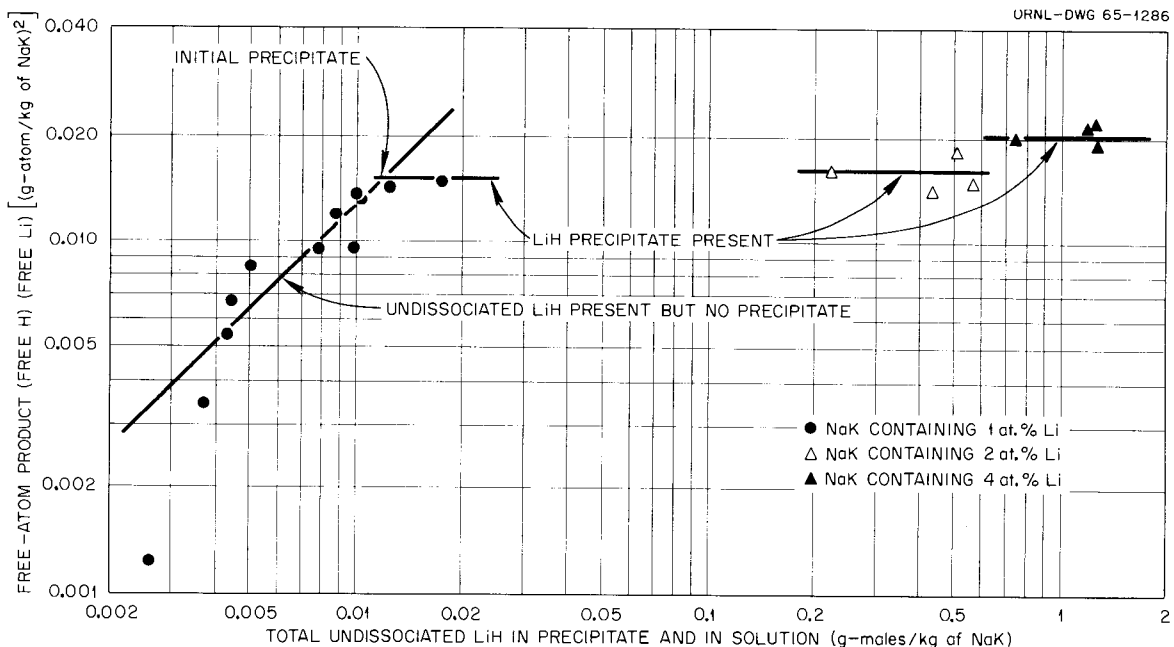


Fig. 17. Solubility Relationships at 1100°F in the H-Li-NaK System.

2, while in the experiments, pressures varied by a factor of 500 and hydrogen uptake by a factor of over 100. Thus our model is sufficient to fit the data. Since thermodynamic evidence alone cannot prove the necessity of species such as the undissociated LiH, the equilibria above must at present be regarded only as a credible hypothesis. It is, however, of interest to note that it was not necessary to invoke nonideal behavior to interpret the data.

Uncomplicated agreement with Sieverts' law in the present investigation indicates the dissolved species to be substantially monoatomic in hydrogen. Consistent with the above evidence for undissociated LiH in solution, similar expressions for undissociated NaH and KH species may be formulated. Other dissolved hydrogen species, such as free hydrogen atoms or free hydride ion, do not have to be invoked to explain the data we have presented in this report. Instead, the dissolved hydrogen may be regarded as being partitioned between the various alkali metals in proportion to their concentration (or activity) and their respective affinities for hydrogen, the solutions being essentially ideal. Sieverts' law should then be obeyed by unsaturated solutions. The Sieverts coefficient would depend on the composition of the metal solution, remaining constant until precipitation of some species occurs. No further inferences as to the structure of liquid alkali-metal solutions containing hydrogen appear indicated on the basis of the present data.

The above experiments indicate that the addition of small proportions of lithium to NaK can substantially reduce the hydrogen activity at 1100°F. However, experiments at other temperature are required before the potentialities of this technique for hydrogen control in SNAP-8 can be evaluated. The single experiment at 1000°F conducted before this program was terminated did not determine the saturation pressure and concentration, and thus is inadequate for such purpose.

CALCULATIONS RELATIVE TO HYDROGEN IN THE SNAP-8 SYSTEM

Estimate of Steady-State Pressure Resulting from Hydrogen Permeation of System Walls

Hydrogen entering the SNAP-8 primary coolant from the zirconium-uranium hydride fuel element will largely be lost by permeation of the various walls of the primary system. If the entry rate is steady, then a steady-state loss rate and system concentration will result. Hydrogen flow may roughly parallel heat flow, and a major portion of the hydrogen may pass through boiler tubing walls into the mercury Rankine system rather than being directly lost into space. Boiler operation may tend to accumulate the hydrogen in the condenser outlet, where it could lead to substantial operating problems.

In order to conduct both bench- and engineering-scale experiments and evaluations in a manner that is relevant to the SNAP-8 program, an estimate of the steady-state behavior of hydrogen in the primary system

is desirable. One useful approach is to assume that the presence of NaK will not affect the steady-state permeation rates from the system, but will only serve to carry hydrogen around the system. Our experimental work has shown that this is basically true. As a result, in estimating the steady-state pressure, we may use permeabilities based on gaseous systems with clean oxide-free walls. We shall also assume the validity of the dependence of permeation rate on the square root of pressure, although this has not been proven at the lowest pressures. We shall assume that the pressure at any point depends on Sieverts' law for hydrogen solubility in NaK. We shall also assume a set of materials, sizes, and temperatures for the SNAP-8 primary, which at one time were thought to be representative, but doubtless since then have been subject to some modification. Such modification is not expected to affect major conclusions.

In the steady state the input to the system will equal the permeation losses through the system. The concentration of the dissolved hydrogen in the NaK will remain constant as it circulates, since the circuit time is far shorter than the time to reach the steady state. We may regard the NaK in any region as exhibiting a hydrogen pressure characterized by Sieverts' law at that temperature. The metal, at similar temperature, will have a hydrogen permeation rate depending on the area, thickness, and permeability coefficient. We may write

$$I = X \cdot \sum_{\text{loop}} \frac{K A}{S \theta} = P X ,$$

where

I = hydrogen input rate into primary, cc (STP)/hr,

X = hydrogen concentration in NaK, cc (STP) per gram of NaK,

K = hydrogen permeation coefficient, cc (STP) mm hr⁻¹ cm⁻² atm^{-1/2},

S = Sieverts' hydrogen solubility coefficient, cc (STP) g⁻¹ atm^{-1/2},

A = wall area of loop section, cm²,

θ = wall thickness of loop section, mm,

P = permeation factor for loop = $\sum_{\text{loop}} KA/S\theta$.

Table 12 shows one calculation of the permeability factor for the SNAP-8 primary circuit. Materials, dimensions, assumed temperatures, permeability coefficient, and Sieverts' coefficients are given for various items or regions in the circuit. Regions of substantial dimensions are treated in two parts of different temperatures. The permeation factor for the entire system is 5668, of which the 0.125-in.-wall Croloy 9M boiler tubing comprises (2249 + 1514 = 3763) about 66%.

If one assumes an input rate of 67 cc (STP) of H₂ per hour, the estimated steady-state concentration is 1.18 × 10⁻² cc (STP) per gram of NaK. At 1100°F this concentration, according to Sieverts' law, would be in equilibrium with hydrogen at a partial pressure of 2.4 × 10⁻⁵ atm.

Table 12. Calculation of Permeation Factor P for Primary Coolant System

$$P = \sum KA/S\theta$$

Item or Point	Material	Length (in.)	Diameter (in.)	θ , Thickness (in.)	A, Area (ft ²)	Region	Mean Temperature (°F)	A/ θ (cm ² /mm)	S ^a	K ^a	KA/S θ
Core exit						Exit	1300				
Piping from core to boiler	Type 316 stainless steel		2	0.049	7.8	All	1300	5,822	2.15	0.260	704
Boiler						Inlet	1299				
Tubing	Croloy 9M	35.5	1	0.125	72.3	Hot half	1249	10,576	2.21	0.470	2249
						Cool half	1149	10,576	2.34	0.335	1514
Shell, annular cylinder	Type 316 stainless steel	35.5	19.87 OD 14.63 ID	0.090	30.6	Hot half	1249	6,217	2.21	0.1805	508
						Cool half	1149	6,217	2.34	0.0815	216
						Exit	1099				
Piping from boiler to pump	Type 316 stainless steel		2	0.049	6.2	All	1099	4,627	2.41	0.0527	101
Pump casing	Type 316 stainless steel			0.250	0.8	All	1099	117	2.41	0.0527	3
Piping to parasitic heater	Type 316 stainless steel		2	0.049	4.2	All	1099	3,135	2.41	0.0527	69
Parasitic heater shell	Type 316 stainless steel	30	10	0.083	7.5	All	1100	3,305	2.41	0.0530	73
Pumping to core	Type 316 stainless steel		2	0.049	7.9	All	1100	5,896	2.41	0.0530	130
Core entry						Inlet	1100				
Reactor core shell	Type 316 stainless steel	20	9-3/16	0.109	4.9	Inlet dome	1100	168	2.41	0.0530	4
						Cool half	1150	654	2.34	0.0818	23
						Hot half	1250	654	2.21	0.1810	54
						Exit dome	1300	168	2.15	0.2600	20
											5668

^aSolubility, S, and permeability, K, values at a given temperature were based on data obtained at ORNL.

As indicated above, the major part of the losses would be into the mercury boiler system. No back pressure of hydrogen from this region was assumed in this model, which visualized the hydrogen as being swept by the mercury vapor to the condenser outlet, where it would tend to accumulate. Unless it was returned with the liquid mercury to the boiler, its subsequent fate was not a subject of this investigation, although its importance to the SNAP-8 system should be considered by the proper investigators.

Removal of Hydrogen from SNAP-8
Primary NaK by Cold Traps, Windows, and Solid Getters

The steady-state hydrogen pressure in the SNAP-8 primary system was estimated above to be about 2.4×10^{-5} atm, corresponding to approximately 1 ppm of H in NaK. On the basis of our solubility studies for hydrogen in NaK, summarized in Fig. 15, it may be estimated that the precipitation of solids may be anticipated if this solution is cooled to a temperature slightly above 300°F.

If such a temperature is possible in any part of the SNAP-8 primary system (i.e., in certain pump regions), then solid hydride could accumulate there at a rate which would also depend on how fast NaK passed through this region.

In order to minimize both this possibility and perhaps more importantly to reduce the permeation of hydrogen into the mercury boiler, reduction of the hydrogen concentration in the primary NaK could be of value. Several means of doing this can be considered. These include direct cold trapping and the use of highly permeable windows, solid getters, or soluble getters.

Direct Cold Trapping

If cold trapping is to be employed, then the rate of passage into the trap, at mainstream concentration, and the trap effluent concentration must be taken into account. This is described in the following, which applies to all types of bypass traps.

$$I + mX_T = mX + PX ,$$

where m is the grams of NaK per hour passing through the trap, and X_T is the concentration of hydrogen in the trap effluent.

If we define r as the fraction of original untrapped hydrogen in the mainstream, which persists in the mainstream after trapping at given bypass rate,

$$r = \frac{X}{X_0} = \frac{I + mX_T}{X_0(m + P)} ,$$

we may show

$$\frac{m}{P} = \frac{1 - r}{r - \frac{X_T}{X_0}} = \frac{1 - r}{r \left(1 - \frac{X_T/X_0}{r}\right)}$$

Thus the trap must reduce the concentration to a lower fraction (X_T/X_0) than is actually effective (r) in the mainstream, unless an infinite bypass rate m is to be employed.

Values of the equilibrium precipitation temperatures may be used to estimate X at various temperatures. An extension of Fig. 15 is shown as Fig. 18, in which the logarithm of the terminal hydrogen solubility is plotted against the reciprocal of absolute temperature.

For $r = 0.02$, $X_0 = 1$ ppm, and $X_T = 0.01$ ppm, a NaK cold-trapping temperature of perhaps 140°F or lower is indicated at equilibrium by Fig. 18. A bypass rate for this condition is estimated as

$$m = P \left[\frac{1 - 0.02}{0.02 \left(1 - \frac{0.01/1}{0.02}\right)} \right] = 5668 \times 98 = 556,000 \text{ g/hr}$$

or

$$m = 3.5 \text{ gpm .}$$

Thus the contents of the primary system would go through the main loop about once every 10 sec and through the bypass about once every 400 sec.

If the mainstream concentration is reduced thereby to 2% of its original value, the rate of permeation from the primary system, in particular into the mercury boiler, would be similarly reduced.

It would therefore appear possible to reduce effectively the mainstream hydrogen concentration in the SNAP-8 primary NaK by cold trapping to temperatures of the order of 140°F or lower. However, to cool the bypass stream from 1100°F to such a temperature may well not be attractive, and other means of hydrogen removal will be considered below.

Windows

One possibility of reducing the hydrogen concentration in the SNAP-8 coolant would be to provide a suitable area of material highly permeable to hydrogen. In this way the loss of hydrogen to space could be increased and the steady-state concentration in the coolant thereby reduced. This

is a problem of parallel flows, in which the conductivities are additive. The permeation factor for the SNAP-8 system was given above as

$$P_o = \sum \frac{K A}{S \theta} = 5668 .$$

The permeation factor for any window may be similarly evaluated. Here

$$I = P_o X_o = (P_o + P_w) X .$$

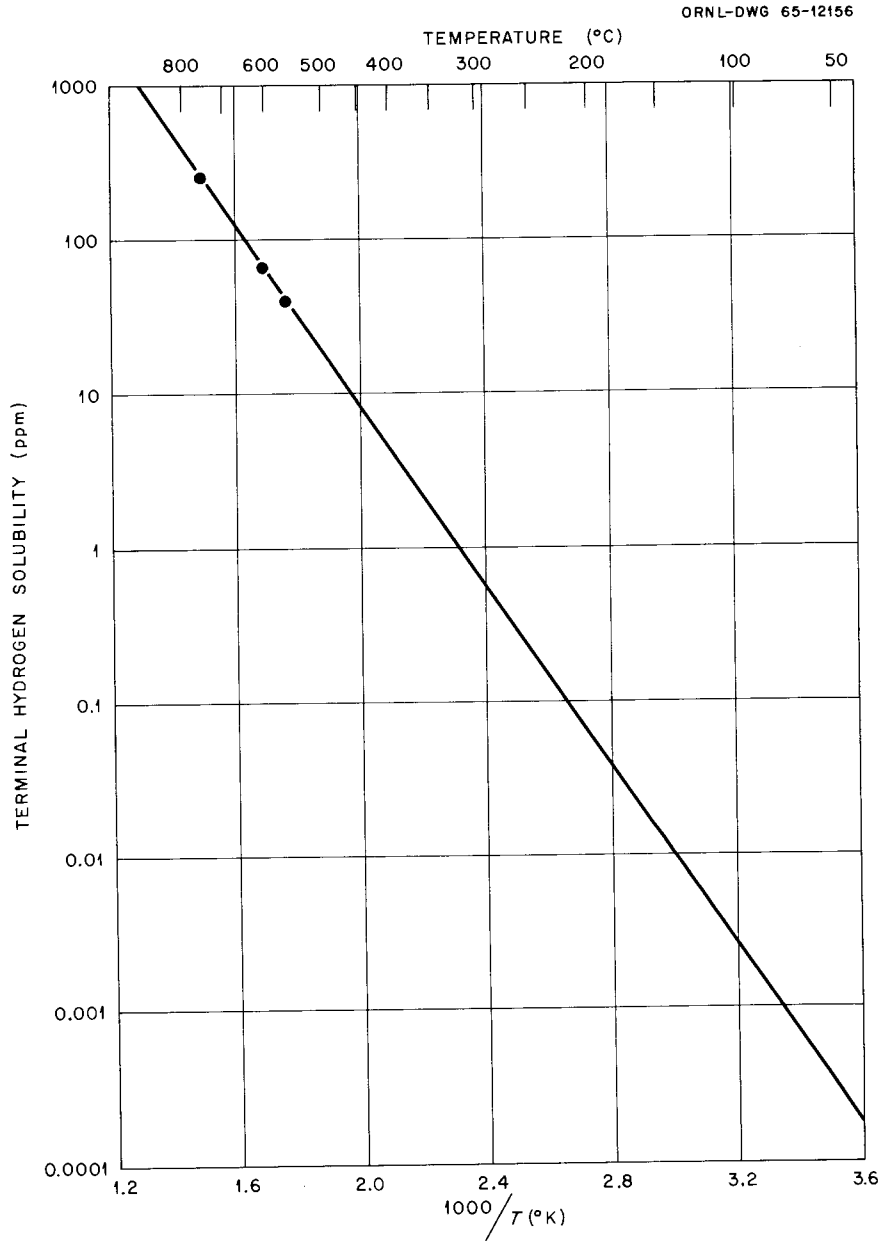


Fig. 18. Extrapolation of Terminal Solubility Data for Hydrogen in NaK.

Thus, the resultant remaining concentration ratio may be expressed:

$$r = \frac{X}{X_0} = \frac{P_0}{P_0 + P_w} .$$

It is desirable thereby to get the permeation factor of the window, P_w , much higher than that of the original coolant circuit, P_0 .

A survey of the literature has indicated that highest permeabilities at SNAP-8 temperatures are indicated for niobium and palladium-silver alloy. At 1100°F, the permeation coefficient for niobium²¹ is 100 cc (STP) mm cm⁻² hr⁻¹ atm^{-1/2}. Permeation coefficients for palladium-25% silver alloy²² extrapolated to 1100°F provide an estimated permeation coefficient of 77 cc (STP) mm cm⁻² hr⁻¹ atm^{-1/2}. It is doubtful that this alloy is compatible with NaK.

Although at low hydrogen concentrations a zirconium window might permit hydrogen to permeate at rates of interest, hydride precipitation occurs at fairly low hydrogen pressure; avoiding this could present a problem. Permeation might also be inhibited by external or internal oxide films, which would be stable. Zirconium will not be considered further.

To examine the size window that might be required, let us rearrange the above formula to read

$$P_w = P_0 \frac{1 - r}{r}$$

or

$$\frac{A_w}{\theta_w} = \frac{P_0}{K_w S} \frac{1 - r}{r} .$$

If we wish to reduce the hydrogen concentration to 1% of the original value by using a niobium window of 1 mm wall thickness, the area/thickness requirement of the window is

$$\frac{A_w}{\theta_w} = \frac{5668}{100 \times 2.41} \times \frac{1 - 0.01}{0.01} = 2328 \text{ cm}^2/\text{mm} .$$

The area/thickness of the boiler tubing is about 21,200 cm²/mm and of the remainder of the system 36,980. Thus, the size of the window region would constitute an appreciable part of the SNAP-8 primary circuit. Unless some way were found to replace original type 316 stainless steel piping with niobium, the use of windows appears marginal.

The use of window regions in a bypass circuit will involve considerations similar to those for cold traps and will require larger areas. The increased area will also require consideration of the associated larger heat loss potential.

In summary, the use of any materials except niobium for a window to reduce hydrogen concentration in the SNAP-8 primary coolant appears prohibitive. The use of niobium could be considered, but to us appears marginal.

Use of Solid Getters

The question of getters implies unclad materials, since otherwise the cladding becomes a sort of internal window, becoming thus a resistance in series. Solid getters involve a solid solution of hydrogen in the metal in most cases because the desired pressures are low. The equilibrium concentrations of hydrogen in the NaK and in the getter metal each follow Sieverts' law:

$$X_1 = S_1 P_1^{1/2} \quad \text{and} \quad X_2 = S_2 P_2^{1/2} .$$

In order to gain a preliminary understanding of the gettering phenomenon and to permit a simple comparison of materials of potential interest, an elementary static gettering situation is considered here in which a getter metal is placed in NaK and the hydrogen is partitioned between them. If we let W_1 be the weight of NaK and W_2 the weight of getter metal, the fraction of the hydrogen remaining in the NaK is

$$r = \frac{WX}{W_1 X_1 + W_2 X_2} ,$$

or if $P_1 = P_2$ (at equilibrium),

$$\frac{W_2}{W_1} = \frac{S_1}{S_2} \frac{1-r}{r} .$$

In order to make comparisons, it is necessary to evaluate the Sieverts coefficient, S_i , for materials of interest (Table 13). A temperature of 400°C was used because data were available for the various materials at that temperature. The Sieverts coefficient for NaK at this temperature is 10 ppm mm^{-1/2}. The conclusions are believed to be qualitatively correct at other temperatures of interest. It is evident that only a small proportion of yttrium would be sufficient to getter the NaK. Zirconium would be adequate only if less cleanup were desired.

The above thoughts on getters do not take into account the influx or outflow of hydrogen through system walls. However, getters that were inadequate in the static case described above would probably be ineffective in the more realistic dynamic situation.

Of the potential hot getter materials, only zirconium and yttrium appear to be adequate. Extensive areas and masses are likely to be required for zirconium if this material has to be used in the alpha or solid-solution range. The ability of hot getters to continuously maintain

Table 13. Estimated Sieverts' Coefficients for Materials of Interest as Hydrogen Getters

	Niobium ^a	Zirconium ^b	Yttrium ^c
X, ppm H	63.1	220	5000 (sat'd)
P, mm	0.1	10 ⁻⁴	2.3 × 10 ⁻⁶
X/P ^{1/2} = S _i	210	22,000	3,300,000
S _{NaK} /S _i	0.05	0.0005	0.000003

^aS. Komjanthy, J. Less Common Metals 2, 466-80 (1960).

^bE. A. Gulbransen and K. F. Andrews, J. Metals 7, 136-44 (1955); also C. E. Ellis and A. D. McQuillan, J. Inst. Metals 85, 89-96 (1956-1957).

^cE. S. Funston, "Physical Properties of Yttrium Hydride," Nuclear Metallurgy, vol. III, pp. 51-56, Inst. of Metals, Div. of AIME, Symposium, 1960.

a low concentration in the solution under steady hydrogen input conditions could be limited by hydrogen diffusion rates in the solid, leading to requirements of thin sections and high contact areas, with associated large NaK holdup volumes. The compatibility of unclad yttrium metal with high-temperature NaK has not been ascertained, but compatibility problems are not anticipated.

Use of Soluble Getters, Including Lithium

There are reasons to believe that certain materials that are soluble in NaK could be used to inhibit hydride activity in NaK by forming filterable precipitates.

The use of calcium, barium, or magnesium as soluble getters for oxygen, carbon, or hydrogen was mentioned by Siegel and his co-workers²³ in 1955 and by others²⁴⁻²⁶ subsequently, and the possibility of using lithium is being considered. Experiments have demonstrated the use of calcium in oxygen removal²⁵ and in carbon removal²⁶ in dynamic systems, with mitigation of attack by these substances, but no experimental data on the use of this or other soluble materials for hydrogen removal have been found. Calcium could indeed be considered as a soluble getter to precipitate hydrogen, as suggested,²³ but the large amount of hydrogen resulting from continued entry of hydrogen into the SNAP-8 primary system appears to overextend its capabilities, as shown below. It would be satisfactory from a nuclear point of view and would doubtless be adequately compatible in a dilute NaK solution with SNAP-8 structural metals under operating

conditions. The composition-pressure-temperature relationships of calcium and of barium hydrides²⁷ are almost the same, and solid solubilities in NaK would likely be similar. However, if enough calcium were originally dissolved in the SNAP-8 primary NaK to account for all the hydrogen to be produced, a concentration of about 2 wt % would be required. No NaK data are available, but the solubility relation given by the Liquid Metals Handbook, Na-NaK Supplement, for the amount (weight percent) of calcium soluble in sodium,

$$\log_{10} w = 2.5629 - 1545.6/T ,$$

where T is in degrees K, implies that a temperature of 410°C (750°F) is required to keep this concentration of calcium in solution. Since cold trapping would have to be at temperatures of, perhaps, 400°F, it would be necessary to keep the system saturated with calcium.

It follows that both calcium hydride precipitation and calcium dissolution for makeup would each have to be at the lowest temperature of the system, or one or the other could precipitate in undesired locations. Precipitated hydride might cover calcium metal and inhibit its subsequent dissolution. To say the least, these requirements would complicate the development of a successful system involving calcium.

Barium is more soluble (in pure sodium, 40 wt % above about 100°C), but it has a neutron absorption cross section of about 1 barn, and the various isotopes produce a number of radioactive isotopes. Larger masses and precipitate volumes would be required. It is possible, however, that it could be used as a soluble getter if more attractive materials could not be found. No reports of experiments on the use of this or other soluble materials for hydrogen removal have been found, although the possibility was suggested by Siegel in 1955.²³

Possibility of Lithium-Enhanced Cold Trapping

It has appeared that the use of lithium as a soluble getter offers the potentiality of effective hydrogen removal from the SNAP-8 primary NaK by cold trapping at reasonable temperatures, along with acceptable compatibility with structural metals at SNAP-8 temperatures. The use of the readily available ⁷Li would give a very low neutron cross section (0.03 barn) and no radioactive by-products from neutron reactions.

Containment does not appear to be an appreciable problem. In reporting results for the Sunflower Program, it was concluded²⁸ from the experiments using lithium-lithium hydride mixtures with temperature cycled between 1165 and 1600°F that:

This moderate depth of penetration (3 to 5 mils for Type 316 SS, 1 to 3 mils for Haynes 25) by lithium hydride corrosion exhibited by both the Haynes alloy No. 25 and the type 316 SS after the long exposure of 5166 hours in Test 15 indicates a compatibility to the corrosive medium which would permit both

materials to be strongly considered for use in the heat receiver of the Sunflower System.

The observed attack was of the crevice and dissolution type, rather than intergranular.

Several tests were reported by Carlander²⁹ in which the corrosion resistance of type 316 stainless steel and of Inconel to NaK containing 1 to 30 wt % Li at 1500°F was measured. The most stringent conditions of temperature differential, NaK flow rate, and time were those in two tests with 5% Li which ran for 1000 hr. In these tests, attack of up to 1.5 mils occurred in the Inconel and up to 6 mils in the cold region of the stainless steel. The addition of lithium to the NaK did not decrease the normal corrosion resistance of Inconel to NaK, but it did slightly decrease that of type 316 stainless steel. Although the data obtained were erratic and were derived from only a cursory examination of the problem, they did indicate that no catastrophic increase in attack would result from the addition of lithium to NaK contained in a nickel-base alloy or an austenitic stainless steel.

Thus at the SNAP-8 temperatures the proposed dilute solution of lithium (~5 at. %) in NaK is expected to be acceptably compatible with the structural metals involved. However, these indications require verification by suitable loop tests.

The decomposition pressure of lithium hydride in equilibrium with lithium metal and hydrogen is given by Heumann and Salmon³⁰ as

$$\log_{10} P_{\text{mm}} = 9.9258 - \frac{8224}{T},$$

where T is in degrees K. Therefore the decomposition pressure of lithium hydride at 1100°F is calculated to be 2.7 mm. The equations of Herold⁹ for NaH or KH decomposition, respectively,

$$\log_{10} P_{\text{mm}} = 11.66 - 6100/T,$$

$$\log_{10} P_{\text{mm}} = 11.69 - 6175/T,$$

indicate that the decomposition pressures of NaH and KH at 1100°F are each approximately 4×10^4 mm. Thus the affinity of lithium for hydrogen is much greater than that exhibited by sodium or potassium. There is a correspondingly strong indication that at low hydrogen concentrations in NaK which contains lithium, precipitation of lithium hydride might prevent further increases in the concentration of dissolved hydrogen. It should be possible to conduct cold trapping of hydrogen at much higher and more readily achievable temperatures in the presence of added lithium than in pure NaK without lithium.

A process may be visualized in which perhaps 5 at. % ⁷Li (1.1 wt %) would be added to the SNAP-8 primary NaK. This amount of lithium is indicated by Carlander²⁹ to be soluble at 200°F. Since 3.3 at. % lithium

is sufficient to accommodate all the hydrogen expected to enter the primary coolant system, the lithium content would be depleted to about 1.7 at. % at the end of operation, unless means were provided to maintain its concentration. Even with this steady but slow depletion of lithium, circulation of a bypass stream through a cold trap at a suitable temperature could maintain the free-hydrogen concentration in the mainstream at levels below a few percent of the steady-state level which would have resulted from diffusion through system walls in the absence of lithium. The amount of hydrogen entering the secondary mercury Rankine system should be reduced by at least this proportion.

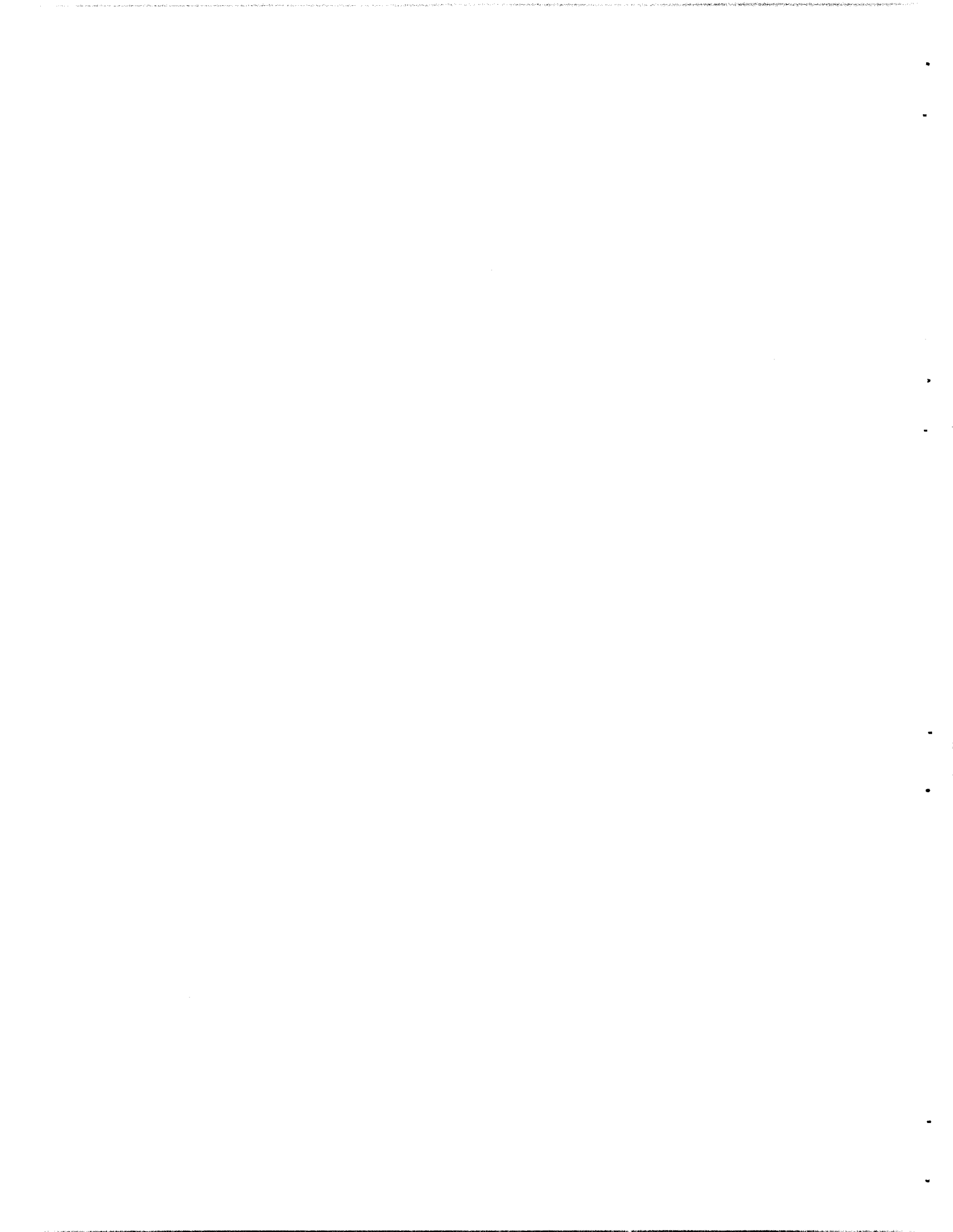
Evaluation of the potentialities of lithium hydride cold trapping requires knowledge of how the hydrogen partial pressure is related to lithium concentration at relevant temperatures. This requires an understanding of lithium-hydrogen chemistry in NaK solution and determination of the parameters or constants that characterize it.

A few scouting experiments have been made at 1100°F that appear to confirm the views stated above. These experiments and some conclusions that may be extracted from them were described in a previous section.

REFERENCES

1. R. M. Barrer, Diffusion In and Through Solids, Cambridge University Press, New York, 1951.
2. D. W. Rudd and J. B. Vetrano, Permeability of Metals and Enameled Metals to Hydrogen, NAA-SR-6109 (Oct. 30, 1961).
3. E. A. Steigerwald, The Permeation of Hydrogen Through Constructional Materials, Thompson Ramo Wooldridge Technical Memo ER-4776 (Nov. 30, 1961). (More recently, see ref. 3a.)
- 3a. E. A. Steigerwald, The Permeability of Hydrogen Through Materials for the Sunflower System, NASA-CR-54005 (May 1964).
4. Saul Dushman, Scientific Foundations of Vacuum Technique, 2d ed. (ed. by J. M. Lafferty), pp. 752-58, Wiley, New York, 1962.
5. P. S. Flint, Diffusion of Hydrogen Through Materials of Construction, KAPL-659 (1951).
6. C. L. Huffine and J. M. Williams, Corrosion 16, 430 (1960).
7. T. R. P. Gibb, Jr., pp. 315-509 in Progress in Inorganic Chemistry (ed. by F. A. Cotton), vol. III, Interscience, New York, 1952.
8. M. D. Banus, J. J. McSharry, and E. A. Sullivan, J. Am. Chem. Soc. 77, 2007-10 (1955).
9. A. Herold, Ann. Chem. (Paris) 6, 536-81 (1951).
10. A. Herold, Compt. Rend. 228, 686-88 (1949).
11. E. F. Sollers and J. L. Crenshaw, J. Am. Chem. Soc. 59, 2015-22 (1937).
12. F. G. Keyes, J. Am. Chem. Soc. 34, 779-88 (1912).
13. C. C. Addison, R. J. Pulham, and R. J. Roy, J. Chem. Soc., 4895-4901 (1964).
14. D. D. Williams, J. A. Grand, and R. R. Miller, J. Phys. Chem. 61, 379-80 (1957).
15. V. M. Sinclair, R. A. H. Pool, and A. E. Ross, pp. 35-56 in Nuclear Reactor Chemistry, Second Conference, Gatlinburg, Tennessee, October 10-12, 1961, TID-7622.
16. A. Thorley and C. Tyzack, pp. 365-97 in Thermodynamics of Nuclear Materials, IAEA Symposium, Vienna, Austria, May 21-25, 1962.

17. C. C. Addison, R. J. Pulham, and R. J. Roy, *J. Chem. Soc.*, 116-21 (1965).
18. D. W. McClure and G. D. Halsey, Jr. (thesis, University of Washington), *J. Phys. Chem.* 69, 3542-47 (1965).
19. G. Goldberg, The Rapid Determination of Low Concentrations of Oxygen and Hydrogen in Alkali Metals by a Modified Amalgamation Technique, ORNL-P-539 (Conf-721-4) (paper presented at 8th Conference on Analytical Chemistry in Nuclear Technology, Gatlinburg, Tennessee, October 1964).
20. M. H. Armbruster, *J. Am. Chem. Soc.* 65, 1043-54 (1943).
21. E. A. Steigerwald, The Permeation of Hydrogen Through Constructional Materials, Thompson Ramo Wooldridge Technical Memo ER-4776 (Nov. 30, 1961). (More recently, see ref. 3a.)
22. Bishop Platinum Company; quoted in: R. E. Corridon, Research in Diffusion of Hydrogen Through Palladium, NASA Report ATL-D-877 (July 1962).
23. S. Siegel et al., "Basic Technology of the Sodium Graphite Reactor," *Proc. U.N. Intern. Conf. Peaceful Uses At. Energy*, Geneva, 1955 9, 321-30 (1955).
24. M. Davis and A. Draycott, *Proc. U.N. Intern. Conf. Peaceful Uses At. Energy*, Geneva, 1958 7, 94-110 (1958).
25. F. L. Bett and A. Draycott, *Proc. U.N. Intern. Conf. Peaceful Uses At. Energy*, Geneva, 1958 7, 125-31 (1958).
26. W. L. Anderson, Removal of Carbon from Liquid Sodium Systems, NAA-SR-6386 (1961).
27. C. J. Smithells, Metals Reference Book, 3d ed., vol. II, p. 575, Butterworths, Washington, D.C., 1962.
28. E. J. Vargo, D. B. Cooper, and J. B. Pearson, Jr., The Containment of Molten Lithium Hydride at Elevated Temperatures, esp. p. 37, NASA-CR-54053, Thompson Ramo Wooldridge Report ER-5787 (Feb. 15, 1964).
29. R. Carlander, "Inconel and Stainless Steel in NaK Containing Lithium," ANP Project Quart. Progr. Rept. June 10, 1956, ORNL-2106, pp. 151-52.
30. F. K. Heumann and O. N. Salmon, The Lithium Hydride, Deuteride and Tritide Systems, KAPL-1667 (Dec. 1, 1956).



Appendixes



APPENDIX A

FLWSHEETS FOR CORROSION LOOPS

ORNL-DWG 65-12426

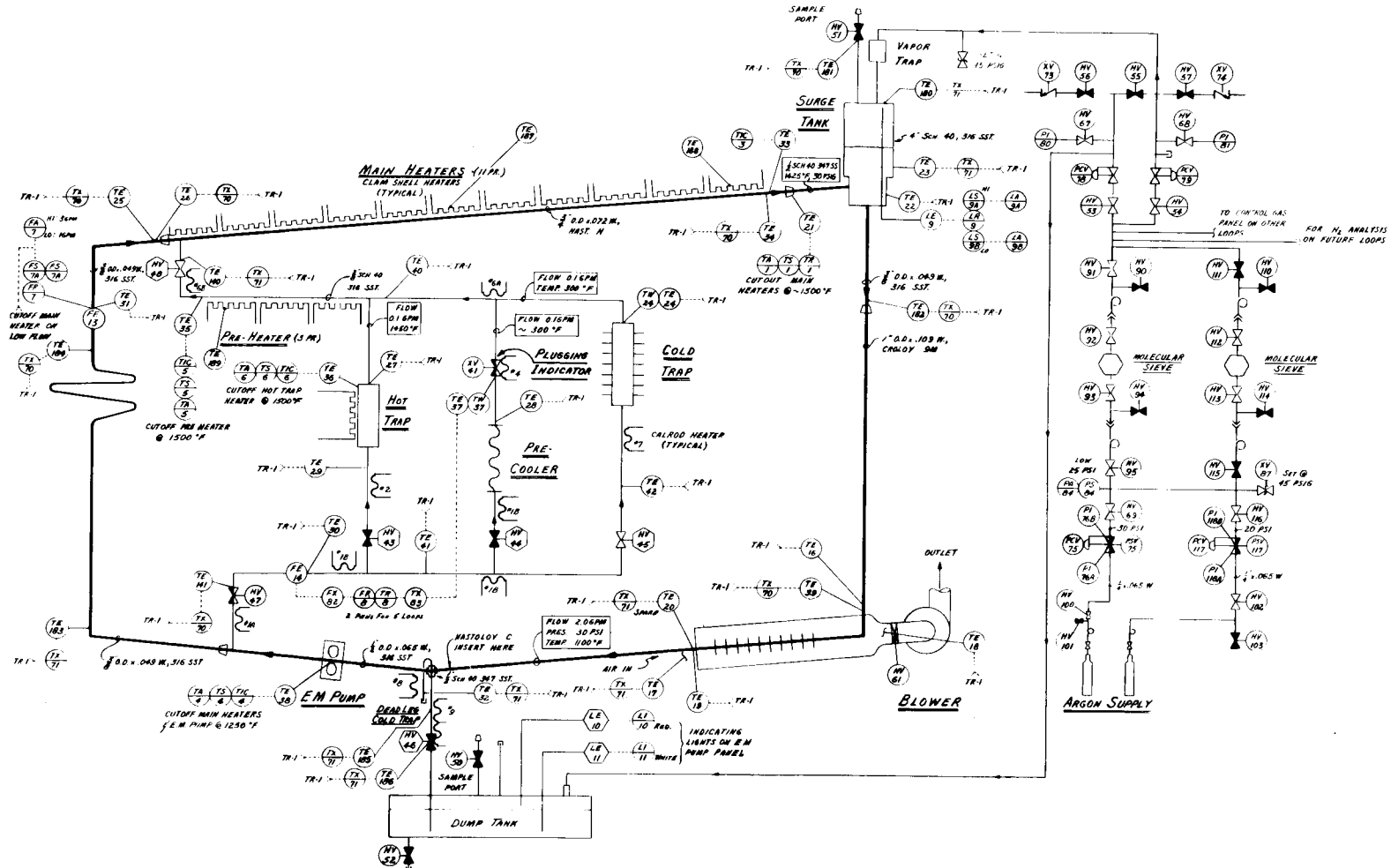
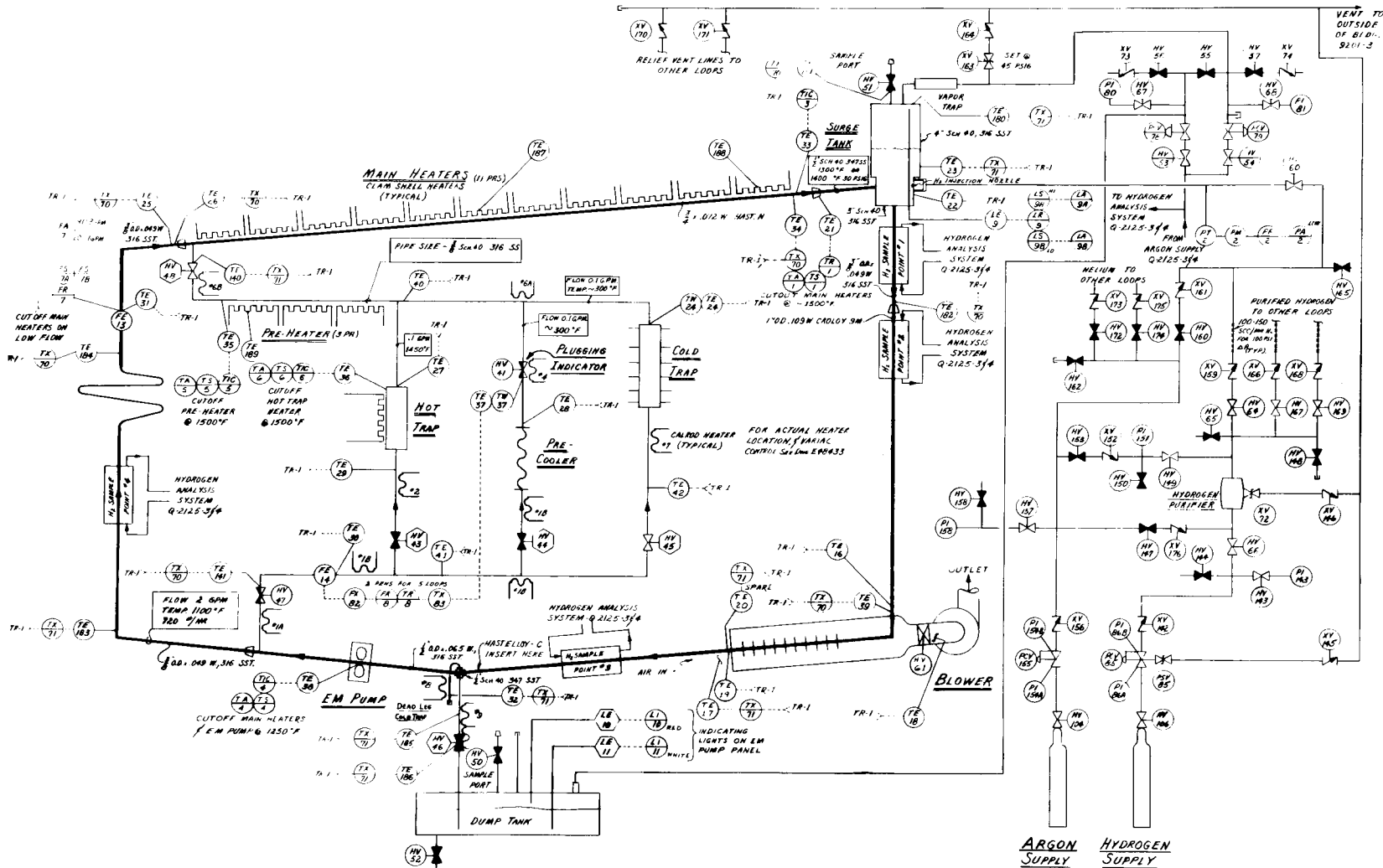
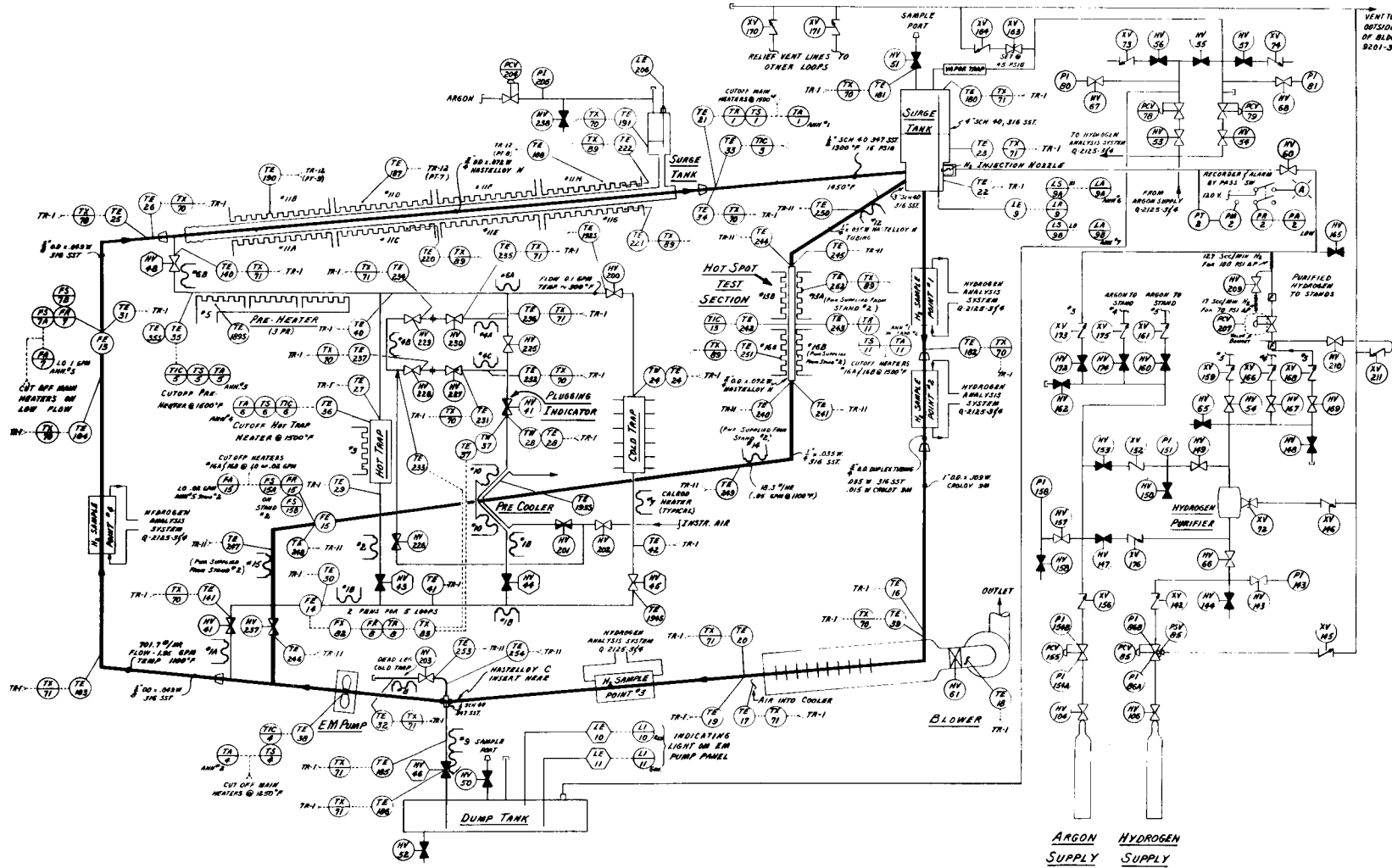


Fig. A.1. Flowsheet for Loops Without Hydrogen Injection.



180

Fig. A.2. Flowsheet for Loops with Hydrogen Injection.



181

Fig. A.3. Flowsheet for Hot-Spot Loop.

APPENDIX B

DRAWING LIST, SNAP-8 CORROSION LOOPS

Mechanical Drawings Used on Loops 1 Through 14

<u>Dwg. No.</u>	<u>Title</u>
C-48029	Support Detail, Lava Bushings
C-48188	Cold Leg Detail
D-48413	Cold Trap Details & Assembly
D-48414	Fill Tank Details & Assembly
D-48415	Plugging Valve Cooler & EM Pump Cell
D-48448	Loop Leak Pan
D-48449	Hot Trap Details
D-48450	Surge Trap
E-48451	SNAP-8 Corrosion Loop Elevation Assembly
E-48452	SNAP-8 Corrosion Loop Sections & Details
D-48455	NaK Sampler Assembly
E-48457	Supports & Shielding
E-48458	Assembly & Details - Air-Cooled Heat Exchanger
E-48459	Details - Air-Cooled Heat Exchanger
E-48460	Assembly & Details of Equipment Supports
E-48461	Blower & Duct Supports
D-48466	NaK Sampler Detail Sheet No. 1
D-48467	NaK Sampler Detail Sheet No. 2
D-48476	Piping Details
D-48477	Corrosion Specimen Detail
D-48501	Location Detail Corrosion Specimens
E-48502	Equipment Supports & Duct Details
D-48503	Surge Tank H ₂ Injection Loops
C-48507	Portable Ladder
D-48508	Heater Bank Trough Supports
C-48510	Detail of Fill Tank Expansion Coil
D-48517	Molecular Sieve
D-48518	Cooler and Plug Indicator Alternate

<u>Dwg. No.</u>	<u>Title</u>
E-48530	H ₂ Detection Sleeves
E-48533	Splash Guard
D-48604	Right-Angle Valve Drive
D-48609	NaK Sampler Transporting Vessel
D-48612	Cold Finger (Modification)
E-48625	NaK Jacket
C-48629	Flowmeter Expansion Loop
D-48725	Hoke 1403 Modification
C-48731	Plugging-Tube Layout
C-48732	Access Door in Shield

Mechanical Drawings Used Only on Loops 13 and 14

E-48736	Bi-Metal Sleeve on Croloy HX, Loop 13
C-48828	Support for EM Flowmeter in Hot-Spot Line
C-48829	Support for Hot-Spot Test Section
D-48830	Hot-Spot Test Section and Piping
D-48834	Surge Tank
E-48835	NaK Jacket
D-48837	Corrosion Specimens - Location Details
D-48838	Specimen Details
E-10350-R-001	Cold Finger, Modification No. 2
D-SK-BCG-12-14-64	NaK Sampler for Argon Test, Loop 14
E-10359-R-001	Elevation and Assembly, Loop 14
E-10359-R-002	Hydride Trap Assembly and Details, Loop 14
E-10359-R-003	Section of Main Assembly, Loop 14
D-10359-R-004	By-Pass Economizer, Loop 14
E-10359-R-005	Details of Hydride Trap, Loop 14
E-10359-R-006	Details of Jackets for H ₂ Sleeves, Loop 14
E-10359-R-007	Assembly and Details - H ₂ Detection Sleeves, Loop 14
E-10359-R-008	Bi-Metal Sleeve on Croloy HX, Loop 14

Electrical Drawings Used on Loops 1 Through 13

<u>Dwg. No.</u>	<u>Title</u>
D-48382	Elevation & Wiring Diagram Common Loop Recorder Panel
E-48394	Front Elevations Control Panels
E-48425	Wiring Diagram Loop Supply Power
E-48426	Schematic Wiring Diagram Power System
E-48427	Schematic Diagrams - Power & Controls
E-48428	Plan View - Electrical Equipment Layouts
E-48429	Elevations & Details Electrical Equipment Layouts
D-48430	Front Elevation & Wiring Diagram Variac Control Panel
D-48431	Control Cabinet Assembly & Wiring for EM Pump
D-48432	Front Elevation & Wiring Diagram-Instrument Panel
E-48433	Heater & Thermocouple Layout
E-48620	Heater & Thermocouple Layout with Alt. Plug Indicator
E-48621	Schematic-Power System with Alt. Plug Indicator
E-48637	Heater & TE Layout with Alt. Plug Indicator & NaK Jacket
E-48638	Schematic Diagram - Power
E-48653	Schematic - Power System, Alt. Plug Indicator & Cooler
C-48734	Heater & TC Layout for Plugging Tube
C-SK-48831	Heater & TC Layout for Hot Spot Section

Electrical Drawings Used Only on Loop 14

E-10359-R-500	Heater and Thermocouple Layout
E-10359-R-501	Schematic Wiring Diagram
E-10359-R-502	Schematic Wiring Diagrams, Std. 4
E-10359-R-503	Schematic Wiring Diagrams, Std. 1
D-10359-R-504	Wiring Diagram, Cabinet No. 1, Std. 4
D-10359-R-505	Wiring Diagram, Cabinet No. 2, Std. 1
D-10359-R-506	Wiring Diagram, EM Pump, Std. 4
D-10359-R-507	Wiring Diagram, EM Pump, Std. 1
D-10359-R-508	Front Elevation on Panels, Std. 4
D-10359-R-509	Front Elevation of Panels, Std. 1
D-10359-R-510	Assy. and Wiring Diagram, Common Recorder

Instrument Drawings Used on Loops 1 Through 14

<u>Dwg. No.</u>	<u>Title</u>
Q-2125-1	Instrument Flow Diagram Without H ₂ Injection (Loops 1 & 10)
2	Instrument Flow Diagram with H ₂ Injection
3	Instrument Flow Diagram Hydrogen Analysis System
4	Instrument Flow Diagram Hydrogen Analysis System
5	Flowsheet Loop 5
7	Flowsheet Loop 7
8	Flowsheet Loop 8
9	Flowsheet Loop 9
10	Hydrogen Analysis System Panel Board Layout
11	Panel Cutout
12	Panel Cutout
13	Panel Cutout
14	Hydrogen Analysis System Piping Layout & Schematic
15	
18	Flowsheet Loop 1A
19	Flowsheet Loop 2
20	Resistance Level Sensor Assembly & Details
21	Test Unit Details & Assembly
22	MGO Tamping Tool
23	H ₂ Detection Station Test Unit
24	H ₂ Valve Operating Procedure
26	Modification of Plugging Indicator Valve
27	3/8" Magnetic Flowmeter - Details & Assembly
28	EM Flowmeter Details
31	Flowsheet Loop 4
32	Flowsheet Loop 13, Hot Spot Loop with H ₂ Injection
33	Flowsheet Loop 14

APPENDIX C

CHEMICAL ANALYSES OF LOOP MATERIALS^a

Material	Analysis	Composition (wt %)															
		C	S	Si	P	Mn	Cr	Ni	Mo	Cu	Fe	W	B	Co	V	Al + Ti	Cb + Ta
Type 316 SS, 1/2-in.-OD, 0.065-in.-wall tubing	Specification ^b	0.08	0.030	0.75	0.030	2.00	16-18	11-14	2-3								
	Ladle	0.048	0.010	0.49	0.015	1.66	17-21	13.74	2.26	0.14							
	Check ^c	0.048	0.009	0.48	0.020	1.58	17.3	13.6	2.23								
Type 316 SS, 3/8-in.-OD, 0.049-in.-wall tubing	Specification	0.08	0.030	0.75	0.030	2.00	16-18	11-14	2.3								
	Ladle	0.048	0.010	0.44	0.015	1.66	17-2	13.74	2.26	0.14							
	Check ^c	0.044	0.007	0.45	0.021	1.63	17.0	13.5	2.28								
Croloy 9M, 1-in.-OD, 0.109-in.-wall tubing	Specification	0.15	0.03	0.25-1.00	0.03	0.30-0.60	8-10		0.90-1.10								
	Ladle	0.11	0.012	0.51	0.014	0.47	8.68		0.98								
	Check ^c	0.094	0.008	0.41	0.019	0.41	8.33		0.93								
Hastelloy N, 3/4-in.-OD, 0.072-in.-wall tubing	Specification	0.02-0.08	0.020	1.0	0.015	1.0	6-8	Bal	15-18	0.35	5.0	0.5	0.01	0.2	0.5	0.5	
	Ladle	0.06	0.010	0.62	0.001	0.47	6.96	Bal	16.17	0.001	4.22	0.20	0.002	0.18	0.33	0.02	
	Check	0.044	0.008	0.63		0.39	7.09	Bal	15.6		4.1						
Type 316 SS, 1 1/2-in. bar	Specification	0.08	0.030	1.00	0.045	2.00	16-18	10-14	2-3								
	Ladle	0.056	0.010	0.55	0.016	1.78	17.46	12.43	2.77	0.14				0.08			
	Check	0.053	0.007	0.46	0.029	1.67	17.8	12.2	2.73								
Type 316 SS, 3-in., sched 40 pipe	Specification	0.08	0.030	0.75	0.030	2.00	16-18	11-14	2-3								
	Ladle	0.040	0.004	0.34	0.026	1.30	17.27	13.40	2.74								
	Check	0.046	0.007	0.66	0.023	1.70	16.7	13.0	2.24								
Type 316 SS, 4-in., sched 40 pipe	Specification	0.08	0.030	0.75	0.030	2.00	16-18	11-14	2-3								
	Ladle	0.056	0.016	0.44	0.012	1.68	17-44	13.21	2.31								
	Check	0.050	0.011	0.45	0.028 ^d	1.61	17.5	12.2	2.20								
Type 316 SS, 1/4-in. plate	Specification	0.08	0.030	1.00	0.045	2.00	16-18	10-14	2-3								
	Ladle	0.045	0.011	0.54	0.022	1.75	17.23	12.78	2.26	0.17							
	Check	0.042	0.008	0.43	0.016	1.53	16.9	12.6	2.15								
Type 347 SS, 1/2-in., sched 40 pipe	Specification	0.08	0.030	0.75	0.030	2.00	17-20	9-13									
	Ladle	0.039	0.008	0.56	0.018	1.72	18.95	11.07									
	Check	0.037	0.006	0.58	0.019	1.63	18.9	10.9									
Type 316 SS, 0.050-in. sheet ^f	Specification	0.08	0.030	1.00	0.045	2.00	16-18	10-14	2-3								
	Ladle																
	Check	0.054	0.010	0.50	0.018	1.84	17.6	13.8	2.08								

^aUnless otherwise noted, all check analyses are the results of one analysis.

^bSingle values are maximum percentages for specification values.

^cAverage of three analyses.

^dAverage of two analyses.

^eThe ASTM specification calls for ten times the carbon content, but less than 1%.

^fFrom ORNL-3604.

APPENDIX D

LOOP OPERATING HISTORIES

ORNL-DWG 65-8927

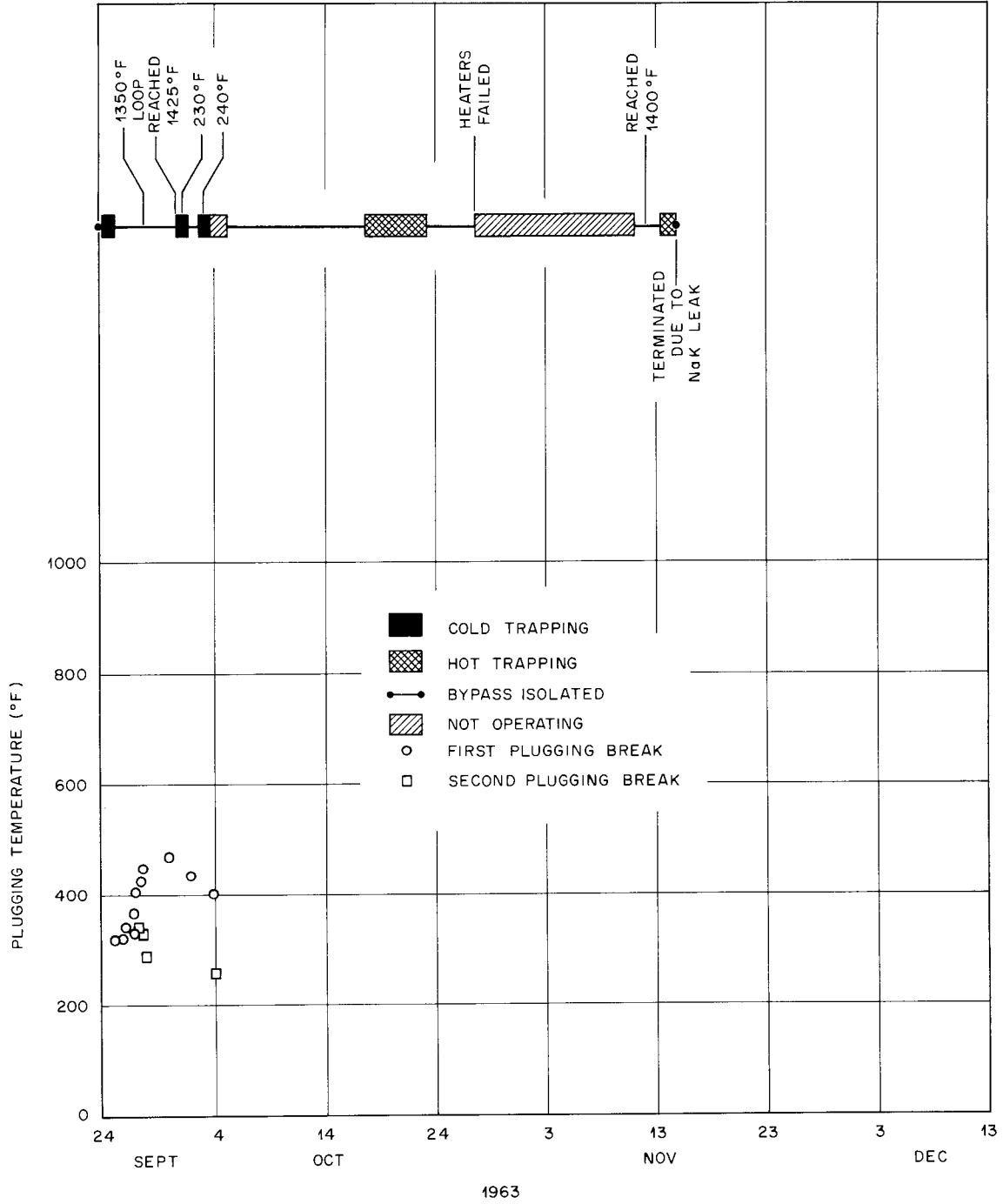


Fig. D.1. Operating History of Loop 1.

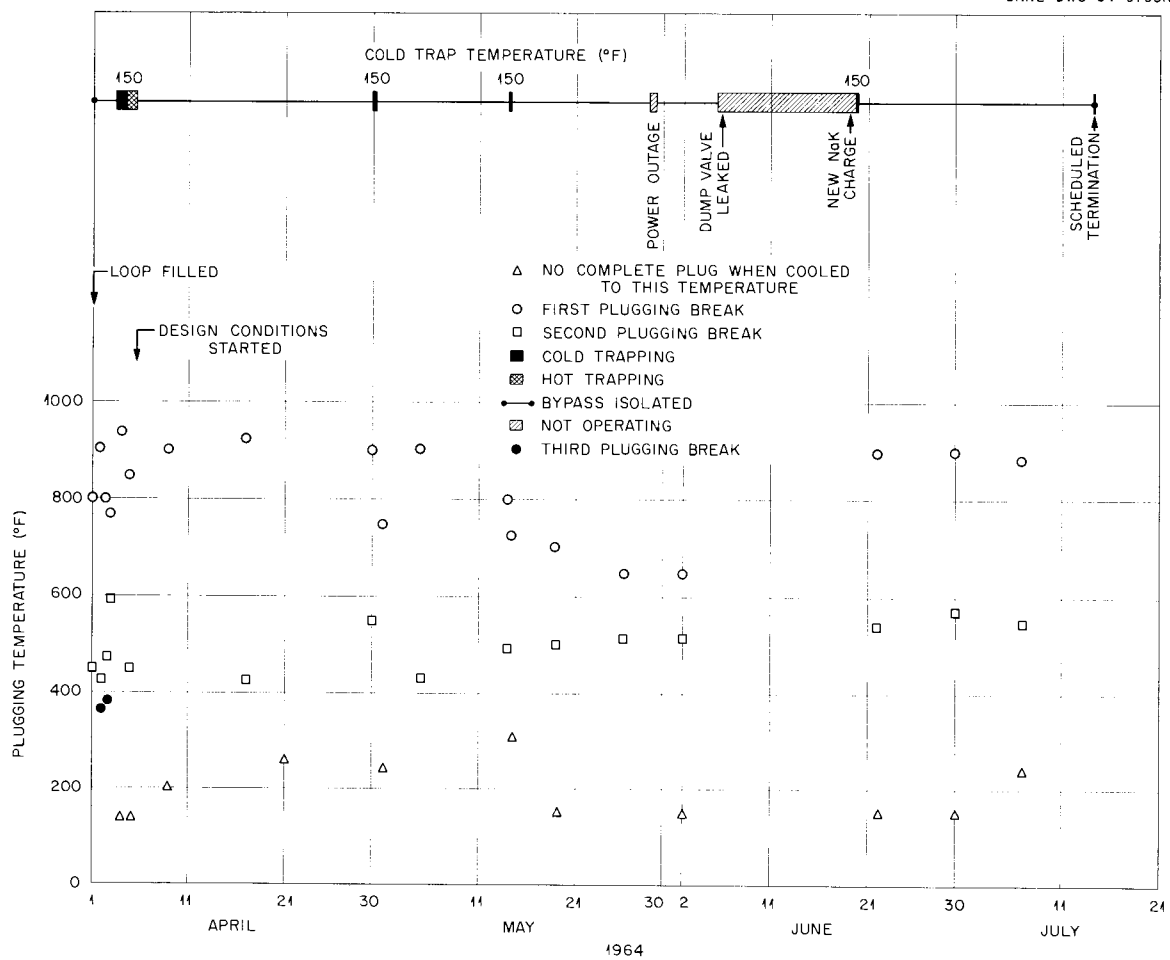


Fig. D.2. Operating History of Loop 1A.

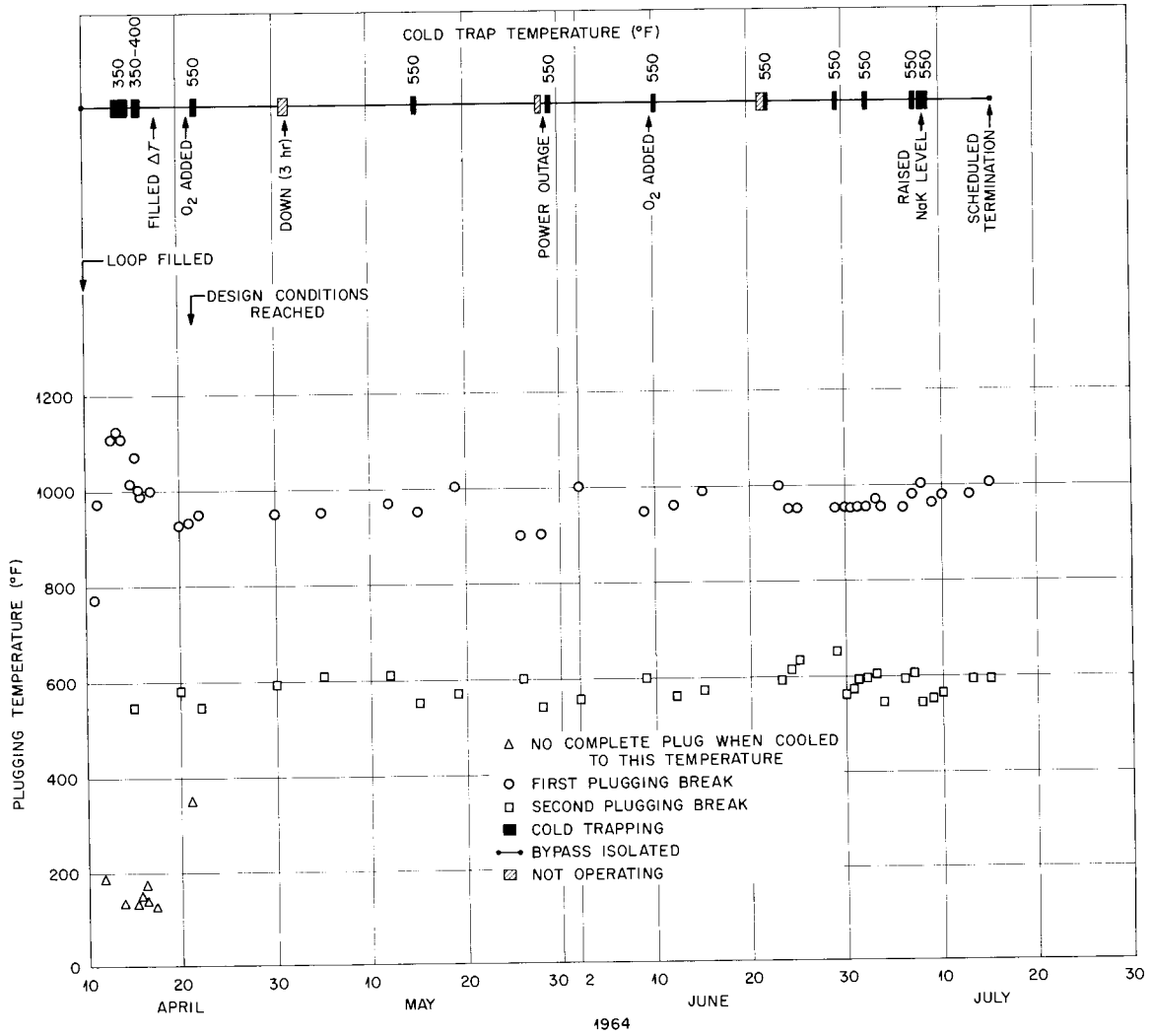


Fig. D.3. Operating History of Loop 2.

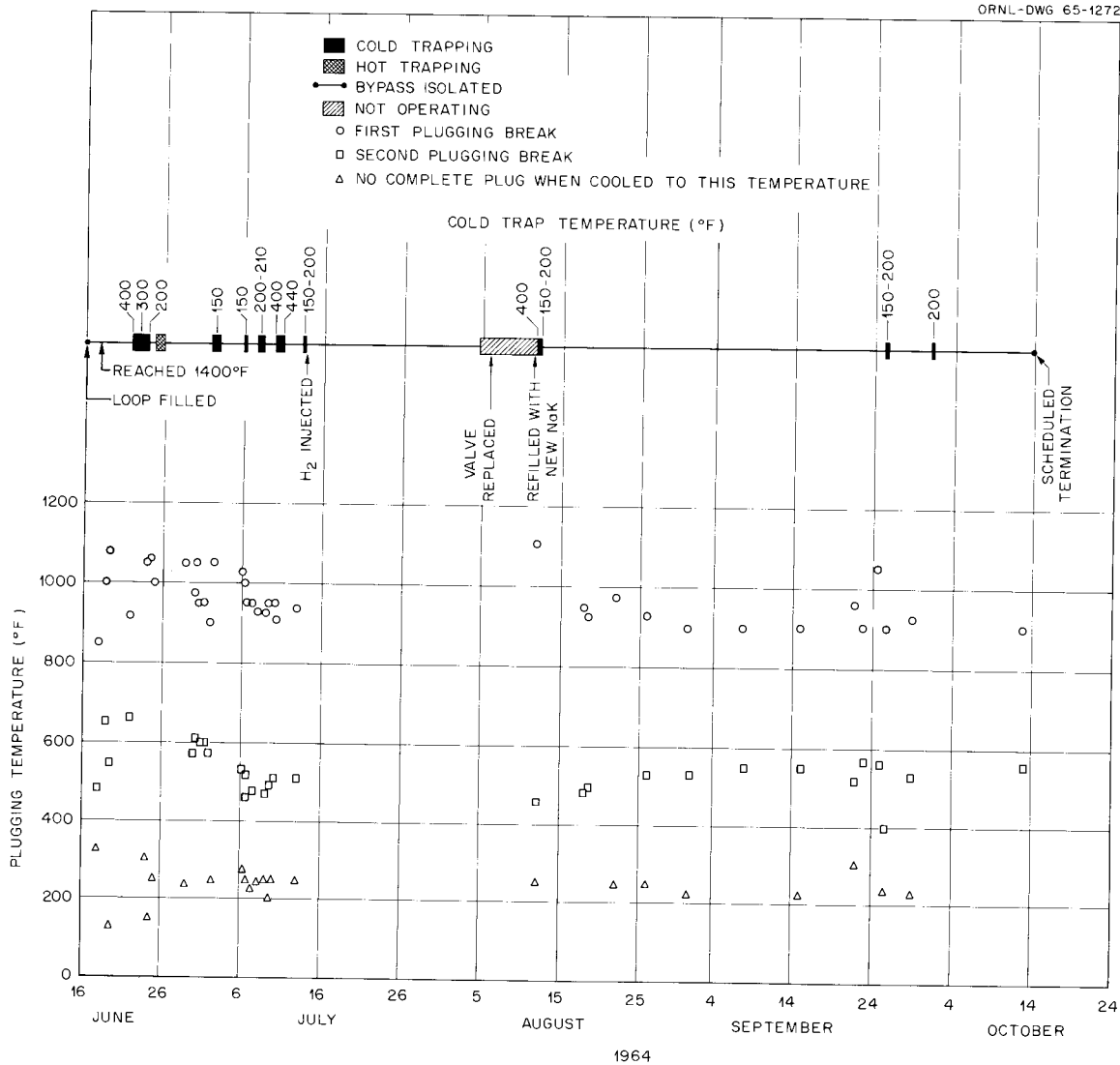


Fig. D.4. Operating History of Loop 4.

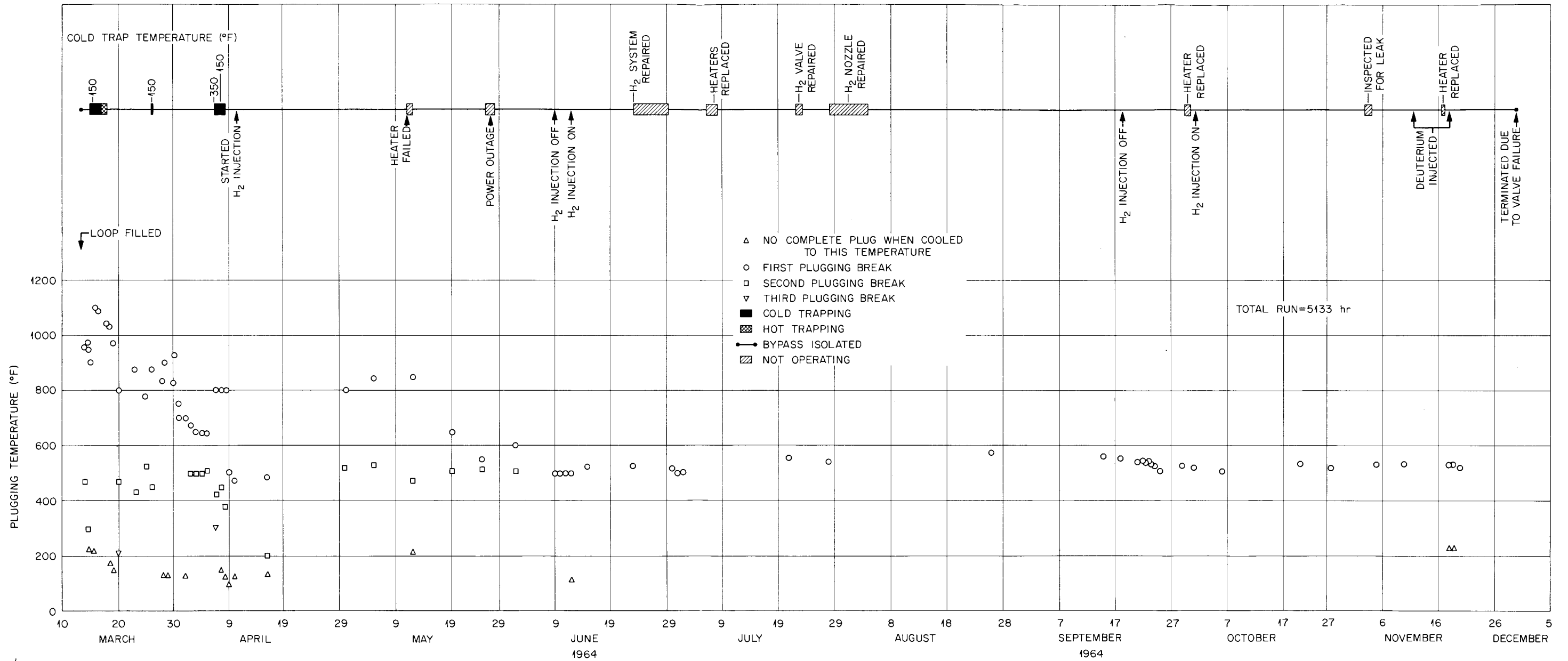


Fig. D.5. Operating History of Loop 5.

ORNL-DWG 64-9797

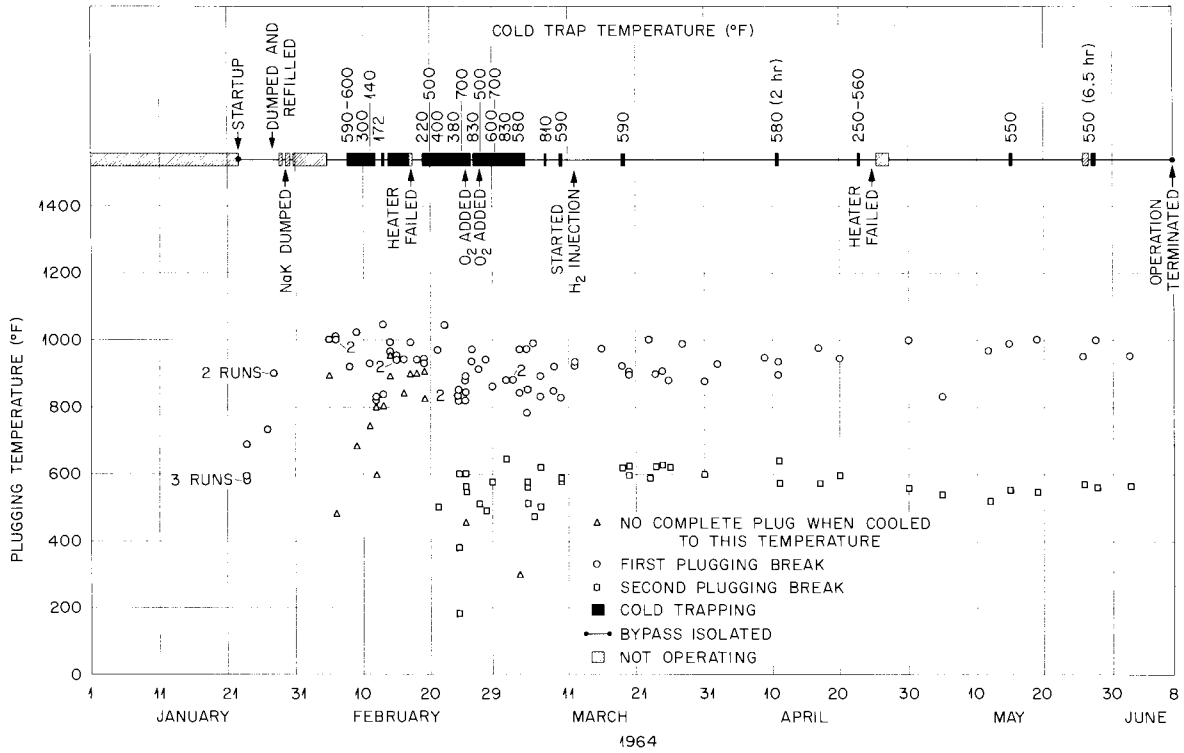


Fig. D.6. Operating History of Loop 7.

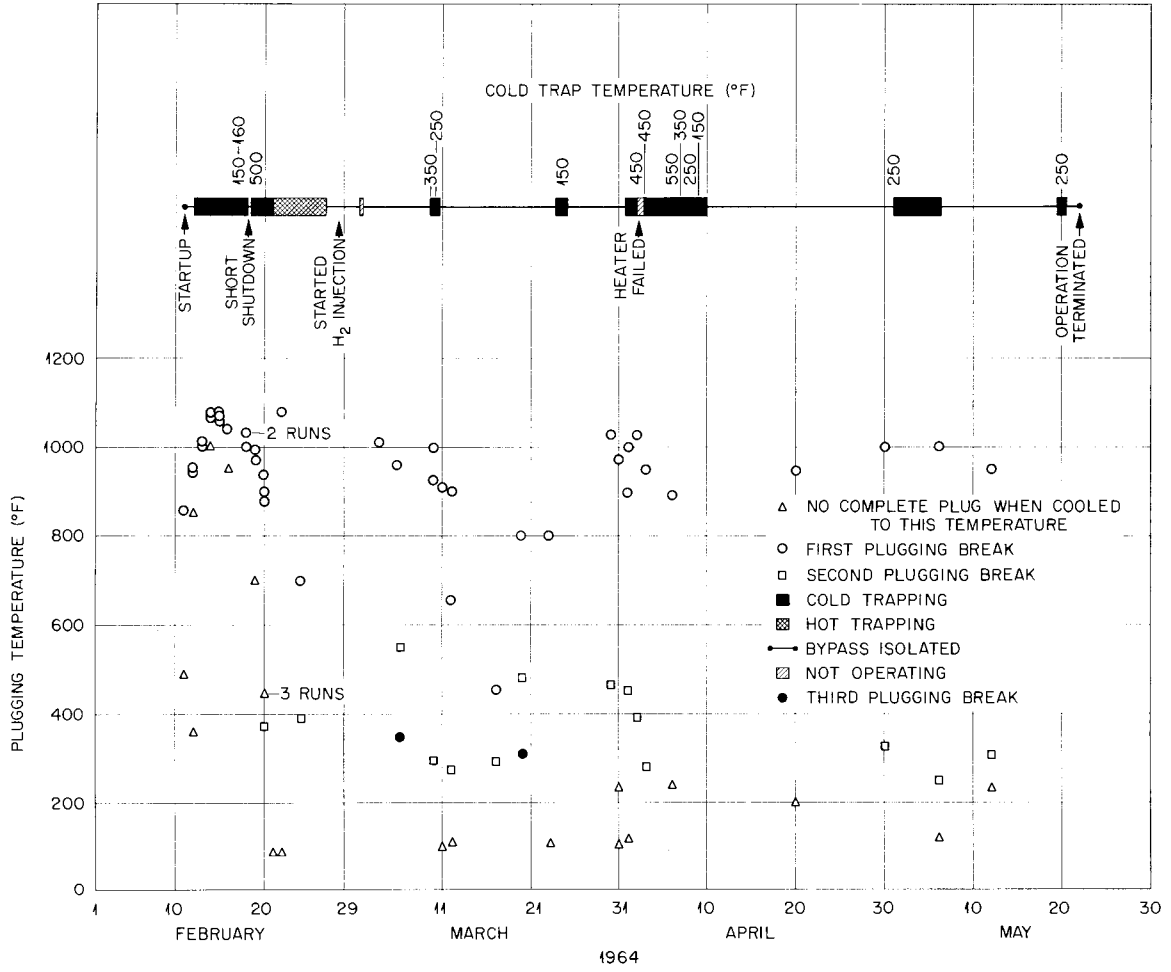


Fig. D.7. Operating History of Loop 8.

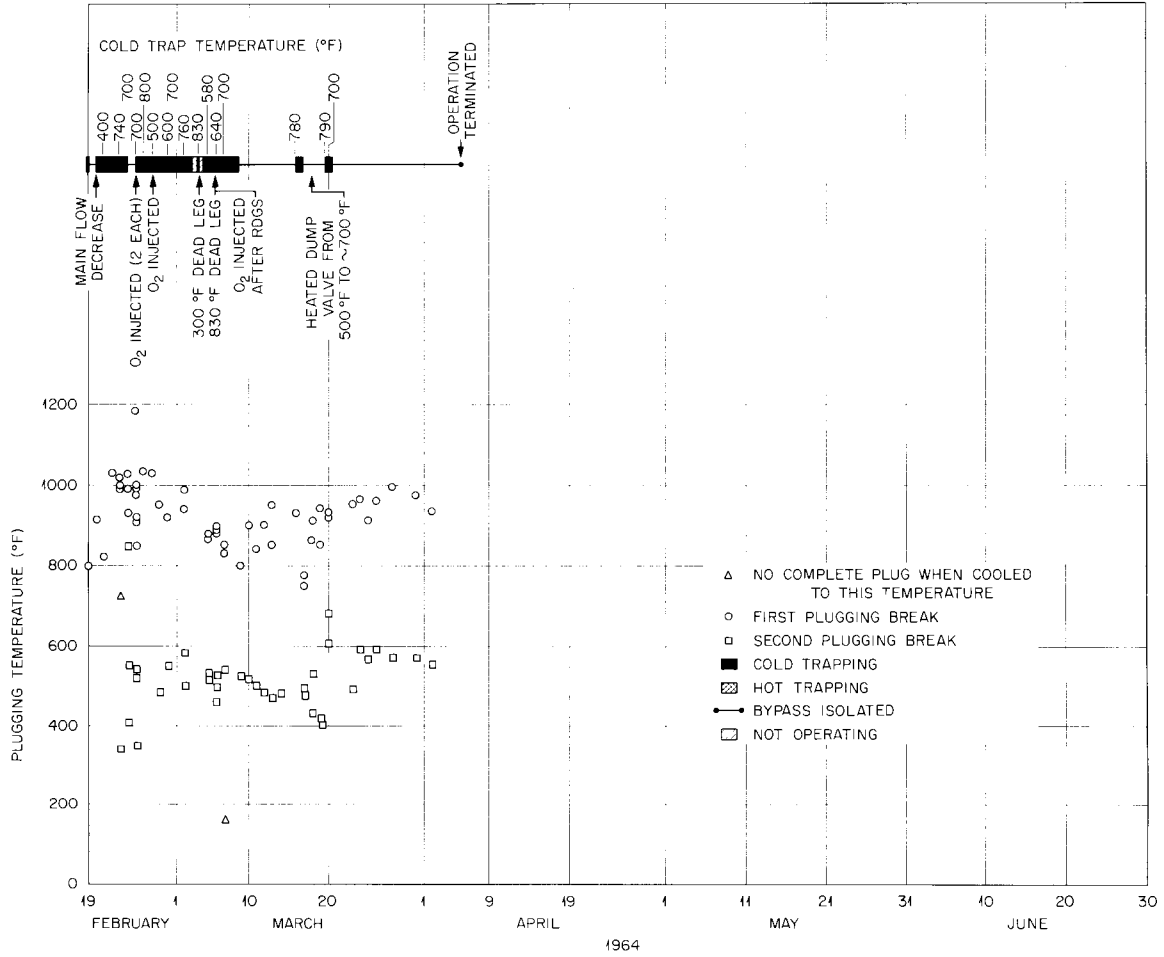


Fig. D.8. Operating History of Loop 9.

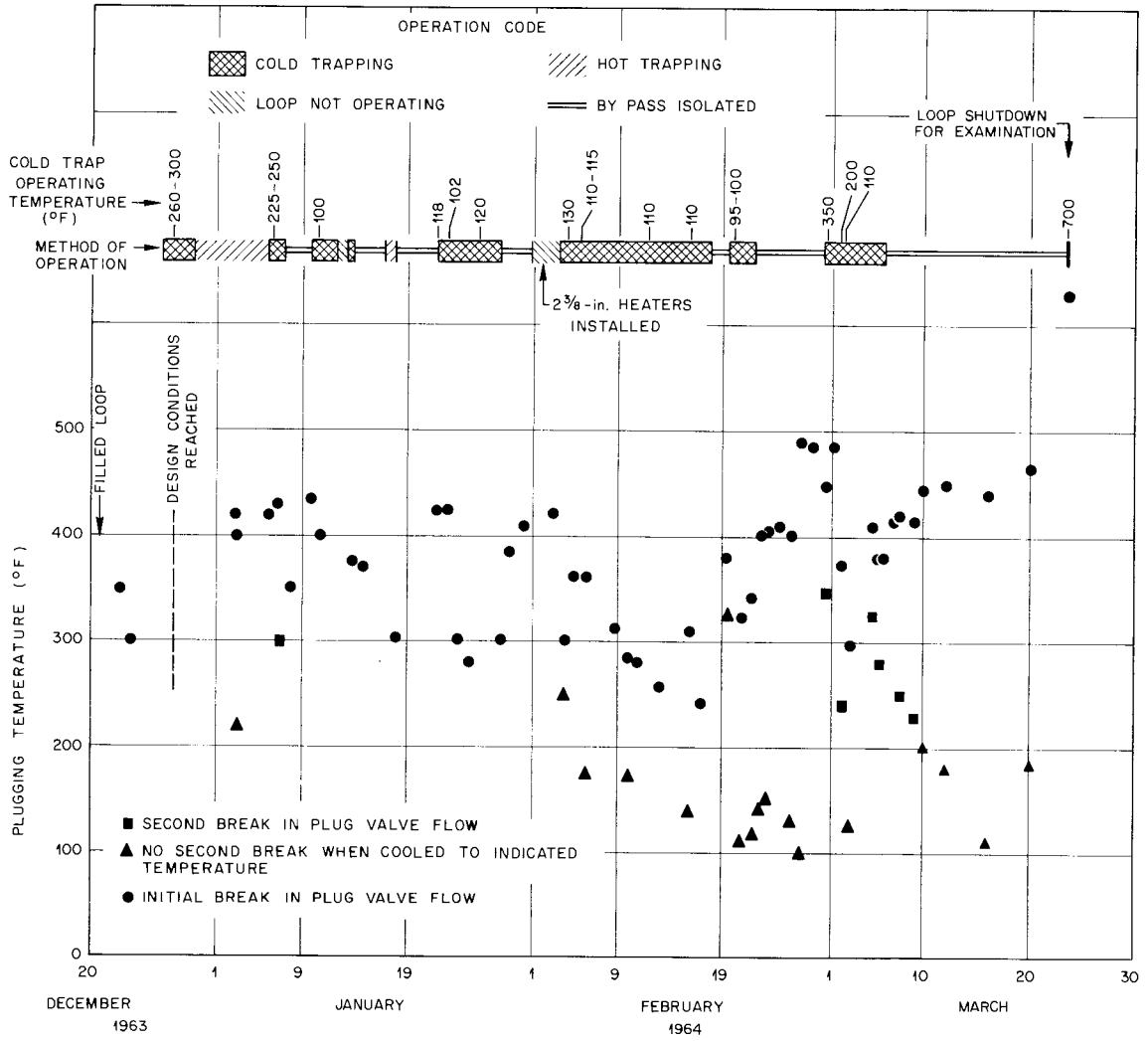


Fig. D.9. Operating History of Loop 10.

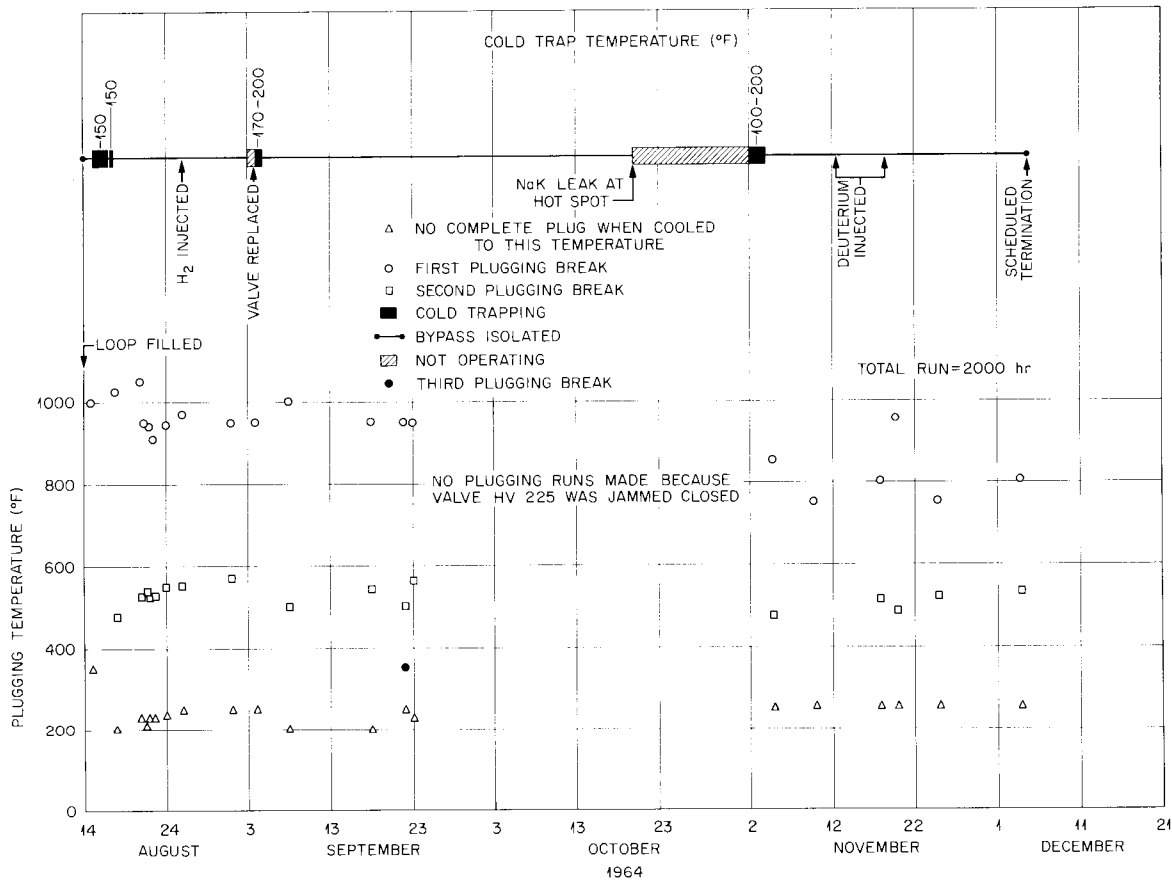


Fig. D.10. Operating History of Loop 13.

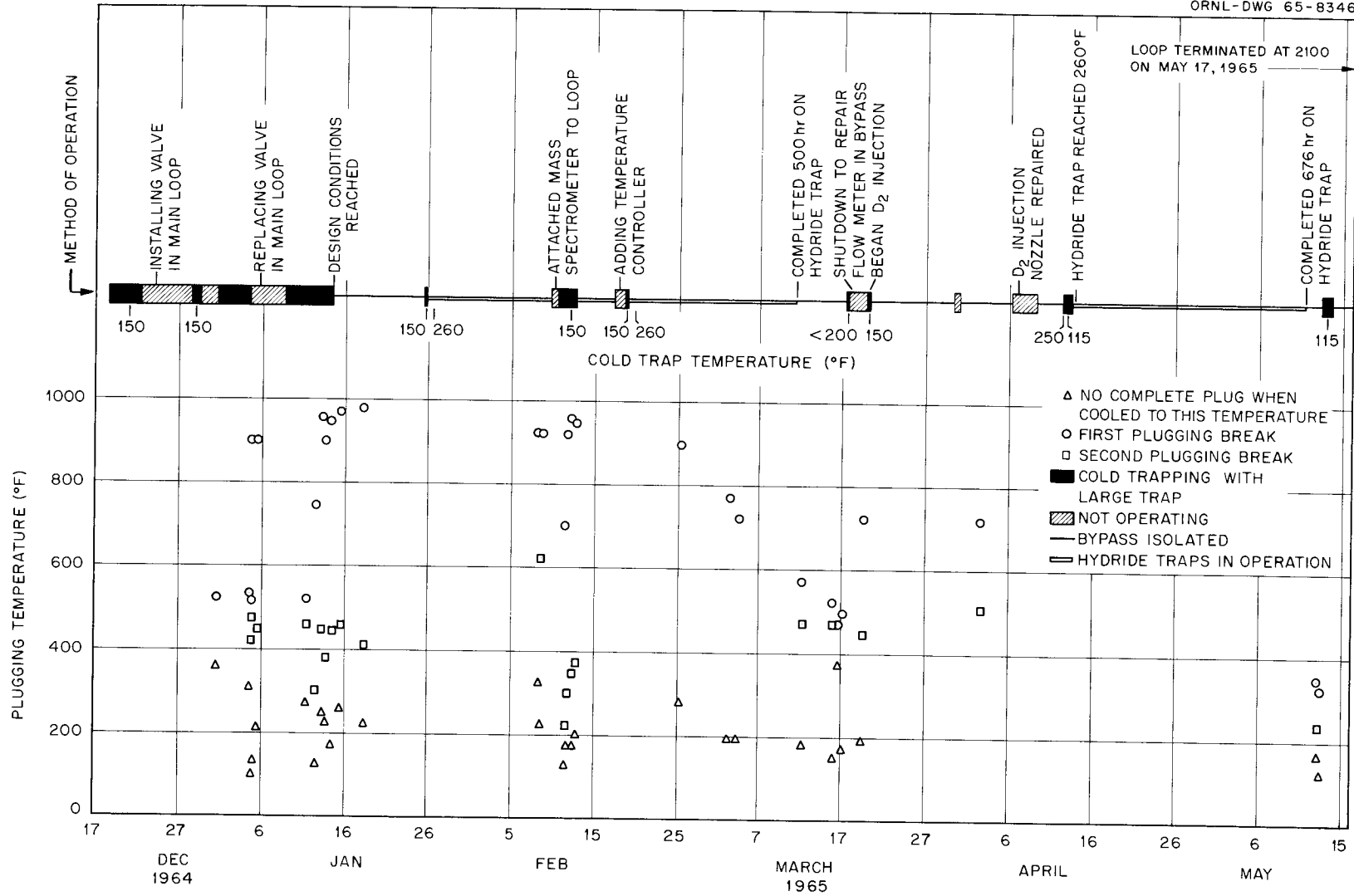


Fig. D.11. Operating History of Loop 14.

APPENDIX E

EVALUATION OF CHROMIZED HASTELLOY N SURFACE

Samples of chromized Hastelloy N from SNAP-8 fuel element tubing obtained from Atomics International and from ORNL's loop piping were examined to establish the degree of similarity of the two products. To perform this evaluation, metallographic examination and electron microprobe techniques were employed. Included in the study were samples of tubing as chromized and samples given a high-temperature heat treatment¹ to simulate actual fuel element processing. All chromized piping and samples used in the ORNL test loops were given the postchromizing heat treatment.

Metallographic examination indicated various and random degrees of chromizing in both the SNAP-8 and ORNL tubing. To further delineate the extent of chromium enrichment, electron microprobe examination was used to obtain chromium concentration profiles.

The main emphasis was placed on examination of chromized tubing that had received the postchromizing heat treatment, since this was the material to be used in the reactor and in the corrosion loops. However, other samples were also examined to gain an appreciation for the relationship between microstructure and the extent of chromium enrichment. The results of these examinations are summarized in Table E.1.

The data clearly show that the degree of chromium enrichment achieved during chromizing is quite variable. Some of the material failed to receive any chromium enrichment, while other material was enriched to as much as 75% chromium. The postchromizing heat treatment generally resulted in a decrease in the degree of chromium enrichment at the surface and caused the point of maximum chromium concentration to shift to a point several tenths of a mil beneath the surface.

The data also reveal at least a qualitative correlation between microstructure and chromium concentration. Samples that showed no diffusion zone when examined metallographically also showed no chromium enrichment when examined by the microprobe. Conversely, samples showing a distinct diffusion zone metallographically always showed some degree of chromium enrichment when examined by the microprobe. In general, the data indicate that the width of the diffusion zone as determined metallographically represents the thickness of material that received at least 2% chromium enrichment. As expected, a phase layer, when present at the surface, was found to contain a high (approximately 75%) chromium concentration.

Material containing no diffusion zone but an extensive gradient of massive precipitates (ORNL 13X) failed to show any chromium enrichment by microprobe examination. The gradient of precipitates indicates the infusion of some element into the material, but the identity of the element was not established by these examinations.

¹Vacuum annealed at 1750°F for 12 hr plus 45 min at 1900°F in air.

Table E.1. Results of Examination of Chromized Hastelloy N Surfaces^a

Cr_s = chromium concentration at surface, %
 $Cr_m(d)$ = maximum chromium concentration, %
 d = depth at which the maximum concentration occurs, mils
 t = thickness of the chromium-enriched region, mils
 Cr_t = chromium concentration of base metal at distance t from surface, %

Tube Designation	Condition	Cr_s	$Cr_m(d)$	d	t	Cr_t	Microstructure
A.I. 2820	As chromized	75			1.4	9	Phase layer surface plus diffusion zone and subsurface precipitates
A.I. 3831	As chromized	23.5			1.2	8	Diffusion zone plus subsurface precipitates
		32.5			1.0	7	Diffusion zone plus subsurface precipitates
		58			1.0	8	Diffusion zone plus subsurface precipitates
		18.5			0.8	7	Diffusion zone plus subsurface precipitates
A.I. N674	As chromized	14.5	18.5	0.02	1.0	7	Diffusion zone plus subsurface precipitates
A.I. N674P	Heat treated	10.5	14.5	0.34	1.55	7.5	Diffusion zone plus subsurface precipitates
A.I. N685P	Heat treated	16.5	20	0.18	1.6	8	Diffusion zone plus subsurface precipitates
A.I. N633P	Heat treated	11	14	0.15	0.8	7	Diffusion zone plus subsurface precipitates
ORNL-31A	As chromized	19.5	24	0.15	1.4	7	Diffusion zone plus subsurface precipitates
		19.5	20.5	0.10	1.1	6	Diffusion zone plus subsurface precipitates
		19.5			1.1	6.5	Diffusion zone plus subsurface precipitates
ORNL 38A	As chromized	7	8	0.10	0.9	7	No diffusion zone; subsurface precipitates
ORNL 43A	As chromized	7	8	0.15	1.0	5.5	No diffusion zone; subsurface precipitates
ORNL 4B	Heat treated	10.5	14.5	0.22	1.2	7	Diffusion zone plus subsurface precipitates
ORNL 16B	Heat treated	31.5			1.48	8.5	Diffusion zone plus subsurface precipitates
ORNL 13X	Heat treated	6.5					No diffusion zone; massive subsurface precipitates extending into wall

^aAll data are semiquantitative. No corrections have been made for absorption or secondary fluorescence.

Since large variations in the degree of chromium enrichment occur on the surface of both the SNAP-8 and the ORNL material, it is impossible to make any definitive statement as to the similarity of SNAP-8 and ORNL materials. It is evident that the material being used in the corrosion loops is at least representative of some of the material being used in the SNAP-8 reactor, but it is also apparent that some of the material being used in the SNAP-8 system is not represented in the corrosion-loop tests. This is particularly so regarding the materials with high chromium concentrations. The experience gained in the loop tests indicated that, although chromium is one of the corroding elements, the overall corrosion rate is very low in low-oxygen-content NaK. Even if the corrosion rate of the high-chromium-content surfaces used in the SNAP-8 reactor were higher than that indicated for the lower chromium material used in the loop tests, the higher rate would prevail only during the initial period of corrosion. During this period, the chromium content would be reduced to that existing in the material used in the loop tests. Consequently, this would affect only the first few tenths of a mil of the tubing surface. Therefore, it is believed that the information generated in the corrosion-loop tests adequately portrays the corrosion compatibility of materials possessing the initially higher surface concentration of chromium.

From the standpoint of carbon migration, the surfaces with the higher chromium content could be expected to be more active carbon getters, and this would in turn influence the surface ductility. The extent to which this would occur and affect the design would be dependent on numerous variables outside the scope of these corrosion studies.

APPENDIX F

METHODS OF ANALYSES

Examination of the various loops for measurement and identification of mass transfer was performed primarily through the use of weight change measurement of insert specimens, chemical analyses, and metallographic examination. Descriptions of the techniques are presented in the following paragraphs.

Weight Change Measurement

Each loop contained insert specimens at the various points around the loop, as shown in Fig. 1 of Corrosion-Loop Materials Studies. Insert specimens were of the same general alloy composition as the tubing in which they were placed, except for specimens 12, 15, and 16, which were Hastelloy C and 316, respectively, in Croloy 9M tubing. Specimens 1, 2, 3, and 4 were loose-fitting tubular specimens fastened into place by a wire threaded through a hole in one end of the specimen and welded to the tubing wall. Specimens 5, 7, 12, and 13 were close-fitting tubular specimens fastened into place by the scheme depicted in Fig. F.1. Specimens 8, 9, 10, 11, 15, and 16 were midstream flat-rectangular specimens fastened into place on a wire rod placed along the center line of the heat exchanger tubing. Specimen 14 was a cylinder rolled from sheet stock and held in place by the spring-back pressure on the tubing walls. Specimen 6 was a tubular specimen placed upright on the bottom of the surge tank

ORNL-DWG 65-12425

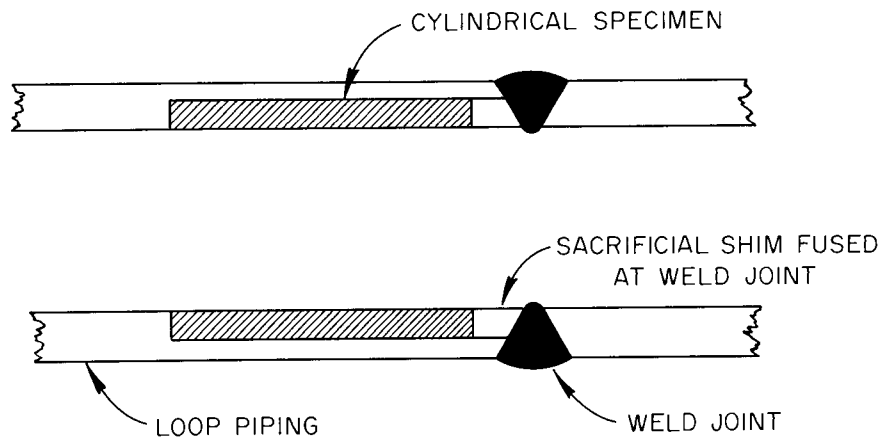


Fig. F.1. Cross Section Showing Insert Specimen Arrangement for Specimens 5, 7, 12, and 13.

Table F.1. Description of Insert Specimens

Specimen No.	Material	Geometrical Shape	Dimensions	Surface Finish on Exposed Surfaces	Fabrication History
1, 2, 3, 4	Chromized Hastelloy N	Thin-walled cylinder	1×0.560 in. OD \times 0.010-in. wall	16 rms	Chromized at Chromizing Corp.; heat treated 1750°F – 12 hr in vacuum, 1900°F – 45 min in air
5	347 SS	Thin-walled cylinder	1×0.682 in. OD \times 0.020-in. wall	16 rms	Machined from $\frac{1}{2}$ -in. sched 40 pipe (same starting material used in loop construction)
6, 13	316 SS	Thin-walled cylinder	1×0.375 in. OD \times 0.020-in. wall	16 rms	Machined from $\frac{3}{8}$ -in.-OD \times 0.049-in.-wall tubing (same starting material used in loop construction)
7	Croloy 9M	Thin-walled cylinder	1×0.778 in. OD \times 0.030-in. wall	16 rms	Swaged 1-in.-OD \times 0.120-in.-wall tubing to 0.786-in.-OD \times 0.140-in. wall; then machined to size (same starting material used in loop construction)
8, 9, 10, 11	Croloy 9M	Flat sheet	$1 \times \frac{11}{16} \times 0.030$ in.	16 rms	Split 1-in.-OD \times 0.120-in. wall tubing and cold rolled to 0.030–0.033 in. strip; fully annealed prior to finishing (same starting material used in loop construction)
12	Hastelloy C	Thick-walled cylinder	$3\frac{1}{16} \times 0.778$ in. OD \times 0.415 in. ID	16 rms	Machined from 1-in.-diam bar
15, 16	316 SS	Flat sheet	$1 \times \frac{11}{16} \times 0.010$ in.	As rolled	Cold rolled 0.050-in. sheet to 0.010 in., bright annealed
14	316 SS	Thin-walled cylinder	$1 \times \frac{9}{32}$ in. OD \times 0.010 in. wall	As rolled	Cold rolled 0.050-in. sheet to 0.010 in., bright annealed; rolled into cylindrical shape

and held in place by a wire welded to the bottom of the tank and bent over the top of the specimen. In choosing the corrosion area of the various specimens for calculation of corrosion rates, the area exposed to the mainstream flow was selected.

For specimens 1, 2, 3, and 4, only the inside surface area was used in calculating the corrosion rates. This would make the corrosion rates conservatively high for these specimens because that portion of flow occurring around the outside of specimens would increase the actual area over which corrosion had occurred, thus making the actual corrosion rate somewhat less than that used in the calculation.

Details of specimen fabrication are reported in Table F.1. Prior to placement in a loop, each specimen was appropriately marked, measured, acetone degreased, and weighed. After test exposure the loops were cleaned by reaction with butyl alcohol, rinsing with flowing water, and blowing dry with flowing air. The specimens were then carefully removed, rinsed in water and acetone, dried with flowing helium, and reweighed.

Adjustments were made in the calculated weight changes to allow for carbon migration. This was done by determining the pre- and posttest carbon content of a specimen and appropriately correcting the weight change so that weight loss or gain due to carbon migration would not be reflected in the corrosion rates. Therefore, the adjusted corrosion rates indicate the rates of metal migration only. Usually the adjustments caused by carbon migration were inconsequential. However, in cases of severe decarburization (such as specimen 7 in all loops), a significant correction resulted.

Chemical Analyses

Carbon Migration

Several methods were used for the detection and evaluation of the character and degree of carbon migration. As previously mentioned, pre- and posttest analyses were performed on the insert specimens to determine the amount of carbon gain or loss. Samples for these analyses consisted of portions of the total cross section of the sample thickness, giving an average analysis for each sample before and after test. The extent and character of carbon migration across the tubing walls at selected locations in the loop were also determined. This was done by machining consecutive layers from the inside surface, collecting the chips, and analyzing for carbon by the combustion method. From these data, graphs were made showing the concentration of carbon as a function of distance across the tubing wall from the inside surface (see Figs. 24 to 32 of Corrosion-Loop Materials Studies).

Analysis of decarburized tubing always indicated a thin surface portion containing more carbon than the substrate. Since tool contamination may have been responsible for this, a different technique was used to

confirm this phenomenon. The piping was machined, from the outside, down to a 0.002-in.-thick cylinder. Analysis of the cylinder confirmed that the carbon content increase near the surface was real. The value measured was ~0.02% as compared to 0.002% in the substrate.

Decarburization was also qualitatively measured by metallographic examination of the piping wall. The approximate degree of decarburization was manifested by the thickness of the region of grain growth. However, one should note that decarburization extended well beyond this region, as clearly shown by the carbon profile curves.

Metal Migration

Three methods of chemical analysis were used to establish the character of metal migration. Standard wet chemical analysis was used for the identification of elements present in mass-transfer deposits when enough deposit was available for this technique. Electron microprobe examinations were used to identify elements of mass-transfer products in situ. This technique was also used in examining corroded surfaces to determine the elements that were selectively removed. An attempt was also made to use x-ray-fluorescence analysis for the examination of corroded surfaces; however, the results were not sufficiently quantitative for useful interpretations.

Metallographic Examinations

Examinations were made selectively of both loop piping and insert specimens to determine the nature of mass-transfer deposits, the stability of materials, and the effect of corrosion on the microstructure. Standard procedures were used except as indicated in the discussion of phase-identification studies.

ORNL-3898
 UC-33 - Propulsion Systems and
 Energy Conversion
 TID-4500 (46th ed.)

INTERNAL DISTRIBUTION

- | | |
|------------------------|--------------------------------------|
| 1. G. M. Adamson, Jr. | 20. H. G. MacPherson |
| 2. J. M. Baker | 21. R. E. MacPherson |
| 3. S. E. Beall | 22. A. J. Miller |
| 4. M. Bender | 23-24. R. B. Parker |
| 5. E. G. Bohlmann | 25. H. W. Savage |
| 6. D. W. Cardwell | 26. H. C. Savage |
| 7. C. E. Center (K-25) | 27. A. W. Savolainen |
| 8. E. L. Compere | 28. J. E. Savolainen |
| 9. F. L. Culler | 29. M. J. Skinner |
| 10. J. H. DeVan | 30. A. Taboada |
| 11. B. Fleischer | 31. A. M. Weinberg |
| 12. A. P. Fraas | 32. J. C. White |
| 13. J. H. Frye, Jr. | 33. Biology Library |
| 14. W. R. Grimes | 34-36. Central Research Library |
| 15. W. O. Harms | 37. Reactor Division Library |
| 16. M. R. Hill | 38-39. ORNL - Y-12 Technical Library |
| 17. W. R. Huntley | Document Reference Section |
| 18. W. H. Jordan | 40-59. Laboratory Records Department |
| 19. C. E. Larson | 60. Laboratory Records, ORNL R.C. |

EXTERNAL DISTRIBUTION

61. Aerojet-General Corporation, Sacramento
62. Aerojet-General Nucleonics (NASA)
63. Aerospace Corporation
64. Air Force Foreign Technology Division
65. Air Force Surgeon General
66. Air University Library
67. AiResearch Manufacturing Company, Phoenix
68. Army Ballistic Research Laboratories
69. Army Director of Transportation
70. Aro, Inc.
- 71-72. Canoga Park Area Office
73. Central Intelligence Agency
74. Director of Defense Research and Engineering (OAP)
75. Douglas Aircraft Company, Inc., Newport Beach
76. Electro-Optical Systems, Inc.
77. General Dynamics/Convair (AF)
- 78-79. General Electric Company (FPD)
80. General Electric Company (MSVD)
81. Monsanto Research Corporation
- 82-83. NASA Goddard Space Flight Center
- 84-86. NASA Marshall Space Flight Center
87. Naval Air Development Center
- 88-89. Office of the Chief of Naval Operations (OP-03EG)

- 90. Pratt and Whitney Aircraft Division (NASA)
- 91. Westinghouse Electric Corporation, Lima
- 92. Westinghouse Electric Corporation, Lima (AF)
- 93. Research and Development Division, AEC, ORO
- 94-95. Reactor Division, AEC, ORO
- 96-439. Given distribution as shown in TID-4500 (46th ed.) under Propulsion Systems and Energy Conversion category (75 copies - CFSTI)

NASA Distribution Order No. C-220-A

- 440-442. NASA, Washington, D.C., Attn: P. R. Miller (RNP), F. Schulman (RNP), George C. Deutsch (RR)
- 443-444. NASA Scientific and Technical Information Facility, Bethesda, Maryland, Attn: NASA Representative
- 445. NASA Ames Research Center, Moffet Field, California, Attn: Librarian
- 446. NASA Goddard Space Flight Center, Attn: Librarian
- 447. NASA Langley Research Center, Attn: Librarian
- 448. NASA Manned Spacecraft Center, Attn: Librarian
- 449. NASA George C. Marshall Space Flight Center, Attn: Librarian
- 450. NASA Jet Propulsion Laboratory, Attn: Librarian
- 451-466. NASA Lewis Research Center, Attn: Librarian (2 copies), Henry O. Slone, Bernard Lubarsky, D. G. Beremand, P. L. Stone (2 copies), J. P. Merutka, R. W. Schaupp, L. E. Light, Normal T. Musial, Reliability and Quality Assurance Office, T. A. Moss, Louis Rosenblum, R. F. Mather, I. I. Pinkel
- 467. NASA Western Operations Office, Santa Monica, California, Attn: John Keeler
- 468-469. NASA Western Operations Office, Azusa Field Office, Attn: J. G. Kennard, F. Herrmann
- 470-473. Aeronautical Systems Division, Wright-Patterson Air Force Base, Attn: Librarian, George E. Thompson, George Sherman, T. Cooper
- 474-475. U.S. Atomic Energy Commission, Washington, Technical Reports Library, Attn: J. M. O'Leary
- 476. U.S. Atomic Energy Commission, CANEL Project Office, Attn: Herbert Pennington
- 477-478. U.S. Atomic Energy Commission, Germantown, Attn: Carl E. Johnson, Herbert Rothen
- 479-480. U.S. Atomic Energy Commission, Technical Information Service Extension
- 481-482. U.S. Atomic Energy Commission, Washington, Attn: M. J. Whitman, J. D. Lafleur
- 483. Argonne National Laboratory, Attn: Librarian
- 484-487. Brookhaven National Laboratory, Attn: Librarian, D. Gurinsky, C. Klamut, O. E. Dwyer
- 488-490. Thompson Rama Wooldridge, Inc., Attn: Librarian, E. Vargon, E. E. Steigerwald
- 491. U.S. Naval Research Laboratory, Attn: Librarian
- 492. Advanced Technology Laboratories, Attn: Librarian
- 493-495. Aerojet-General Corporation, Attn: Librarian, R. S. Carey, H. Derow

- 496-499. Aerojet-General Nucleonics, Attn: Librarian, B. Farwell, P. Young, M. Parkman
- 500-502. AiResearch Manufacturing Company, Phoenix, Attn: Librarian, E. A. Kovacevich, John Dannen
- 503. AiResearch Manufacturing Company, Los Alamos, Attn: Librarian
- 504-507. Atomics International, Attn: Librarian, John Page, H. Gereke, D. J. Cockeram
- 508. AVCO, Research and Advanced Development Department, Attn: Librarian
- 509. Babcock and Wilcox Company, Alliance, Ohio, Attn: Librarian
- 510. Battelle Memorial Institute, Attn: Librarian
- 511. The Boeing Company, Attn: Librarian
- 512. Curtiss-Wright Corporation, Attn: Librarian
- 513. E. I. du Pont de Nemours and Company, Inc., Attn: Librarian
- 514. Electro-Optical Systems, Incorporated, Attn: Librarian
- 515. Ford Motor Company, Aeronutronics, Attn: Librarian
- 516. General Atomic, John Jay Hopkins Laboratory, Attn: Librarian
- 517. General Electric Company, San Jose
- 518. General Electric Company, Vallecitos, Attn: Librarian
- 519. General Motors Corporation, Allison Division, Attn: Librarian
- 520. Hamilton Standard, Attn: Librarian
- 521. Hughes Aircraft Company, Attn: Librarian
- 522-523. Lockheed Missiles and Space Division, Attn: Librarian, John N. Cox
- 524. Marquardt Aircraft Company, Attn: Librarian
- 525. The Martin Company, Attn: Librarian
- 526. The Martin Company, Nuclear Division, Attn: Librarian
- 527. Martin-Marietta Corporation, Metals Technology Laboratory
- 528. Massachusetts Institute of Technology, Attn: Librarian
- 529. McDonnell Aircraft, Attn: Librarian
- 530-531. MSA Research Corporation, Attn: Librarian, R. C. Andrews
- 532. North American Aviation, Inc., Attn: Librarian
- 533. Pratt and Whitney Aircraft Corporation, Attn: Librarian
- 534-536. Pratt and Whitney Aircraft, CANEL, Attn: Librarian, K. J. Kelly, Robert Strough
- 537. Republic Aviation Corporation, Attn: Librarian
- 538. Rocketdyne, Attn: Librarian
- 539. Solar, Attn: Librarian
- 540. Southwest Research Institute, Attn: Librarian
- 541. Sylvania Electric Products, Inc., Attn: Librarian
- 542. Temescal Metallurgical, Attn: Librarian
- 543. Union Carbide Metals, Attn: Librarian
- 544. United Nuclear Corporation, Attn: Albert Weinstein
- 545. University of Michigan, Attn: Librarian
- 546. Vought Astronautics, Attn: Librarian
- 547. Westinghouse Electric Corporation, Aerospace Department, Attn: Librarian
- 548. Westinghouse Electric Corporation, Astronuclear Laboratory